NTNU

Norwegian University of
Science and Technology

Wilkinson Power Divider

A Miniaturized MMIC Lumped Component Equivalent

Tron Torgersen

Master of Science in Electronics

Submission date: June 2009

Supervisor: Guennadi Kouzaev, IET

Co-supervisor: Morten Olavsbråten, IET

Norwegian University of Science and Technology
Department of Electronics and Telecommunications

Problem Description

Design of miniaturized Wilkinson Power Divider using MMIC technology.

Assignment given: 15. January 2009
Supervisor: Guennadi Kouzaev, IET

Wilkinson Power Divider

-

A Miniaturized MMIC Lumped Component Equivalent

NTNU, 2009

Contents

P R A C T I C A L

Simulations

Measurements

Conclusion

Introduction

This report will describe the simulation of a Wilkinson Power Divider, realised using lumped components to minimize its size. Every step in the process, from calculating the lumped component values to the final Momentum s-parameter simulation is discussed. All relevant theory is described in the theory section.

The report is divided into two main parts: theory and practical. The theory part is subdivided into three parts: the circuit, the technology and the tools.

The circuit deals with anything related to the Wilkinson Power Divider, including a thorough analysis. The technology describes the MMIC (Microwave Monolithic Integrated Circuits) technology as well as some related subjects like electromagnetic coupling (cross-talk). The tools section is about the software tools and the theoretical tools that have been used in the project. The theory part should give the reader all the necessary knowledge to understand the practical part of the report.

The practical part starts with an overview of the design flow in numerical order. Each of these parts is then detailed, making the development of the final layout easy to follow. A number of figures showing all of the relevant setups in the computer design tool are included. All relevant graphs are included and commented.

In the measurements part, all of the s-parameter results from both practical measurements and the simulations done for comparison is given. The chapter starts with a short text on measurements in general and then goes through how the measurements for this report were done. Measurements and simulations are performed on both single and coupled inductors.

A basic understanding of RF electronics is assumed. It is important to understand that only information relevant to the project is included in the theory part. This means that key information on some subjects might have been omitted because it is not relevant to this particular project.

The main goal of this project is to produce the Wilkinson Power Divider using TriQuints 0.5 μm TQPED process in as small area as possible. The response of the circuit should also be made as close as possible to the ideal Wilkinson Power Divider. An important additional goal is to learn to use a relevant high-frequency design tool (Agilent ADS) and to get a good understanding of MMIC technology, including the components used and various effects such as cross-talk. During the project a practical measurement on components produced using the TriQuint process has been done, which gives a good understanding of practical measurements using probe station and network analyzer.

The design and simulation process has been done on a computer using ADS (Advanced Design System) from Agilent Technologies. This program package allows the running of s-parameter simulation on a schematic setup using component models from the vendor that takes into account the parasitic effects of each component. It also has the opportunity to run an s-parameter simulation on the final layout using a process based on the method of moments.

The final layout is reached in three steps from the regular distributed Wilkinson Power Divider. Figure 1 show these steps sequentially.

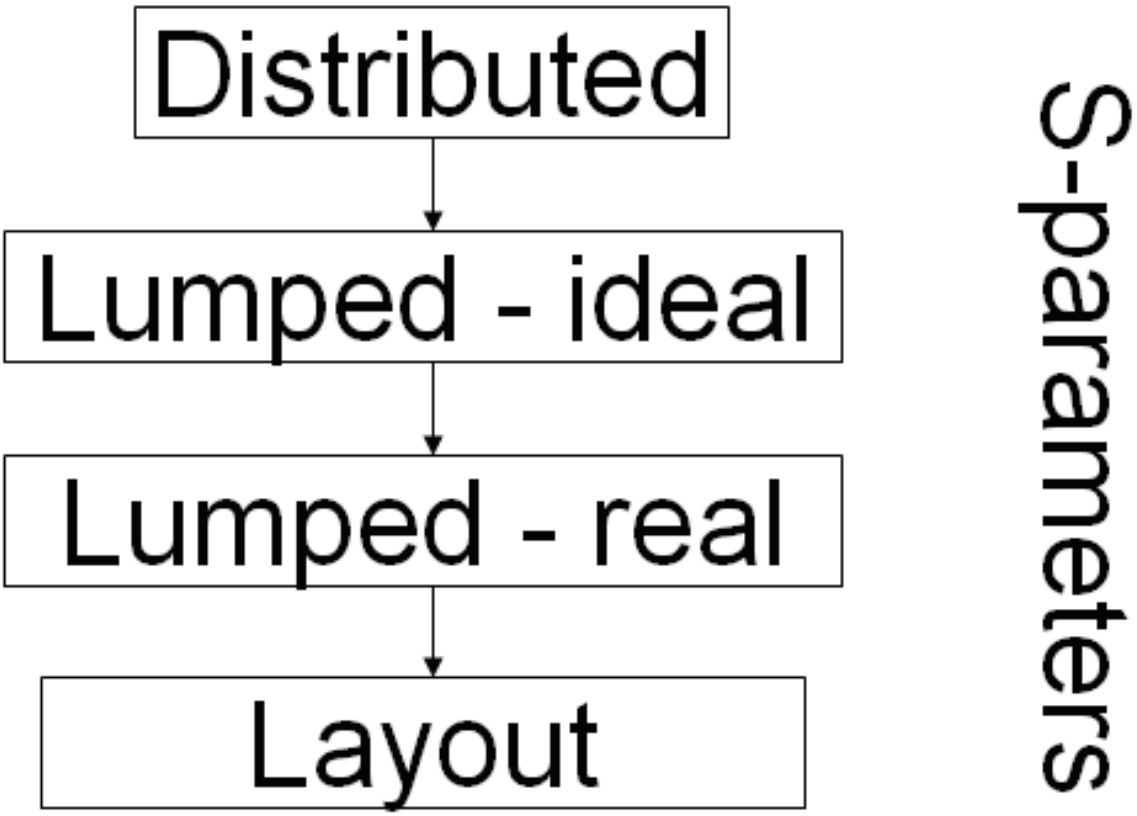

Figure 1: The various steps involved in reaching the final layout from the lumped component Wilkinson Power Divider.

The goal is to try to make the s-parameters at each step as close as possible to the previous step. This should, ideally, make the s-parameters of the final layout close to that of the ideal circuit. Because of the parasitic resistance, inductance and capacitance of the components as well as the effects of the transmission lines and cross-talk this is, as we will see, not possible to achieve.

Every step of the conversion from distributed to the final lumped component layout is described in the practical section. The s-parameters are then described and comments are made about the reasons for any deviation from the previous step. To get the desired response from the circuit, ADS's optimize function has been used. This function allows optimization on specified parameters, using goals like input and output match.

Finally, the key results and findings are summarised in the summary at the end. The conclusion section also includes a comparison of measurement and ADS simulation results, and a brief run-through of sources of error for the deviation between measurement and simulation results.

Important process data etc. is included as Appendixes.

THEORY

The Circuit

Wilkinson Power Divider

The Wilkinson Power Divider was introduced by Ernest J. Wilkinson in 1960 [8].

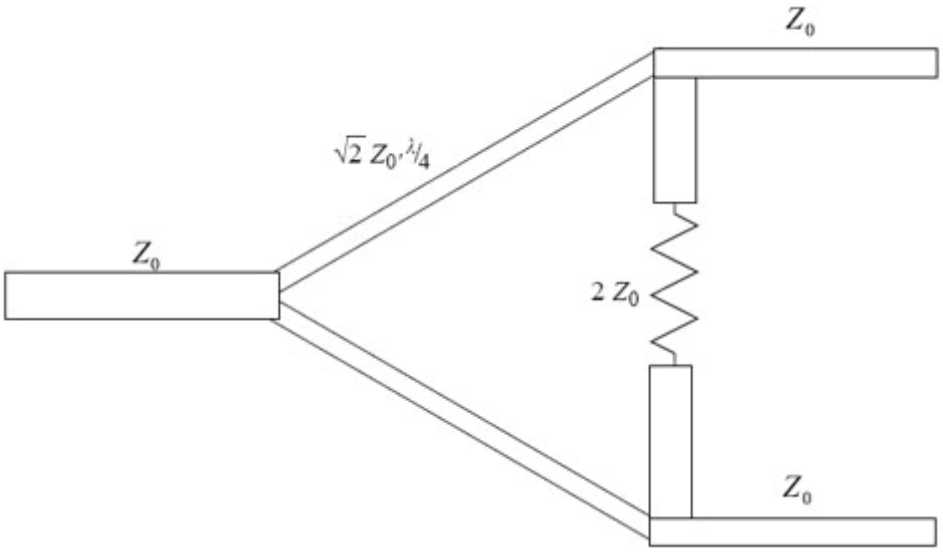

Figure 2: Wilkinson Power Divider (from [9]).

The purpose of the Wilkinson Power Divider is to split the power of the input equally between two output ports, ideally without loss. It can also be used in the reverse direction – as a power combiner. Other properties of the Wilkinson power divider is that all ports are matched, the two output terminals are isolated from one another, and that it is reciprocal. Resiprocality means that you get the same result if you send the signal from one port to another in either direction.

Three-port networks can not be reciprocal and matched without being lossy [10]. The solution to this, in the Wilkinson Power Divider, is to add a resistor between the two outputs. This resistor absorbs energy if there is a mismatch between the outputs. It also helps isolating the two outputs when the circuit functions as a power combiner.

Assuming a system impedance of 50 Ω, 50 Ω would have to appear at the input for this to be matched. With the two loads being 50 Ω each in parallel, we would achieve match if they both were transformed to 100 Ω (two 100 Ω loads in parallel equals 50 Ω). The way that this is achieved in the original Wilkinson Power Divider is by the use of quarter-wave transformers. We can see that this if possible by looking at the formula for a quarter-wavelength transmission line:

$$Z_{in} = \frac{Z_0^{\,2}}{Z_{load}}$$

By using lines with the appropriate characteristic impedance, we can theoretically transform the 50 Ω loads to any real impedance. To transform the 50 Ω loads to 100 Ω, we would need lines with characteristic impedance of 70.7 Ω.

S-Parameters

Figure 3 shows the S-parameter matrix of an ideal Wilkinson Power Divider.

$$[S] = \frac{-j}{\sqrt{2}} \begin{bmatrix} 0 & 1 & 1 \\ 1 & 0 & 0 \\ 1 & 0 & 0 \end{bmatrix}$$

Figure 3: S-parameter matrix for an ideal Wilkinson Power Divider.

The s-parameter matrix tells us:

- That the ports are matched (S_{11}, S_{22} and S_{33} equals 0)
- That ports 2 and 3 are isolated (S_{23} and S_{32} equals 0)
- That the power present at port 1 is equally divided between ports 2 and 3 (S_{12}, S_{13}, S_{21} and S_{31} equals -3 dB with a 90˚ phase shift)
- That the circuit is reciprocal (S_{mn} equals S_{nm})

Improving the Bandwidth

One of the biggest drawbacks of the Wilkinson Power Divider is that it has a quite narrow bandwidth. This can be improved by adding a quarter-wavelength section in front of the power combiner. In this way the impedance transformation is done in two steps, thereby improving the bandwidth.

The bandwidth of the power divider can also be increased by splitting the two quarter wavelength sections into multiple sections with a resistor between each section [11]. A common realisation is to use three sections instead of one. More than this can also be used to further increase the bandwidth. This obviously makes the circuit more complex, with added loss and increased area consumption on the chip.

A four section power divider is reported to have a VSWR < 1.11 at a 2:1 bandwidth and isolation between the outputs better than 26 dB. This can be compared to a traditional two-output Wilkinson Power Divider which has a VSWR < 1.22 at a 1.44:1 bandwidth and isolation of at least 20 dB.

Lumped Components

At low frequencies the size of the quarter-wavelength segments can get exceedingly large. The most popular way to reduce the size of the circuit is probably to replace the transmission lines with its lumped components equivalents.

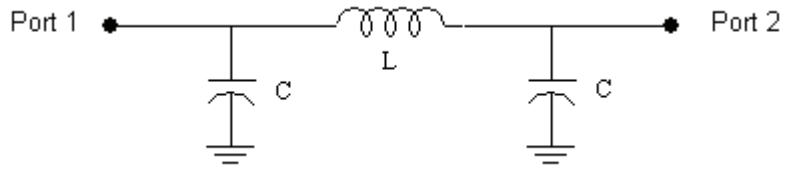

Figure 4: Lumped components equivalent to distributed transmission line.

One way to realise the ideal transmission line with lumped components is to use a series inductor and two shunt capacitors as shown in Figure 4. The component values can be quite easily calculated using the following reasoning:

We know that the resonant frequency of a LC-circuit is $1/\sqrt{(LC)}$ [12], so we set this equal to the centre frequency that we design the circuit for. Since we have two unknowns and only one equation, we need another equation. This can be obtained by setting the impedance of the lumped equivalent equal to that of the distributed transmission line. The impedance of the lumped circuit will be $\sqrt{(L/C)}$, and setting this equal to $\sqrt{2}\ Z_0$, which is the characteristic impedance of the transmission line, we end up with the following two formulas:

$$\sqrt{\frac{L}{C}} = \sqrt{2}Z_0$$

$$\frac{1}{\sqrt{LC}} = \omega_0$$

which is easily solved to yield:

$$C = \frac{1}{\sqrt{2}\omega_0 Z_0}$$

$$L = \frac{\sqrt{2}Z_0}{\omega_0}$$

Formula 1: Formulas for calculation of inductor and capacitor values for lumped components Wilkinson Power Divider.

The resulting lumped components Wilkinson Power Divider is shown in Figure 5, along with the regular Wilkinson circuit. The values were calculated at the central frequency, so that even with ideal components the two topologies will only be equivalent at this frequency.

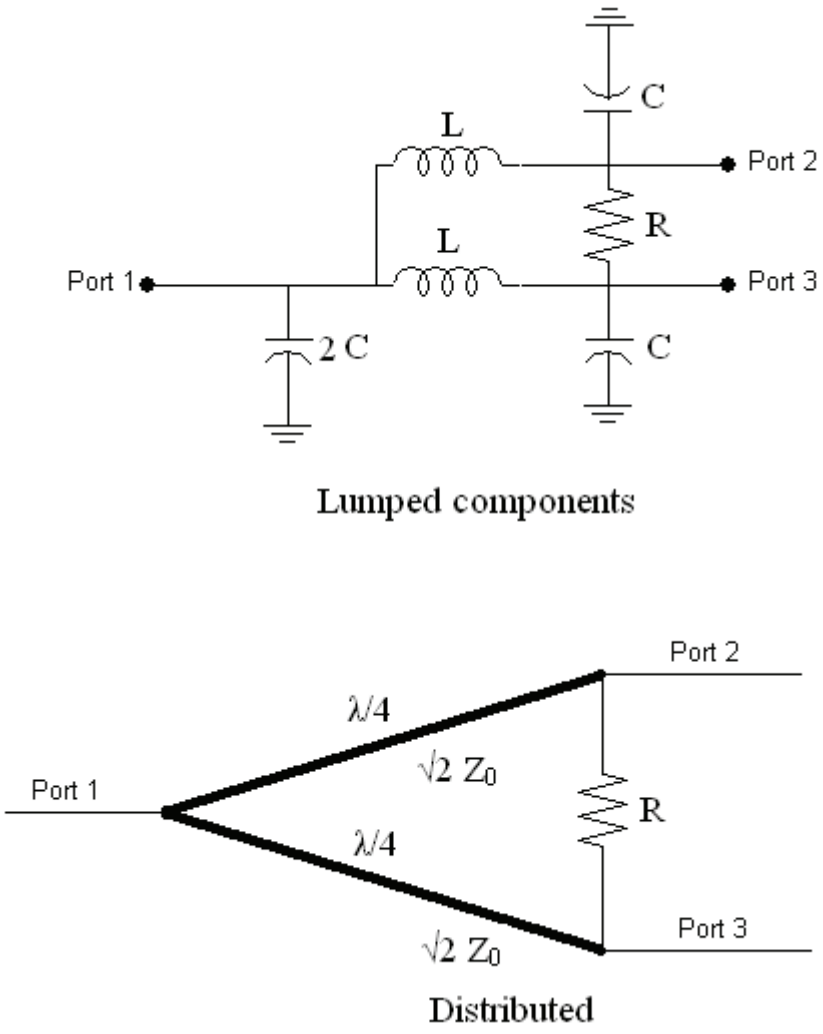

Figure 5: Wilkinson Power Divider. Lumped and distributed realisations.

To study the differences between the quarter wavelength transmission line and the lumped components equivalent shown in Figure 5, an Agilent ADS (see separate Chapter on ADS under the tools section) s-parameter simulation is performed on both realisations. The resulting S_{11} and S_{21} values for both realisations are displayed in separate Smith charts in Figure 6. Because of symmetry, we must have that $S_{22} = S_{11}$ and $S_{12} = S_{21}$.

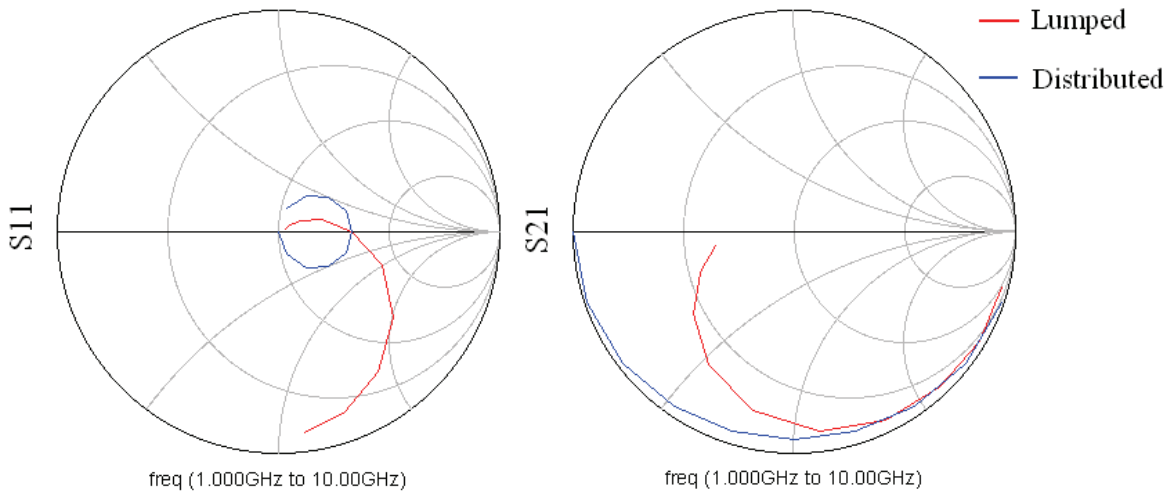

Figure 6: S_{11} and S_{22} for ideal transmission line and lumped components equivalent simulated in Agilent ADS.

We can clearly see from the left chart, that the two topologies are only equal at the design frequency of 5 GHz. Here the value of S_{11} is purely real and equals 2 for both topologies. The lumped components show an inductive behaviour below this frequency and a capacitive above, while the distributed line behaves in an opposite manner. At frequencies above the design frequency, the input mismatch will be grater (higher voltage standing wave ratio) for the lumped components realisation than for the transmission line.

The left chart shows that the S_{21} value of the two realisations is also different. At 10 GHz, where the transmission line is a half wavelength, we see that the signal is transmitted without loss and an 180˚ phase shift on the transmission line. The S_{21} value of the lumped components realisation deviates greatly from this value at this frequency.

Analysis

This section is based on [13].

To find the s-parameters of the Wilkinson Power Divider, we need to find the incident and reflected voltages at all the ports. To do this we can use even- and odd-mode analysis (see separate section on even/odd mode analysis under The Tools Chapter):

We start by applying a voltage source with impedance Z_0 at port 2 with port 1 and 3 terminated with Z_0 (Z_0 being the system impedance). The circuit can now be split in two along the horizontal axis, with a positive port at the upper half and a negative at the lower half, as shown in Figure 7. This circuit has odd symmetry which means that the symmetry line becomes a virtual short. We can now treat the upper and lower parts of the circuit as separate.

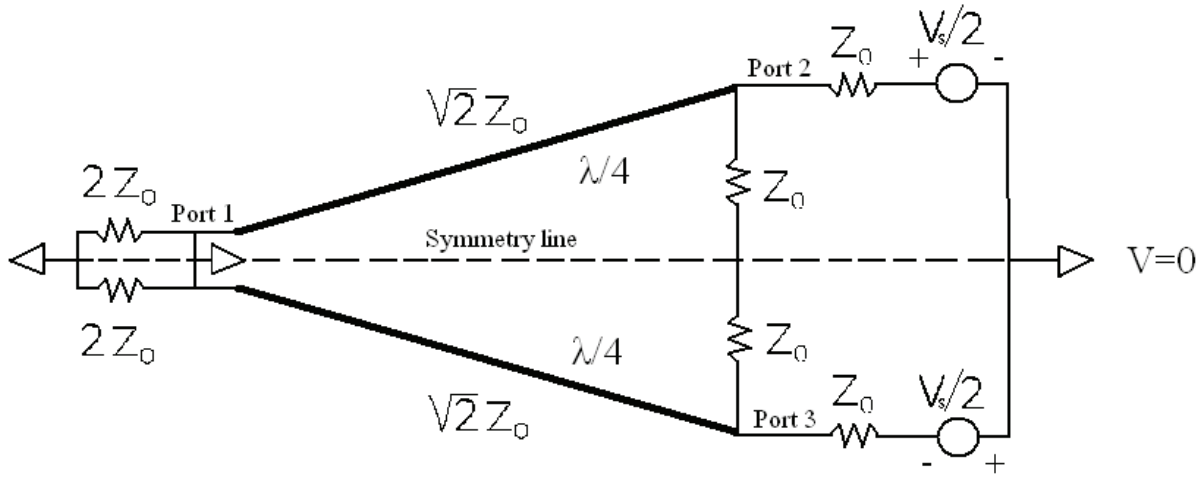

Figure 7: Setup for odd mode Wilkinson Power Divider analysis

We can see directly that V_1^o (o indicates odd) is zero since this port is short circuited. Since the line is a quarter wavelengths, the short is transformed to an open at port 2 and 3. So from simple voltage division we find $V_2^o=V_s/4$ *and* $V_3^o=-V_s/4$.

We now use the even mode circuit in Figure 8 to find the even mode voltages. Since we have even mode symmetry, the symmetry line represents a virtual open. The $2*Z_0$ resistor at port 1 transforms (using the quarter wavelength formula) to Z_0 at ports 2 and 3. Using simple voltage division again, we find $V_2^e=V_s/4$ and $V_3^e=V_s/4$. If we apply the telegraphers equation with the boundary conditions, we find that $V_1^e=-jV_s/(2\sqrt{2})$.

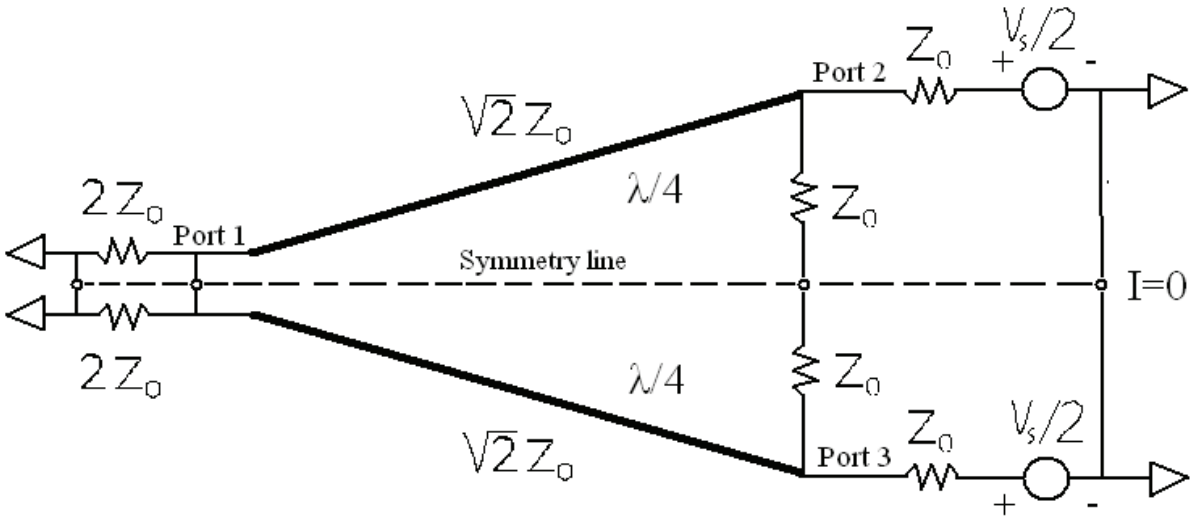

Figure 8: Setup for even mode Wilkinson Power Divider analysis.

By adding the odd and even voltages (superposition), we find the total voltages at the ports, which is the sum of the incident and reflected voltages. Doing this gives $V_1=-jV_s/(2\sqrt{2})$, $V_2=V_s/4$ and $V_3=0$. Since ports 1 and 3 is terminated in Z_0, the reflected voltages at these two ports must be zero, so $V_1^+=0$, $V_1^-=-jV_s/(2\sqrt{2})$, $V_3^+=0$ and $V_3^-=0$. Now, since the source impedance at port 2 is matched to the line impedance, which is electrically small, we must have that $V_2^+=V_s/2$ and $V_2^-=0$.

We have now calculated the necessary voltages to find S_{12}, S_{22} and S_{32}:

$$S_{12}=\frac{V_1^-}{V_2^+}=\left(\frac{-jV_s}{2\sqrt{2}}\right)\frac{2}{V_s}=\frac{-j}{\sqrt{2}}$$

$$S_{22}=\frac{V_2^-}{V_2^+}=(0)\frac{2}{V_s}=0$$

$$S_{32}=\frac{V_3^-}{V_2^+}=(0)\frac{2}{V_s}=0$$

From symmetry we must have that $S_{13}=S_{12}$, $S_{33}=S_{22}$ and $S_{23}=S_{32}$. While reciprocity gives; $S_{21}=S_{12}$ and $S_{31}=S_{13}$.

To find S_{11}, we move the source to port 1 and use even symmetry (see Figure 9).

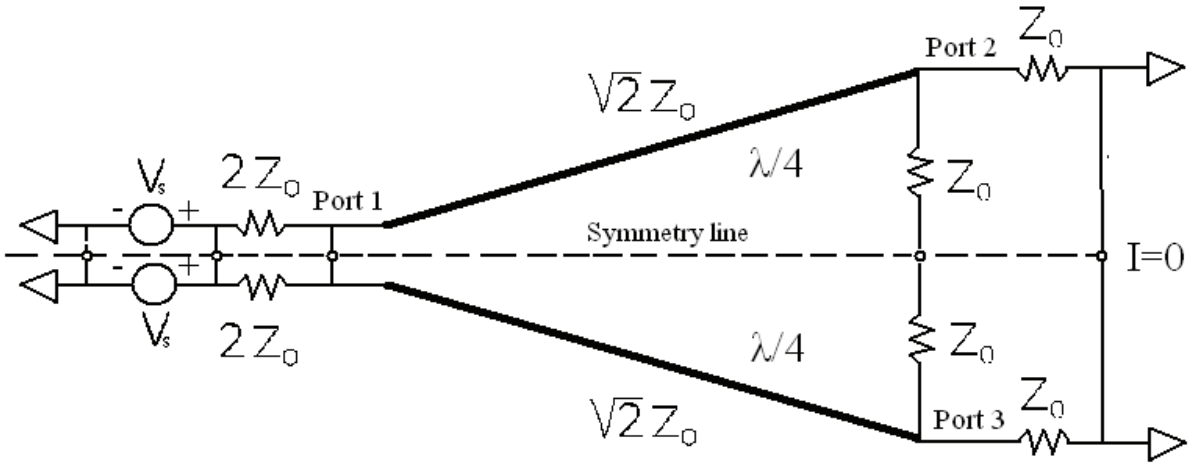

Figure 9: Setup for even mode Wilkinson Power Divider analysis to find S_{11}.

Using the upper half of the circuit, we transform the load at port two to the input and apply voltage division to find $V_1=V_s/2$.Using the same logic as for V_2 above, we find $V_1^+=V_s/2$ and $V_1^-=0$. Now S_{11} is easily found as:

$$S_{11} = \frac{V_1^-}{V_1^+} = (0)\frac{2}{V_s} = 0$$

This should complete the calculation of scattering parameters, and give the s-parameter matrix for an ideal Wilkinson Power Divider:

$$S = \begin{bmatrix} 0 & \frac{-j}{\sqrt{2}} & \frac{-j}{\sqrt{2}} \\ \frac{-j}{\sqrt{2}} & 0 & 0 \\ \frac{-j}{\sqrt{2}} & 0 & 0 \end{bmatrix}$$

Figure 10: S-parameter matrix for an ideal Wilkinson Power Divider.

Practical Use of the Wilkinson Power Divider

The Wilkinson Power Divider can be an integrated part of a larger system, or fabricated as separate parts. Important parameters for separate power dividers are; frequency range, number of outputs, type of connections, isolation, insertion loss, VSWR and temperature range.

For any power divider it is important that the impedance level is matched at all the ports. 50 Ω is standard impedance for nearly all stand-alone power dividers. For system integrated ones it can be different if this is beneficial.

Wilkinson Power Dividers are a widely used type of circuit. Some examples of its practical uses are: antenna sharing, test labs and in-building networks. It is used for a wide range of communication signals like: GSM, PCS, WCDMA and UMTS [14].

Radio frequency (RF) systems (i.e. radio or television) with multiple channels commonly use the Wilkinson Power Divider because the output ports are well isolated, and thus prevent cross-talk [15].

Examples of Systems Employing Wilkinson Power Dividers

1. In [16] three Wilkinson Power Dividers are used to feed an ultra-wideband (UWB) antenna array in a one-to-four configuration. A defected ground structure is used to create a notch in the frequency characteristic to avoid interference with WLAN systems operating in the same frequency range as the UWB. The defective ground involves removing some of the ground plane below the transmission line. This gives a resonance with the line at some frequency that is determined by the size of the removed section. Symmetrical spiral defects are used in this design. To adjust the rejected frequency band, the size of the spirals is changed.

   To achieve wide enough bandwidth, the quarter wavelength sections of the Wilkinson Power Divider are constructed from three separate parts. This is a well known method for increasing the bandwidth of the power divider, at the expense of increased dimensions. To obtain the correct frequency band, the length and width of the transmission lines or the resistance values of the sections is changed.

2. Wilkinson Power Dividers is often used to feed multiple antennas in an antenna array from a single source. [17] gives one example of such utilization. In this design, six Wilkinson Power Dividers is used to split the input signal to the eight elements of a Vivaldi antenna array operating at the lower UWB at 2-4 GHz. This array is intended used for through-wall imaging systems. The antenna elements are constructed as tapered slots.

   This design offers an example of a power divider that is not matched to 50 Ω. It is instead designed for minimum reflection at 100 Ω (both input and output loads) since this is the characteristic impedance of the antenna elements at the design frequency. As in the previous example, this design uses Wilkinson Power Dividers constructed from three sections to achieve good bandwidth. The input is connected directly to two power dividers, giving an input impedance of 50 Ω (2x100 Ω in parallel).

3. [18] offers an example of a two-way commercially available Wilkinson Power Divider. It has N type female connections and is designed for the frequency range of 0.7 to 2.7 GHz. It is designed to handle 40 watts of power on both input and outputs, and exhibits low insertion loss while having a good isolation between output ports.

   The power combiner can be used for a wide range of applications within its RF band. Examples include amplifier combining and antenna splitting. It is used in a lot of systems including the 800 MHz cellular, GSM 850, 900, 1800 & 1900, GPS, UMTS, RFID and 2.3 GHz & 2.5 GHz WiMAX.

The Technology

Monolithic Microwave Integrated Circuits (MMIC)

MMIC is an acronym for Monolithic Microwave Integrated Circuit. Monolithic indicates that both passive (resistors, inductors etc.) and active elements (i.e. transistors) are fabricated on the substrate, while microwave means that the circuits are operating in the 300 MHz to 300 GHz frequency range.

MMIC's biggest advantage over earlier techniques like hybrid design is that it is easily mass produced making it cost-effective for large quantities. Smaller quantities are often cheaper using hybrid design, because of the high start-up cost for MMIC production. Other advantages of MMIC technology are that the circuits can be made very compact and reliable with low parasitics. This allows high frequency operation from small chips; an important element in modern technology.

In the MMIC technology's childhood, gallium arsenide (GaAs) was the preferred substrate material, and is still the dominant material today. Gallium arsenide is very well suited for MMIC circuits because of its relatively high resistivity, high permittivity and low loss tangent. The biggest drawback of GaAs is its high cost compared to i.e. silicon.

MMIC designs make use of both distributed and lumped components. Especially at high frequencies, distributed components are practical because of their small size. Even components like antennas can be produced directly on the chip at these frequencies. Distributed components can also be used for functions such as matching and bias networks.

The very first functioning MMIC designs were produced in the late 1960's. During the 1970's the technology was gradually improved, culminating in the IEEE establishing a symposium dedicated to GaAs IC development in 1979 [1].

Important MMIC Parameters

Following is a list of important parameters specifying the electrical properties of the materials that makes up the MMIC chip.

Conductivity (σ)
Conductivity is a measure of how well the material conducts electric current. The definition of conductivity is the ratio of the electric field applied to a material to the electric current density that it produces.

A high value means that the material is a good conductor and the material is classified as a conductor. A low conductivity means that the material conducts current poorly, in which case it is classified as an insulator. Semiconductors usually have a conductance somewhere between these two classifications, though the conductivity of semiconductors is highly dependent on doping, electromagnetic fields and temperature. The conductivity of most materials is temperature dependent [19].

Permittivity (ε)
The permittivity of a material tells us the ratio between the electric displacement (**D**) and the electric field (**E**). It can be taught of as a measure of how well the material "conducts" electric fields. To account for losses in the material, complex permittivity can be used. The imaginary part then represents the loss. This value is normally frequency dependent, and can also be dependent upon direction, in which case the material is called anisotropic.

In practice, the permittivity is usually expressed as a value relative to the permittivity of free space, called relative permittivity. The relative permittivity is given as: $\varepsilon_r = 1 + \chi_e = \varepsilon/\varepsilon_0$, where χ_e is the electric susceptivity of the material and ε_0 is the permittivity of free space.

The loss tangent (tan δ)
The loss tangent is defined as the ratio between the imaginary and the real part of the permittivity. A high loss tangent means high loss in the material. Typical values can be around 0.0005. The loss is dominantly converted to heat in the substrate/dielectric.

Permeability (μ)
The permeability is analogous to the permittivity, the difference being that it accounts for the materials magnetic properties, instead of the electrical, as is the case with permittivity. The permeability is also commonly expressed in a real and an imaginary part. For most materials used for substrate or dielectric in MMICs the value of the permittivity is the same as that of air (vacuum).

MMIC Lumped Components

Resistors

Resistors are components that are used for many purposes, including feedback networks, power dividers, impedance matching and stabilisation. Resistors are made up from a lossy material with a given resistivity ρ expressed in Ω-m. The physical dimensions of the resistor also determine its value. Increased cross-section lowers the resistance value, and increased length increases the resistance. The width of the resistor should be kept as close as possible to that of the connecting microstrip line, since deviating cross-section leads to discontinuity effects.

Some important parameters for resistors are: power rating, temperature coefficient, tolerance, maximum voltage and current handling, noise, stability and maximum frequency. In MMIC all resistors are realised as planar components. Planar resistors can in general be divided into three categories: chip (thin- and thick-film), MCM – Multichip Modules (PCB's, cofired ceramic and thin-film on silicon) and monolithic (e.g. bulk resistors). Common for all these types is that the voltage standing wave ratio (VSWR) is very large for low sheet resistance (ohms/square). On the other hand, the thermal resistance increases sharply as the sheet resistance is increased, so that a compromise between these two factors must be made.

Mesa resistors
Resistors in MMIC technology can be realised using doped areas of the substrate. This kind of resistors will, however, have low accuracy, be prone to resistivity drift due to aging and be highly temperature dependent. For Gallium Arsenide it is approximately 300 ppm/˚C, meaning that the resistance increases sharply when the temperature increases. Thin-film resistors have, in comparison, about 30 ppm/˚C temperature dependence.

Semiconductor resistors also have a limited range of field strengths where the voltage-current relationship is linear, so that the resistors need to be long if it is to handle large voltages [1].

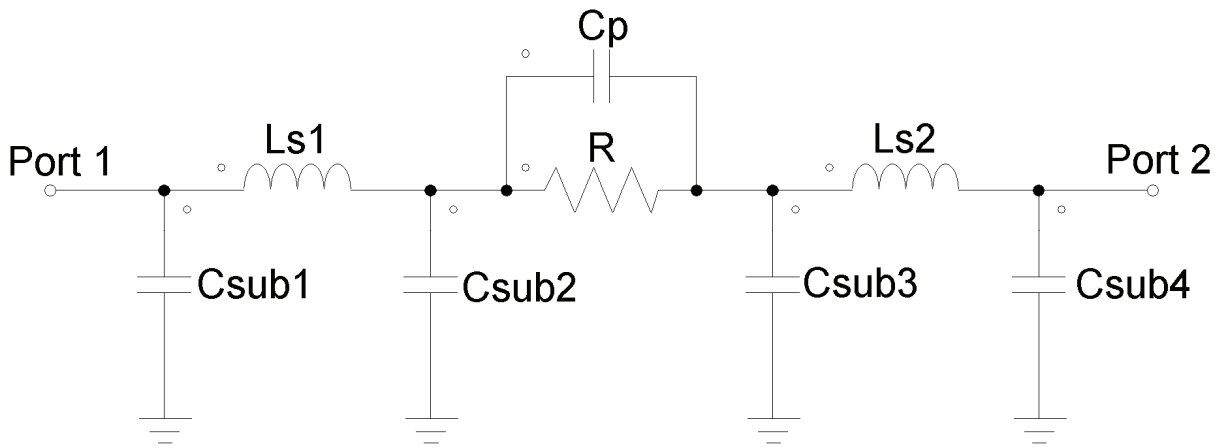

Figure 11: Thin-film resistor equivalent.

Thin-film resistors
A better way to make resistors in MMIC technology is to use resistive metal resistors where the technology allows these. These are produced by a sputtering process. Common materials are compounds like NiCr (nichrome) and TaN (tantalum nitride). Resistors produced by this method are highly temperature and frequency independent. They are usually located directly above the substrate and are connected by a local metal layer.

Figure 11 shows an equivalent circuit of a microstrip mounted thin-film resistor (all equivalent circuits in this section is from [5]). The inductors are due to the connections to the rest of the circuit, as well as the length of the resistor itself, while Csub1, Csub2, Csub3 and Csub4 is due to the substrate capacitance to the ground plane. C_p is the parasitic capacitance between the two ports.

Inductors

Inductors are constructed using lengths of transmission lines. They need to be narrow to achieve high inductance with low parasitic inductance. Only relatively small inductances can be achieved in this way because of space limitations and the fact that resistance and current capacity demands limits the narrowness of the lines. Fabrication processes technology also limits the minimum line width.

Today nearly all inductors are constructed as spirals. This utilises the available space in an efficient way, and also achieves increased inductance by mutual coupling between the turns. A difficulty in realising these kinds of inductors is, however, that the inner segment needs to be connected to the outside circuit. There are many ways to do this; using an air bridge or using a separate metal layer for the underpass is two methods. The chosen technology limits the available choices in practice.

When constructing MMIC inductors, one wants to achieve the proper inductance with as low resistance as possible (resulting in the highest Q-factor), in as small area as possible. These two concerns are contradictory, so a trade-off has to be made. The Q-factor tells us how much energy is dissipated in the inductor relative to its inductance (capacity for storing magnetic energy), or the ratio of reactance to resistance. It is a frequency-dependent value, and some formulas for calculating the q-value is given below.

Other important factors for inductors are the current carrying capability and the parasitic effects.

$$Q = 2\omega \frac{|W_E| - |W_M|}{P_{diss}}$$

Formula 2: General formula for calculation of the Q-factor of inductors. W_E is the energy stored in the electric field, while W_M is the energy stored in the magnetic field.

$$Q = \frac{f_{res}}{BW}$$

$$Q_{eff} = \frac{\mathrm{Im}[Z_{in}]}{\mathrm{Re}[Z_{in}]} = \frac{X}{R} = \frac{\omega L_e}{R}$$

Formula 3: Q-factor formulas. BW is the 3-dB bandwidth.

The inductance is increased by increasing the total length or reducing the spacing between turns or the width of the line. All of these modifications increase the resistance and thereby reduces the Q-factor. Longer lines with smaller gap between turns also increase parasitic capacitance. The current carrying capacity is mainly determined by the line width, but also depends on factors such as the shape of the inductor and the thermal coupling to the surrounding environment and its temperature. Multiple metal layers can be used to increase current capacity (and Q-factor) if available.

A number of techniques can be employed to increase the Q-factor of an inductor. One method is to decrease the line width of the turns closest to the centre of the inductor. This increases the Q-factor because it limits the effects of the so-called eddy currents. The eddy currents are created by the magnetic field that surrounds the inductor when it passes through the inner turns. According to Lenz's law, a current is induced that tries to cancel the applied field. This induced current is circular and will cancel the original current on one side of the conductor while it adds to the current on the other side of the conductor. The result is that the effective resistance is increased, and thereby the Q-factor is decreased. Since the induced eddy currents are strongly dependent on frequency, the effect is only critical at higher frequency. By reducing the size of the inner turns, or making the centre of the inductor hollow, the effect is reduced.

Other techniques for improving the Q-factor are using micromachining, high resistivity substrate, multilayer layout and wide traces with high conductivity. The voltage difference between the inductor and the ground plane and magnetic loss due to the magnetic fields that penetrates the substrate leads to loss in the substrate. To reduce this loss, we can place a ground shield between the inductor and the lossy substrate. This can be done with a patterned ground shield in for instance metal, polysilicon or n^+. This technique is most relevant in low resistance substrates like silicon (Si).

Another factor that must be taken into account is the resonant frequency of the inductor, since it can only be used at a frequency well below the resonant frequency. The main reason for this is that the resonant frequency is highly dependent upon process variations. A small change in any of the inductors parameters changes the resonant frequency which means that the inductance close to the resonant frequency is very sensitive with regards to changes in line width etc. This concern becomes especially important at higher frequencies.

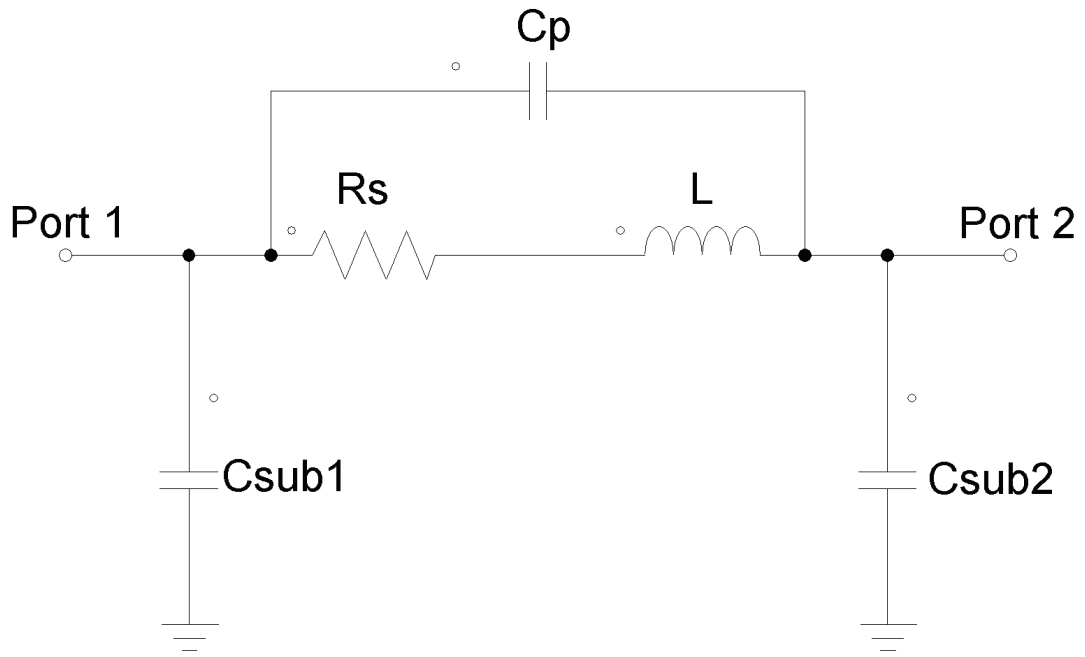

Figure 12: *A model of a lumped MMIC inductor.*

Figure 12 shows a model of a coiled inductor. From this model it is easy to see that the inductor will suffer from parallel resonance at a certain frequency, and that it will, in fact, behave as a capacitor at higher frequencies. The physical origin of Cp in Figure 12 is the capacitive coupling between adjacent lines. This coupling can be reduced by reducing the number of segments in the inductor or increasing the distance between adjacent turns.

Capacitors

Interdigital capacitors

There are two types of capacitors in common use. Interdigital capacitors are one of these. They are constructed from a number of interleaved microstrip fingers. A capacitive effect will exist between each of them. The biggest advantage of this method is that they have very good accuracy. The major drawback being that the achievable capacitance is quite limited. When designing these capacitors it is important to keep the size very small compared to the wavelength, so that it can be treated as a lumped element.

Metal-Insulator-Metal capacitors

The most common type of capacitor in MMIC is Metal Insulator Metal (MIM) capacitors. MIM capacitors consist of a dielectric sandwiched between two metallic layers. Using small separation distances and high permittivity dielectrics, high capacitances can be achieved using small areas. Square capacitors are the most common, though any shape, like circular and triangular is possible.

An important parameter for capacitors is its Q-factor, with its formula given below. R_S is the equivalent series resistance, C is the total capacitance and f is the operating frequency. A capacitor will have both series and parallel resonance. As the frequency is increased from DC,

the capacitance will decrease until it reaches the series resonance frequency, where the capacitance is zero. The reactance of the component is then inductive until the frequency where it reaches parallel resonance, where it appears as a highly resistive component. Other important capacitor parameters includes; maximum voltage and current ratings and insulation resistance.

$$Q = \frac{1}{2\pi f C R_S}$$

Formula 4: Capacitor Q-factor.

Figure 13 shows an equivalent circuit for an MIM capacitor.

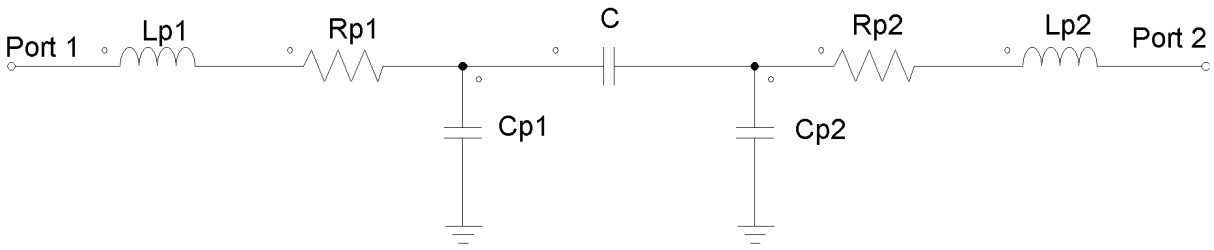

Figure 13: Capacitor lumped model.

Via holes

In MMIC design one needs to have some kind of connection to ground, often several. This is achieved by the use of via holes. A via hole is a conducting connection to the bottom ground plane. It can function as a thermal conducting path as well as an electric path. Via holes can be produced in several ways. For thick substrates (> 100 um) etching (wet or dry) is the most common. For thinner substrates mechanical or laser methods can be used [36]. Drilling and cutting is preferable with soft substrates, while etching or laser beam processing is used for hard substrates [2].

It is important to take into account the parasitic effects of the via holes when designing a circuit. The dominant parasitic is often the inductance, though the parasitic is highly dependent upon the chosen technology, at least at high frequencies. Figure 14 shows an equivalent lumped components circuit of a via hole. The main parasitic will be the inductance L2, because the via is relatively long (150 μm, typically).

Combining several via holes together to one single hole can cause problems at high frequencies, as the via holes are not ideal and dangerous feedback paths can exist [1]. It is also important to take into consideration that coupling exists between adjacent via holes at high frequencies, and that the via holes will radiate energy when the frequency becomes high enough.

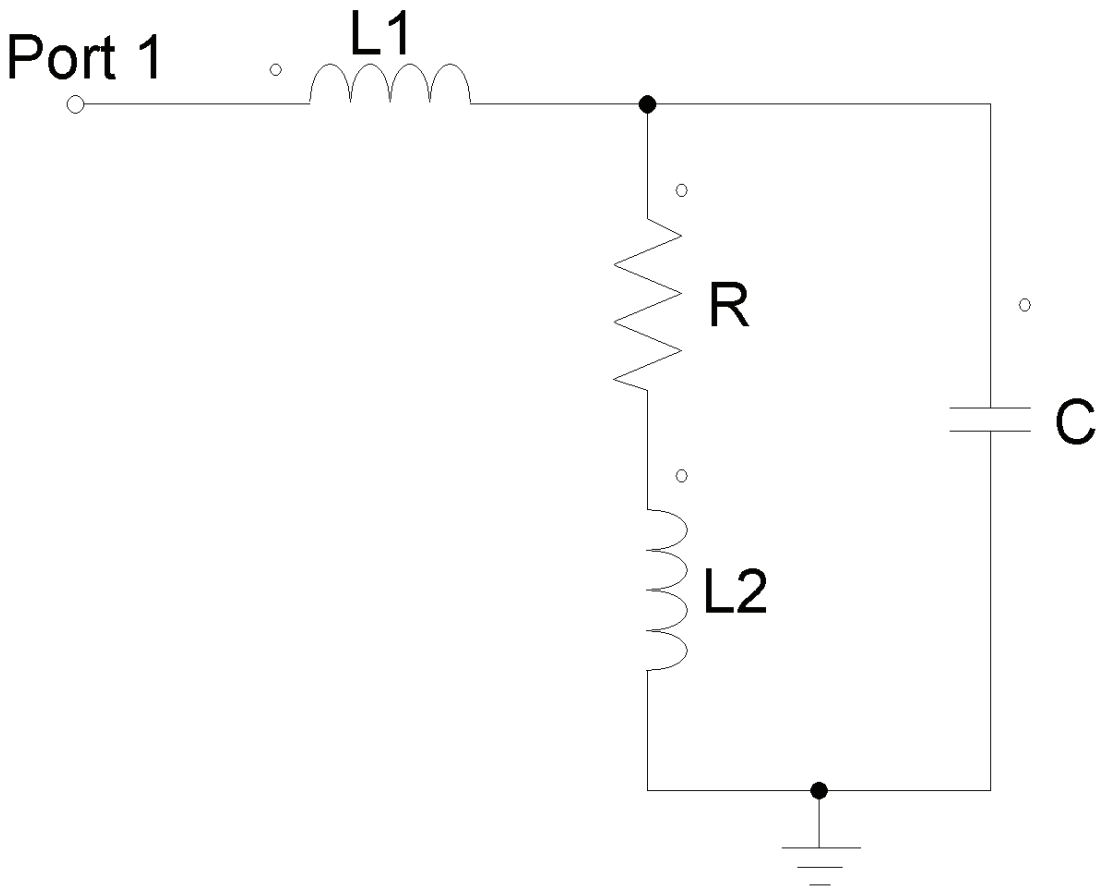

Figure 14: Via hole equivalent circuit.

Parasitics in MMIC lumped components

Every length of metal represents an inductance, every conductor (unless being a superconductor at very low temperatures) has some resistance and every separated pieces of metal with different charge will have a capacitance between them. This means that every structure in MMIC has some capacitance, resistance and inductance.

At high frequencies these parasitic effects starts to become significant and needs to be taken into account when designing a circuit. Models often exist to account for these effects. When using computer tools in the design, models are often supplied by the chosen manufacturer. These models are not 100 % accurate though, and electromagnetic (EM) simulation normally has to be applied to validate the design.

Lumped components can be considered as discrete when their size is a fraction of a wavelength. As a rule of thumb the distributed nature of the components needs to be taken into account when the frequency exceeds 20 GHz [37].

Electromagnetic Coupling

Any electric charge that is accelerated (change of direction or speed) emits electromagnetic radiation. This means that for circuits operating at AC, any conducting structure will theoretically radiate energy. The structure needs, however, to be a substantial fraction of a wavelength to be a good radiator, which means that the problem of unwanted electromagnetic coupling gets worse with increasing frequency. The radiation will be strongest at any discontinuity like bends, and junctions.

The radiation from one part of the circuit will affect the electrons in other conducting parts of the circuit, making the signal in different parts of the circuit affect each other. This phenomenon is called *cross-talk*, and can adversely affect the performance of the circuit.

Since the strength of electromagnetic radiation is inversely proportional to the square of the distance, structures that are close together experiences the strongest coupling. Cross-talk can therefore be reduced by increasing the distance between the components, including the transmission lines. Parallel lines with small separation distance are an example of a structure where strong coupling would occur. Some large structures like inductors is also surrounded by a strong electromagnetic field, which means placing two inductors close together can lead to strong coupling.

Besides increasing the separation distance between components, shielding can be used to limit cross-talk. An example of this could be a grounded wire separating two inductors, thereby reducing the electromagnetic coupling between them. Factors like component orientation can also affect the coupling. In [20] an example of the strong dependence of the coupling between two adjacent MMIC inductors upon their orientation is given.

Radiation is not the only mechanism behind component coupling. Closely spaced conductors will experience a capacitive effect, and conductors that carries a current will have a inductive effect between them. This means that some of the signal will be coupled from one part of the circuit to another.

Basic Transmission Line Theory

Electric Field

A force will exist between all electric charges. Charges of equal polarity will repulse each other, while opposite charges will attract. The strength of the force (*F*) between them depends on the strength of the charges (*q*) and the distance between them (*r)*. This effect is expressed in Coulombs law, which is fundamental to all electromagnetics.

$$F = \frac{q_{source} q_{test}}{4\pi\varepsilon_0 r^2}$$

Formula 5: Coulombs law.

From Coulombs law we can find the force acting on an electric charge due to the other charges in its vicinity, but most of the time we want to know what force an imaginary charge would experience if it was placed at a certain point. This is where the concept of a field arises. By removing the "test" charge from Coulombs law we have a vector quantity that tells us the strength and direction of the force that a charge of a given size (in coulombs) will experience if placed in at a given point in the space where the expression is valid. This is analogous to the concept of gravitational fields, where the force of an object of a given mass can be found if placed at a given point (i.e. in the vicinity of earth).

The English chemesist and physicist Michael Faraday found in 1831 that a current will flow in an electric loop that penetrates a changing magnetic field (**B**) [21]. This means that not only electric charges are the source of electric fields (**E**), but also changing magnetic fields will induce an electric field. This is important as it leads to the possibility for propagating electromagnetic waves. Faradays law in differential form is given below.

$$\nabla \times \mathbf{E} = -\frac{\partial \mathbf{B}}{\partial t}$$

Formula 6: Faradays law.

Magnetic Field

If you run a current through two parallel wires you will find that a force is acting between them. The direction of the force depends on the direction of the currents. Current run in the same direction will make the wires attract, while current in the opposite direction makes the wires repel each other. This force is not due to electric forces, but is due to magnetic forces that exists between moving electric charges (electric current),

Any conductor carrying a current, *I,* can be thought of as having a circular magnetic field surrounding it. The direction of the field can be found by making the right hand thumb point in the direction of the current. The rest of the fingers of the right hand will then follow the direction of the magnetic field if you curl your hand around the conductor. If a steady line

current is flowing in a conductor, the magnetic field that surrounds it can be found from Biot-Savarts law, given below. This is analogous to Coulombs law in electrostatics.

$$d\mathbf{B} = \frac{\mu_0}{4\pi}\frac{I(d\mathbf{I}\times\mathbf{r})}{r^3}$$

Formula 7: Biot-Savarts law.

A varying electric field will source a magnetic field just as a changing electric field will source a magnetic field.

Electric and Magnetic Fields in Matter

When a dielectric material is subject to an electric field it will be polarized. A dielectric material can generally be thought of as a material that is not a conductor. The polarization is due to two effects: stretching and rotation of atoms and/or molecules, which in sum gives a lot of little dipoles pointing along the direction of the field [6].

A materials ability to get polarized is proportional to the electric field provided the material is linear, and that the field is not too strong. This polarizability is summed up by the dielectric constant of the material. If a charge is contained within a dielectric with high dielectric constant, the force it exerts on nearby charges will be reduced because the material is polarized in such a way that it limits the electric field. When dielectrics are involved it is easiest to work with the displacement **D**, with its relation to the electric field **E,** for a linear media, given below.

$\mathbf{D} = \varepsilon\mathbf{E}$, $\varepsilon = \varepsilon_r\varepsilon_0 = \varepsilon_0(1 + \chi_e)$

Formula 8: Displacement is proportional to the electric field. ε is the permittivity, ε_r the relative permittivity, ε_0 the permittivity of free space, and χ_e the electric susceptibility.

When a magnetic material is subjected to a magnetic field it will be magnetized. There are two general types of magnetic materials: paramagnets that acquire magnetization parallel to the applied magnetic field, and diamagnets that acquire magnetization opposite to the magnetic field. Ferromagnets are a type of material that retains the magnetization after the magnetic field has been removed.

Just as with the dielectric materials, the effect of a magnetic field on a linear magnetic material, can be expressed using a material-dependent constant, in this case called relative permeability, and the relation between the magnetic field **B**, and the **H** field is given below.

$\mathbf{B} = \mu\mathbf{H}$, $\mu = \mu_r\mu_0 = \mu_0(1 + \chi_m)$

*Formula 9: Constitutive relation between **B** and **H** field. μ is permeability, μ_r relative permeability, μ_0 permeability of free space and χ_m the magnetic susceptibility.*

Maxwell's Equations

$$\begin{cases} \nabla \cdot \mathbf{D} = \rho_f & (i) \\ \nabla \cdot \mathbf{B} = 0 & (ii) \\ \nabla \times \mathbf{E} = -\dfrac{\partial \mathbf{B}}{\partial t} & (iii) \\ \nabla \times \mathbf{H} = \mathbf{J}_f + \dfrac{\delta \mathbf{D}}{\partial t} & (iv) \end{cases}$$

Formula 10: Maxwell's equations in differential form. ρ_f is the free electric charge and J_f is the free current (current not attributable to bound currents caused by magnetic fields).

Maxwell's equations along with the force law, contains all the theoretical information of classical electrodynamics.

$$\mathbf{F} = q(\mathbf{E} + \mathbf{v} \times \mathbf{B})$$

Formula 11: The force law.

The last term in equation iv (commonly referred to as Amperes law) was added by Maxwell. This term is important as it allows for propagating electromagnetic waves. By decoupling **E** and **B** in Maxwell's equations we get the wave equations for **B** and **E**.

$$\Delta^2 \mathbf{E} = \mu_0 \varepsilon_0 \frac{\partial^2 \mathbf{E}}{\partial t^2}, \ \Delta^2 \mathbf{B} = \mu_0 \varepsilon_0 \frac{\partial^2 \mathbf{B}}{\partial t^2}$$

*Formula 12: Maxwell's equations decoupled for **B** and **E**.*

We see that electric charge in motion produces travelling electromagnetic waves, and that electromagnetic waves (travelling through free air or a dielectric) will affect electric charges that it passes. This is the basis for electrical communication.

Transmission Line Modes

We have seen that travelling electromagnetic waves made up of electric and magnetic fields is possible. In free space the two fields will both be transverse to the direction of travel. This can be seen from Formula . This type of wave is therefore called a transverse electromagnetic (TEM) wave.

Electromagnetic communication through air is not always favourable, since the waves spread out in the space, and energy is lost at the receiving point. Some kind of waveguide is therefore used extensively. There are many different kinds of waveguides. Some examples is: hollow waveguides (circular or rectangular), dielectric waveguides and parallel plate waveguides. For signal distribution on electric chips or circuit boards, printed lines like microstrip, coplanar wave guide or slot line is used. All these structures can be looked at as waveguides.

When the electromagnetic wave propagates through uniform media like air or a dielectric, the wave mode can be the TEM one. If the wave propagates through more than one media, like what is the case in coplanar wave guides (propagation through air and dielectric), the propagating mode can not be pure TEM. This means that there must be a longitudinal component of the electric or the magnetic field, or both. For a TEM mode to exist there needs to be at least two conducting lines (or planes), which means that TEM waves can not exist, for instance, in hollow waveguides.

A propagating wave through a waveguide will in general have electric and magnetic fields in all directions (x, y and z axis in the Cartesian coordinate system). This mode of propagation is called hybrid mode, and includes the components E_x, E_y, E_z, H_x, H_y and H_z.

Often, at low frequencies, the longitudinal field components are negligible, and can be ignored when doing calculations. The mode is then called quasi-TEM, since it is approximated as a TEM wave, even though it has electric and/or magnetic components in the direction of propagation.

If the waveguide has a longitudinal component of the electric field, and no magnetic component in the direction of travel, the mode is called transverse magnetic (TM). If, on the other hand, there exists a longitudinal magnetic component, and no electric component in the direction of travel, the mode is called TE.

The TE and TM modes have periodic variations in the transverse direction. TE_{10}, for instance, means that there is no electric field component in the longitudinal direction, and that the electric field has one periodic variation along the first axis, and is constant along the second axis. For a rectangular waveguide, this means that the electric field along the longest side varies from zero at the edges to a maximum at the centre. The variation is sinusoidal. Along the other direction, the field is constant. The widest side is always numbered first in a rectangular waveguide.

Both circular and rectangular waveguides has countable and infinite number of TE and TM modes. The various modes can only exist above a certain frequency, called the cut-off frequency. For communication, only the mode(s) with the lowest cut-off frequency is used, to avoid signal distortion. The mode with the lowest cut-off frequency is called the dominant mode.

Printed transmission lines also have propagating modes. If modes other than the dominant mode are exited, this can distort the signal and cause malfunctioning. It is therefore important to use technology that can handle the frequency you are using. Thinner substrates allows for higher frequencies. The use of wide traces to make high-impedance lines makes the transmission line more prone to higher order modes.

If modes below the cut-off frequency of that mode are exited, this mode will decay exponentially, and is called evanescent. These modes are also called parasitic modes, and have the same influence as reactive components on the circuit.

Transmission Line Parameters

Most of the information in this section is from [7].

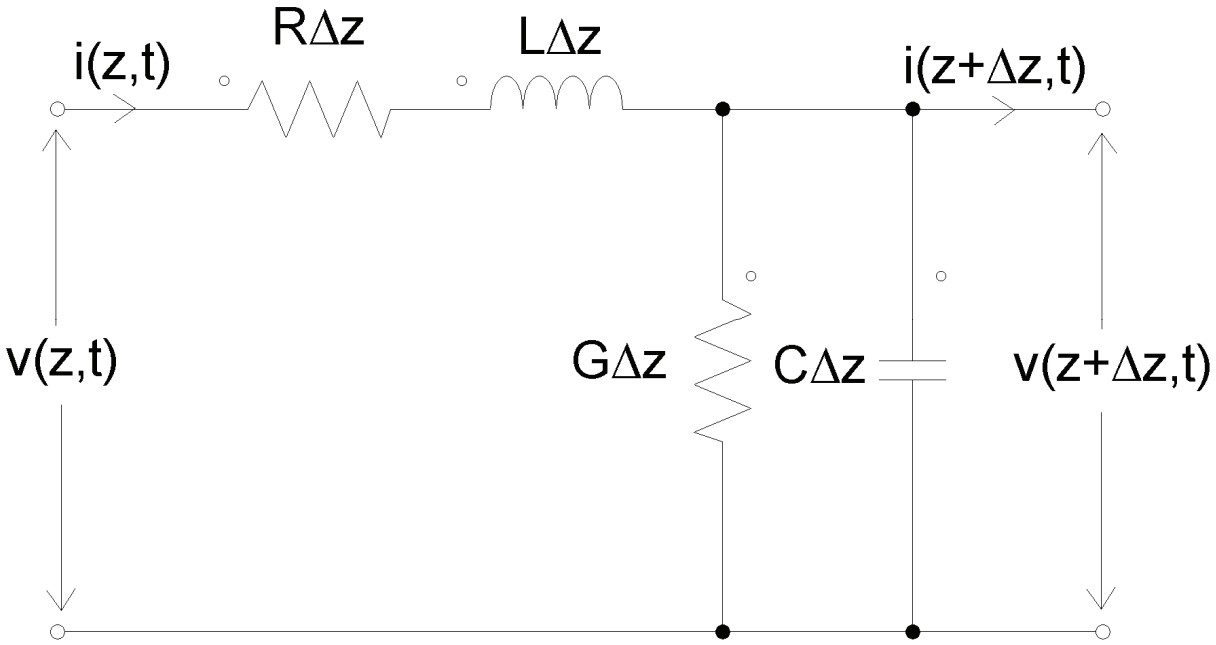

Figure 15: Equivalent circuit of an infinitesimal two- conductor transmission line of length Δz.

Figure 15 shows how a transmission line segment can be represented by lumped components. From this setup we can find the time-harmonic transmission-line equations (Formula 13), that shows how the voltage and current varies along the length of the transmission line. *R* is the series resistance due to the conductor not being perfect and therefore has a resistivity. The transmission line will also have a series inductance, *L*, because all conducting lines have some inductance. The parallel conductivity, *G*, is caused by the isolation between the two conductors not being perfect, and there will also be a capacitive effect, *C*, between the two conductors.

$$-\frac{dV(z)}{dz} = (R + j\omega L)I(z)$$
$$-\frac{dI(z)}{dz} = (G + j\omega C)V(z)$$

Formula 13: Time-harmonic transmission-line equations.

To characterise the wave propagation on a transmission line, the propagation constant is used (see Formula 14). This constant is, in general, complex, and contains information about both the loss and the phase variation along the line. If the phase constant is not a linear function of frequency (which it generally is not), the line is said to be dispersive since various frequency components travels with various velocities.

$$\gamma = \alpha + j\beta = \sqrt{(R + j\omega L)(G + j\omega C)}$$

Formula 14: Propagation constant. γ (in 1/m) is the propagation constant, α the attenuation constant (in Np/m) and β the phase constant (in rad/m).

Another key transmission line parameter is the characteristic impedance, Z_0, (see Formula 15). This value gives the ratio between the current and the voltage on the line. For both the characteristic impedance and the propagation constant definitions it is assumed that there is only one propagating wave (no reflections).

$$Z_0 = \frac{R + j\omega L}{\gamma} = \frac{\gamma}{G + j\omega C} = \sqrt{\frac{R + j\omega L}{G + j\omega C}}$$

Formula 15: Characteristic impedance.

$$LC = \mu\varepsilon$$

Formula 16: Useful relation between inductance (L), capacitance (C), permeability (μ) and permittivity (ε).

Microstrip Transmission Lines

This section is based on information found in [2].

To connect the components to each other, we need to use some sort of connecting lines. One of the most commonly used microwave transmission line is the microstrip line. Figure 16 shows a section of a microstrip line. It is one of the simplest forms of transmission lines, consisting of a conducting line above an infinite ground plane, separated by a substrate.

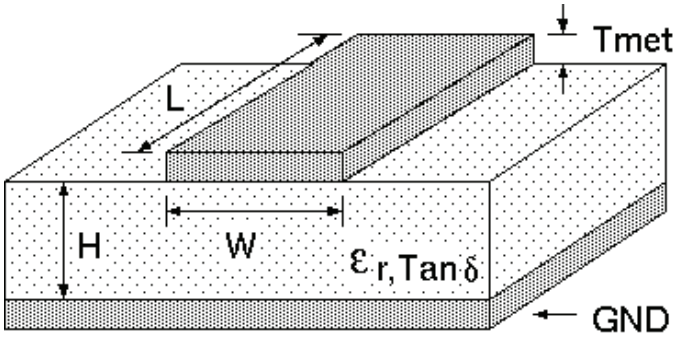

Figure 16: Microstrip transmission line cross section [22].

It can be seen from Figure 16 that the microstrip structure is open, which means that the electric and magnetic fields, will (theoretically) extend to infinity. Along with the finite height of the conducting line, this makes the structure very difficult to analyze. Infinitely thin top conductor and metallic shielding is therefore normally assumed when analyzing the structure.

Since the electromagnetic field will propagate in both air and the substrate, the propagating wave can not be a pure transverse electromagnetic (TEM) wave, and both the electric and the magnetic fields must have a longitudinal component. The reason for this is that the phase velocity in air and the substrate is different, and therefore a TEM mode can, in theory, only exist at DC.

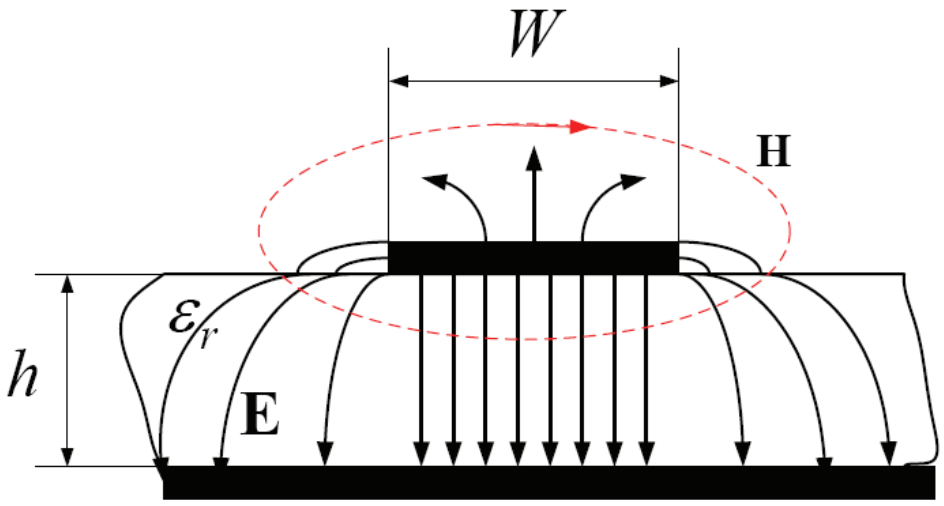

Figure 17: Electric and magnetic field distribution for a microstrip transmission line [38].

The phase velocity for the entire structure must lie somewhere between the velocity in air and the velocity in the substrate. Experiments have shown that more and more of the electromagnetic field will exist in the substrate as the frequency is increased. This means that the effective permittivity (the permittivity that the combined structure appears to have) approaches that of the substrate for frequencies approaching infinity. It also means that the velocity of the propagating wave decreases as the frequency is increased. Since the propagation speed is frequency dependent, the microstrip transmission line is a dispersive structure. Figure 18 shows the dependence of phase velocity, *v(f)*, on frequency. Below a certain frequency, the velocity is nearly constant, and this region is commonly called the quasi-static region.

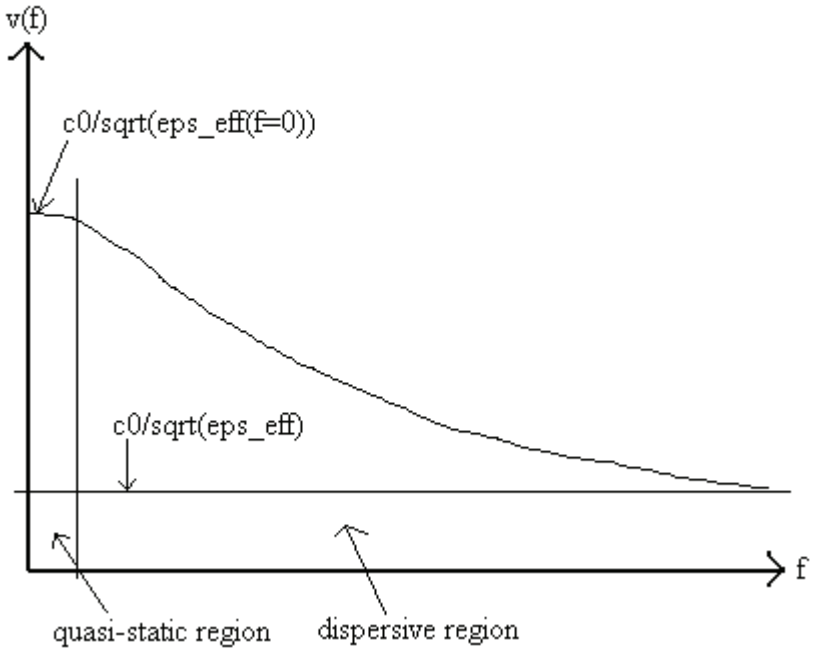

Figure 18: Phase velocity versus frequency on a microstrip line.

Because of the boundary conditions of electromagnetic theory, the discontinuity that the electric field undergoes at the boundary between the substrate and air increases with increased dielectric constant of the substrate. The magnetic field does not experience a discontinuity though, because the permeability is equal in both air and the substrate.

To ease calculations on microstrips, it can be assumed, for low frequencies, that the field-distribution is quasi-TEM. An example of this field distribution can be seen in Figure 17. The validity of the assumption depends on factors like substrate- and transmission line geometry, but is normally valid up to roughly 1 GHz. The field distribution deviates from a quasi-TEM mode at high frequencies mainly because of the magnetic field that has a considerable transversal component at higher frequencies. The electric field, on the other hand, has a negligible longitudinal component beneath the cut-off frequency of the first higher-order mode.

All microstrip transmission lines suffer from loss, which can be divided into three categories: conductor loss, substrate loss and radiation loss. The conductor loss is due to the electrical properties of the material used. Different materials have different loss, so it is advantageous to use a material with high conductivity. As the frequency is increased, most of the current will

be concentrated in the outer part of the conductor. This phenomenon is often referred to as skin effect, and results in higher resistivity, and higher loss, as the frequency increases. The skin effect has a predominantly square root dependence on frequency. The bottom of the strip will have higher current density than the top. The current in the ground plane will be mostly concentrated directly below the strip.

Substrate loss can be subdivided into two categories: loss in the substrate itself, and loss due to high conductivity of the substrate. The loss in the substrate is normally specified by the loss tangent. The use of a substrate with low loss tangent is preferable to avoid unnecessary losses. Since the substrate loss is proportional to frequency it will be the dominant loss at high frequency. To avoid loss due to substrate conductivity, a material with high resistivity is preferable. Gallium Arsenide (GaAs) is one example of such a material that is a good isolator. Silicon (Si) on the other hand is a poor isolator, and therefore has substantial conduction loss.

The radiation loss occurs when energy is radiated to the surrounding environment. This effect is most pronounced when the wave length is relatively small compared to the dimension of the circuit, and also depends on its geometry. When designing antenna structures this radiation is desired. In other designs it is normally an unwanted effect. A substrate with high dielectric constant reduces the radiation.

From a practical view point, the microstrip transmission line has relatively low radiation and dispersion compared to other transmission lines. Since it is unshielded it will have relatively high electromagnetic coupling to nearby transmission lines, as opposed to i.e. coplanar wave guides. An inherent difficulty with microstrip transmission lines is components that need grounding. In this case a substrate via hole is needed. This takes up relatively much area on the chip, and can affect the circuit performance.

A microstrip transmission line can normally have characteristic impedance between 20 and 120 Ω. Wider lines leads to lower characteristic impedance. As the line width increases, higher order modes will appear, limiting the maximum practical width of the line. The minimum width of the line is normally limited by the technology that is used to produce it. It should be noted that characteristic impedance increases slightly with increasing frequency.

The main reason that the microstrip transmission line is so popular is that it is relatively easy to fabricate. It has also received a lot of investigation during the years so that the theory is well developed, and accurate engineering formulas are available.

TriQuint 0.5 µm TQPED process

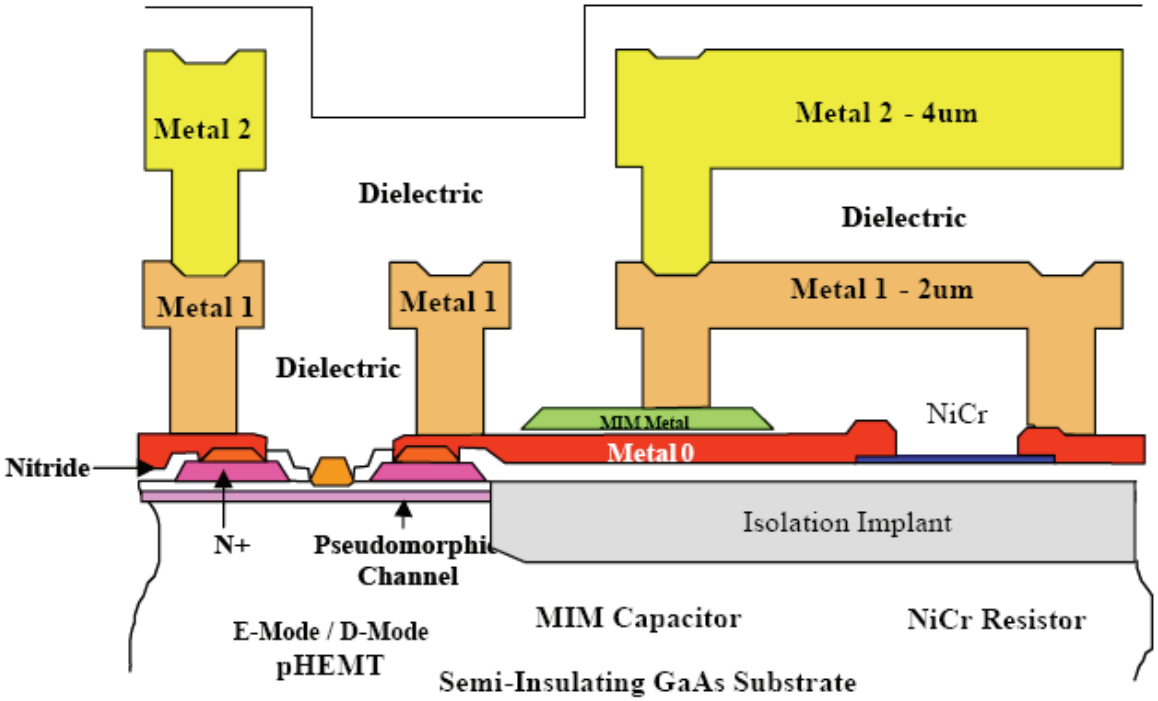

Figure 19: 0.5 µm TriQuint TQPED device cross section.

The process that has been used for this project is TriQuints 0.5 µm TQPED process. A cross section of this process is shown in Figure 19. The entire production process description available from TriQuint at [23] is included as Appendix A2.

The targeted applications for this process are, according to TriQuint:

- Low noise amplifiers
- Linear, low loss and high isolation RF switches
- Converters
- Integrated RF front ends

The process can also be suitable for other applications.

The main features of the process are:

- Depletion mode transistors with -0.8 V pinch off and enhancement mode transistors with +0.35 V threshold voltage.
- Two global, and one local, connection layers.
- High precision NiCr resistors with very low temperature dependence.
- High value Metal Insulator Metal (MIM) capacitors.

The three metallic interconnect layers all have different resistivity and current density capacity, with metal layer two having the highest current density capacity and lowest resistivity. Metal layer zero has the poorest current density capacity and highest resistivity of

the metallic interconnect layers. This should be considered when doing the layout of the circuit.

All of the passives are designed to have high q-values. It is possible to use bulk resistors for high resistance in a small area, though this is not recommended as they have high temperature coefficient, low accuracy and poor current density capacity.

Further information on the process data is available in the process specific design manual from TriQuint, which is only available to users who have signed the non-disclosure agreement.

The Tools

Advanced Design System

Advanced Design System (ADS) is a computer aided design tool (CAD) from Agilent Technologies. The version that has been used for this project is the 2008 release - 2nd update, released September 18th. It allows for design of circuits in both the RF and microwave range.

ADS are in common use in universities around the world, making it a well known tool for a large number of electronics graduates. This, along with being a marked leader in a number of fields, has made ADS the industry leader in high-frequency design [24]. Among the innovative functions of ADS is the Harmonic Balance function which was the first commercially available simulator of its kind when it was introduced in the early 1980's. It also has the only commercially available timed synchronous data flow simulator for system-level simulation [24].

The key components when designing a circuit in ADS is; a schematic window where the circuit is drawn and simulated, a data display window where the simulation results can be displayed in various forms, and a layout window where the physical components are laid out and simulated using electromagnetic simulators.

Schematic Window

The schematic window uses symbols to represent simple components like inductors and resistors or more complex circuits like filters and amplifiers. These are connected in the proper way and are then ready for simulation. A whole range of different simulations is available like S-parameters, transient and harmonic balance. The circuit can also be optimized with regards to chosen parameters, or we can find the expected yield with a given component variance.

A large number of so called "smart components" are available, like couplers, bias networks and impedance matching networks. These components are used in the schematic like any other components, and the smart components functionality is specified using a design guide. In this way commonly used circuits can be designed easily.

Before the design of a circuit, a foundry has to be chosen. The components for the given technology can be installed in ADS using a library, making these available in the design. The components are based on accurate models that allows for high-accuracy simulations.

Data Display Window

The data display window is used for display of the simulated results. These simulation results can be displayed in a number of ways. If we choose to plot the results, then three different plots are available; polar, smith and rectangular plots. We choose the data we want to be

displayed – different measurements, even from different simulations, can be displayed in the same plot. If we choose to display complex variables, we need to specify what part of the variable we want to be displayed; the real or the imaginary part. We can choose to plot the decibel value or even the dBm value.

Another way to display the data is to use lists where the data is displayed in numeric format.

For both plots and lists, we have the opportunity to use equations to specify our data. A large number of mathematical expressions and operations as well as different functions are available. Some examples of these are; minimum/maximum value, absolute value and decibel value. Using functions, nearly all kind of settings and plot data can be accessed.

To avoid spending lots of time setting up the data display, ADS comes with predefined Design Libraries that contain pre-configured schematics, data displays, and test benches. These libraries cover a lot of common display requirements, and can be customised to the specific needs. It is also possible to design your own display templates, and use them for various projects.

Layout Window

When a circuit is completed (i.e. shows satisfactory performance) in the schematic window, a physical layout can be produced. A layout can be generated automatically from the schematic, or components can be placed manually in the layout.

The layout window provides the opportunities for drawing a large range of various shapes like circles and arcs, and also has the ability to manipulate the shapes and components in a number of ways, like rotation and mirroring. The components are connected together with traces or other conducting shapes. A tool exists to check if the wanted connectivity is achieved.

When the layout is completed, it is ready for electromagnetic simulation. Prior to this the substrate needs to be specified. This can be loaded from a file, if available, or created manually. To perform the electromagnetic analysis, the program needs to know all the specifics of the dielectrics, like thickness and permittivity, as well as the specifics of the conducting layers. These are then mapped to the layers used in the layout, so that the program knows where the different layers are located. The via-holes must also be specified in the substrate setup.

Before performing the electromagnetic simulation, the circuit can be closely inspected in a 3D-viewer. Among the useful tools included in the viewer is the ability to scale the z-plane and to cut different planes, allowing a clear view of any part of the circuit.

Two different simulators are available in ADS; Momentum and EMDS. Momentum is based on the Method of Moments (see the Method of Moments section under The Tools Chapter). To perform the Method of Moments, ADS first finds the Green's functions for the substrate and the mesh information for the circuit and uses this information to calculate the currents. S-parameters can then be found from these currents.

The necessary meshing can be performed in advance with the resulting cells shown on the layout. There are a number of parameters that can be specified for the meshing, like cell size

vs. wavelength, arc resolution etc. The user even has the opportunity to specify different settings for different layers.

EMDS for ADS is a full 3D EM simulator that can model any 3D shape. The EMDS function has been developed to give good results even for novice users as key functions, like meshing, has been automized. Low memory usage and quick solution times has also been prioritized.

EMDS is well suited for antenna simulation, and antenna parameters like gain, directivity and polarization can be found. The radiation pattern, as well as the field distribution, can be viewed in 3D with the ability to rotate the view as the animation is running.

Using Momentum or EMDS, components can be created from the layout and then used in the schematic window like any other component. S-parameter analysis using Momentum or EMDS needs to be run prior to using the component in the schematic. Different parameters can be set, like length or angle perturbations, and even varying port locations.

Measurements

Because of the small dimensions of the MMIC, we need to use a probe station to make measurements on the pre-assembled circuit. The probe station has microwave probes, and a microscope that makes it possible to position the probes accurately.

The most common instruments used for measurements on MMIC technology is oscilloscope, spectrum analyzer and network analyzer. Both the oscilloscope and the spectrum analyzer need some sort of signal source. An active circuit also needs to be supplied with supply voltage.

This text will focus only on the network analyzer since this instrument is used in the practical measurements.

The key difference between the spectrum analyzer and the network analyzer is that the network analyzer contains the signal source and uses this to examine the response of the device to a known signal. This gives a result that is very easy to interpret, i.e. from a Smith chart. The network analyzer does, however, require significant calibration, which the spectrum analyzer does not. When properly calibrated, it will, on the other hand, give much more accurate results than a spectrum analyzer.

Spectrum analyzers are commonly used to measure signal levels, like carrier, sidebands and harmonics. They can have complex built-in demodulation capabilities, for instance for UMTS. Spectrum analyzers are often used for nonlinear stimulus/response testing with some external source.

Spectrum analyzers display signal level versus frequency, while oscilloscopes displays signal level versus time. By using the Fourier transform, it is possible to convert between these two domains.

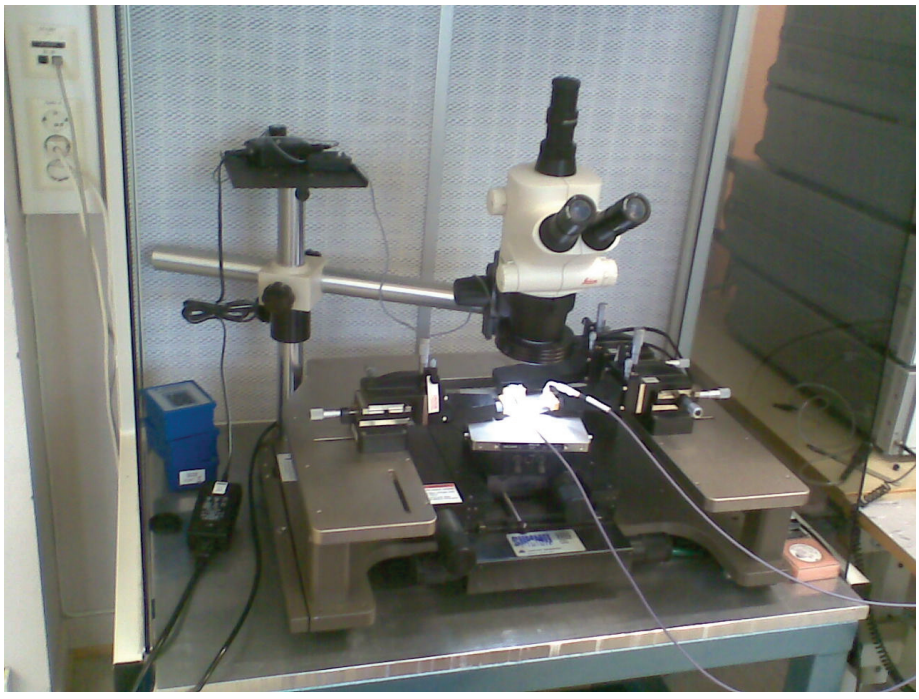

Figure 20: Cascade Microtech Summit 9000 probe station.

Figure 21: Hewlett Packard HP 8510C network analyzer and computer running the the WinCal XE software from Cascade Microtech that controls the analyzer.

Network Analyzer

Most of the information for this section is taken from [25].

For high-frequency applications it is most advantageous to use s-parameters when measuring a component or a circuit. From these s-parameters it is easy to calculate key parameters like gain and reflection coefficient and also other parameters like z-, y- and h-parameters is easy to compute from the s-parameters.

There are two main classes of network analyzers; scalar and vector. The scalar version (SNA) measures only the amplitude of the signal, while the vector version (VNA) measures the phase as well. Vector network analyzers are often called automatic network analyzers (ANA), and sometimes gain-phase meters.

Early network analyzers were not automated since error correction had to be done manually. The first network analyzer to feature built-in error correction was the original HP8510, circa 1982, allowing the error-corrected measurements to be displayed in nearly real time [26].

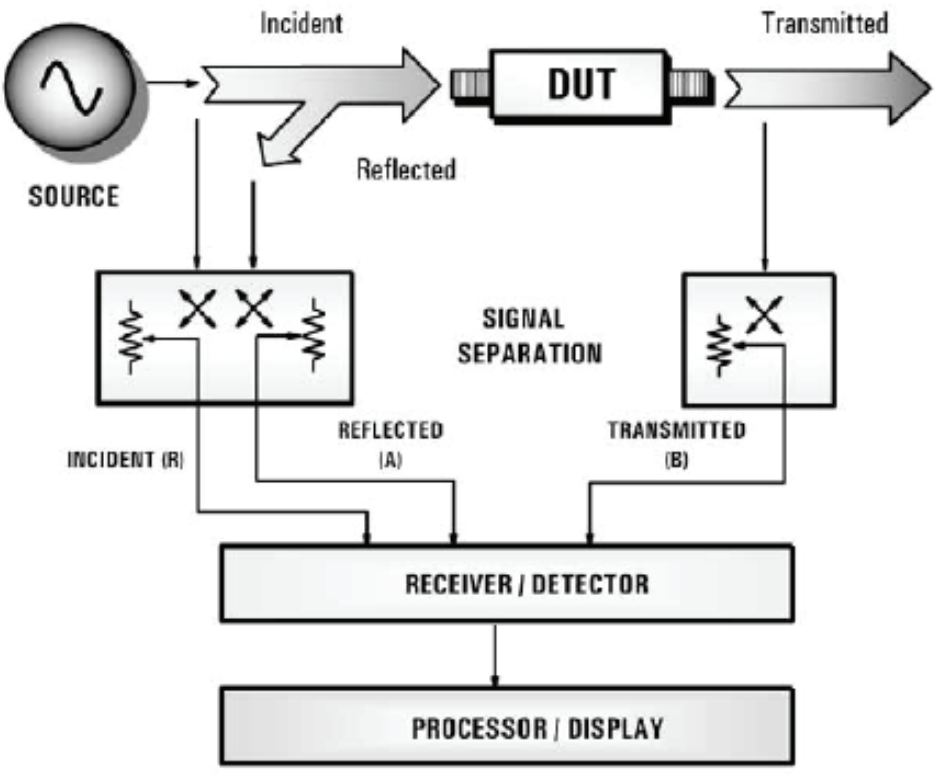

Figure 22: Network analyzer. General block diagram.

A network analyzer uses the concept of transmitted and reflected power waves to calculate the s-parameters. A block diagram of a general network analyzer is shown in Figure 22. We can see that a source that generates a known signal is needed. By measuring reflected and transmitted power, we can find all of the s-parameters. All that is needed for termination is matched loads. A two-port device is shown in the figure, but the device can have any number of ports. The ports not being measured should be terminated with matched loads.

On most modern network analyzers, the source is integrated into the instrument. For accurate measurements, it is important that the source has good frequency resolution and stability. The source has the ability to sweep both frequency and power.

The signal separators are of big importance in network analyzers. To make accurate measurements we must use couplers with high directivity (good isolation of unwanted signal, small loss of through signal and good coupling of wanted signal). At the input, a splitter or directional coupler is used to separate the input (reference) signal and the reflected signal. Splitters have good bandwidth, but are normally quite lossy. Directional couplers, on the other hand, have low loss and good isolation and directivity, but limited bandwidth. In particular, they are not practical at low frequencies.

A directional coupler can also be used to separate the reflected wave from the incident one, but limited bandwidth is a problem here as well. For this reason, a Wheatstone bridge is often used since these works all the way down to DC. They have considerable loss though, which means the signal level is lowered at the DUT input.

To detect the signal, two types of circuits can be used; a diode based circuit or a tuned receiver. The latter is significantly more complex and costly, but offers the best sensitivity/dynamic range and provides harmonic/spurious rejection. Diode detectors have its biggest advantage in its low cost and broad bandwidth. To increase the dynamic range, the input power level is increased. Good dynamic range is very important to achieve measurement accuracy.

A tuned receiver uses a mixer and a local oscillator to convert the signal to a lower frequency. The local oscillator needs to be tuned to the input signal either by locking it to the RF or the mixed-down intermediate frequency (IF) signal. The IF signal is then filtered to improve the sensitivity and dynamic range. To extract the magnitude and phase information from the filtered signal, the signal is converted to digital form using an analogue-to-digital converter. The digital signal is then analyzed using digital signal processing.

The magnitude and phase (for VNA) information needs to be conveyed to the user in a convenient form. This is the task of the processor/display block in Figure 22. On most network analyzers the data can be displayed in linear or logarithmic plots, and Smith- or polar plots. Another common feature is trace markers which makes it easy to inspect bandwidth, attenuation etc. Most modern network analyzers also have built-in software that makes measurements easier.

Calibration

Measurement errors can be divided into three groups: systematic errors, random errors and drift errors. Systematic errors occur due to the analyzer and test setup not being perfect. These errors can be removed by calibration since they are constant over time.

Random errors, on the other hand, varies over time, and can therefore not be calibrated out. The random errors are mainly caused by noise in the analyzer. The last group of errors is drift, which is mainly due to temperature changes. By letting the instrument reach operating temperature before making measurements, and keeping the ambient temperature constant, these errors can be significantly reduced.

The systematic errors are what we aim to remove by calibration. These systematic errors consist of six terms:

- Directivity (leakage of input signal into measured reflected input signal)
- Cross-talk (leakage from input of DUT to output not passing through the DUT)
- Source mismatch (reflections at the input of the DUT)
- Load mismatch (reflections at the output of the DUT)
- Reflection tracking (ratio of reflected signal and reference (source) signal)
- Transmission tracking (ratio of transmitted signal and reference signal)

Since all six terms applies in both the forward and reverse direction, there is a total of twelve error terms for two-port devices. Full two-port calibration is therefore called twelve-term error correction.

For twelve-term error correction we must use a process known as vector error correction. This process removes the systematic errors by measuring known calibration standards, and correcting for the measured errors in subsequent measurements. Vector error correction is only available on full vector network analyzers (VNA/ANA).

The most common type of calibration standard is the short-open-load-through (SOLT). These components is supplied in a calibration kit (which is quite expensive), and its characteristics is stored in the network analyzer. It is important that these data match the calibration kit used, or the measurements will not be accurate. Another important calibration technique is the through-reflect-line (TRL). This technique is mostly used in microwave non-coaxial setups, for instance waveguides. The reason for the TRL technique being popular is that it is difficult to fabricate good opens and shorts for other transmission lines than coaxial, like waveguides, at high frequencies.

Twelve-term error correction requires the two ports to be used in both directions. The systematic errors can then be compensated for to find the actual s-parameters. Each s-parameter depends on all four s-parameters, and both a forward and a reverse sweep has to be performed to update any s-parameter. The dependence of the actual s-parameter values on the error terms and the measured s-parameters is complex (see Appendix A3), but this calculation is built into the analyzer software and the user does not need to have knowledge of these equations.

Most network analyzers have options that can be used as a trade-off between speed and accuracy. One such option, when performing calibration, is to omit the cross-talk calibration. For most measurements this error has little significance since the leakage is small. Some examples of circuits where this factor can be important are multi-stage amplifiers in the reverse direction, and switches in the open position. The cross-talk calibration should preferably be done by connecting identical DUT's with matched termination at the output to both of the ports. Since this calibration adds noise to the error model (measured level is close to the noise level), it should only be used when necessary.

When doing measurements an option is to use averaging. This makes multiple measurements at each point, and then uses the average value, thus making the measurement more accurate at the expense of measurement time.

Probe Station

Probe stations allows for the testing of small devices like MMICs without mounting and wire-bounding them. This makes them particularly popular in academic research, at Universities etc. They consist of a microscope that makes it possible to work on the small devices – making the connections etc, and, of course, probes [27].

Modern probes can be used up to well over 100 GHz, and is significantly improved since the early probes. The first microwave probe was invented at Tektronix in 1980, and worked up to 18 GHz. They had a major drawback in that they were easily destroyed if bent [28].

Figure 23: Cascade Elite 300 probe station with accessories [29].

Probes normally have three connections; signal at the centre and ground on each side; just like coplanar wave guides. It is also possible to have only one ground pin on one side of the signal pin.

More advanced probe stations can have motorized control of both the microscope and the wafer stage, and can be connected to a computer with software that can control the probes and microscope. Some probe stations is also delivered with a dry chamber for storage of the wafer stage that protects the device from electromagnetic interference, eliminates moisture or frost build-up when using a cold chuck and a dark environment for making light sensitive measurements [30].

Most probe stations have the ability to move the plate that holds the circuit (normally by a vacuum) in both *x*- and *y*-directions, as well as rotate the whole plate. The probes can also be moved in the *x*- and *y*-direction and rotated, but also, obviously, has the ability to be lowered and raised. The probes is connected to the measurement equipment (i.e. a network analyzer), by RF cables. It is important that the effect of these cables is compensated by calibration (de-embedding) so that the measurement results reflect the actual circuit by it self.

When making the measurements, the probes are placed onto the contact pads by manual or automated control. It is important that the probes slide along the surface for some distance (25 um is usually enough) so that the probe tips penetrates the upper layer and makes good electrical contact. This is especially important when using pads made up by such materials as aluminium which oxidizes easily. This oxide layer needs to be penetrated by the probe tips (or removed by other means, i.e., chemically, before making the measurements). It is important to be aware that oxide layers can build between the probe tip and the contact pad while making time-consuming measurement, thus giving false results.

S-Parameters

At high frequencies it is difficult to realise good short circuits and open circuits because of radiation and parasitic effects. Using the Z- and Y-parameters that is common at low frequencies is therefore difficult, if not impossible to achieve with good accuracy. The solution to this problem is to use matched loads which is easily realised in practice. By using these loads we can measure the scattering parameters of the device.

To measure the s-parameters, the signal is applied to each port in succession, and then the reflected power wave is measured at each port. The s-parameters are then calculated as the ratio between the incident and the reflected power waves. If we have a two port system, then the s-parameters will be calculated like this:

$$S_{11} = \frac{V_1^-}{V_1^+}, S_{12} = \frac{V_2^-}{V_1^+}, S_{12} = \frac{V_1^-}{V_2^+}, S_{22} = \frac{V_2^-}{V_2^+}$$

where a + indicates a wave going into the port, and a – indicates a wave going out of the port.

Assumptions

S-parameters can only be applied to linear networks, and is most commonly applied to networks operating in the RF or microwave range. The s-parameters can be applied to circuits with any number of ports, including single port networks. When specifying the s-parameters of a network, one must also supply the system impedance that has been used under measurements, where the ports are located on the actual circuit, as well as other critical factors like temperature, bias currents etc.

The s-parameters are frequency dependent, meaning that they are usually measured over the entire frequency range of interest.

Derived Parameters

A number of parameters characterising the properties of the circuit can be found directly from the s-parameters. Following is a list of some of the most common ones for a two port small-signal linear network:

Scalar logarithmic gain: $20\log_{10}|S_{21}|$

Insertion loss: $-10\log_{10}\frac{|S_{21}|^2}{1-|S_{11}|^2}$

Input return loss: $\left|20\log_{10}|S_{11}|\right|$

Gain
The gain is the amplification of the signal from input to output. It can be expressed in decibel or as a scalar value. It can also be expressed as a complex number by including the phase.

Insertion loss
The insertion loss reveals how much power is lost due to the insertion of the device into the rest of the circuit.

Return loss
The return loss reveals how much of the incident power is lost due to mismatch at the input. It is expressed in decibel.

Even/odd Mode Analysis

This section is based on [31].

Even/odd mode analysis is often used to find the s-parameters of the Wilkinson Power Divider. The even mode involves exciting two ports with the same voltage (or current) of equal polarity, while odd mode involves exciting the two ports with sources of opposite polarity and equal magnitude.

Even/odd mode analysis can be used to simplify the analysis of symmetric circuits. A number of unsymmetrical circuits can be made symmetric by for instance splitting a resistor into two separate resistors. The key element in even/odd mode analysis is that for even mode (same sources) the line of symmetry can be replaced by an open circuit, while in the case of the odd mode (opposite sources) the line of symmetry can be replaced by a short circuit. This makes analysis a lot easier as only half of the circuit needs to be considered.

To see that even mode leads to a virtual open symmetry, while odd mode leads to a virtual short symmetry, we can consider the circuit in Figure 24.

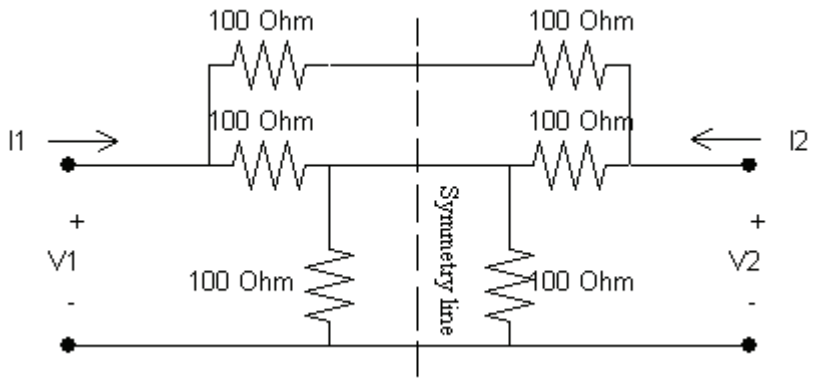

Figure 24: A resistor network with two ports.

We see that with equal sources, no current can flow from one side of the symmetry line to the other, as this would make the circuit unsymmetrical, thus proving that this line is a virtual open. With opposite sources, the currents and voltages must be equal and opposite on the two halves of the circuit, which means that the voltage must be the same on the whole symmetry line. This makes the line of symmetry a virtual short in the odd mode.

To perform the even/odd mode analysis the correct sources needs to be applied to the two ports being considered. This obviously rarely happens in practical cases. To achieve this we can again consider the circuit in Figure 24.

Let's say we wish to perform the even/odd mode analysis on the circuit with a voltage source attached to the left side, and a short circuit on the port on the right side. We can then replace this setup by two voltage sources in series with equal polarity on the left port, and two equal voltage sources of opposite polarity in series on the right port. The magnitude of all the sources needs to be half of the original. This new setup should be exactly equivalent to the original one.

We can now easily achieve the even mode by turning off a voltage source with equal polarity on both ports, and likewise get the odd mode by turning off voltage sources with unequal polarity on both ports. To arrive at the currents and voltages for the circuit as a whole we need to apply superposition.

Superposition

In a circuit where all of the components are linear, the total current in a given branch is the sum of the currents produced by each individual source. This makes it easy to find the total current in a given branch for a circuit with multiple sources, as the current resulting from each individual source can be found with the other sources deactivated, and then the total current is simply the sum of all the individual currents [32].

To deactivate a voltage source, we need to short it, while a current source is deactivated by an open circuit.

This principle applies to any type of source and superposition in electronics can generally be stated as;

> […] whenever a linear system is excited, or driven, by more than one independent source of energy, the total response is the sum of the individual responses. An individual response is the result of an independent source acting alone. [3]

Method of Moments

The Method of Moments (MoM) or Moment Method is a numerical method in the frequency domain based on integral equations. The Momentum function in ADS is based on this, and uses it to obtain a solution in the spectral domain.

An integral equation is an equation where the unknown appears in the integrand. MoM solves these kinds of equations by the use of basis functions. The amplitudes of these functions are then calculated at certain points by making sure that the integral equations are valid at these points. The resulting matrix can then easily be solved using a computer.

The choice of basis functions is very important. These functions can be divided into two classes; sub domain and entire domain. Examples of sub domain functions are piecewise constant, piecewise linear and truncated cosines. These are the most used ones. Of less common use are the entire domain functions. These can be useful when information about the current distribution is known before the calculations are performed. Entire functions can for example be calculated from Maclaurin, Legrende and Hermite polynomials.

The basis functions should be chosen so that the unknown function can be represented accurately with as little computational time as possible. It is important that the basis functions are not smoother than the function they are set to represent.

When using MoM, the circuit needs to be divided into cells. These cells can be either square or triangular. This division into cells is commonly called meshing. Smaller cell sizes results in more accurate solutions at the expense of extra computation time. By choosing the sizes of the cells wisely, accurate results can be achieved with little computation time. An example is transmission lines where the current density tends to be higher and more abrupt at the edges than at the centre due to the skin effect. By using finer size cells at the edges than at the centre this effect can be taken into account. Discontinuities of any type are also typical places where small cell sizes should be employed. Employing triangular and square cells in a wise manner is also an effective way to reduce the number of cells and thereby also the computational time.

The first step in MoM is to calculate the current on each cell by using a coupling Green's function. The way this is done in MoM is to use what is called weighting or testing functions along with the basis functions. These weighting functions can be of the same type as the basis functions. The inner product of the weighting and basis function is taken and the electric field (which is a unique function of the current distribution) is forced to zero at all test points. The resulting matrix equation is used to find a unique set of weights for the matrix functions, which in turn gives the current distribution that satisfies the boundary conditions. The problem must be linear to guarantee that the solution is unique.

[4] and [33] has been used as resources for this section.

Smith Chart

The Smith chart, named after its inventor Phillip H. Smith, is used to plot impedances or admittances, depending on the type of chart. Either one can be represented as a Smith Chart, or they can both be combined into one. The impedance or admittance needs to be normalized to the system impedance before being plotted.

Appendix A1 shows an example of an impedance Smith Chart. The circles with centre on the horizontal axis are constant resistance circles, while the circles with centre on an imaginary vertical axis on the right are constant reactance circles. Using these circles, the normalized impedance is easily plotted. The design of the Smith Chart leads to inductive elements being located at the upper half of the chart, while capacitive elements are located on the lower half. A point at the far right will mean an open circuit, while a point at the far left means a short circuit.

The reflection coefficient can now be easily read directly from the chart. To find the magnitude we measure the length from the centre to the plotted point and divide it by the length from the centre to the edge of the chart. A separate scale for the magnitude of the reflection coefficient is often provided along with the chart. The phase of the reflection coefficient is read from the scale on the outer edge of the chart. This means that the amount of reflection can easily be found by inspecting the Smith Chart, as points further from the centre involves more reflection. A point at the centre of the chart means a matched element, and therefore no reflections. If the plotted curve stays close to the centre of the Smith Chart this means a wide bandwidth, and is often preferable. A constant Standing Wave Ratio (SWR) circle can be drawn, indicating all the frequencies lying within a certain SWR specification.

The Smith Chart in Appendix A1, has in addition to a scale for the magnitude of the reflection coefficient, also scales for SWR, return loss and reflection loss among other, located below the chart. This makes determining these important parameters easy once the desired network has been plotted in the chart. To find these parameters, a circle centred at the origin is drawn, and then a vertical line is drawn from the circle that intersects the scales. Now the desired values can be read directly off the scales.

What makes the Smith Chart so practical for RF engineers is that lumped components or transmission lines can easily be accounted for in the Smith Chart. To plot an inductor in series for example, we just follow the constant resistance circles in the direction of increasing inductance. A transmission line segment will be equivalent to a circle in the Smith Chart. The length of the circle is found from the “wavelengths towards generator” or “wavelengths toward load” scales on the outer edges of the chart.

Series elements are, as we have seen, easily plotted in the impedance Smith Chart. To plot shunt elements we need to convert the admittance into impedance. This is done by drawing a line from the point through the origin with the same length on the opposite side of the chart. This gives the related impedance point. Alternatively a combined impedance/admittance Smith Chart can be used, which makes conversion between impedance and admittance straightforward.

PRACTICAL

Design Flow

1. **Design and simulation of lumped component circuit from distributed Wilkinson.**
   The lumped equivalent capacitor and inductor values are calculated using formula 1 from the section on lumped components under The Circuit Chapter. The circuit constructed with ideal lumped components is then designed and simulated using ADS.

2. **Inductor design.**
   The inductors are designed to achieve the right inductance with as high Q-factor as possible on a limited space.

3. **Setup of the circuit using TriQuint components in ADS's schematic window.**
   The circuit is drawn in the Agilent ADS schematic window.

4. **Optimization of the circuit from ADS's schematic window.**
   An optimization is run to achieve a response as close to the one with ideal components as possible.

5. **Simulation of the circuit using TriQuint components from the schematic window.**
   The circuit using the final component values is simulated.

6. **Layout.**
   The physical layout of the circuit is done.

7. **Momentum simulation and adjustment of the layout.**
   The component placement, connecting line width etc. is adjusted to get Momentum results as close as possible to the ones obtained when running s-parameter analysis from the schematic window. A Momentum simulation is run to check the performance of the modified circuit. Multiple adjustments might be needed before satisfactory performance is achieved. The final s-parameter results are plotted in a graph.

8. **Production and measurements.**
   The circuit is sent to the vendor for production, and the finished wafer is measured to test whether the circuits is within the specifications.

Simulations

Ideal Lumped Components Equivalent

To construct the lumped component Wilkinson Power Divider using ideal components, we need to calculate the capacitor and inductor values using formula 1 from the Lumped Components section. Using these formulas with frequency $\omega_0 = 2\pi*f = 2\pi*5*10^9$ rad/s = $3.14*10^{10}$ rad/s, and system impedance $Z_0 = 50\ \Omega$, yields:

$$C = \frac{1}{\sqrt{2}\omega_0 Z_0} = \frac{1}{\sqrt{2}*3.14*10^{10}*50} pF = 0.45 pF$$

$$L = \frac{\sqrt{2}Z_0}{\omega_0} = \frac{\sqrt{2}*50}{3.14*10^{10}} nH = 2.25 nH$$

The resistor needs to be $R = 2*Z0 = 2*50\ \Omega = 100\ \Omega$.

Using these values we get the circuit in Figure 25.

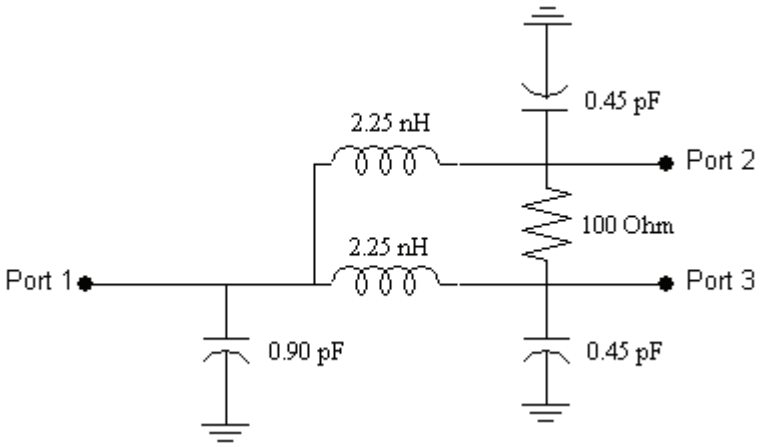

Figure 25: Lumped components Wilkinson Power Divider at 5 GHz and 50 Ω impedance.

We can see that the two capacitors in parallel at the input has been combined into one with value 2*0.45 pF = 0.90 pF.

Simulations

Figure 26 shows the s-parameters vs. frequency for the ideal lumped components circuit. For this case, as well as for the rest of the plots in this part of the report, only S_{11}, S_{22}, S_{21} and S_{32} will be plotted as these parameters gives all the information about the circuit. This is because of the symmetry and reciprocity properties of the Wilkinson Power Divider.

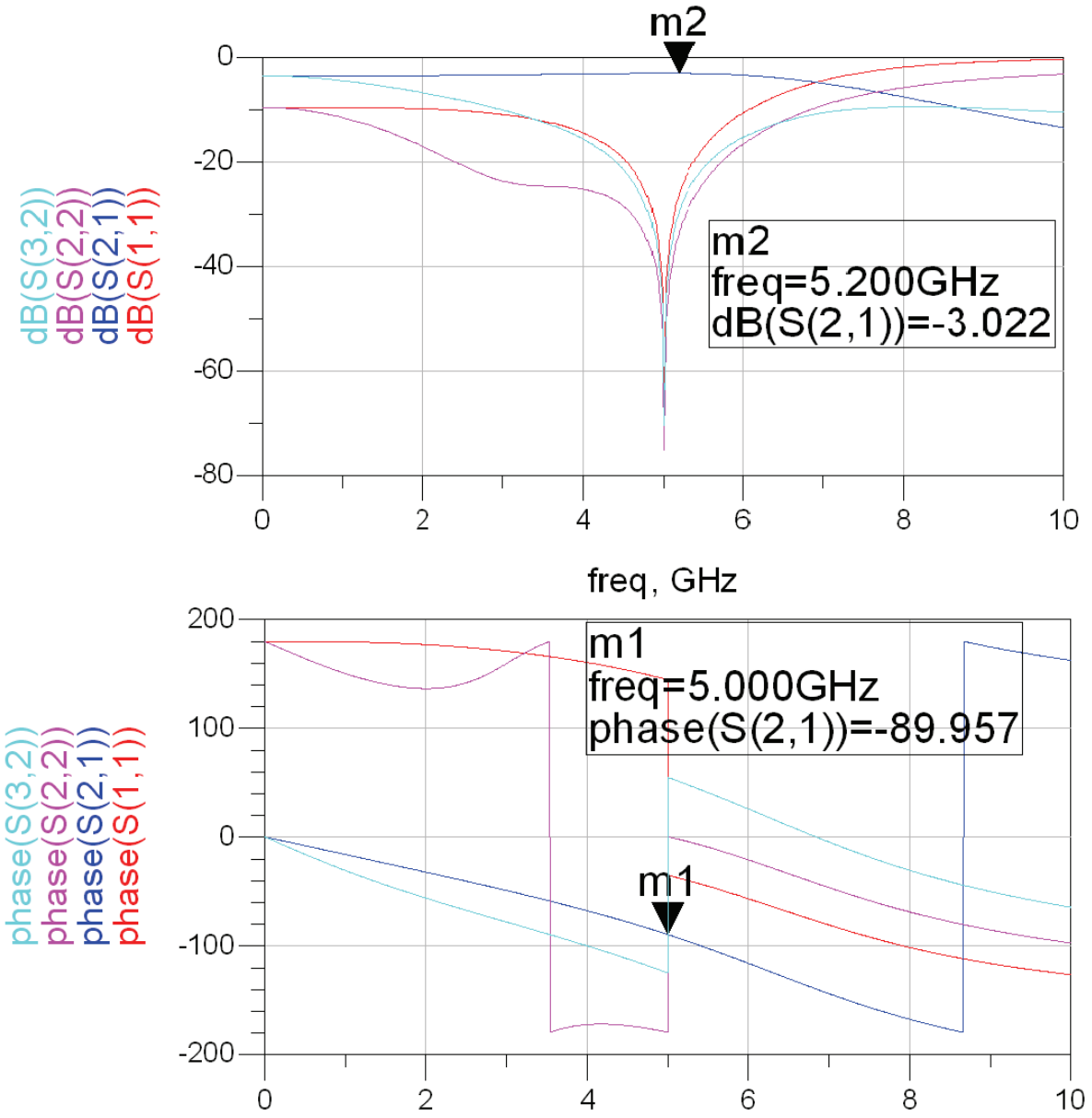

Figure 26: Phase and dB-value of s-parameters vs. frequency for ideal lumped components.

From the plots in Figure 26 we can see that the matching of the input and the output is very good at the design frequency (5 GHz), while the bandwidth, as with the distributed version, is rather poor. S_{21} shows that the attenuation from input to output is 3 dB, meaning that the signal at port 1 is split equally between port 2 and 3 without loss.

From the phase plot we see that all s-parameters except S_{21} show resonance at the design frequency, as we would expect. Inspection of S_{21} at this frequency shows a phase of 90˚, as in the original circuit.

Comparison with Distributed Wilkinson Power Divider

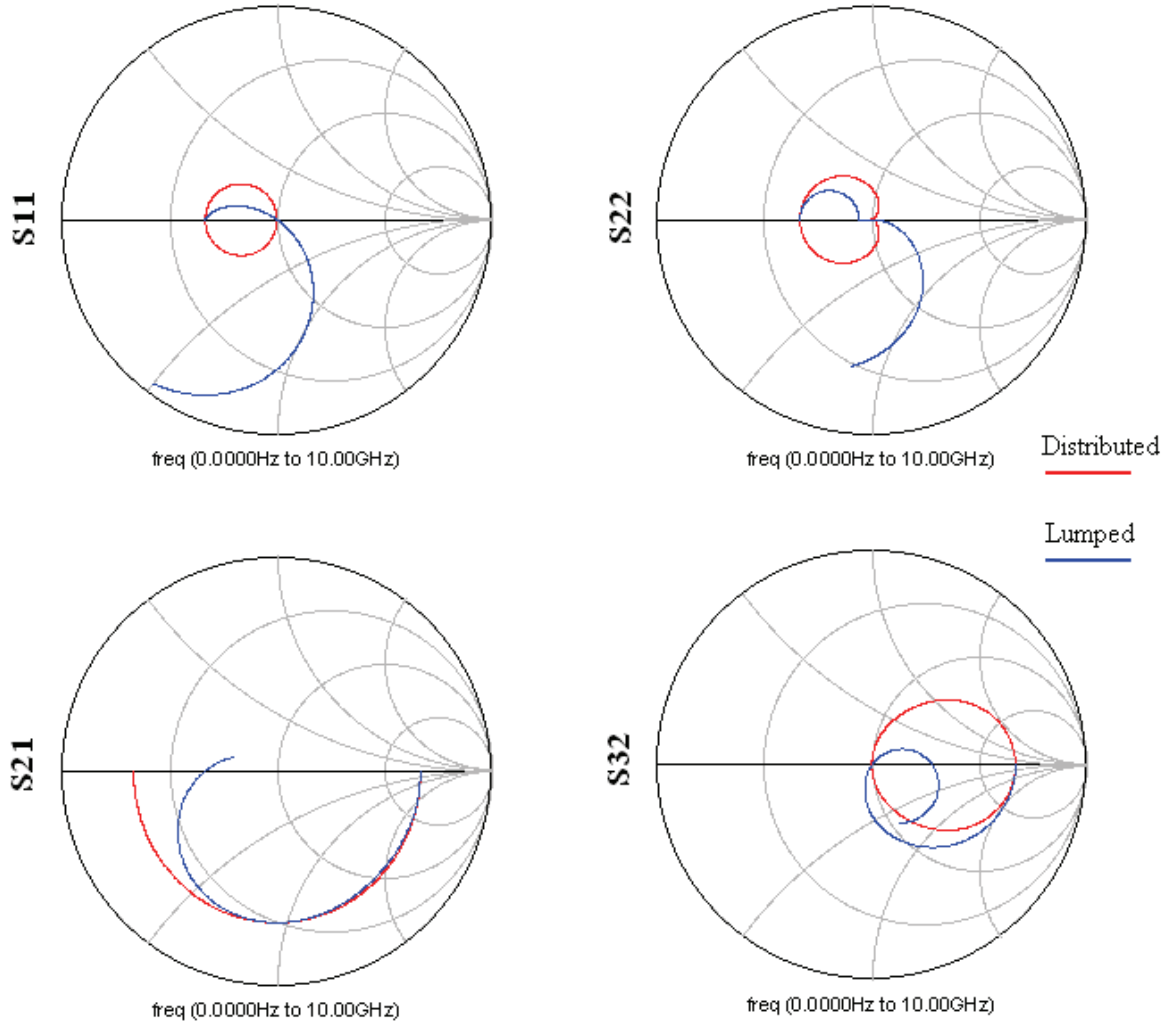

Figure 27: S-parameters for distributed and lumped version plotted in Smith Charts.

The Smith Charts in Figure 27 shows us that we only get a perfect match between the lumped and the distributed circuit at the design frequency. At other frequencies the deviation between the two circuits can be rather large. The practical consequences of this are mainly that the bandwidth might be different. This is especially true for S_{22} (and S_{33}) as we can see that these curves stay close to the centre of the Smith Chart over a significant frequency range in the case of the distributed version. This means that the distributed Wilkinson Power Divider has significantly wider bandwidth on the output ports.

We also notice that we can get arbitrarily close to the centre of the Smith Chart, indicating a perfect match, for S_{11}, S_{22} and S_{32}. Any deviation from this is caused by effects such as round-off errors. This means that $|S_{11}| = |S_{22}| = |S_{32}| = -\infty$ dB at 5 GHz.

Construction of the Inductors

The MMIC spiral inductors need to be designed manually by adjusting the width and length of the inductors lines, as well as the spacing between the turns. This is done by using the inductor_q design in Agilent ADS. This setup tries to achieve the correct inductance while keeping the resistance as low as possible, thereby maximising the Q-factor. To do this the optimize function in ADS is used.

Figure 28: Schematic window setup for design of inductors.

Schematic Window Setup

Figure 28 shows the schematic window setup of the inductor_q design. Instructions for using the setup are displayed in the lower right corner. They are printed below:

1) Enter the desired inductance at the desired frequency
2) Try to start with reasonable values and ranges for width, spacing, turns and length
3) Run random optimize with about 1000 iterations
4) If an error message appears showing "Fatal error occurred while evaluating model `MRINDSBR', instance `L1.L2'." try increasing the minimum length or decreasing maximum width and/or spacing
5) If the correct inductance is not achieved, try adjusting the ranges for width, spacing and length
6) When the inductance is close to the desired one, use tuning to get the correct inductance
7) Check the layout to see if the space has been utilised in a reasonable way
8) Run SP2 and check that the resonant frequency is far enough from the design frequency

The error message in step 4 appears if the chosen values make the inductor unrealisable in practice. I.e. the number of turns will not fit within the chosen length.

Specifications like minimum line width and exclusion distance for the technology that is used should be considered when setting the ranges for line width and spacing.

Data Display Setup

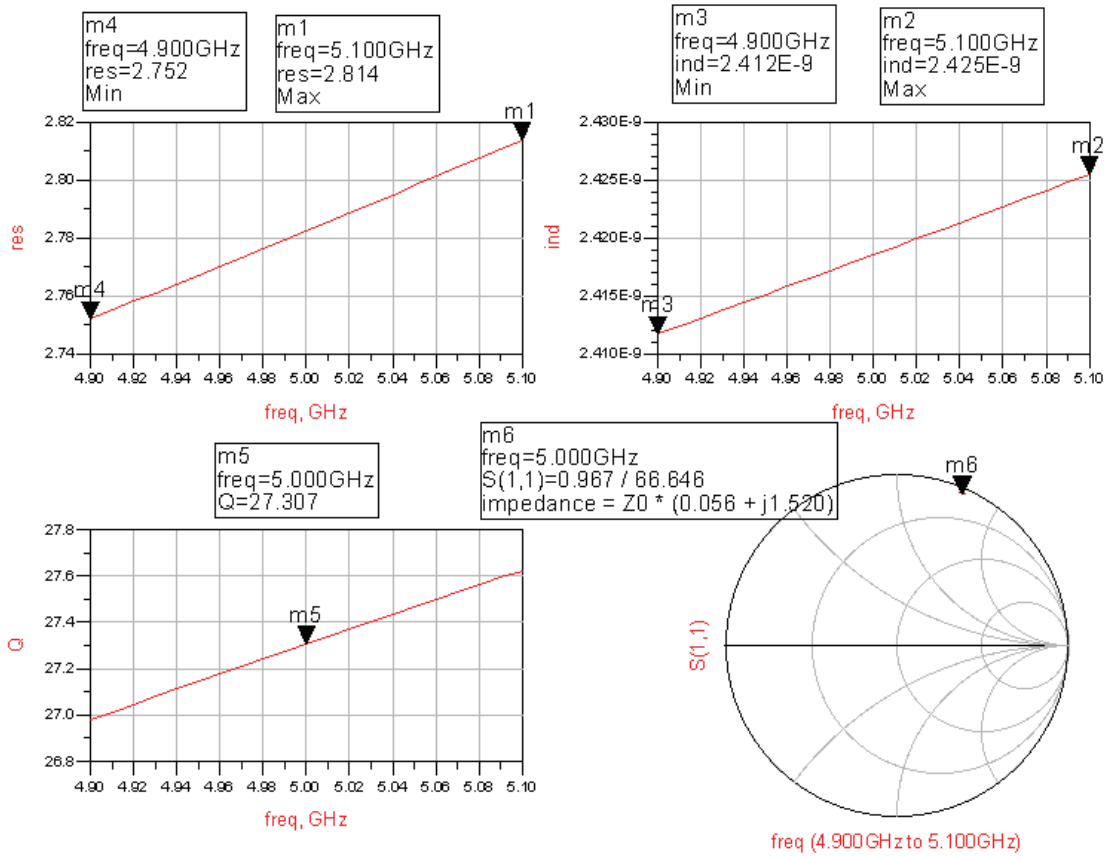

Figure 29: Data display window for the inductor_q design.

In the data display the inductance and resistance of the inductor vs. frequency is plotted in separate plots, as well as the Q-factor, and S_{11} is plotted in a Smith Chart. This should give all the information needed when designing the inductor. The formulas used for finding inductance, resistance and Q-factor from S_{11} are as follows:

$$R = \Re\left\{-50\frac{S_{11}+1}{S_{11}-1}\right\}$$

$$X = \Im\left\{-50\frac{S_{11}+1}{S_{11}-1}\right\}/(2\pi f)$$

$$Q = \frac{\omega L}{R}$$

The formula for Q-factor is from [34].

Results

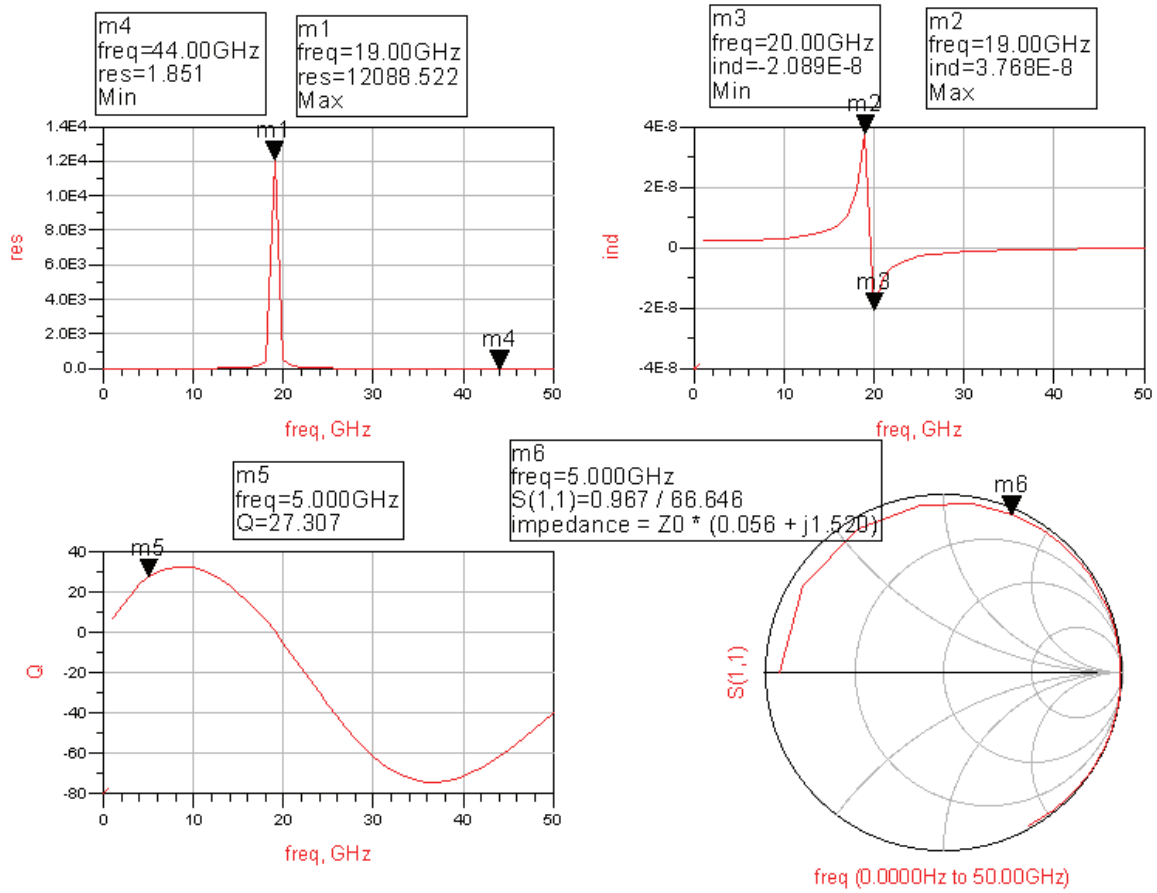

Figure 30: Resistance, inductance and Q-factor for a broad frequency range.

We can see the final inductance, resistance and Q-factor close to the design frequency in Figure 29. Figure 30 shows these values for a broader frequency range. From this figure we can read off the resonant frequency as approximately 19 GHz, which is well above the design frequency. This means that the inductance should be relatively constant with regards to small process variations.

Schematic and Data Display Setup Using TriQuint Components

Schematic Setup

Figure 31, on the next page, shows the setup for the lumped component Wilkinson Power Divider in the schematic window of ADS. The circuit itself is in the middle of the screen. It is drawn using the components from the TriQuint library. Care has been taken, to drawn the circuit as closely as possible to the actual physical realisation to get good agreement between schematic s-parameter simulation and Momentum simulation of the layout. To run s-parameter analysis, we use 50 Ohm terminations on all the ports, with number 1 on the input, and number 2 and 3 on the outputs. Actual ports are also drawn, and can be used for the layout. These are deactivated in the present case.

To use the TriQuint components we must include the TriQuint Netlist Include component. This is placed to the left of the circuit. Between this component and the circuit, a variable equation component and a measurement equation component is placed. The measurement equation component specifies various commonly used parameters like input match (S_{11}), that can be used for instance in a yield specification. The variable equation component contains all of the values that are to be adjusted in order to tune or optimize the performance of the circuit. We can see that most of these variables are set for tuning and/or optimization.

The s-parameter simulation components are placed in the upper left corner, surrounded by a red box. There are three different s-parameter components with different ranges and intervals, so that the circuit response can be inspected for various frequency ranges. It is possible to run multiple s-parameter simulations simultaneously.

The components used for running the yield and optimization are placed inside separate boxes to make the view of the setup clean. The use of optimization is described below. Yield analysis has not been performed on this circuit.

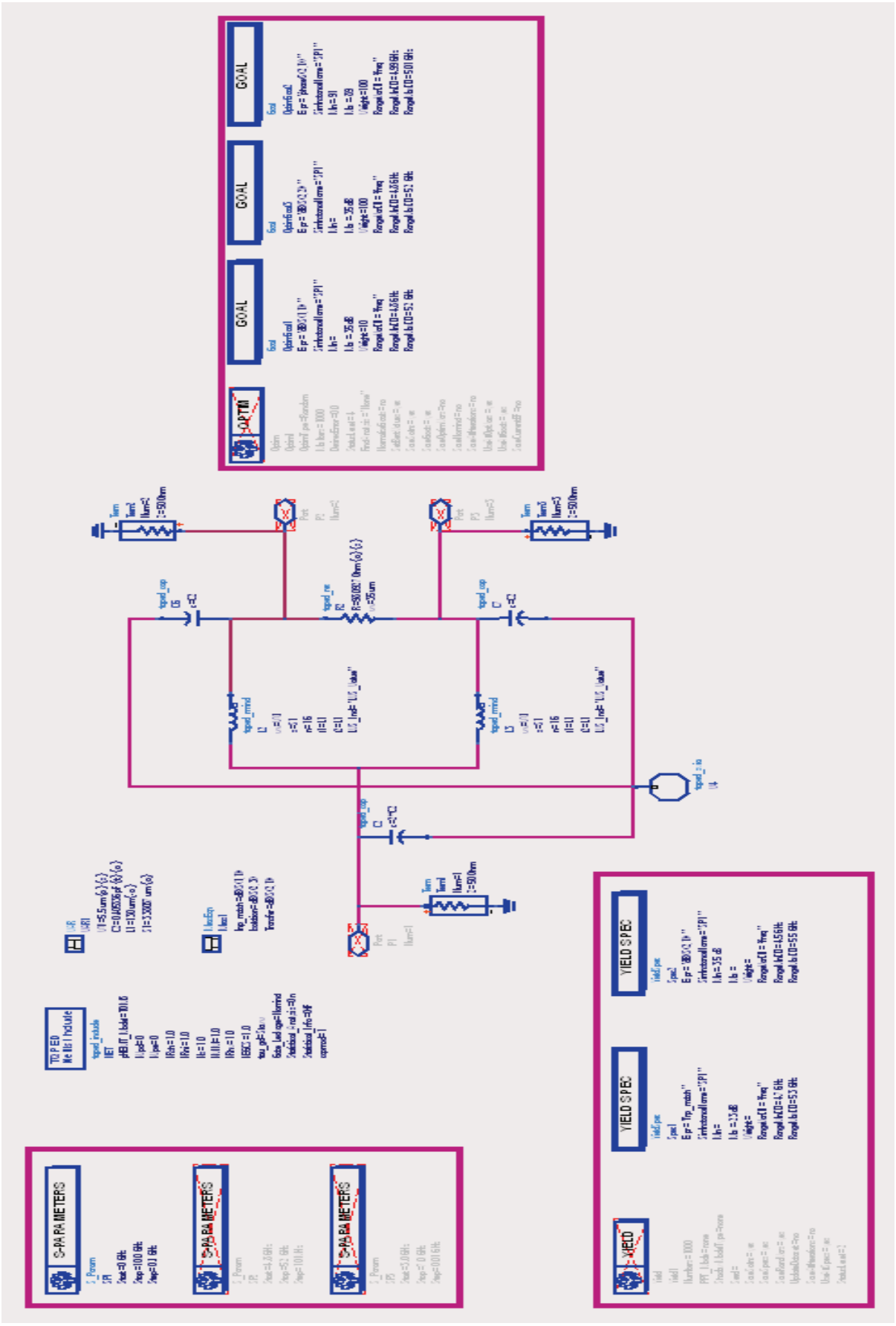

Figure 31: Agilent ADS schematic window setup of the lumped component Wilkinson Power Divider.

Data Display Setup

The setup of the data display window for the s-parameter simulations of the circuit in ADS is shown in Figure 33. In order to use this display window, a single s-parameter analysis from 1 to 10 GHz, with 10 MHz resolution should be run.

The decibel value of S_{11}, S_{22}, S_{23} and S_{21} is plotted in the centre plot. Because of symmetry and reciprocity, all of the s-parameters can be found from this plot. Frequencies from 1 to 10 GHz are displayed. To the right of this plot, minimum values of S_{11}, S_{22} and S_{23} as well as the 5 GHz value of S_{21} is displayed.

On the upper left, the insertion return loss, return loss, voltage standing wave ratio and the 25 dB bandwidth for both the input and output (ports 2 and 3) are displayed. The formulas for these values can be found on the equations page (see Figure 32). These equations are taken from [35].

```
Eqn In_IL=-10*log10(sqr(abs(S(2,1)[40]))/(1-abs(sqr(S(1,1)[40]))))
Eqn In_IRL=abs(20*log10(abs(S(1,1)[40])))
Eqn In_VSWR=vswr(S11[40])
Eqn In_Bandwidth=bandwidth_func(dB(S11),25,1)
Eqn VSWR_marker=vswr(S11[find_index(freq,indep(m7))])
Eqn Out_IL=-10*log10(sqr(abs(S(2,1)[40]))/(1-abs(sqr(S(2,2)[40]))))
Eqn Out_IRL=abs(20*log10(abs(S(2,2)[40])))
Eqn Out_VSWR=vswr(S22[40])
Eqn Out_Bandwidth=bandwidth_func(dB(S22),25,1)
```

Figure 32: Equations used in the data display of Wilkinson Power Divider s-parameters.

In the lower left part of the screen a short description of the setup is given.

On the right side of the screen, the decibel values of S_{11}, S_{22} and S_{32} is plotted in separate plots for close inspection of these important parameters.

In the bottom centre of the screen thee is a slider that can be used to display the input voltage standing wave ratio at various frequencies by sliding the marker to the desired frequency.

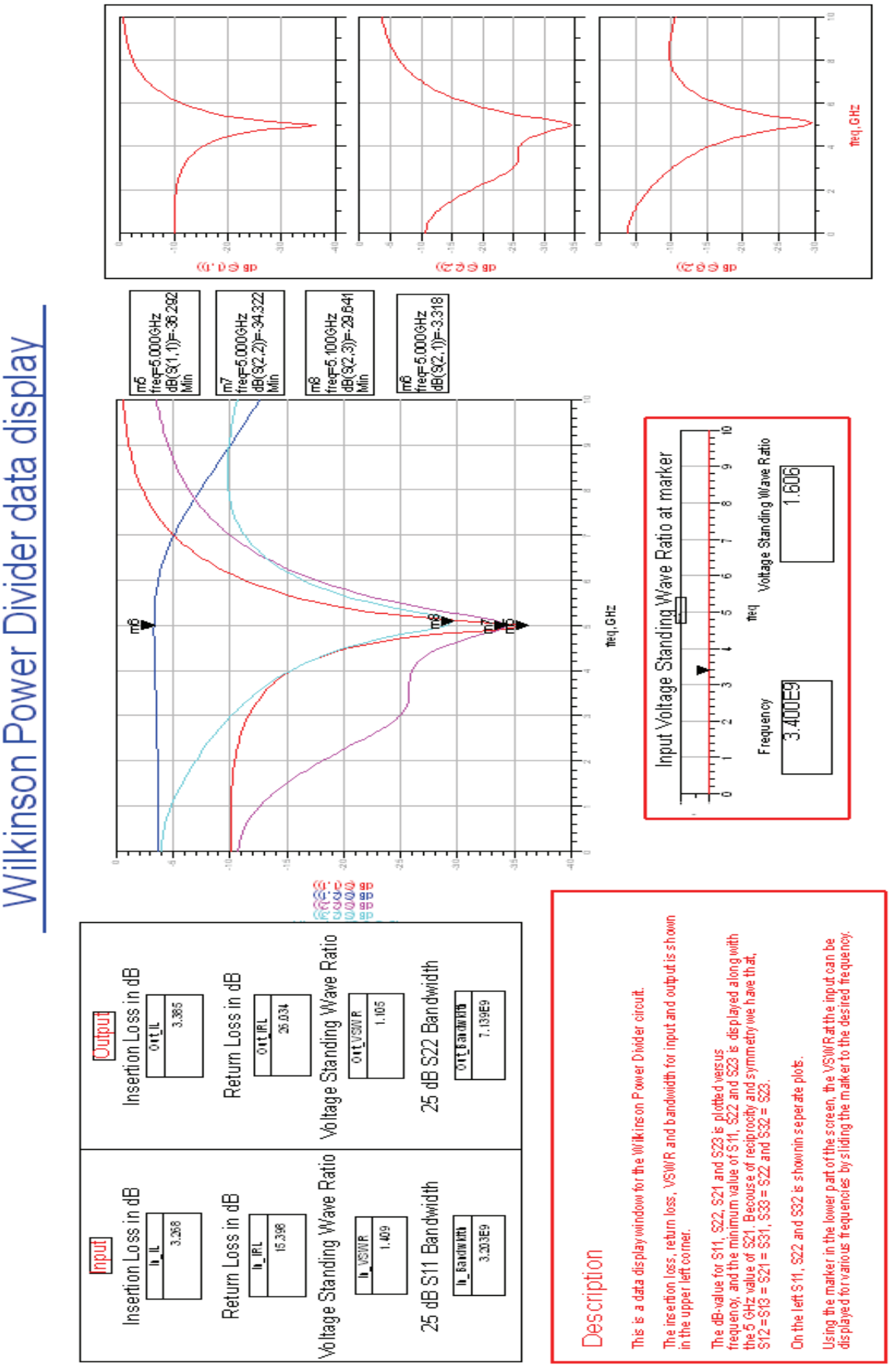

Figure 33: Data display setup for s-parameter simulations of the Wilkinson Power Divider in ADS.

Optimization

To achieve the best possible performance from the circuit, an optimization is run on the circuit. We use the values found using ideal components as a starting point. The values that are used as variables during optimization are; capacitor size, inductor line width and resistance.

The main goal that must be achieved to mimic the behaviour of the distributed line Wilkinson Power Divider is that the phase shift between ports 1 and 2 and ports 1 and 3 is 90˚ at the centre frequency. This goal is specified as phase(S_{21}) and is weighted strongest with 10.

The other goal that must be met is a good match at all the ports at the centre frequency. These goals are taken into consideration by specifying that S_{11} and S_{22} should be below -35 dB in a band of 400 MHz around the centre frequency. These goals are weighted by 1. Because of the symmetry of the circuit it is not necessary to specify S_{33} as it must equal S_{22}. Neither is it necessary to specify separate goals for the isolation between ports 2 and 3 (S_{23} and S_{32}), or the transmission between port 1 and ports 2 and 3 (S_{21}, S_{12}, S_{13} and S_{31}) because these parameters will be taken into account with the given goals.

As always when optimizing a circuit there will be trade-offs, so that optimizing the circuit with regards to a specific parameter will normally make the others suffer. This optimization tries to give a balanced weighting between all the parameters.

A random optimization is then run using 1500 iterations. With results close to those obtained with ideal components, a gradient optimization is run using 500 iterations. A final tuning of the relevant variables can then be attempted. Further improvement of the performance is difficult to achieve, but valuable information about the functioning of the circuit, and the sensitivity of the components, can be learned in this way.

Figure 34 shows the setup for the ADS optimization.

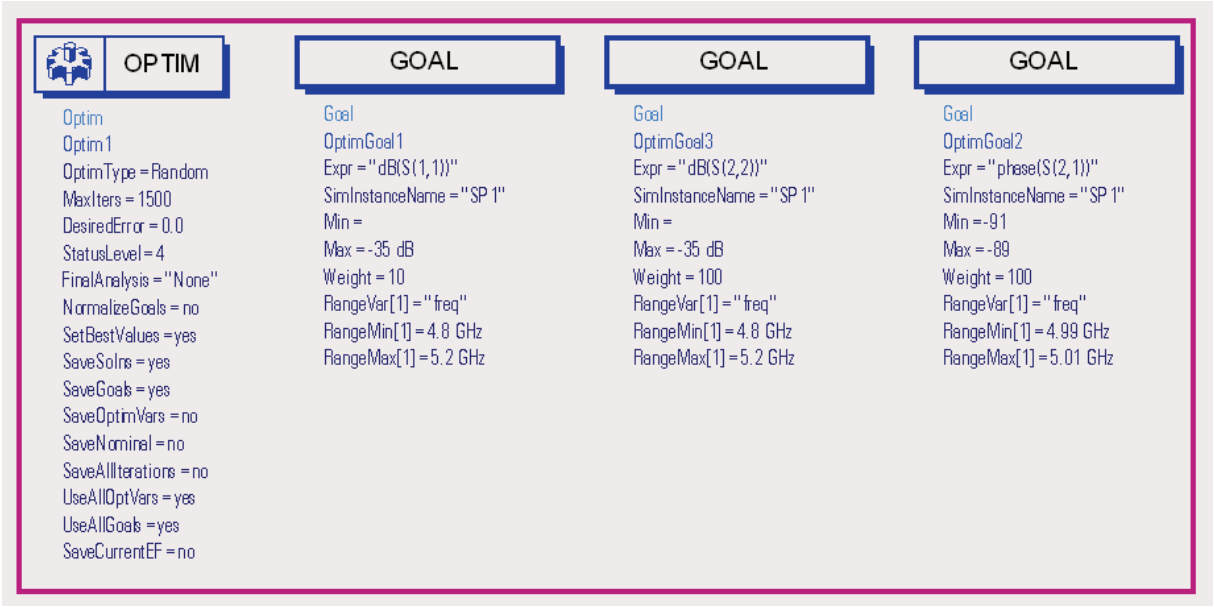

Figure 34: Setup for optimization of the lumped component Wilkinson Power Divider using TriQuint components in ADS.

Simulation Using TriQuint Components

Schematic Window Setup

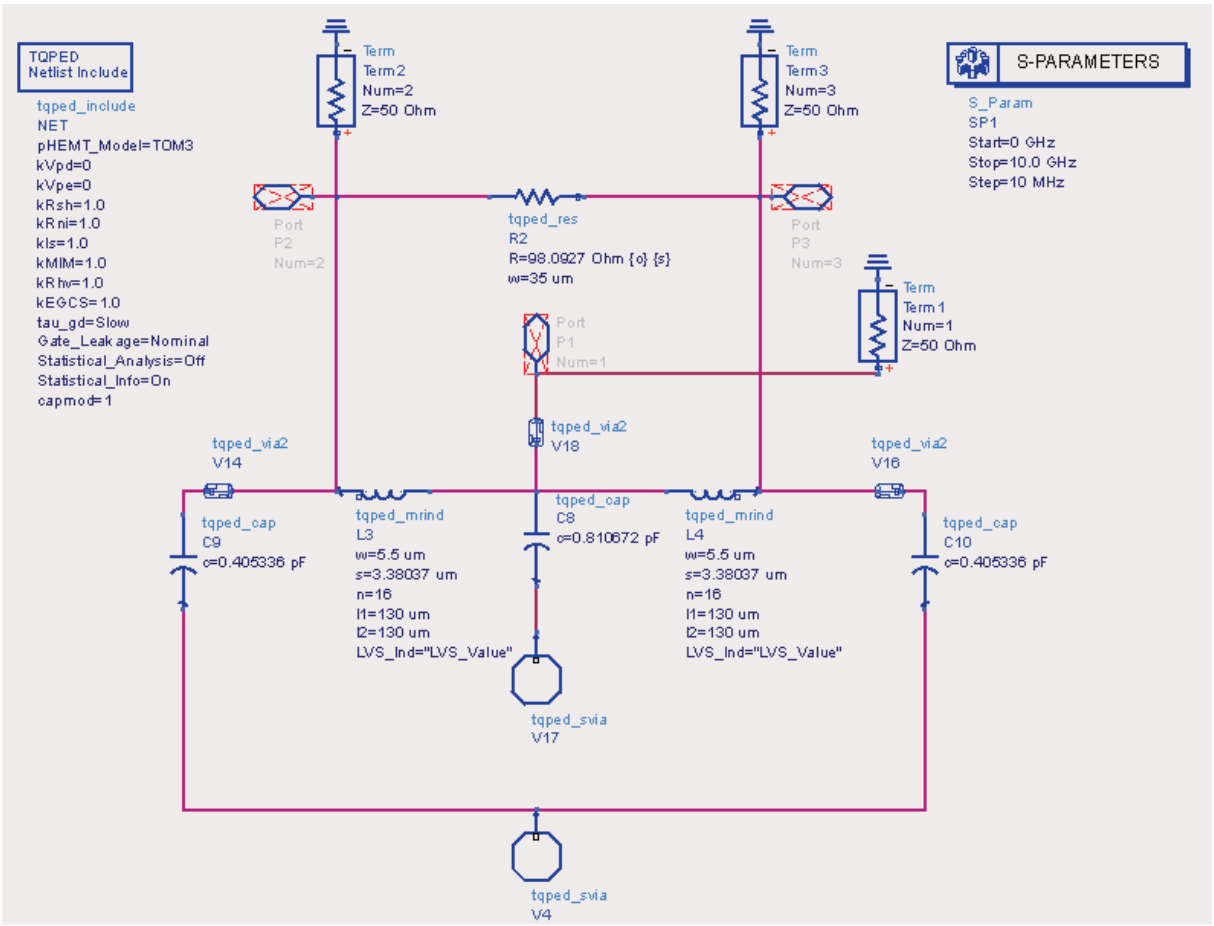

Figure 35: Schematic setup for simulation with TriQuint components.

The component values found during optimization is used in the s-parameter simulation setup shown in Figure 35. Here the via-holes have been included to make the simulation results as close as possible to that of the final circuit.

Simulation Results

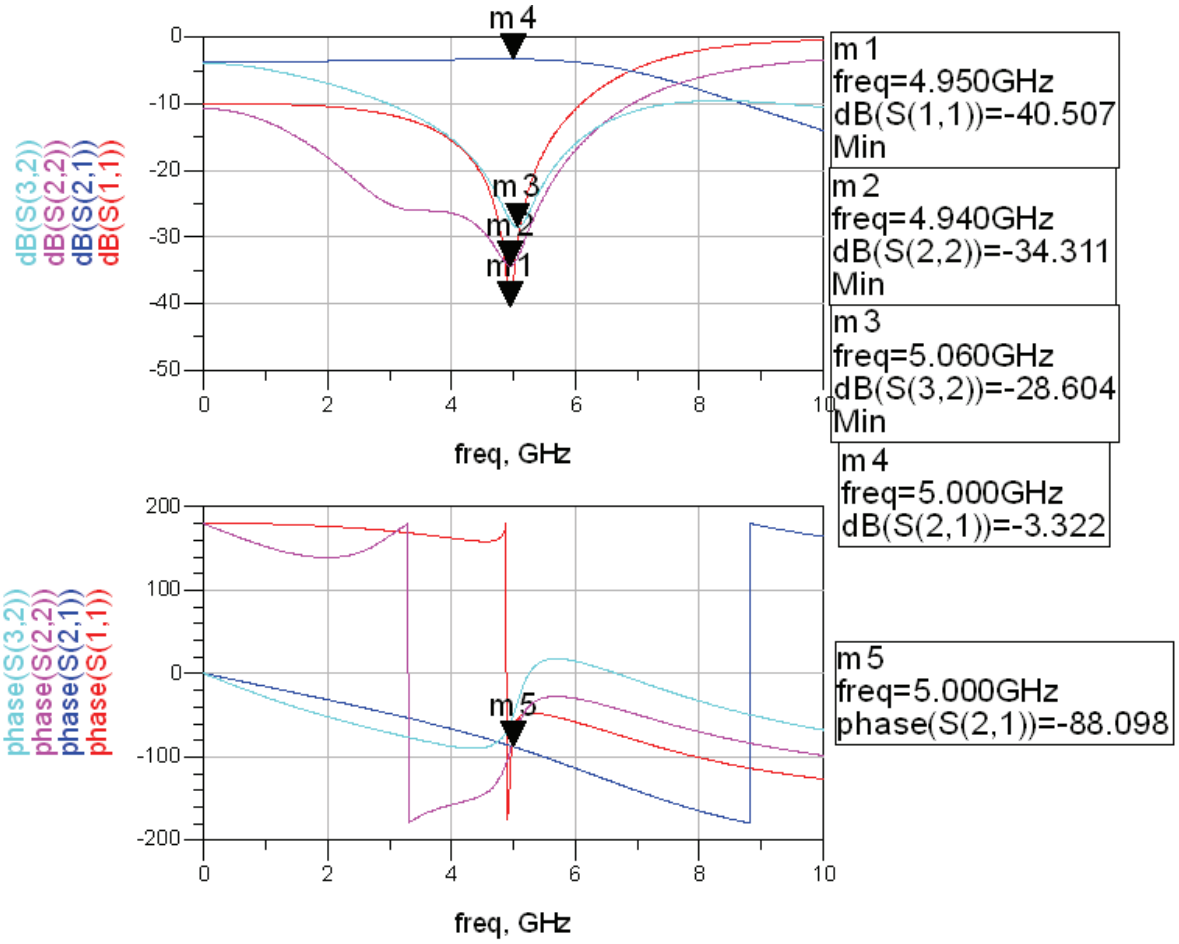

Figure 36: dB and phase response of the circuit with TriQuint components simulated from the Schematic Window.

In Figure 36, we can see the phase- and magnitude- (in decibel) response of the circuit. We see that the centre frequencies is close to the desired frequency of 5 GHz, with the attenuation of both S_{11} and S_{22} being below -30 dB at that point.

The phase response shows that S_{21} (and S_{12}) has a slight deviation of 2˚ from the desired phase shift of 90˚.

Comparison with Ideal Components

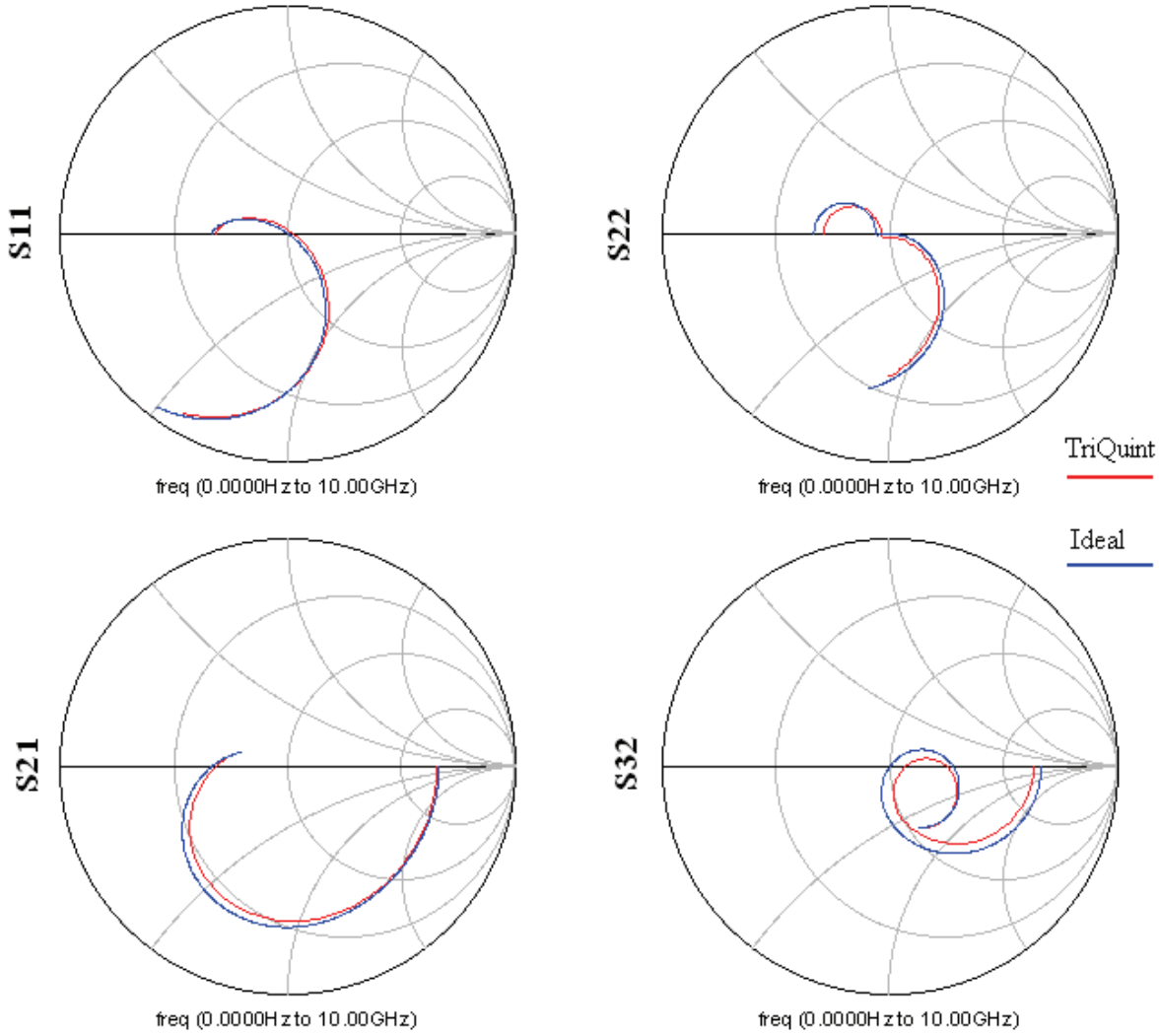

Figure 37: Smith Charts showing the differences between lumped component Wilkinson Power Divider with ideal and real (TriQuint) components.

From the Smith Charts in Figure 37, we can see that we no longer can have a perfect Wilkinson Power Divider, even at the design frequency. This is because of the parasitic effects of the components, mainly the resistive losses. The main reason that S_{32} deviates noticeably from the ideal components case, is that the phase of S_{21} is no longer 90˚. Losses in the two branches, and the fact that the resistor value has been changed from the original 100 Ω, also contribute to this deviation. See Simulation Results under the Momentum Simulation and Final Adjustments section for a more thorough description of this effect.

Layout

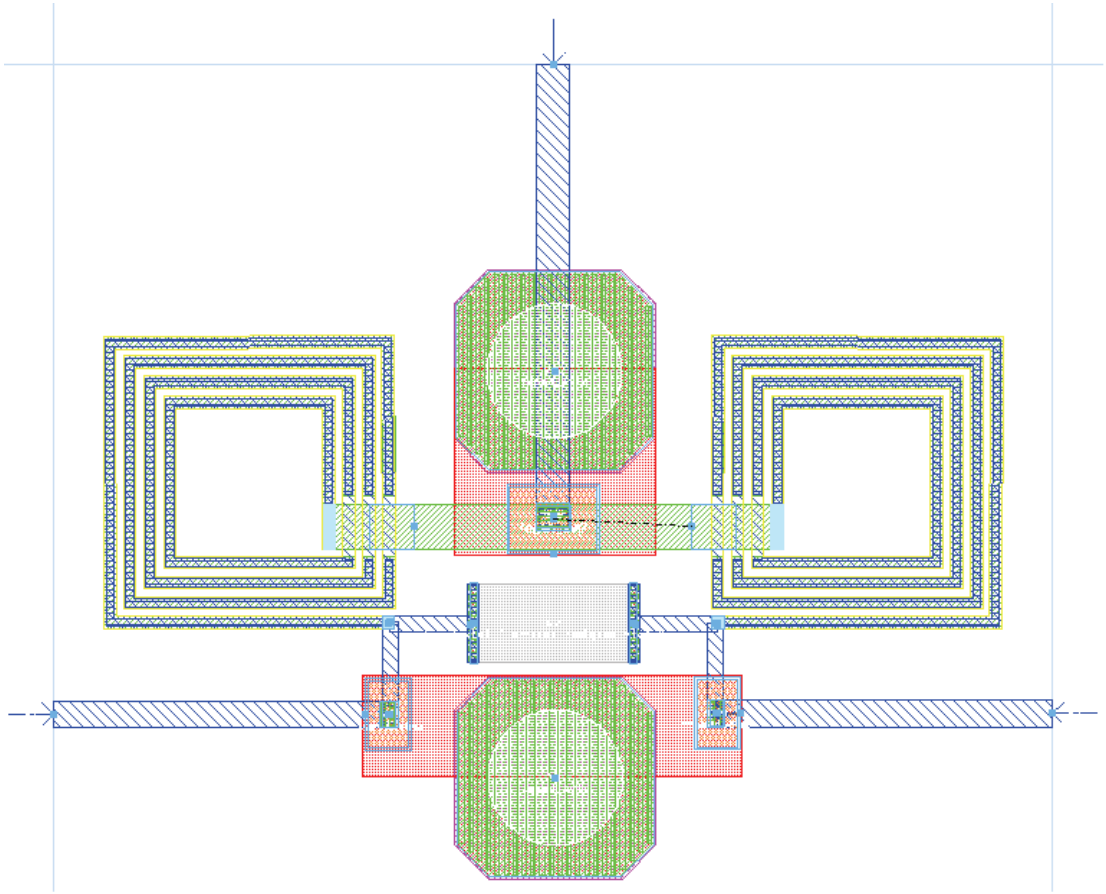

Figure 38: The ADS layout of the lumped component Wilkinson Power Divider.

Figure 38 shows the layout of the circuit in the layout window of ADS. The two inductors are the two spirals on either side, the resistor is the grey component in the centre, the capacitors can be seen to have clearly visible via holes to metal layer one, while the substrate via hole is placed in the low centre of the layout. Metal layer one is drawn in green, layer two in blue and metal layer zero is shown in red. The signals are applied at the points indicated by arrows. Port 1 is at the top while ports 2 and 3 are at the left and right side, respectively.

As can be seen, care has been taken to maintain symmetry between the two sides of the circuit. This is done to make sure ports 2 and 3 have the same phase difference and attenuation with regards to port 1. The two inductors have been placed as far apart as possible to reduce cross-talk between them. This allows the input capacitor and the resistor to be placed between them.

To minimize parasitic inductance, capacitive coupling and loss, the transmission lines has been kept as short as possible and the overlap between different metal layers have been kept as small as possible where this is not desired. The inductors use both metal layer one and two to achieve a high inductance and low resistance on a small space.

A single substrate via hole is used for the output ports (ports 2 and 3) to minimize the area consumption of the circuit. The connections between the via-hole and the connected components should be kept as short as possible to minimize parasitic inductance, as this could lead to unwanted resonances.

The circuit has been designed to have a current carrying capability of 100 mA on either side, and the traces have been designed to be well within this target. The width of the resistor is 35 µm.

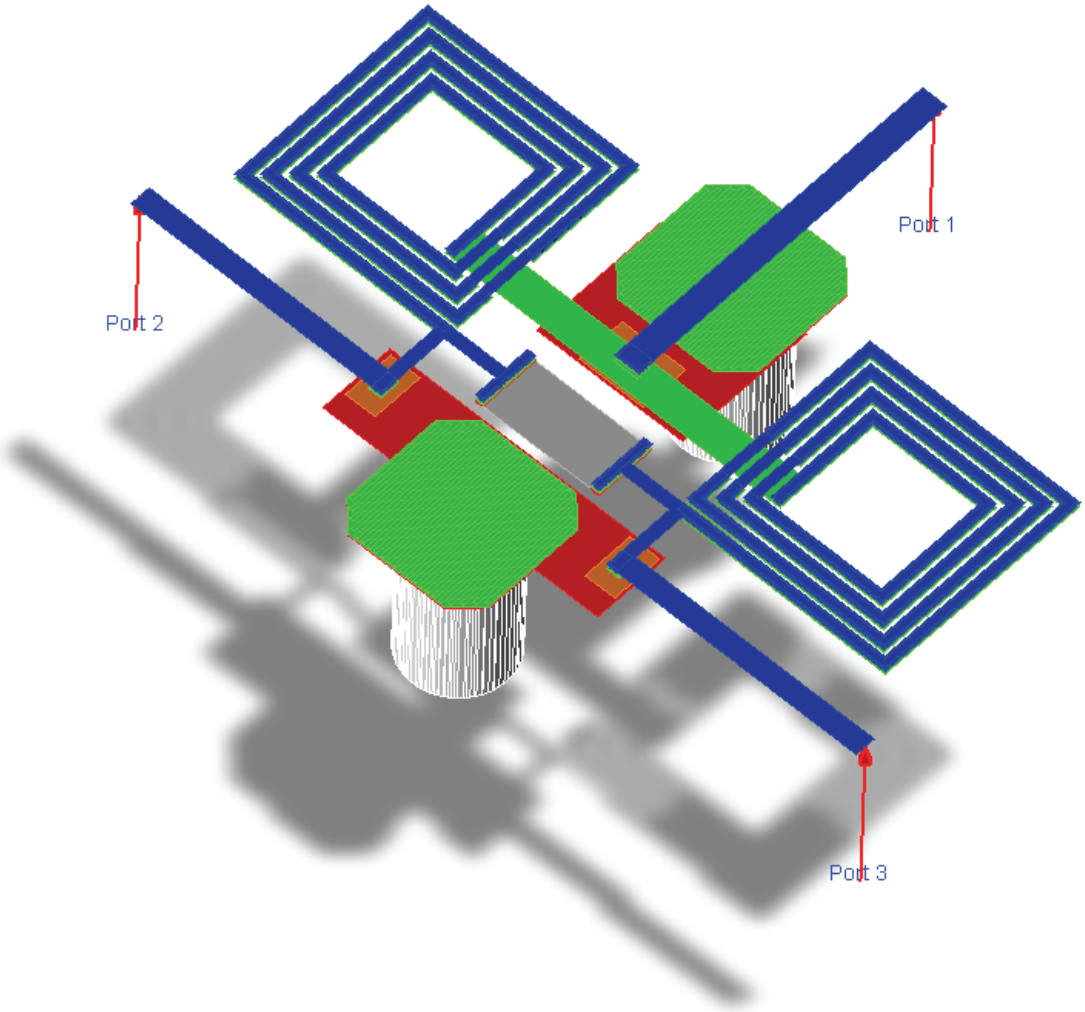

Figure 39: 3D view of the circuit.

Momentum Simulation and Final Adjustments

Adjustments

When the layout has been done as described in the previous chapter, a Momentum simulation is run. The result of this simulation is shown in Figure 40.

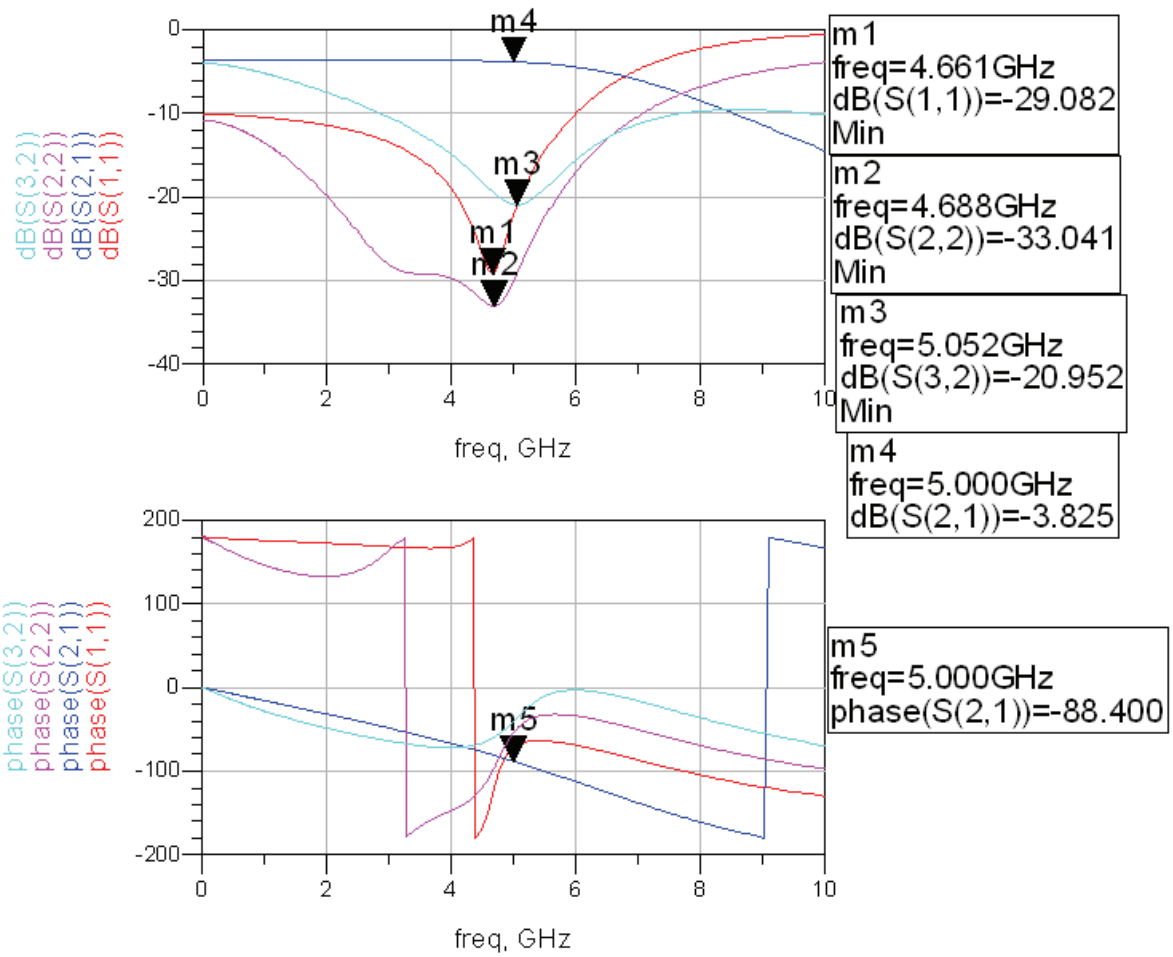

Figure 40: Momentum simulation using values from Schematic optimization.

A can be seen, the results from the simulation is clearly poorer than those from the Schematic Window s-parameter simulation. This is due to the transmission lines that have been added to connect the different components (as well as connections to the external circuitry) and cross-talk. The schematic models from TriQuint are also not 100 % accurate.

To improve on the design, we need to fine tune it. This is done in a number of steps; by changing one parameter at a time, and inspecting the results to see if an improvement is made.

The most natural components to adjust are the capacitors, since the capacitance of these is easy to vary, and there is plenty of space to increase them in the layout. By adjusting the capacitance in steps we arrive at the final component values shown in Figure 41. The other values have been rounded off to two decimals.

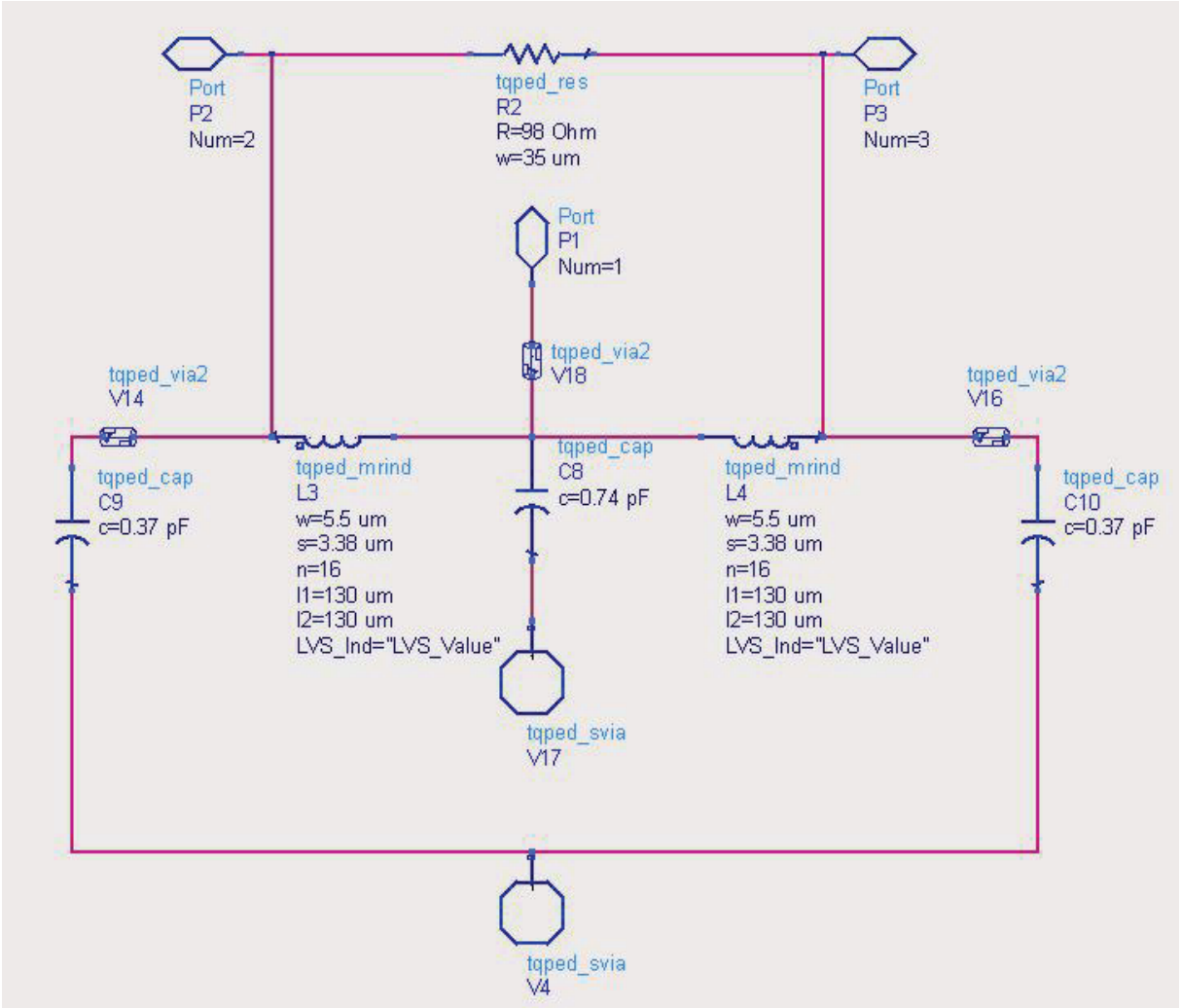

Figure 41: Schematic showing the final component vales of the layout.

Simulation Results

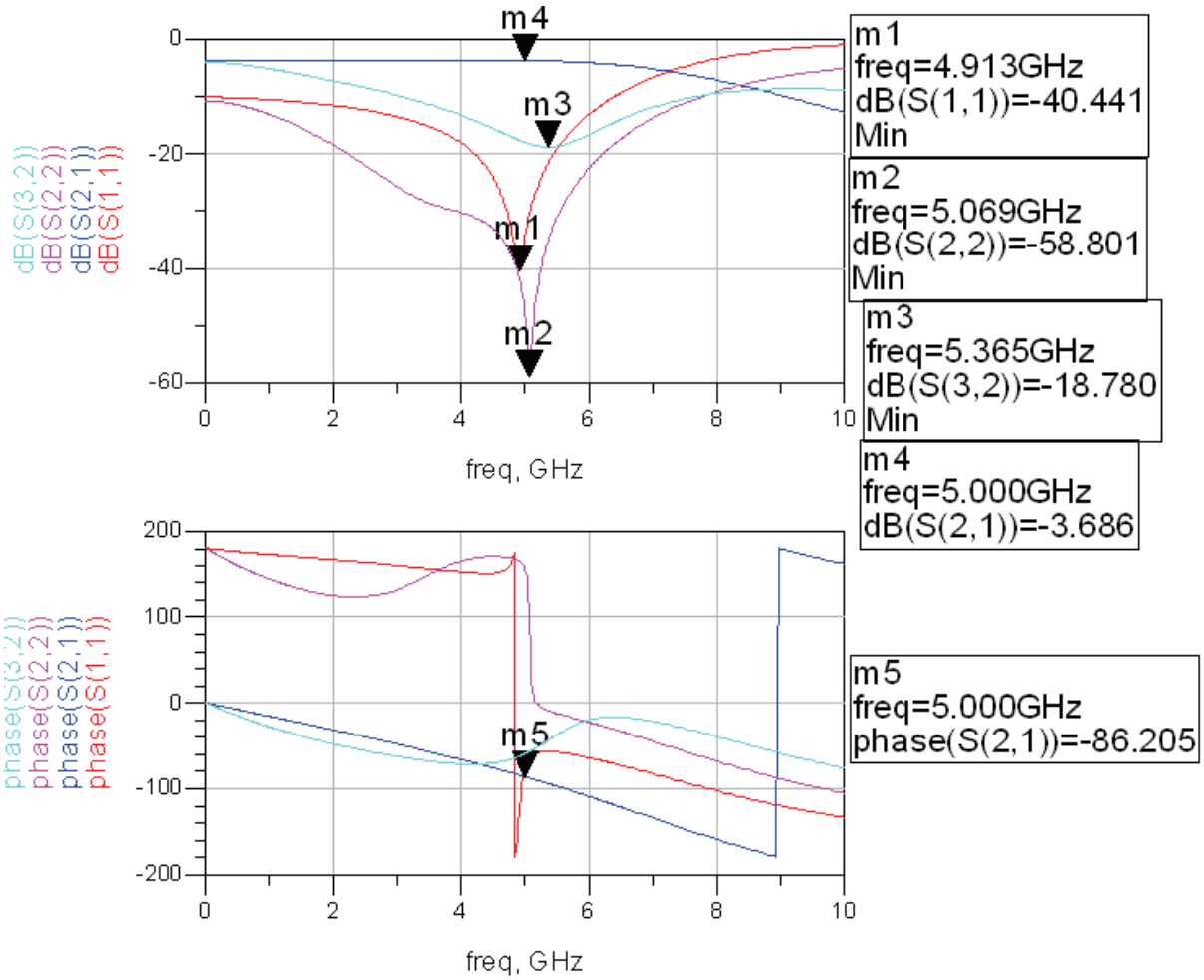

Figure 42: dB and phase response from Momentum simulation of the final layout.

The s-parameters obtained using Momentum simulation on the final layout is shown in Figure 42. We can see that the input and output matches are very good, with both being below -40 dB and with resonances close to the desired frequency of 5 GHz. The loss in the signal path from port 1 to ports 2 and 3 is slightly higher than that obtained in the s-parameter simulation run from the schematic.

The biggest drawback of this realization is that the isolation between ports 2 and 3 is rather poor, with 18 dB attenuation at 5 GHz. If the circuit is to be used as a power combiner with reasonably matched loads, this should, however, not be a problem.

To understand the reason for the poor S_{23} value we need to understand why ports 2 and 3 is isolated in an ideal Wilkinson Power Divider:

Assume that ports 1 and 3 are terminated with matched loads and that a signal is applied to port 2 using a source with matched impedance. Two power waves will be excited from port 2; one going through the resistor, and one going through the two 90˚ branches. Since the total phase shift of the signal through the two branches is 180˚, and the signal through the resistor, theoretically, has 0˚ phase shift, the two waves will add with opposite phase. The power of the two waves will also be equal since the same amount of energy is dissipated in the load at port

1, as is dissipated in the resistor. This means that for an ideal Wilkinson Power Divider we will get perfect cancelation of the signal from port 2 at port 3.

Strictly speaking none of these assumptions is fulfilled in a real realization. First off all; the phase shift from the branches is not -90˚, but -86.2˚ making the total phase shift from port 2 to port 3 -172.4˚; a deviation of 7.6˚ from the desired 180˚. Furthermore, there is a final phase shift in the resistor branch, making the cancelation at port 3 even worse. We can see from Figure 42 that the phase of S_{21} increases with increasing frequency. This explains why S_{32} resonates at a higher frequency than the design frequency (5.37 GHz vs. 5.00 GHz), as the phase difference between the two waves must be closest to 180˚ at this frequency.

A further problem with the practical realization is that the two branches is not loss free. This means that the power of the two waves is not equal, making the cancelation poorer. That the resistor has been changed from the original 100 Ω to 98 Ω to improve the matching at the ports further worsens the cancelation.

If we want to make the isolation between ports 2 and 3 of the physical realization close to that of the ideal circuit, we can make the phase shift of the two branches slightly higher than 90˚ to compensate for the finite phase shift of the resistor branch. To compensate for the losses of the two main branches, we can slightly increase the resistance of the resistor, so that the power of the two canceling waves is equal.

This has been attempted, and while the isolation between ports 2 and 3 indeed improved significantly, the matching at the ports got significantly worse. This was in particular the case with port 1. For this design the matching of the ports has been weighted over the isolation between ports 2 and 3, since for most uses of the circuit, this is not a key parameter.

Comparison with Schematic Simulation

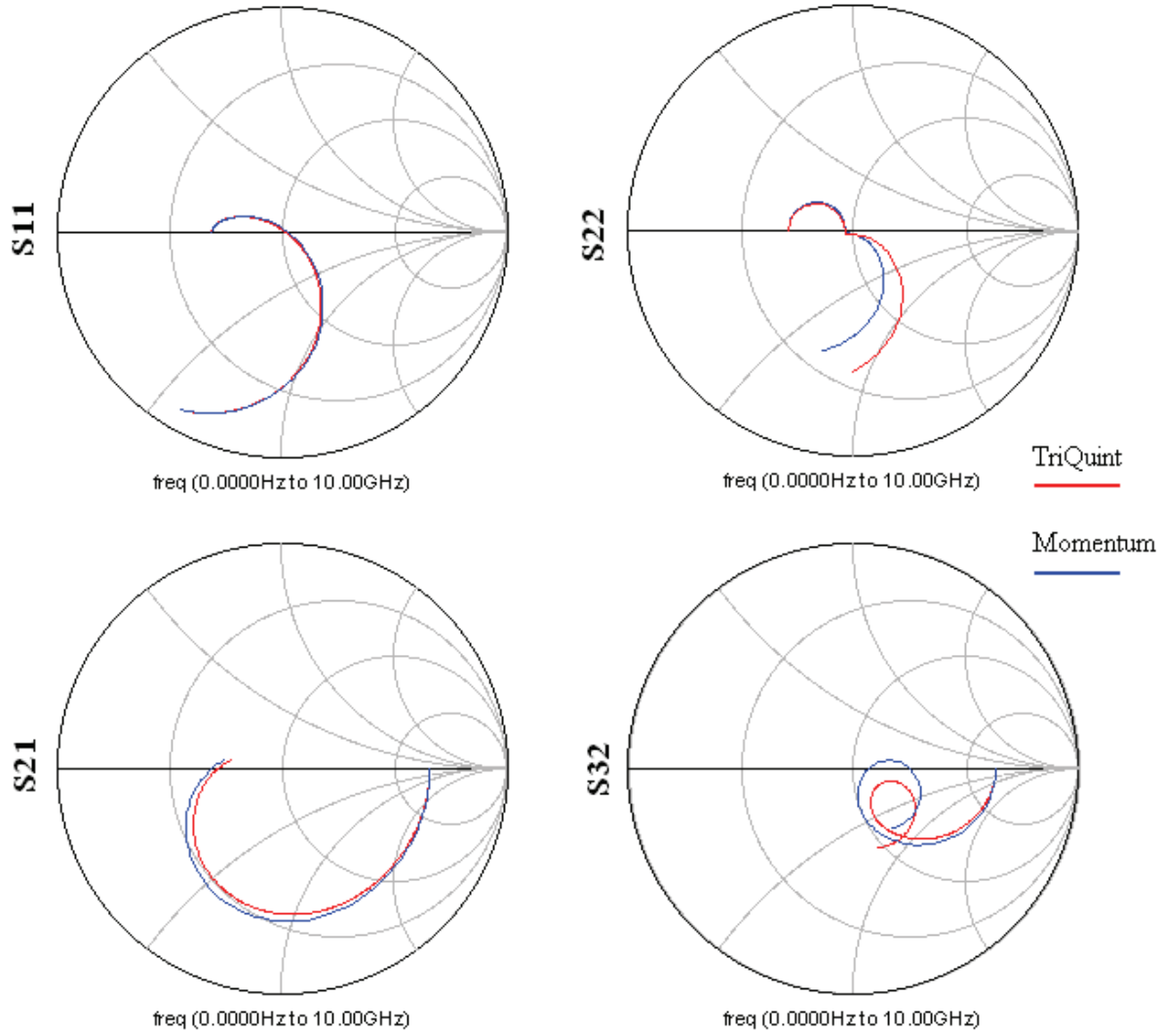

Figure 43: S-parameters from Momentum and schematic window simulation plotted in Smith Charts.

The main deviation from the schematic simulation is that of parameter S_{32}. This is mainly due to extra phase shift and loss due to the transmission lines, and that the capacitance of the capacitors has been adjusted to improve the matching. This has been discussed in detail in the previous section.

The matching at ports 2 and 3 is actually improved over that of the schematic simulation, while the transmission between port 1 and ports 2 and 3 is slightly lossier.

It is instructive to inspect the results obtained from running s-parameter analysis on the same components in both the schematic and layout window. Figure 44 shows these results. The deviation between the two curves is due to the inaccuracy of the TriQuint models, and the effects of the arrangement of the layout (transmission lines and coupling). It is also important to remember that the Momentum simulation is not 100 % accurate, but should, however, be close to the true response as long as a reasonable meshing has been used.

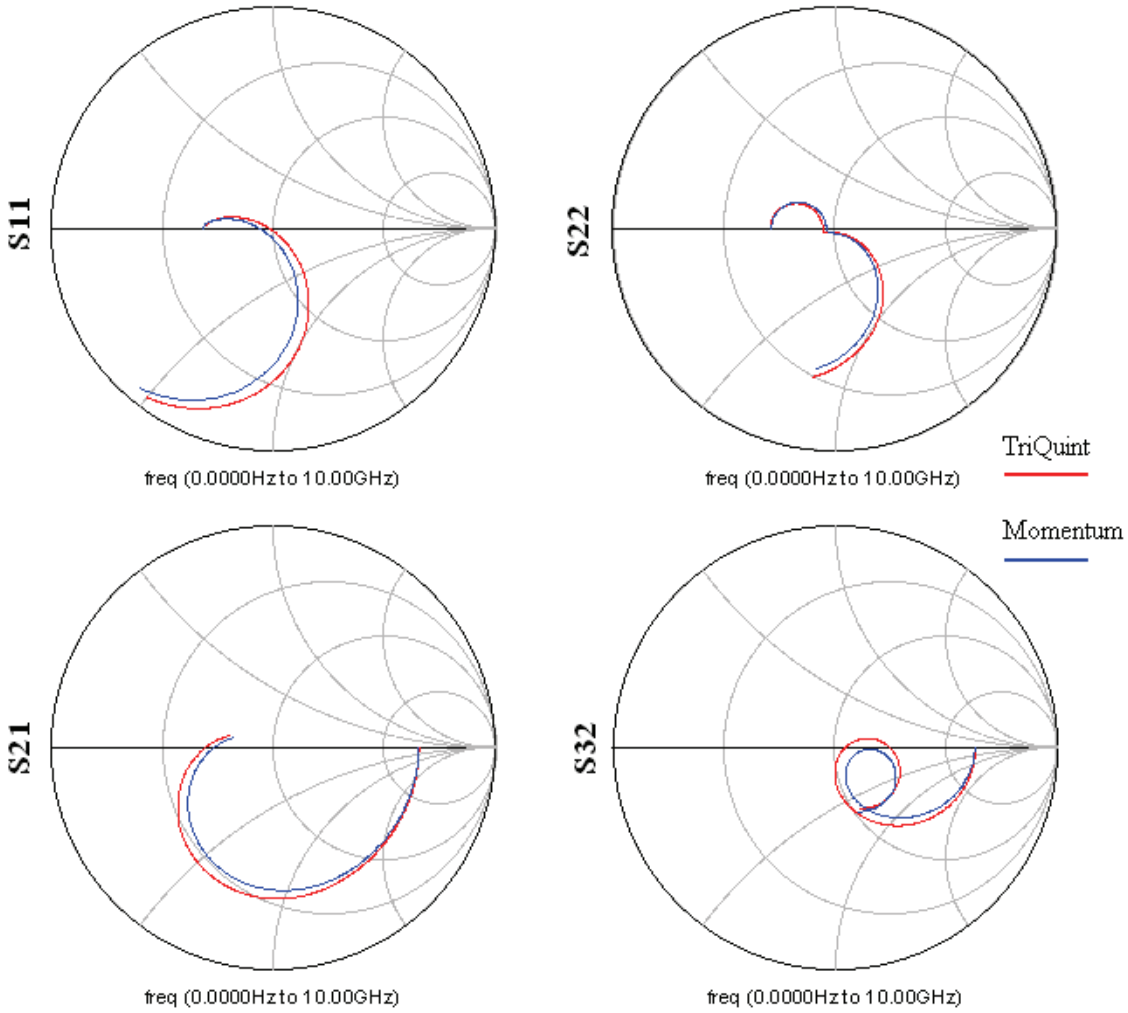

Figure 44: S-parameter simulation from schematic and layout using the same component values for both circuits.

We can see that the results from the Momentum simulation is close to the ones from the schematic simulation, but that further adjustments is necessary to arrive at a satisfactory performance. This will in general be the case when doing the layout.

RF Pulse Response

The Wilkinson Power Divider is often operated with one of its outputs either shorted or open. This situation can be caused by, for instance, the output appliance (i.e. a radio receiver) being removed or even shorted due to some internal damage. It is therefore interesting to see the effect of a RF pulse applied to the input of the circuit when it operates as a power divider, with one of the outputs shorted to ground. One possible use of such a circuit is as a simple RFID, which transmits a replica of a received pulse, with a time delay. This time delay is however impractical to realise on a MMIC chip since it has to be quite large (multiple wave lengths).

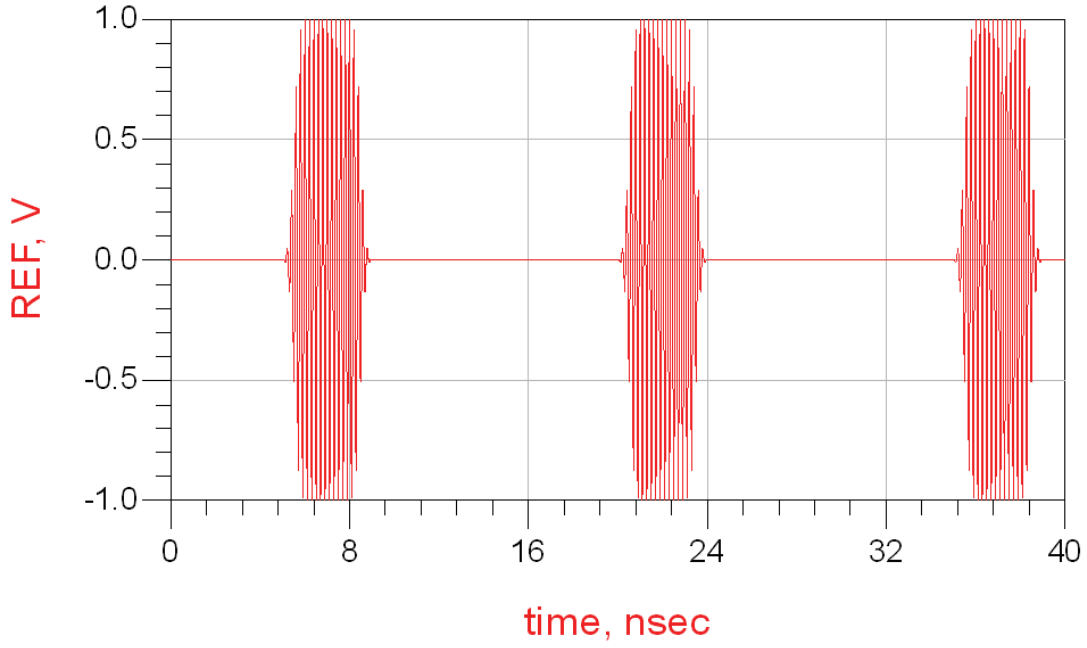

Figure 45: The applied periodic RF pulse.

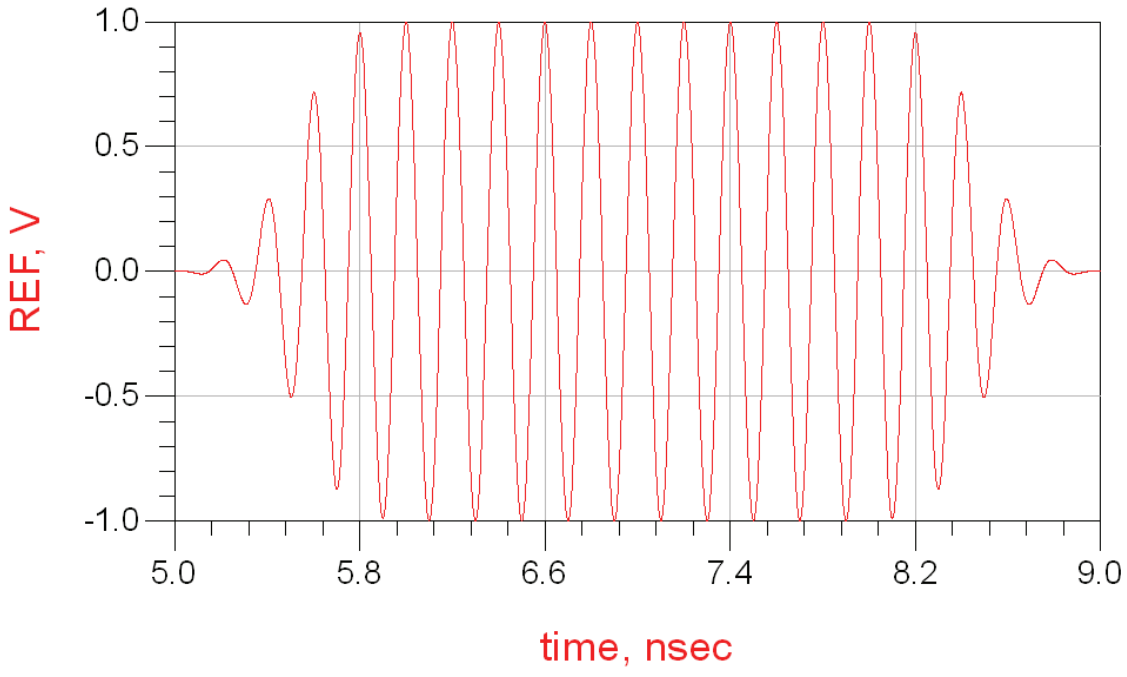

Figure 46: Detailed view of the applied RF pulse.

The effect of a pulse applied to the input of a matched Wilkinson Power Divider will also be studied, as well as the response with the pulse applied to one of the outputs. This also allows us to study the isolation between the two output ports (ports 2 and 3). The effect of a mismatched output is also studied, giving the opportunity to see the effect of reflections at the output. As we can see, the time domain simulations give valuable information that can not be easily obtained from the s-parameters.

Figures 45 and 46 shows the RF pulse that is used in studying the circuit response in the time domain. The pulse is smooth in its rise and fall to keep the frequency spectre narrowly concentrated around the 5 GHz carrier frequency since abrupt changes in the time domain leads to a wide signal in the frequency spectre. A 1 volt amplitude signal is used as the amplitude should not be important since the ADS simulation engine uses a linear solving method.

Schematic Setup

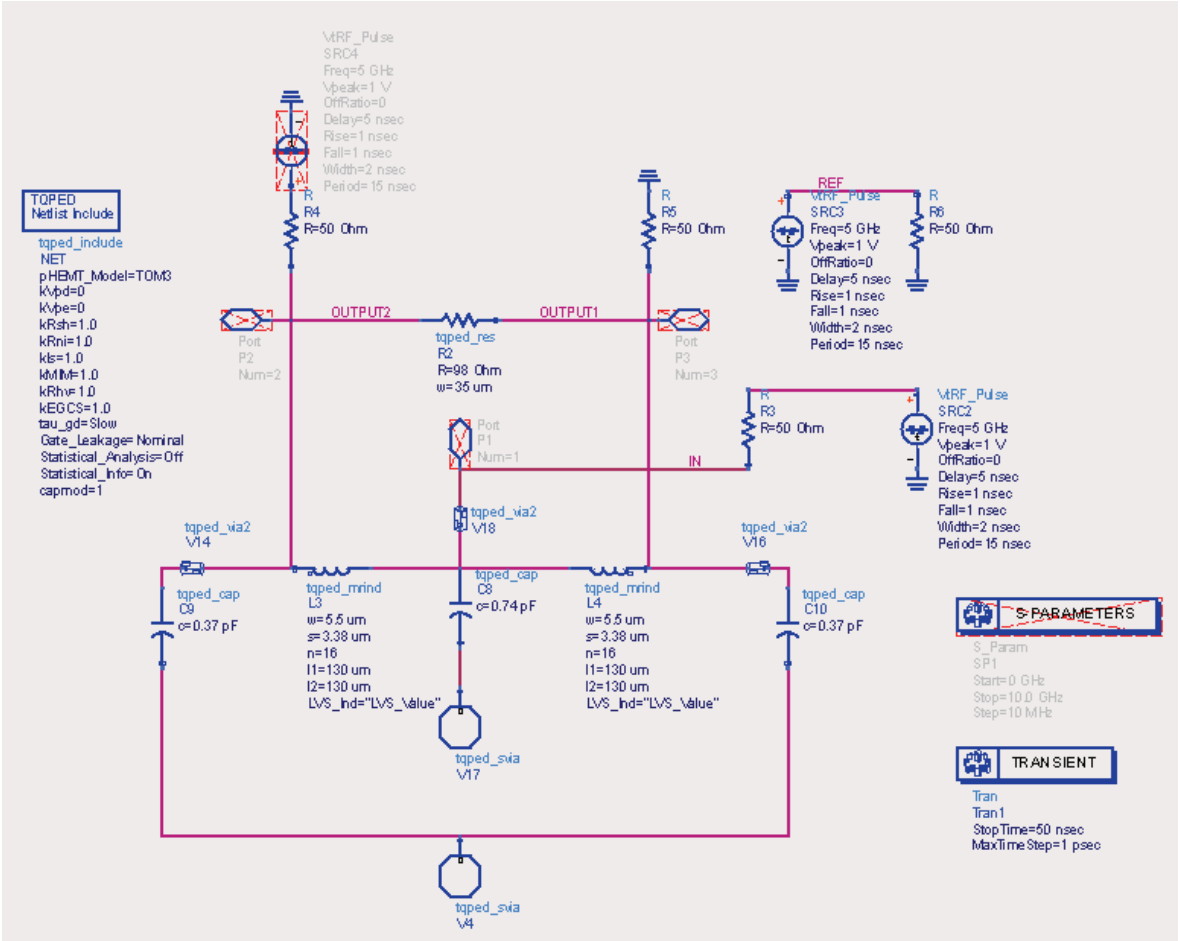

Figure 47: Schematic window setup for the time domain simulations.

The schematic window setup is shown in Figure 47. The component values from the final tuned circuit are used. A 50 ns transient analysis with high resolution is run with a source at either the input or one of the outputs. All signal sources use the same parameters.

Matched Ports

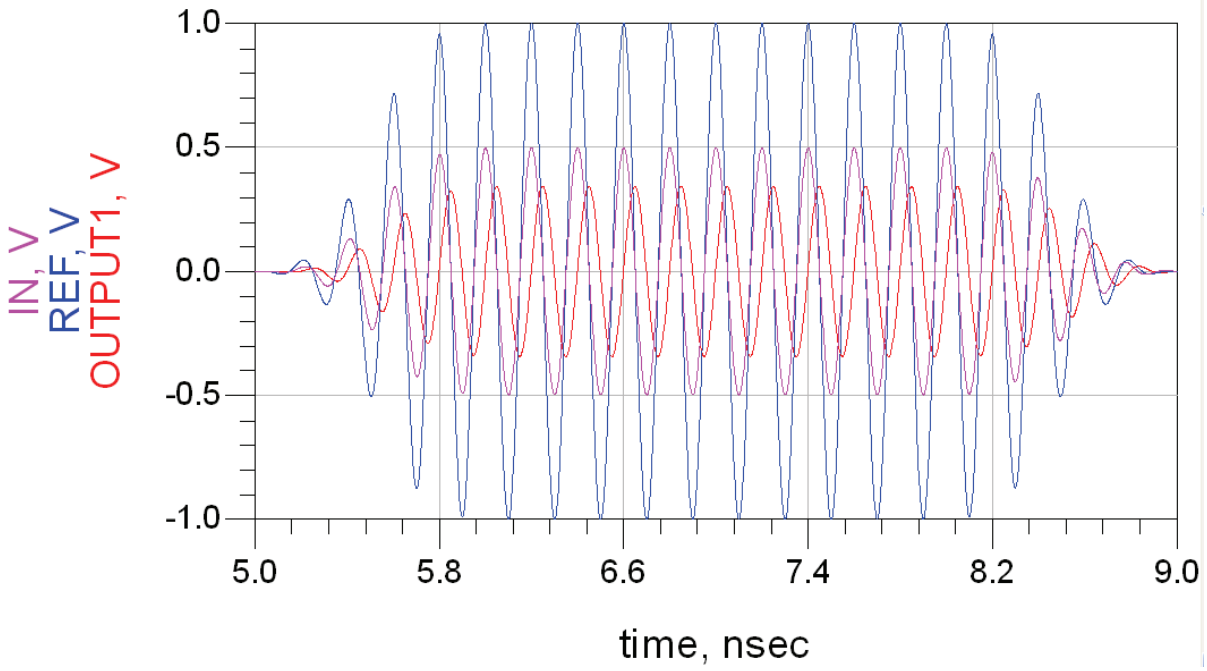

Figure 48: RF pulse applied to input with matched ports.

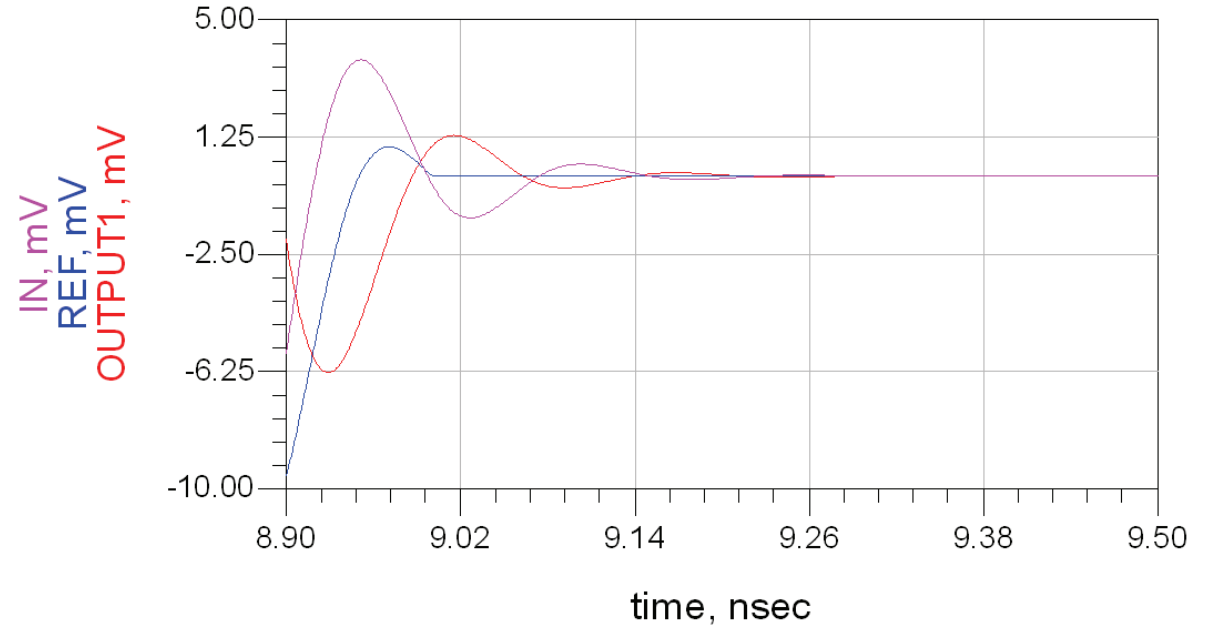

Figure 49: RF pulse applied to input with matched ports. Detailed view of reflections.

Figures 48 and 49 shows the response at the ports with the RF pulse applied to the input port. Only the response at output 1 (port 2) is shown since the response at output 2 is exactly equal. From Figure 48 we can see that the phase difference between input and output is 83.9˚, slightly less than the phase difference of 86.2˚ found in the s-parameter analysis. The probable cause of this difference is that the time domain simulation contains other frequency components than 5 GHz due to transients, and also has small amounts of reflection from

mismatches. This means that the s-parameter result should be most accurate, since this simulation contains only the 5 GHz frequency component.

The voltage at the input is 0.5 V, half that of the supplied voltage, because of the voltage division between the supply and the circuit. At the outputs the voltage is reduced by 156 mV to 344 mV. The current is reduced as well, so that the total power reduction is approximately 3 dB at each port.

From Figure 49 we see that we get multiple reflections after the applied signal is removed (zero volts). These reflections are caused by mismatches. They are quickly reduced to negligible values which indicate that the mismatch is small.

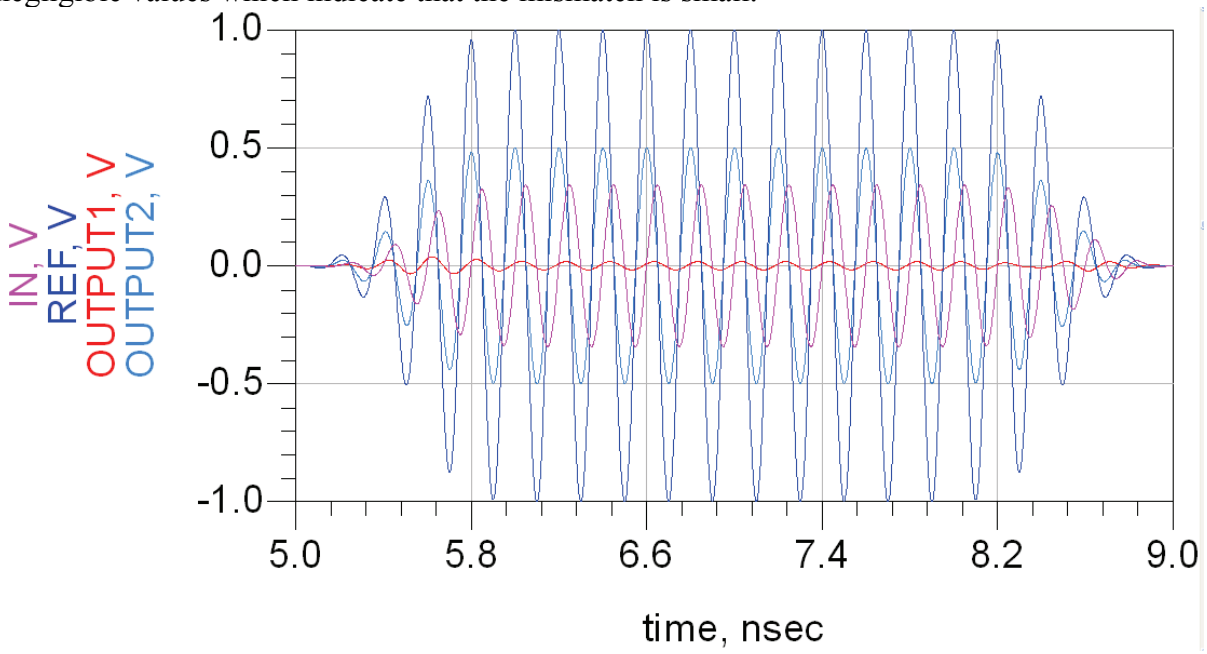

Figure 50: RF pulse applied to output with matched ports.

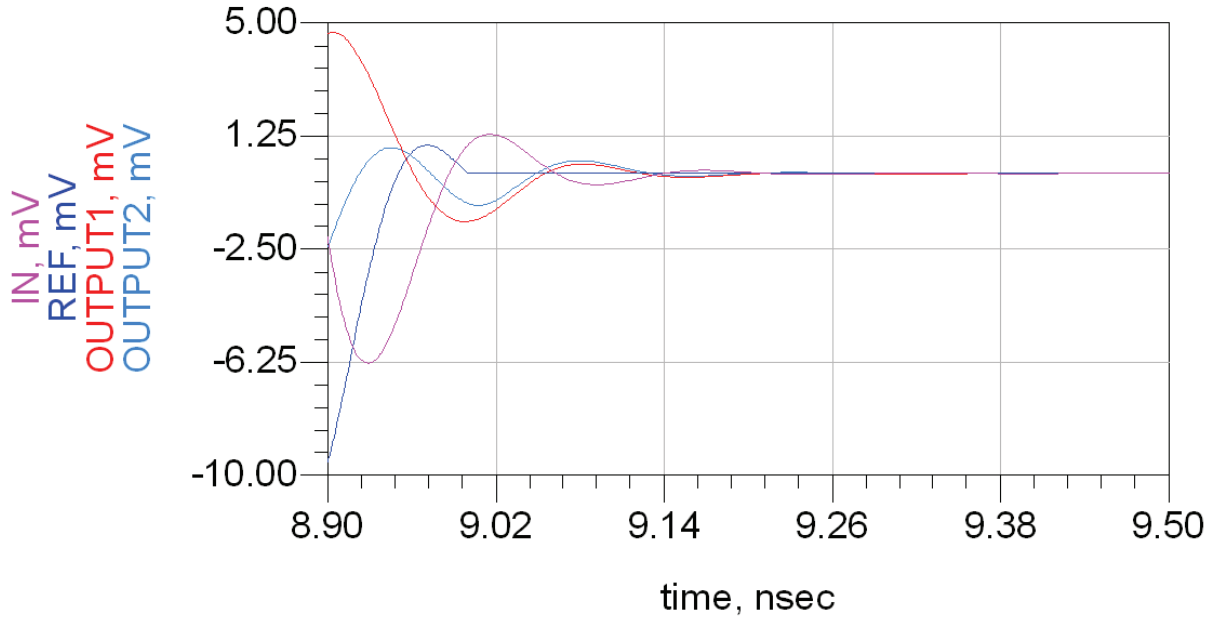

Figure 51: RF pulse applied to output with matched ports. Detailed view of reflections.

Figures 50 and 51 show the equivalent plots with the signal source at output 2. Figure 50 shows that the signal at output 1 is reduced by 471 mV to 31 mV, compared to the signal of 502 mV at output 2. This is a 12 dB reduction in voltage, and shows that the isolation between ports 2 and 3 is good. The signal at the input (port 1) has a 344 mV amplitude.

Mismatched Ports

When the load resistance at port 2 (output 2) is swept from 10 to 100 ohms with the source at the input, we get the results shown in Figures 52 and 53. We can see that, as expected, the voltage swing at the ports depends on the termination resistance. The 100 ohm output resistance give the highest voltage swing at output 2, and the lowest swing at the input, while the voltage swing is nearly constant at output 1, except at the end of the pulse where the 10 ohm termination gives the highest amplitude.

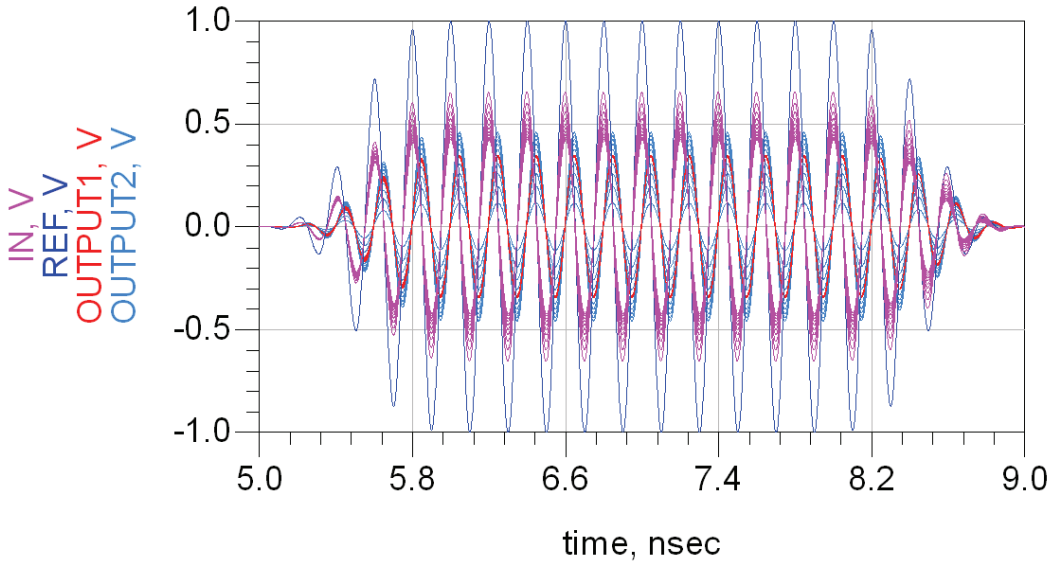

Figure 52: Response with swept output resistance.

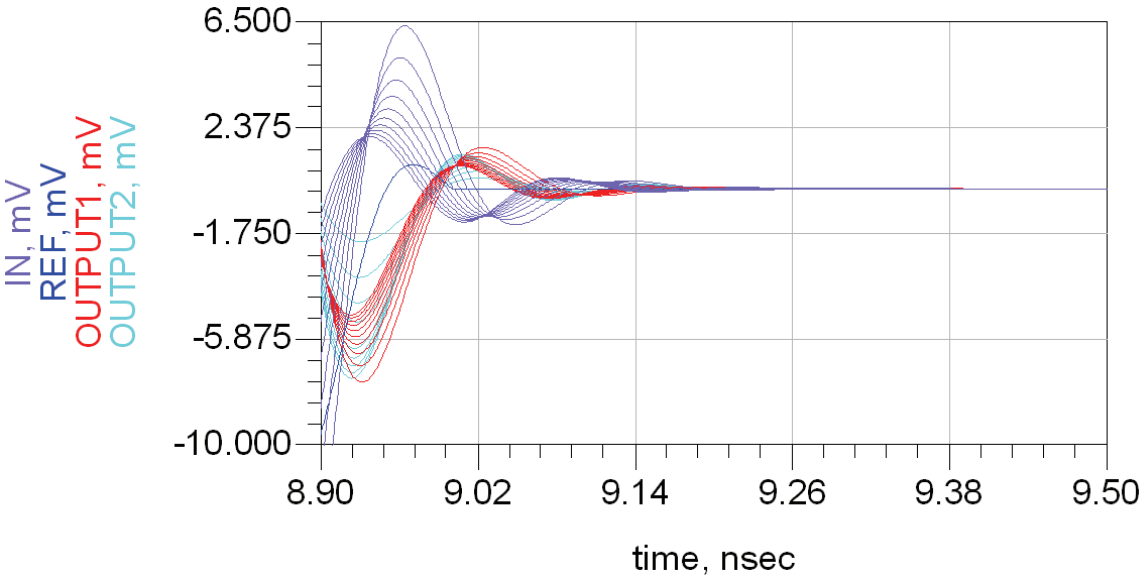

Figure 53: Response with swept output resistance. Detailed view of reflections.

An investigation of the power at all the ports for the various terminations shows that it is highest at output 2 and the input with 50 ohms resistance, and virtually constant for all termination values at output 1. We therefore conclude that a mismatched output leads to reduced power delivered to this port. The voltage and current waves are not necessarily largest with this termination, though.

Output Delay

By putting a delay on the signal at the grounded output we can return the received pulse in the interval between the sent pulses. Figure 54 shows the result when using a 4233˚, 50 Ω delay line. This gives a delay of nearly 5 ns since the signal travels through the line in both directions. We can see from the figure that the amplitude of the returned signal is nearly half that at the input, indicating small losses.

As mentioned in the start of this section, the delay would be difficult to fabricate on the MMIC chip. Special artificial delay lines composed of integrated inductors and capacitors could be one solution to the problem.

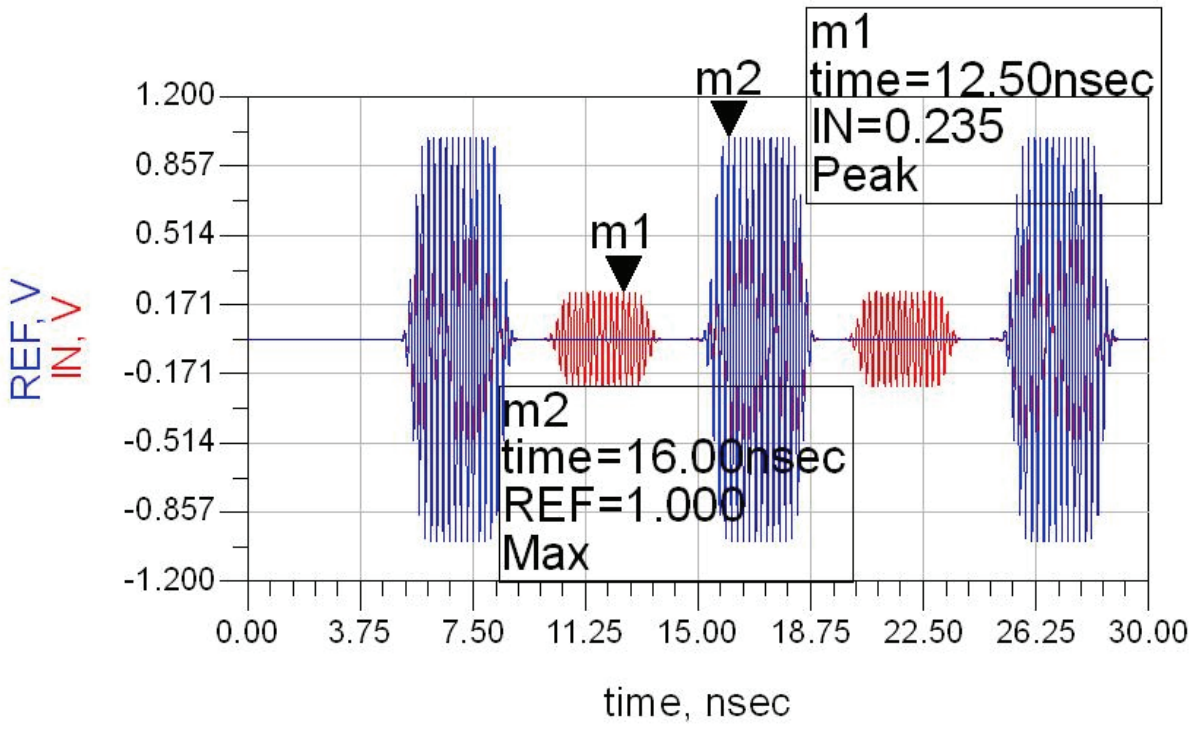

Figure 54: Response of 4233˚ delay line circuit.

Measurements

About the Measurements

As noted earlier, the actual Wilkinson Power Divider circuit could not be produced in time for the deadline of the report. Measurements was instead carried out on single lumped components on test chips already fabricated for the NTNU University, using the same vendor and technology as was intended used for the Wilkinson Power Divider fabrication.

This opened the opportunity to compare ADS simulation results with the measurement results to get an idea of how accurate the produced circuit response would have been, and also see how the ADS settings (like mesh resolution) affects the accuracy of the simulation results. It was also important to get the practical experience of making microwave frequency measurements using probe station and automatic network analyzer (ANA).

Performing the Measurements

The measurements was done using an Cascade Microtech Summit 9000 probe station and an Hewlett Packard 8510C ANA controlled by a remote computer running the WinCal XE software from Cascade Microtech, Inc. The Measurements section of the Tools Chapter shows pictures of the actual probe station and network analyzer that was used for the measurements in this report.

First the small chips was placed on the wafer stage, and held in place by a vacuum. The probe tips were placed on the appropriate pads using the microscope and precision controlled probe arms. When the probe tips made contact with the pads they were slid along the surface a small distance to make sure there was good electrical contact with the gold pads. The probes were roughly centred on the pads. It is important that the same procedure is followed when making all the probe-to-pad connections to get consistent results.

The WinCal software runs on the Windows platform, and makes it easy to do accurate measurements using the ANA. It offers a user-friendly graphical interface for doing the ANA setup (i.e. setting the frequency range), makes it easy to compare measurement results and offers an automatic calibration routine.

After setting the proper parameters, like the probe brand and model and type of calibration i.e. SOLT (short-open-line-through), we ran the auto calibration routine. This makes the calibrations very easy since the program tells you where to place the probes (i.e. open) and then automatically sends the calibration data to the ANA and tests whether the calibration results is adequate. After calibration the effects of all the systematic errors, like the effect of the probes is removed, so that the measurement results reflects (ideally) only the actual circuit.

Eight different components, located on two separate chips, were measured. The layout of these chips can be seen in Appendixes A4 and A5. On the layout of Appendix A4, the SOLT

calibration method was used, while a separate calibration chip had to be used for the other layout, since this contained no calibration components.

The calibration components used determines the reference plane of the measurements. Only the parts of the measured circuit beyond the reference plane of each port affect the measurement results. This means that the effect of the transmission lines on the inductors on the layout in Appendix A4 does not affect the measurements, and only the influence of the component itself is considered. The reference plane has to be equal in the simulations to get comparable results.

Since a separate chip had to be used in the calibration for the measurements of the layout in Appendix A5, the reference plane was not correct. This means that the transmission lines that connect the ports to the inductors influence the measurements.

S-parameter Results

Single Inductors

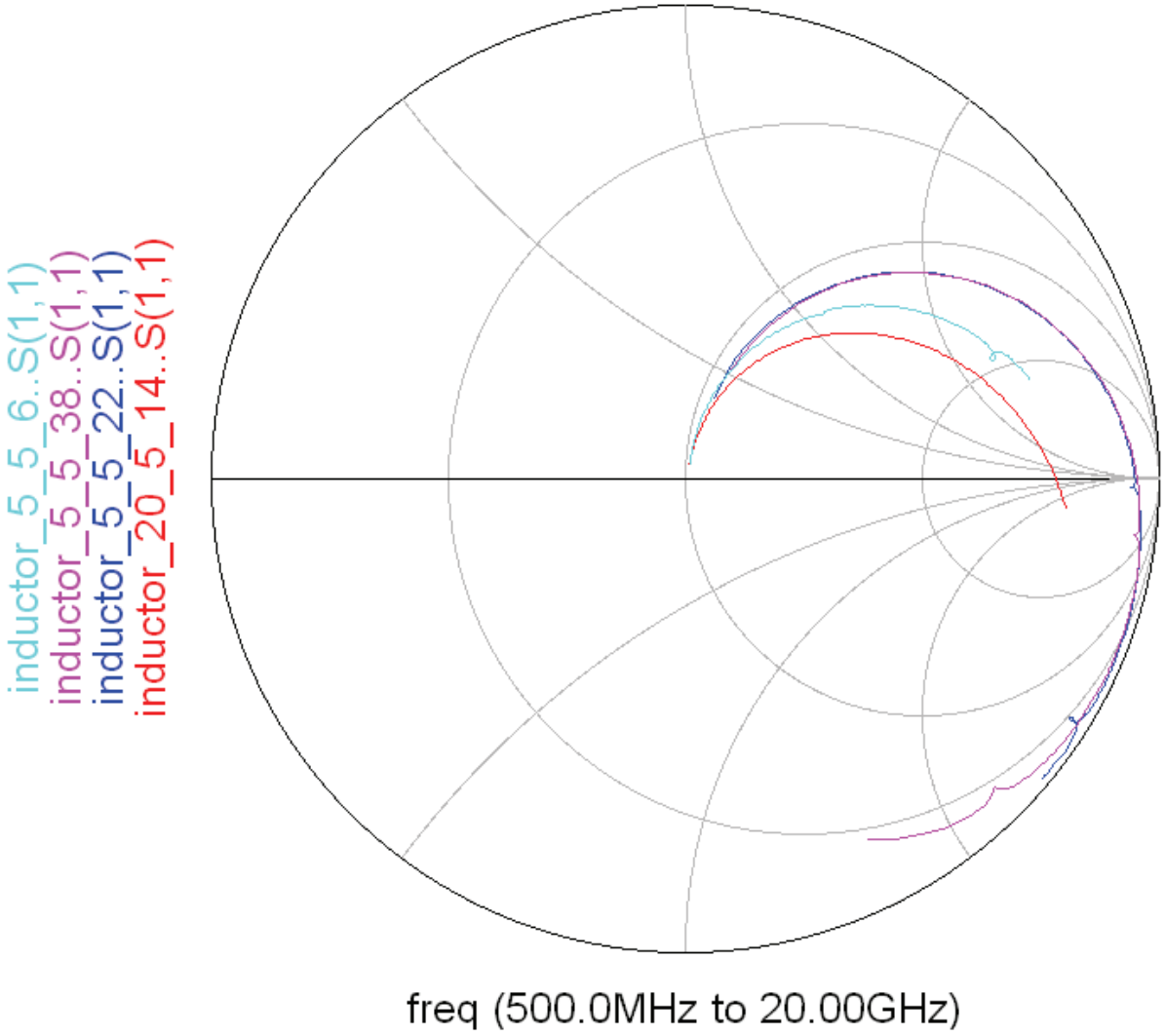

Figure 55: Smith chart showing the measured S_{11} parameters plotted in a Smith Chart.

Figure 55 shows S_{11} from all the four measured inductors on the layout of Appendix A4 plotted in the same Smith Chart, while Figure 56 shows the S_{21} parameters.

From Figure 57 it is easy to see that three of the inductors experience resonance due to the parasitic capacitance, mainly between consecutive turns. The resonance is in parallel, meaning that the resistance at resonance is (theoretically) infinite (see Figure 58). The resonance frequency depends on the construction of the inductors. When constructing inductors, a high resonance frequency is often an important goal since it must be used at frequencies well below the resonance.

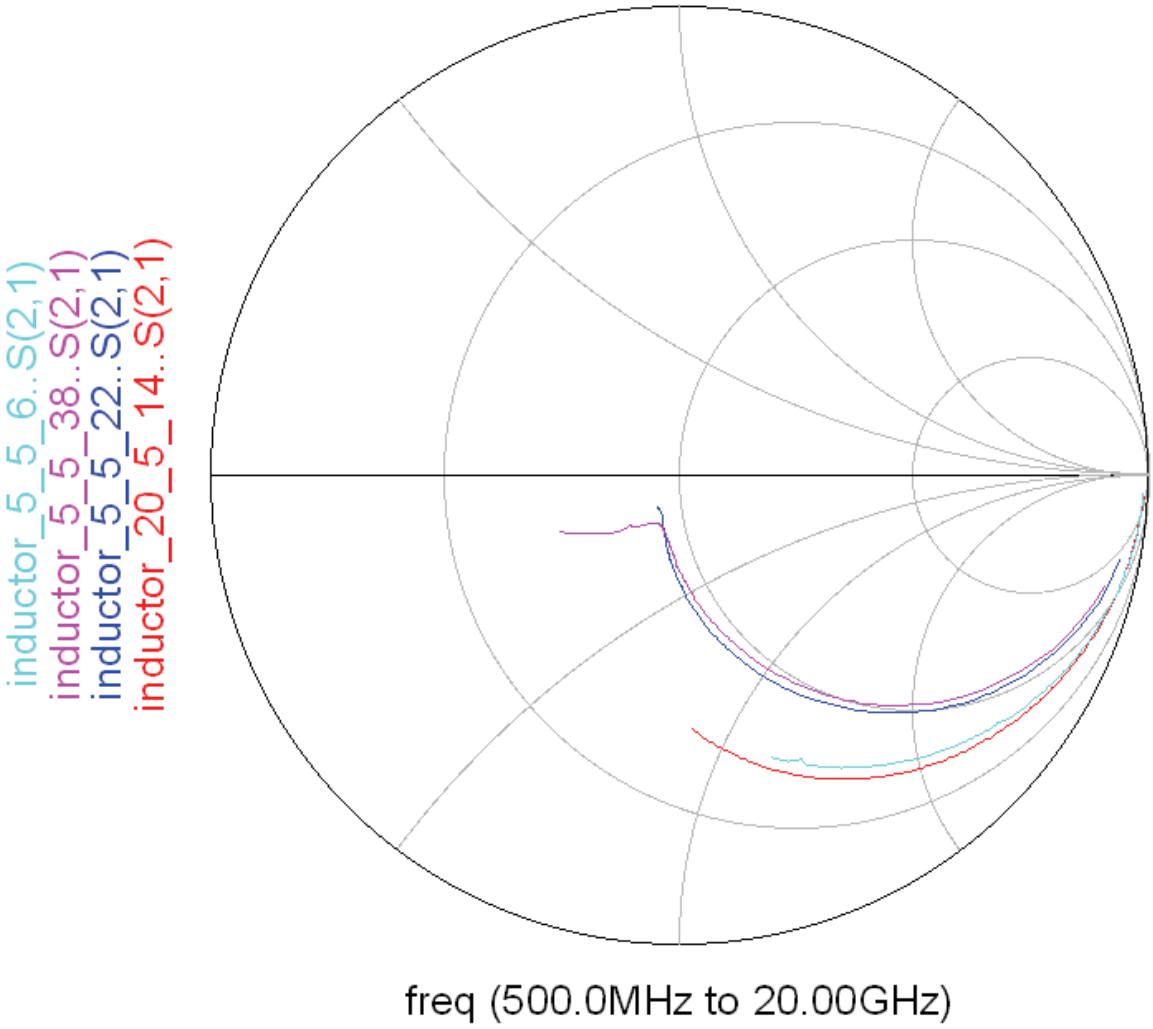

Figure 56: All S_{21} parameters plotted in the same Smith Chart for comparison.

From Figure 57 we can see that the inductor 2 (see Appendix A4) has the lowest resonance frequency, while inductor 1 has no resonance in the measured frequency range (0.5 to 20 GHz). This makes sense since inductor 2 has 38 segments, while inductor 1 only has 6 segments, giving a much lower parasitic capacitance.

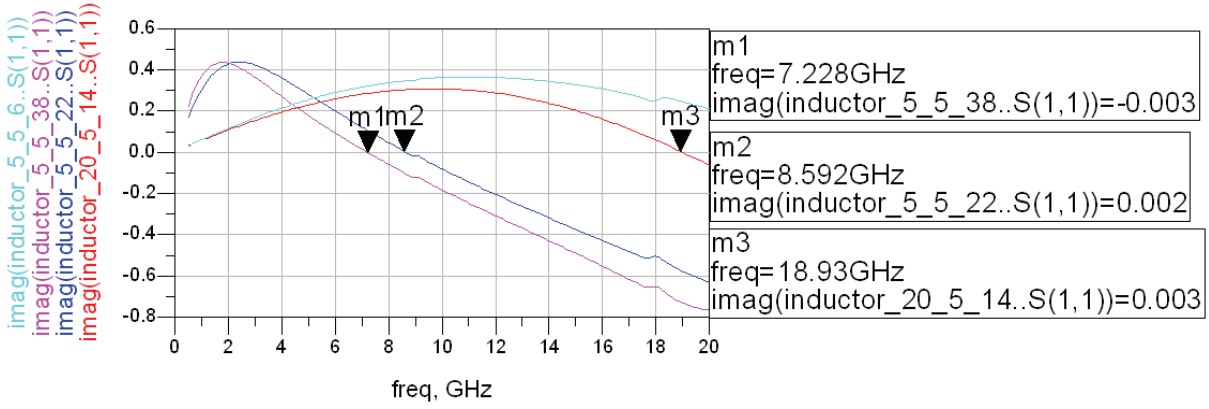

Figure 57: Plot of the imaginary values of the (normalized) s-parameters, along with the resonance frequencies.

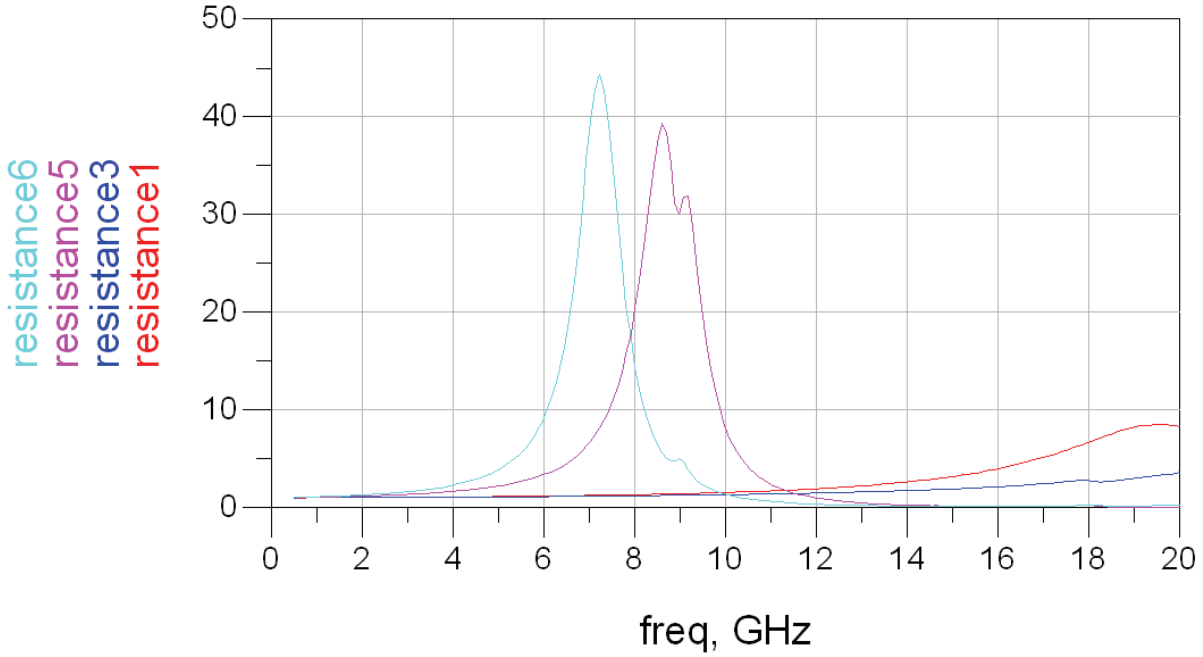

Figure 58: Resistance values of all the inductors plotted in the same diagram.

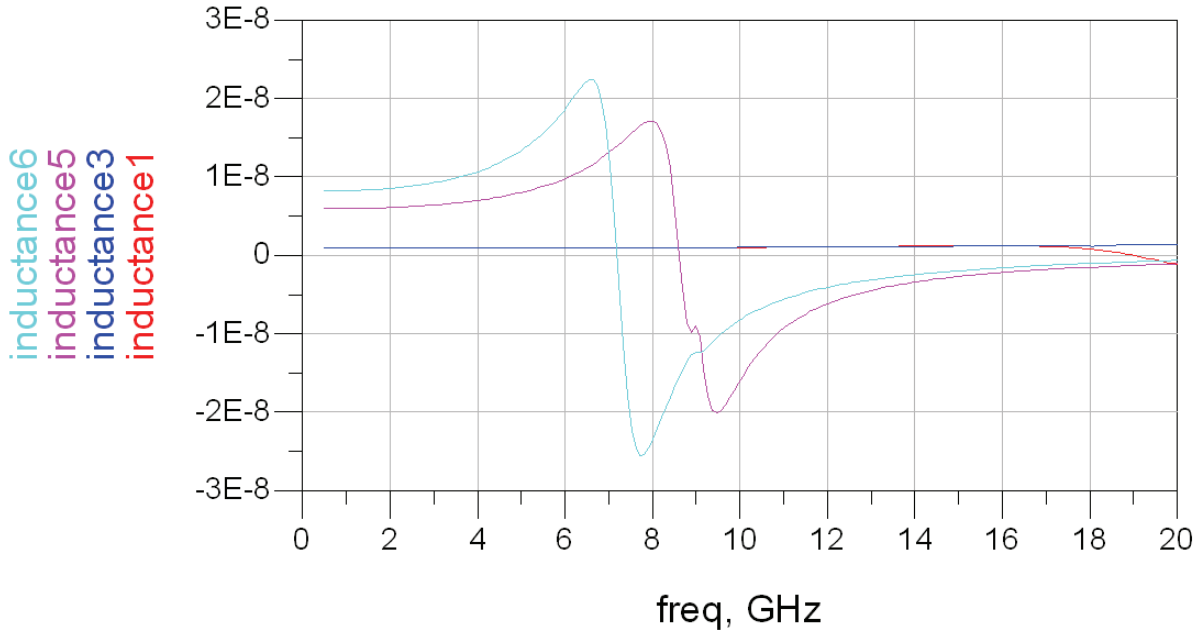

Figure 59: Inductance values of the inductors over the whole frequency span.

Figure 59 shows how the inductors inductance varies over the frequency range. A negative value indicates that it behaves as a capacitor. Inductors 2 and 3 have relatively low resonance frequency. Inductor 2 should therefore only be used up to about 3 GHz while inductor 3 can be used up to 5 GHz. Beyond these frequencies the inductance is very much prone to process variations.

The resistance plot of Figure 58 shows that the resistance of the inductors is fairly small, except at parallel resonance where the resistance increases sharply.

It is interesting to note that inductor 1 has slightly higher inductance and lower resistance over the whole frequency span than inductor 4. Since they occupy the same area on the chip, this indicates that the construction of inductor 1 is a better solution than that of inductor 4, except where the extra current carrying capacity of inductor 4 is needed. Leaving a free area in the centre of the inductor is normally wise because the effect of the most central segments on the inductance is small, while eddy currents running through these segments leads to increased resistance.

Coupled Inductors

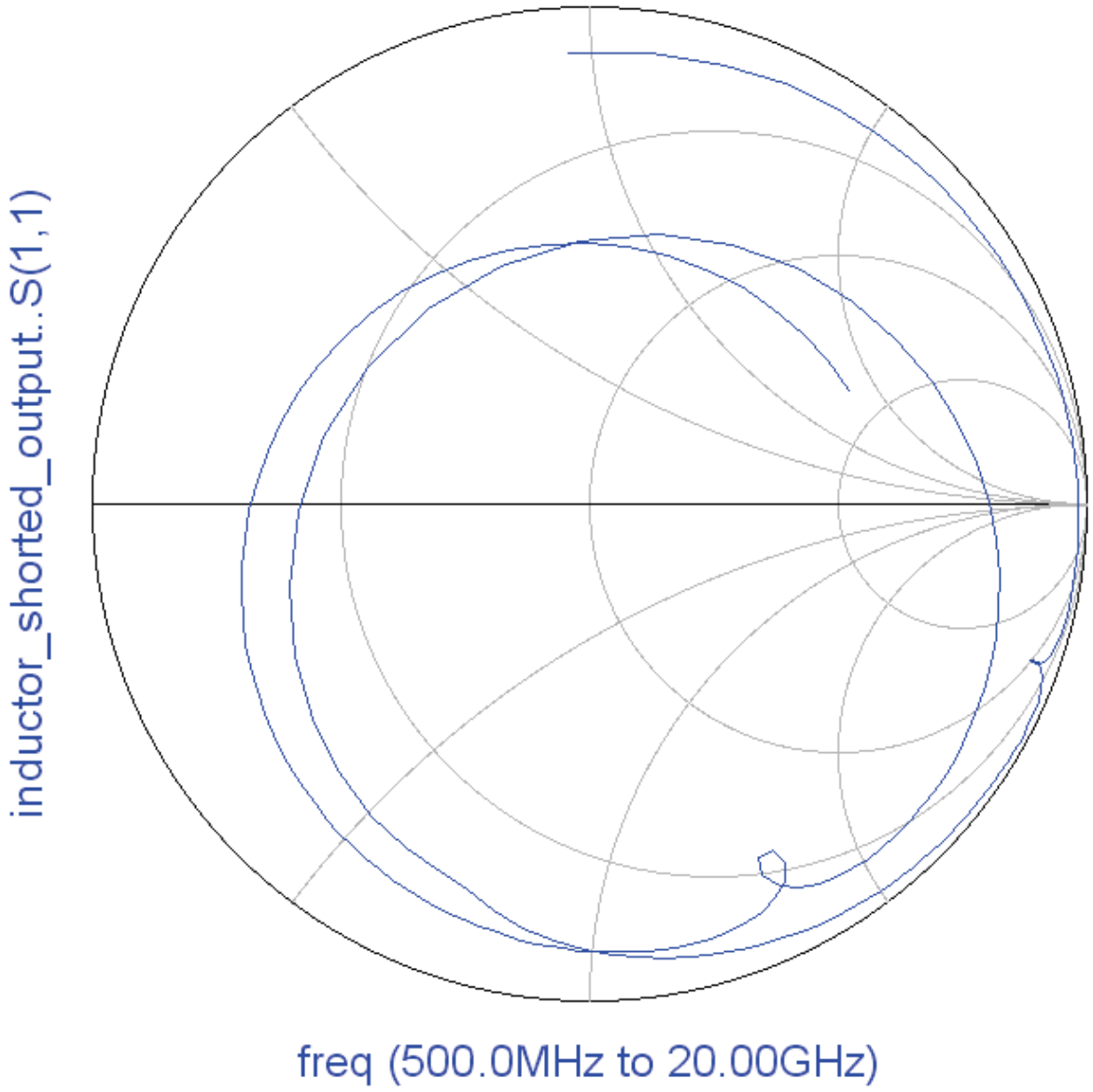

Figure 60: Smith Chart showing s-parameters of a single inductor with shorted output.

To see the effect of electromagnetic coupling between near-by inductors and what effect the separation distance has on the coupling, we performed measurements on two sets of near-by inductors. One pair had a separation distance of one line width, while the other had a separation of three line widths. The layout can be seen in Appendix A5.

The S11 parameters of a single inductor with one of the outputs shorted to ground can be seen in the Smith Chart of Figure 60 while Figure 61 shows the phase plotted separately which makes it easy to inspect the resonance frequencies.

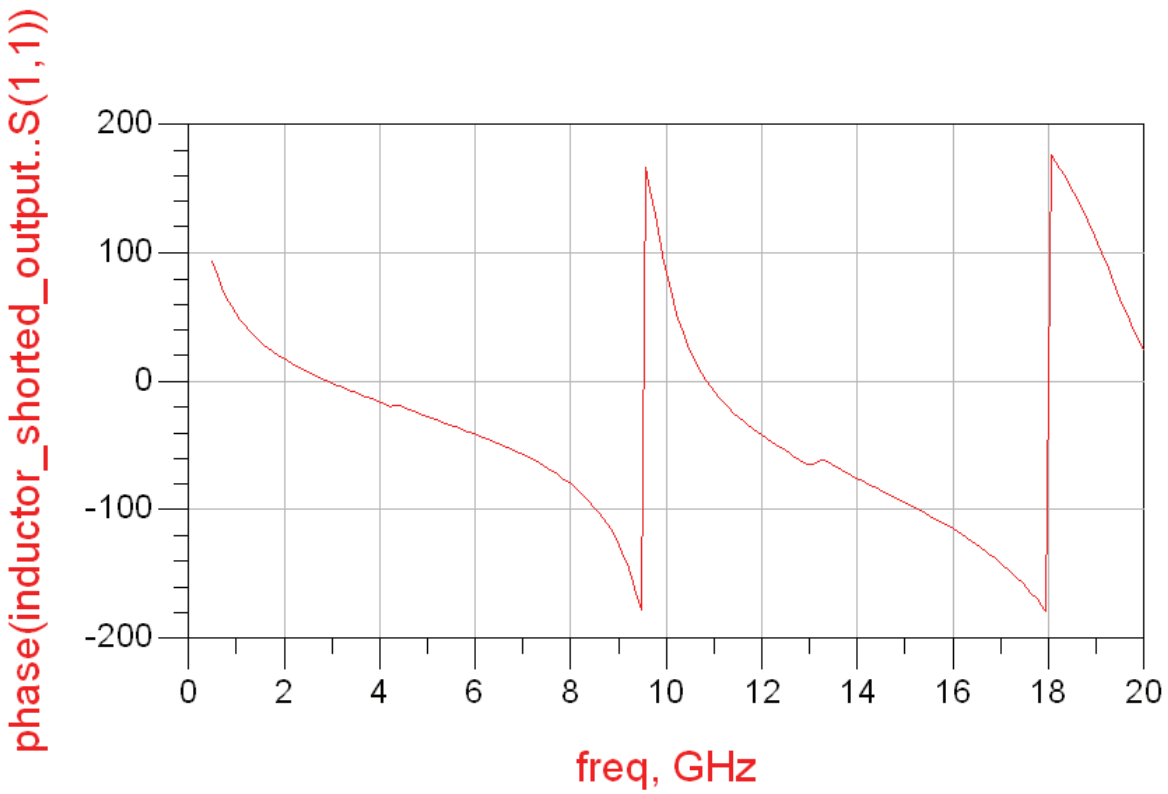

Figure 61: Phase plot of a single inductor shows the resonance frequencies clearly.

The effect that the separation distance has on the electromagnetic coupling can best be seen from Figures 62 and 63. We can clearly see that increased separation between the components gives a reduced coupling over the whole frequency range, and that the coupling can be relatively strong for large and near-by inductors. This is caused by their large surrounding magnetic field.

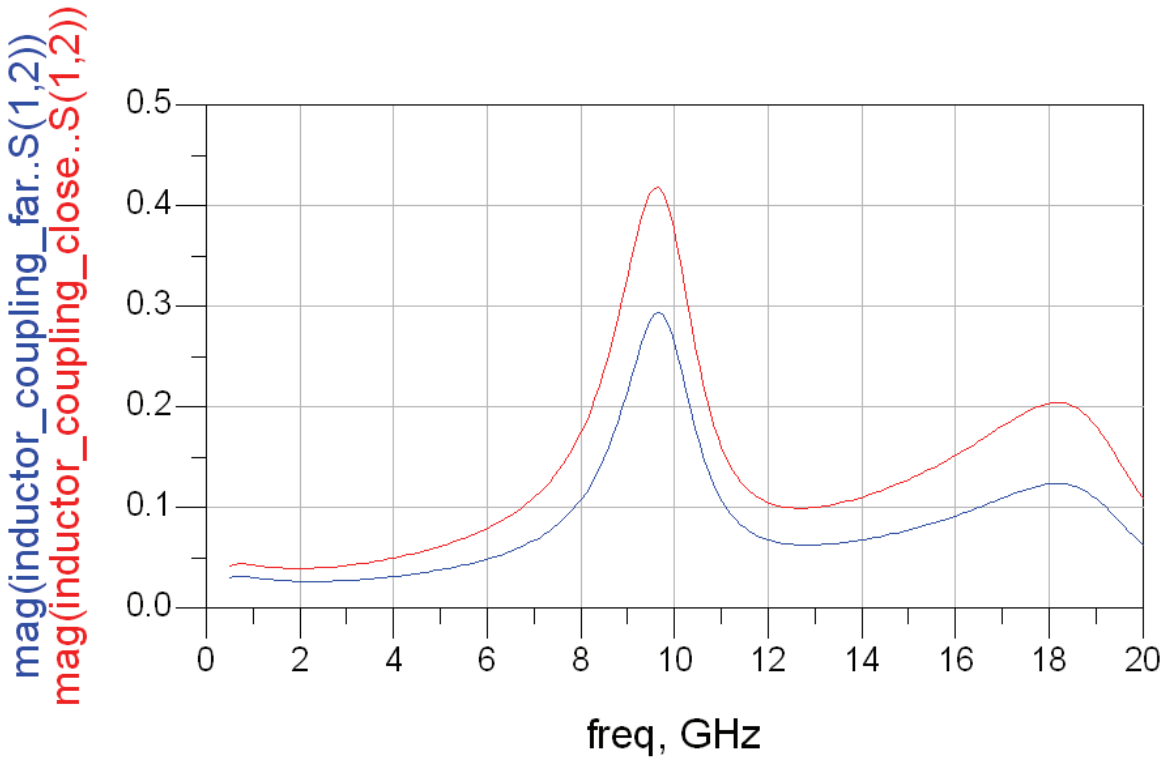

Figure 62: Magnitude of S_{21}.

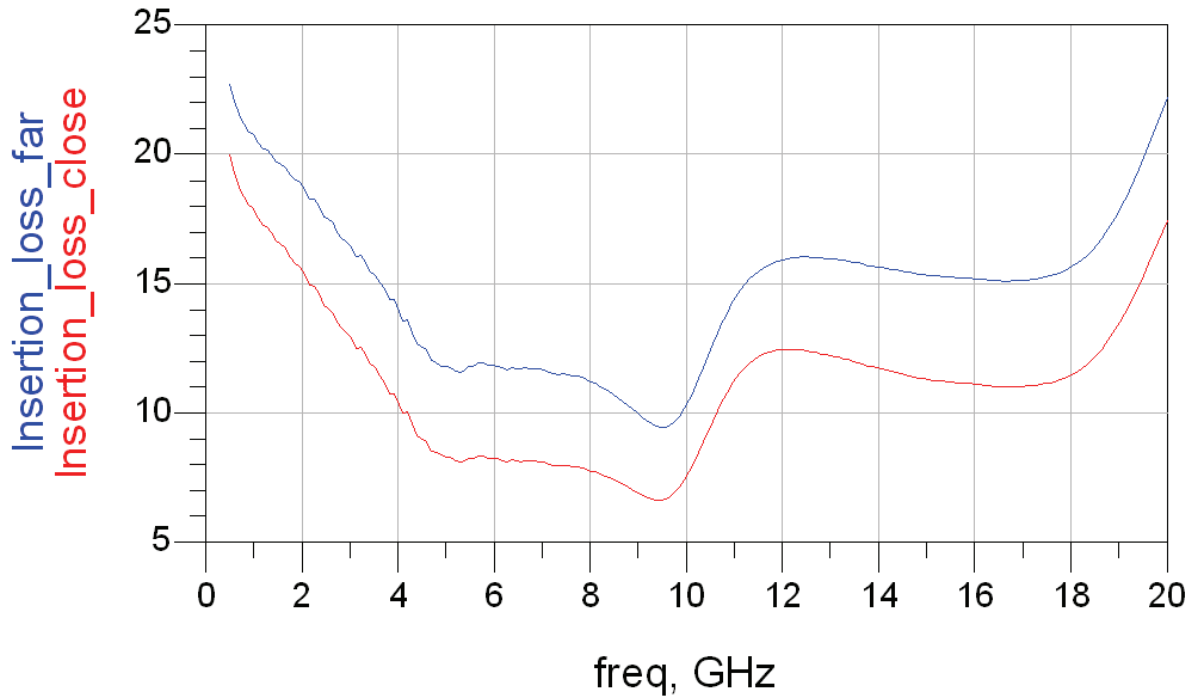

Figure 63: Insertion loss for both coupling measurements.

The separation distance will not be as critical for smaller inductors, which has less powerful magnetic fields around them. Neither will other types of passive components, like capacitors experience the same amount of coupling, though it can not be ignored for capacitors with small separation distance.

The lesson from these measurements should be that components that are susceptible to electromagnetic coupling should be placed as far apart as the available space permits. As mentioned earlier (see [10]) the orientation of the inductors also plays a role in the magnitude of the coupling since opposite or equal current directions influence the coupling.

The inductor with shorted output is resonant at four frequencies in the simulated frequency range. This occurs at 2.9, 9.5, 10.8 and 18.0 GHz. Two of the resonances have a phase of 0 while the other two has an 180˚ phase. We have the best match (closest to the centre of the Smith Chart) at 9.8 GHz. This is the frequency where most of the energy is delivered to the inductor, and not reflected.

The coupling between both the close and far apart coupled inductors is strongest at 9.7 GHz and has a peak at 18.2 GHz. This is close to the resonant frequencies of the single inductor, where the inductor appears as a short (with some resistance) to ground, feeding the signal back in antiphase. A simple equivalent drawing of the two inductors is shown in Figure 64. At resonance the energy fed to the inductors will oscillate between being stored in electric and magnetic form.

This means that coupling will be strongest near the resonance of both inductors. The input matching of the inductors also matters since poorly matched inductors reflects most of the applied signal.

Figure 66 on the next page shows the S_{21} parameter for both measurements plotted in the same Smith Chart.

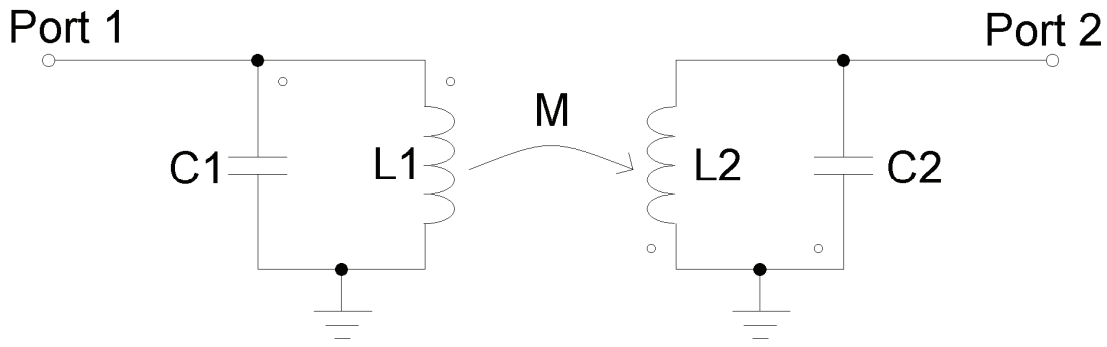

Figure 64: Equivalent circuit diagram of two near-by inductors.

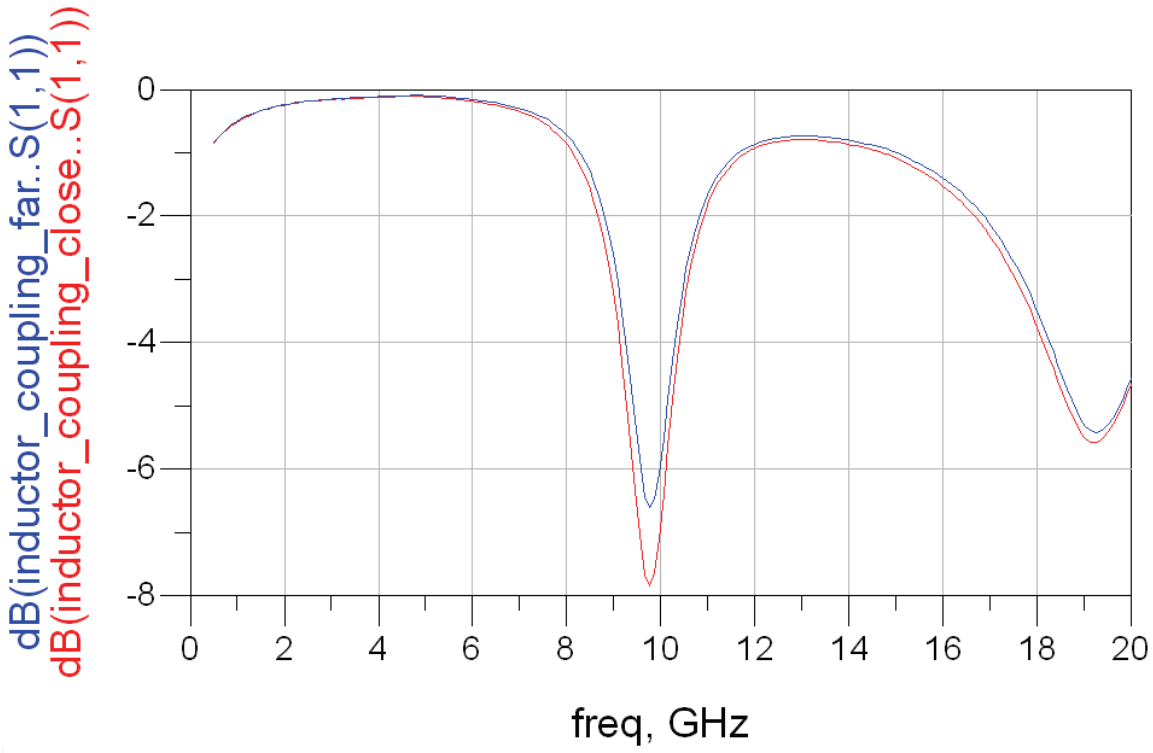

Figure 65: Decibel value of S_{11} for both measurements.

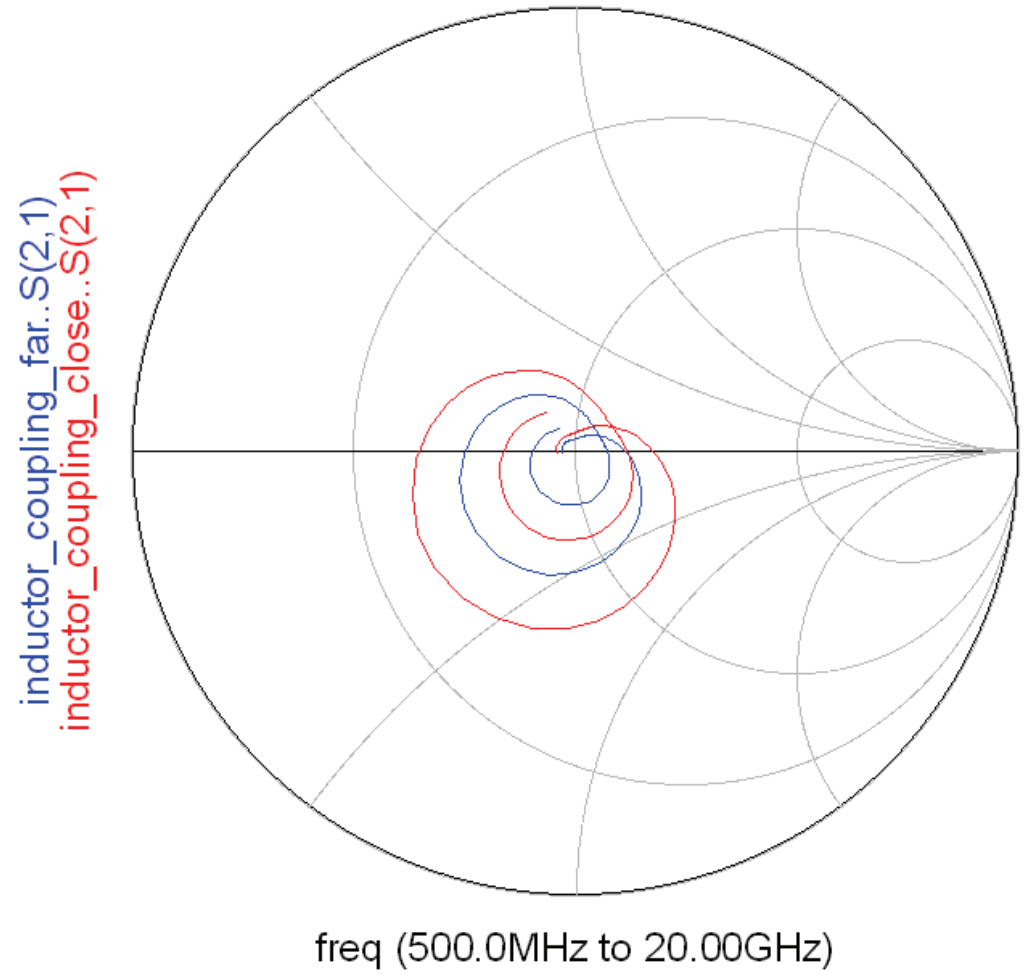

Figure 66: The coupling (S_{21}) of both measurements.

Simulation Results

To be able to compare the measurement results with ADS Momentum- and model results, s-parameter simulation was performed on the same components that we measured in the laboratory. It was then possible to compare the results, and assess the agreement between ADS Momentum simulation and the supplied model from TriQuint and the results obtained from the practical measurements. Comparison is done under the Conclusion Chapter at the end of the report.

Single Inductors

All four single inductors is simulated both from the schematic window, using a model from the manufacturer (TriQuint), and directly from the layout of the component, by the Momentum simulation. The probe pads and transmission line leading up to the component is removed to get the same reference plane as in the measurements. A meshing of 20 cells/wavelength with automatic size edge mesh, thin layer overlap extraction and mesh reduction is used for all Momentum simulations. All simulations use the same frequency span as the measurements (500 MHz to 20 GHz). This is true also for the coupled inductors in the next section.

Figures 71 and 72 plots the Momentum and TriQuint model S_{11} results in the same rectangular plots. As we can see, the results agree fairly well. The decibel values are reasonably close, except for inductor 3 (w=5, s=5, n=6) where there is a clear deviation between the Momentum results and the modelled results. The phase plot of Figure 72 also shows a good agreement between the Momentum phase and the model phase, but the deviation between the two results seems to get larger at higher frequencies, though.

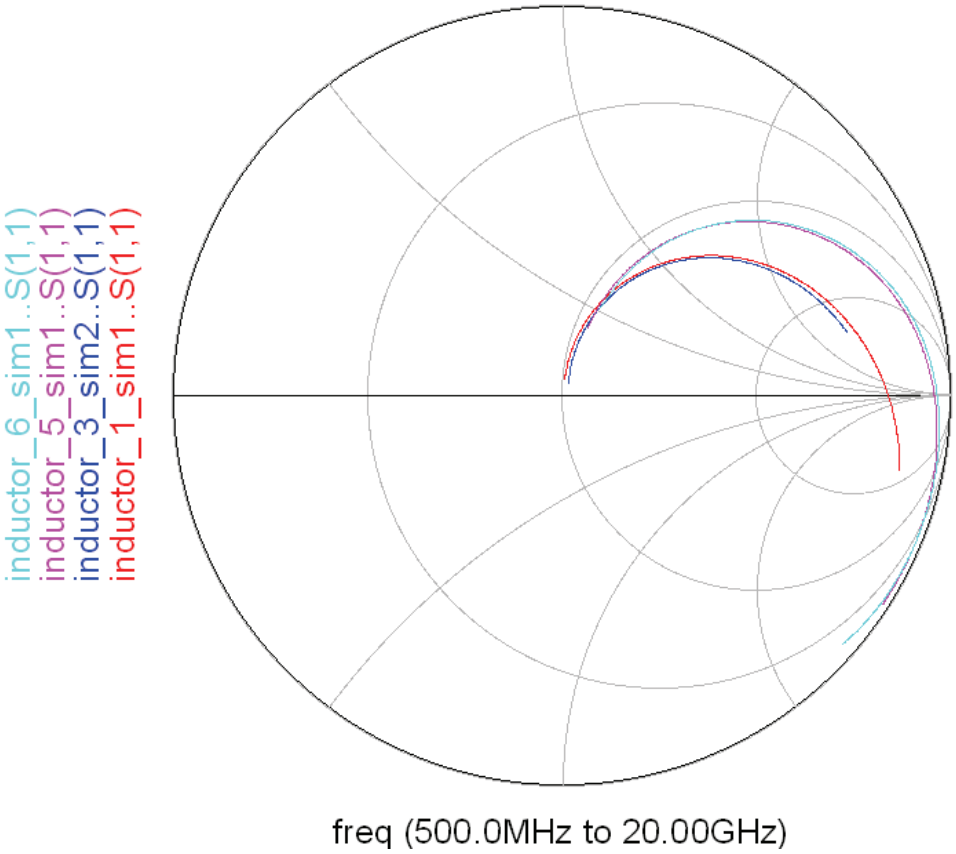

Figure 67: Inductor model S_{11} parameters plotted in Smith Chart.

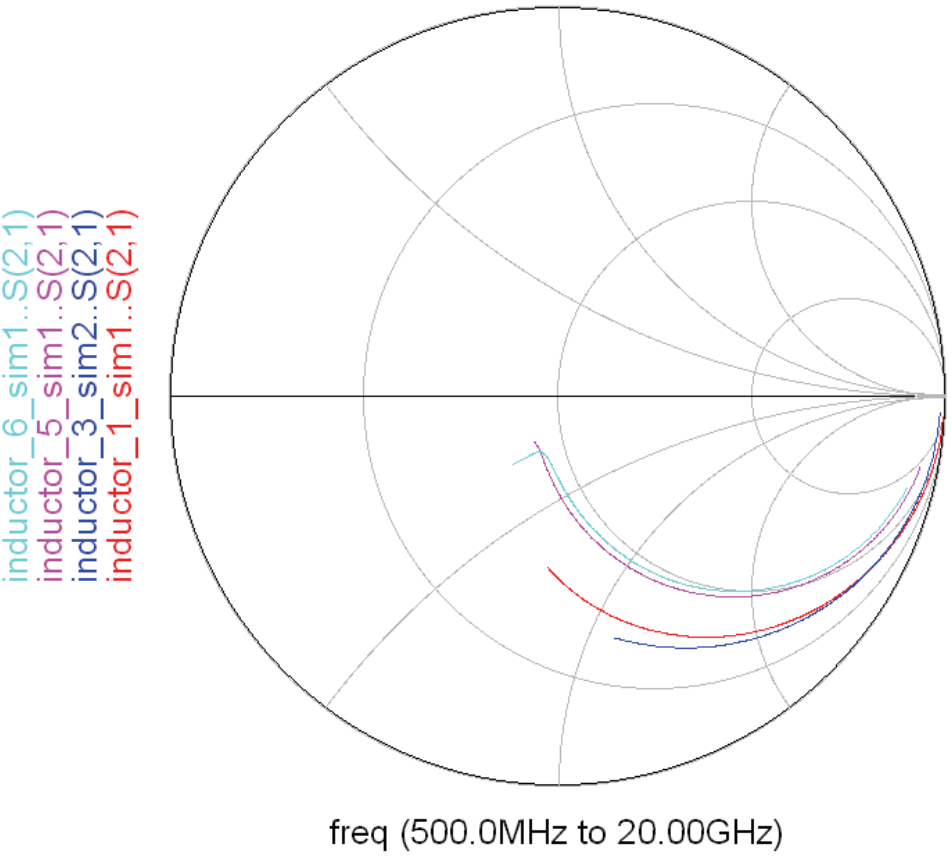

Figure 68: Inductor model S_{21} parameters plotted in Smith Chart.

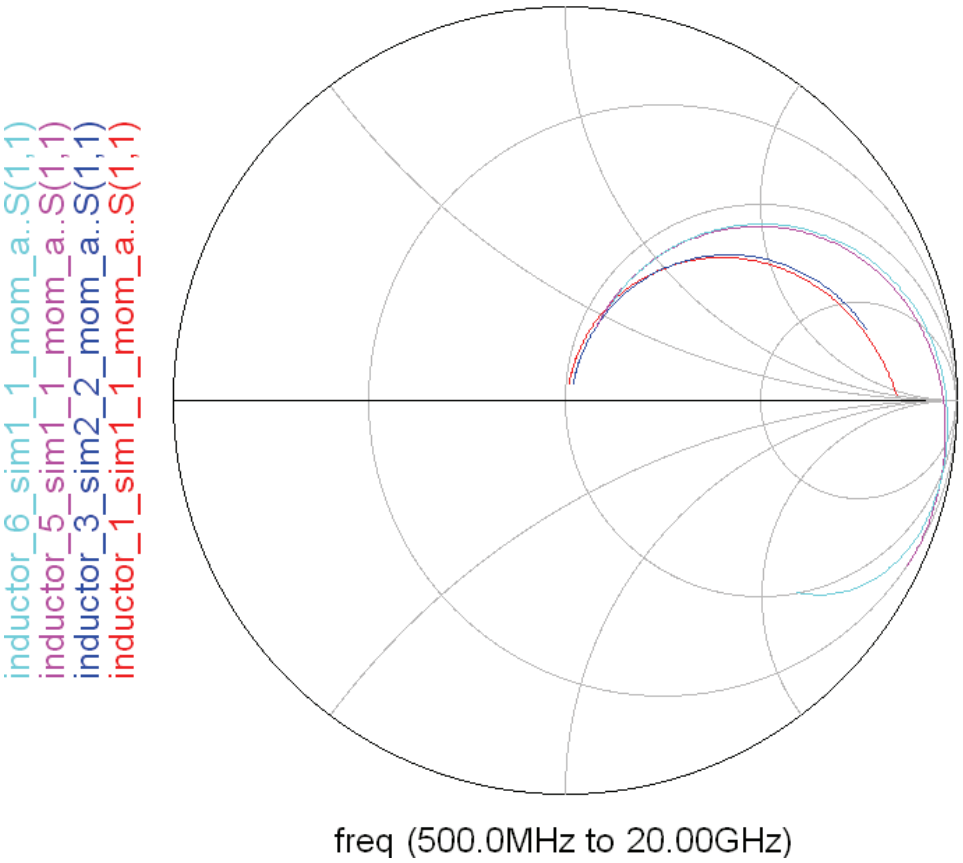

Figure 69: ADS Momentum simulation S_{11} parameters plotted in Smith Chart.

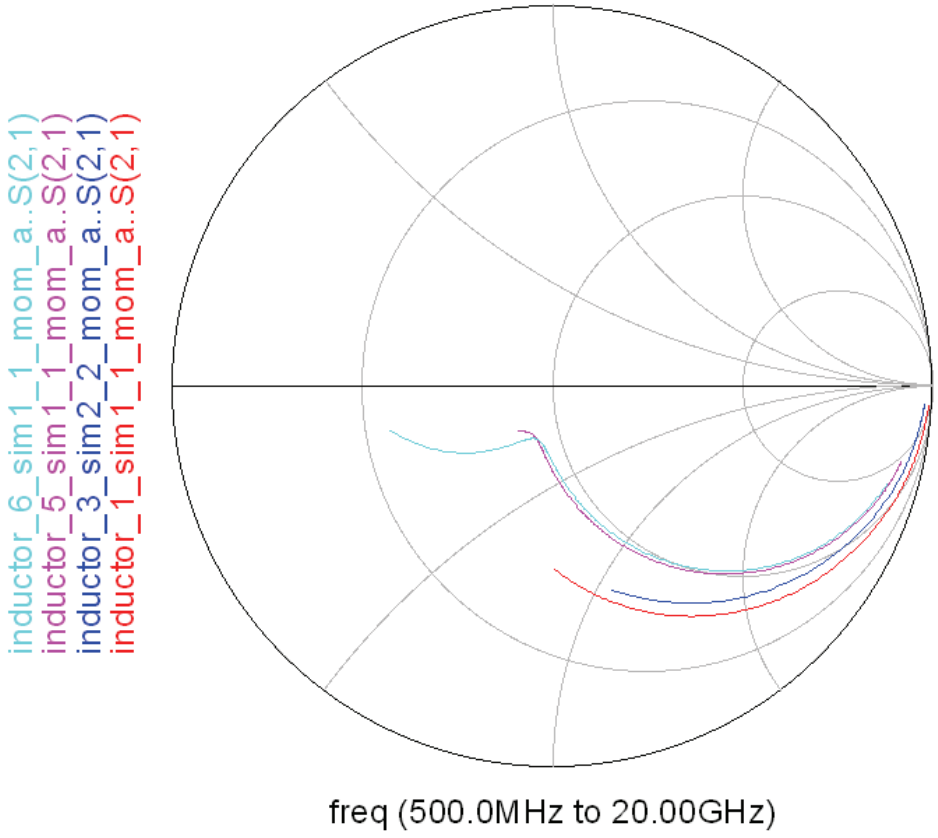

Figure 70: Inductor model S_{21} parameters plotted in Smith Chart.

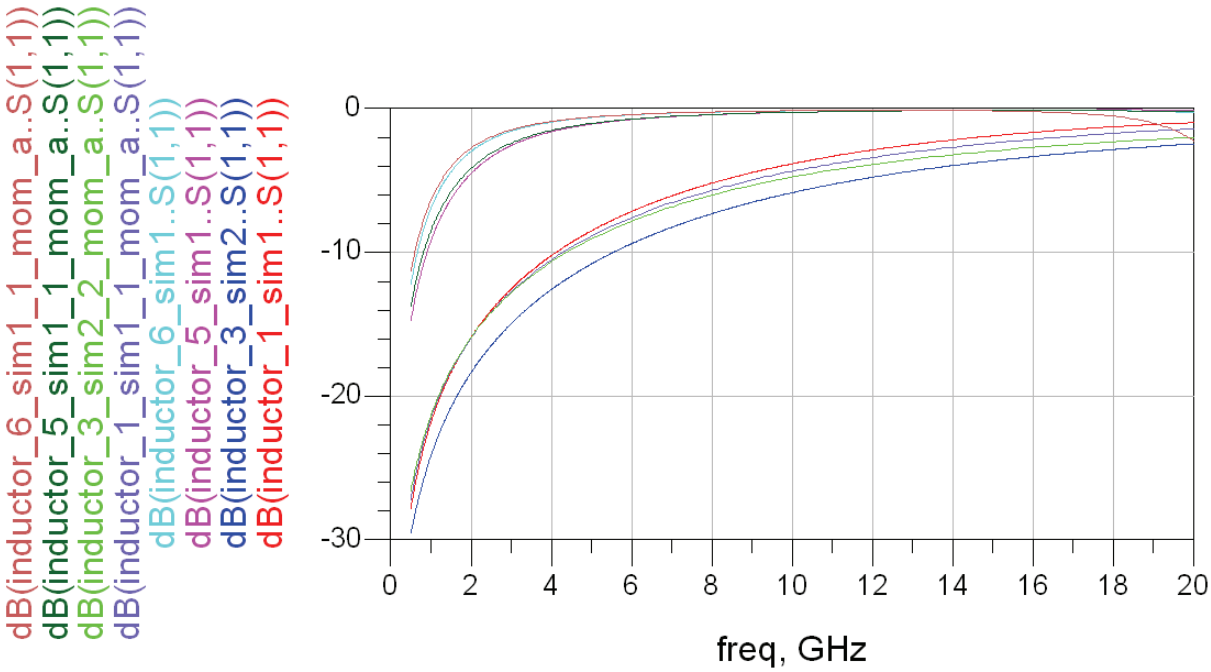

Figure 71: Decibel plot of all Momentum and model S_{11} values.

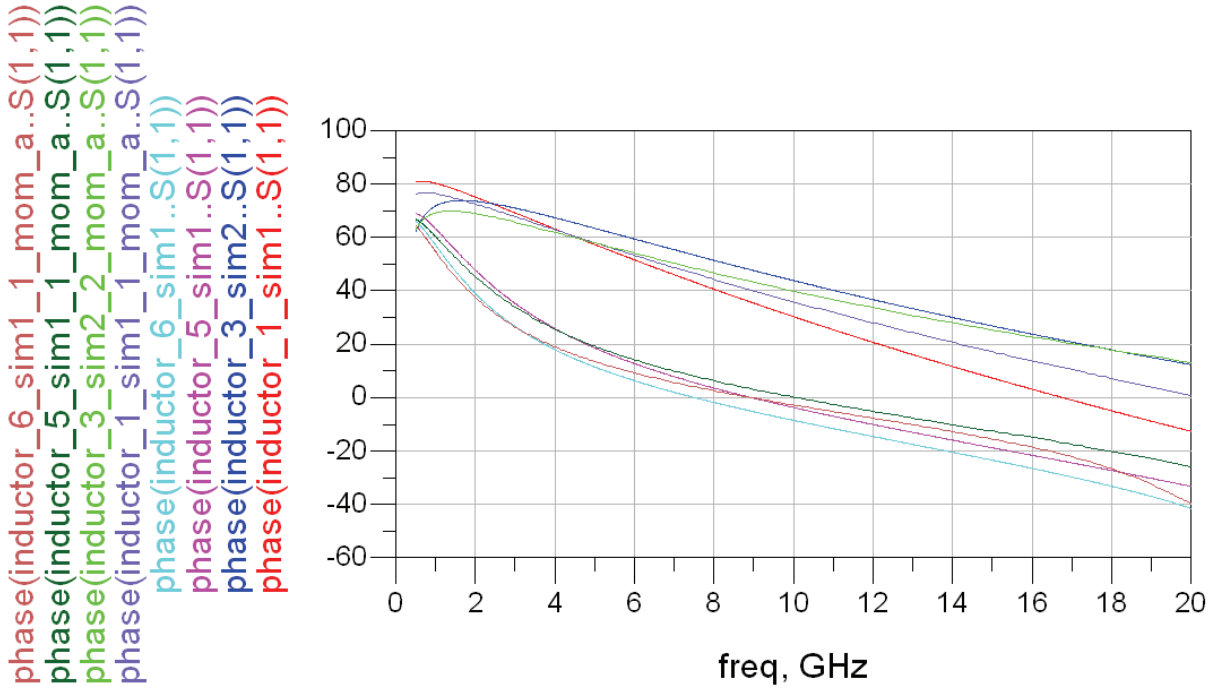

Figure 72: Phase plot of all Momentum and model S_{11} values.

Coupled Inductors

Since two near-by inductors featured in the Wilkinson Power Divider design, it was of interest to study the effect of coupling between closely positioned inductors. The setup can be seen in Appendix A5. There are two variants of inductor coupling. The same inductors with grounded output are used in both setups. A spacing of one line width is used in one setup, while a separation distance of three line widths is used in the other. This allows us to study both the frequency dependence of the coupling and the dependence upon distance between the elements.

Below, the simulation results from ADS Momentum is plotted in both rectangular form (decibel and phase) and Smith Chart. We can see that the inductor is clearly best matched to the 50 Ω source at 9.5 (and 17.7) GHz. It also has four resonant frequencies at; 3.1, 9.3, 10.6 and 16.8 GHz.

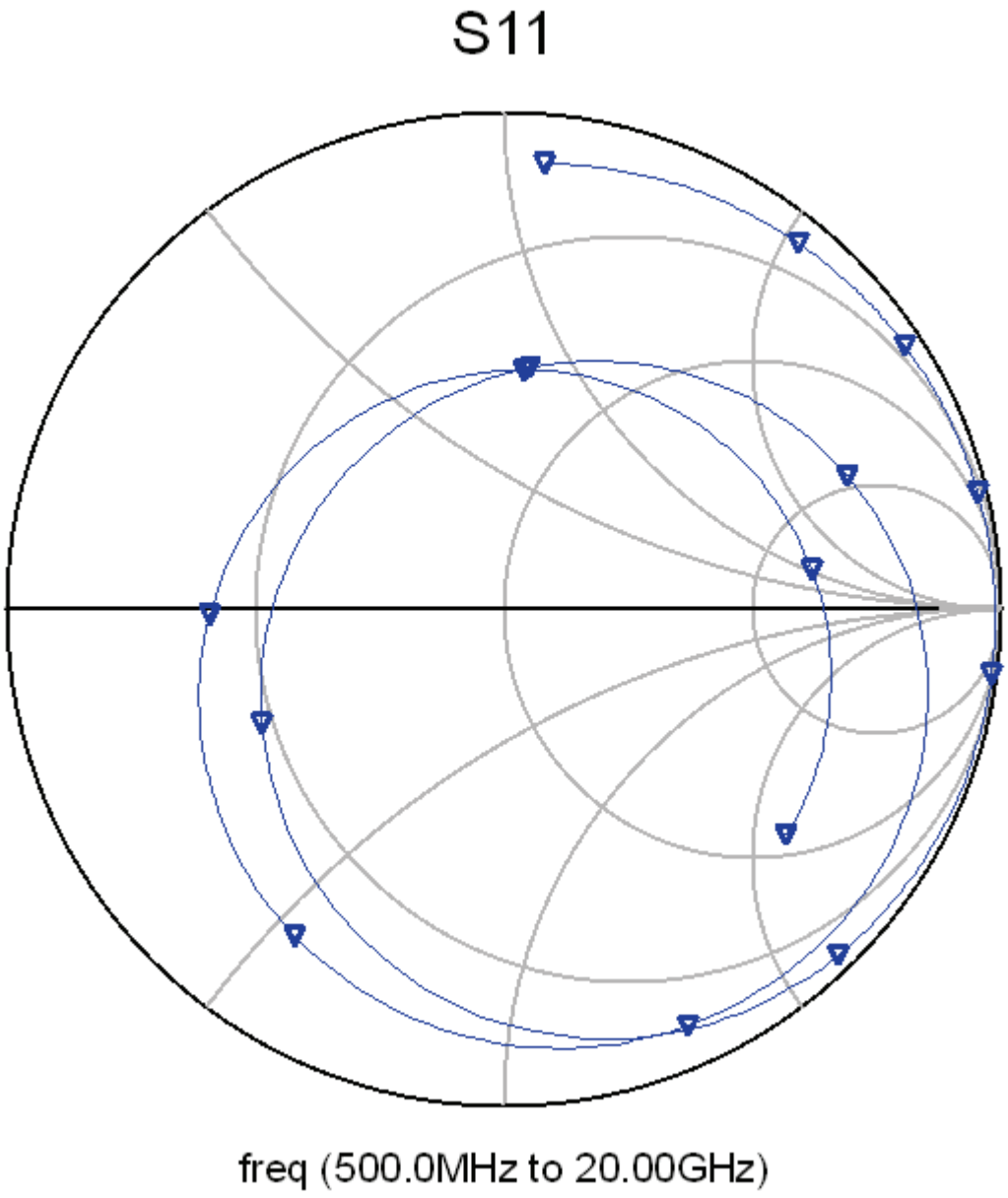

Figure 73: Smith Chart displaying s-parameter of a single inductor with one port grounded.

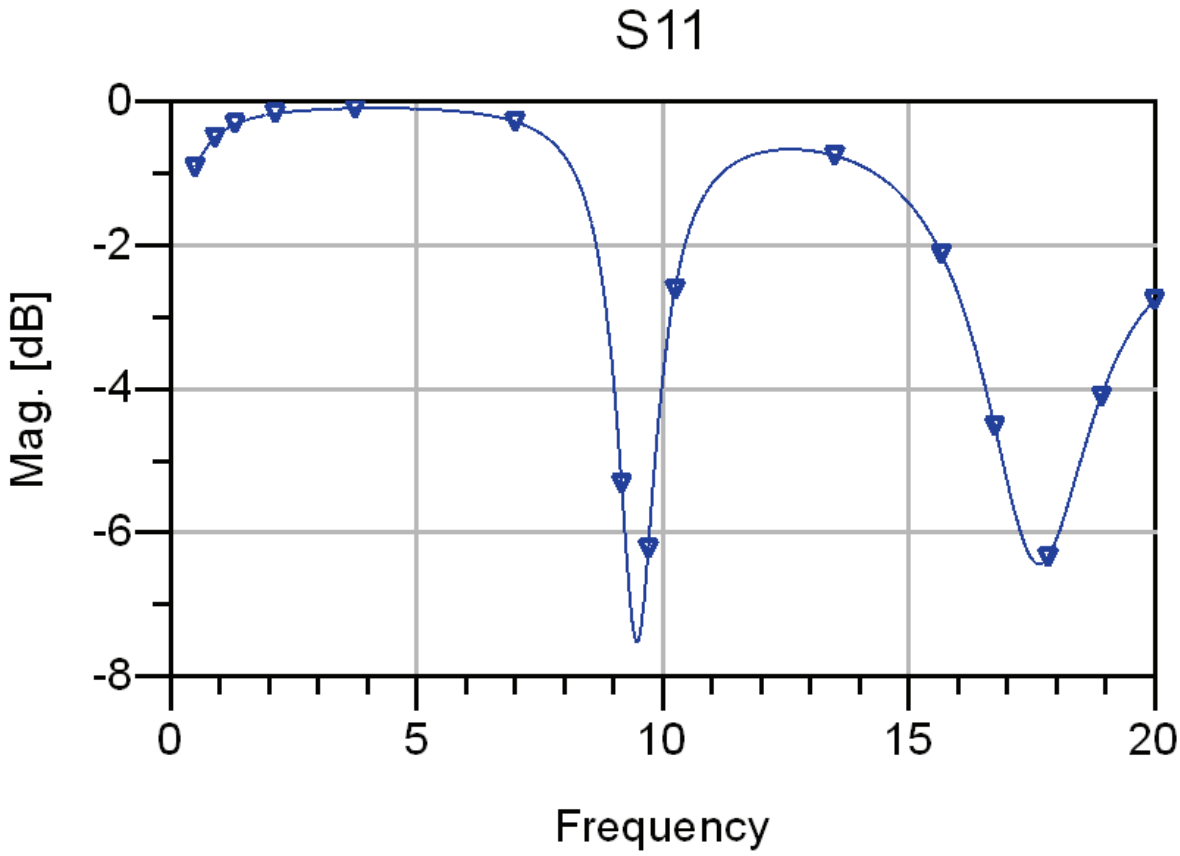

Figure 74: Rectangular plot of the magnitude response of single inductor with grounded output.

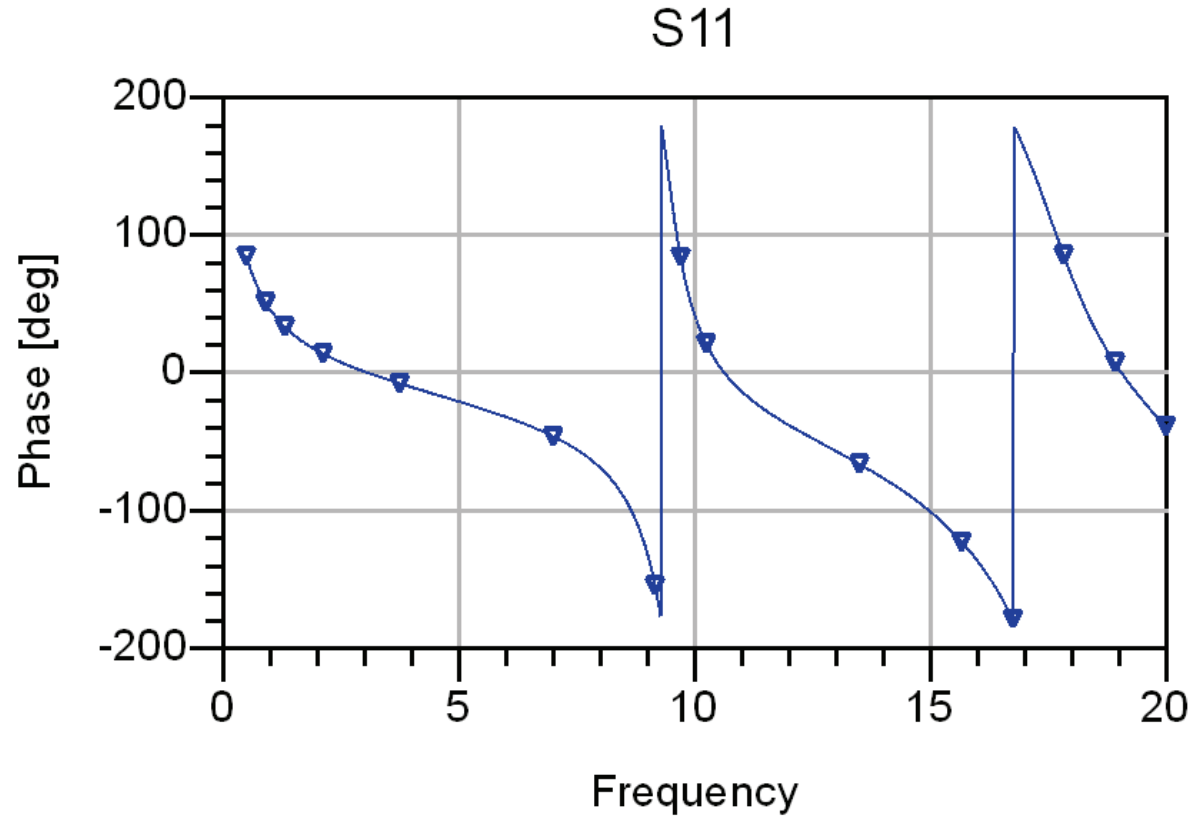

Figure 75: Rectangular plot of the phase response of single inductor with grounded output.

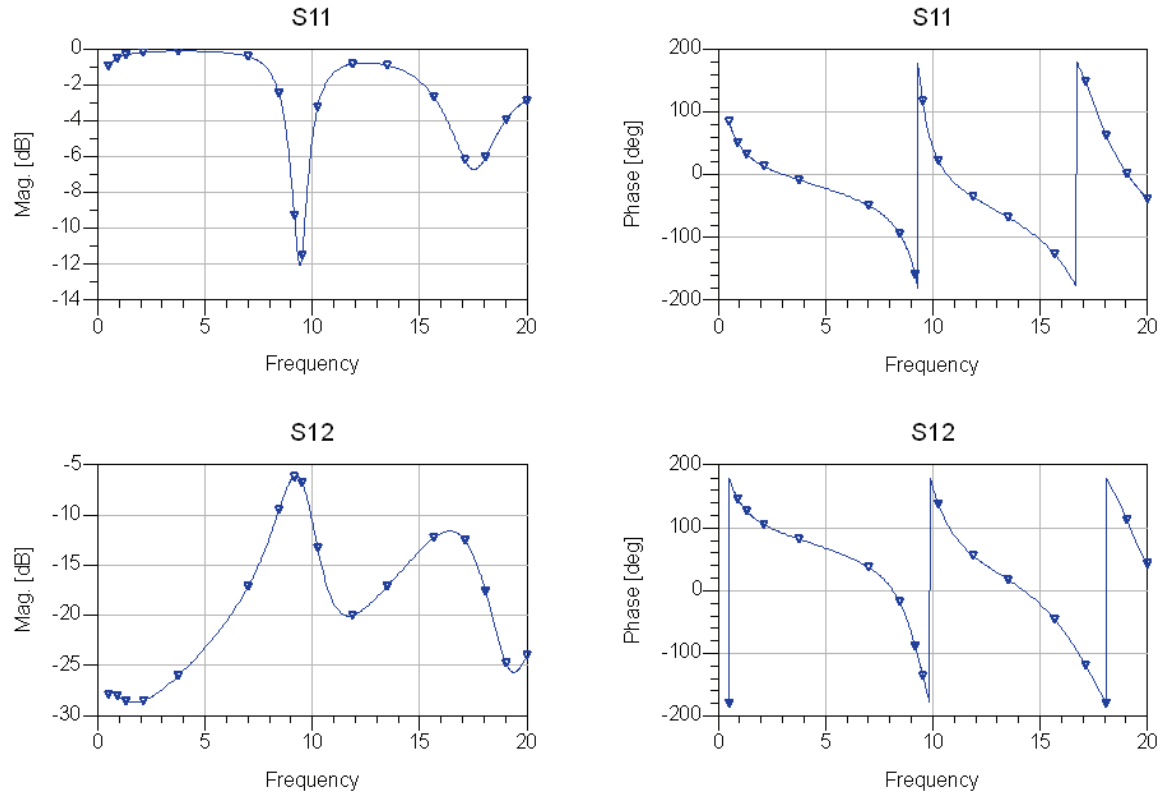

Figure 76: S-parameters from Momentum simulation of electromagnetically coupled inductors – one line width spacing.

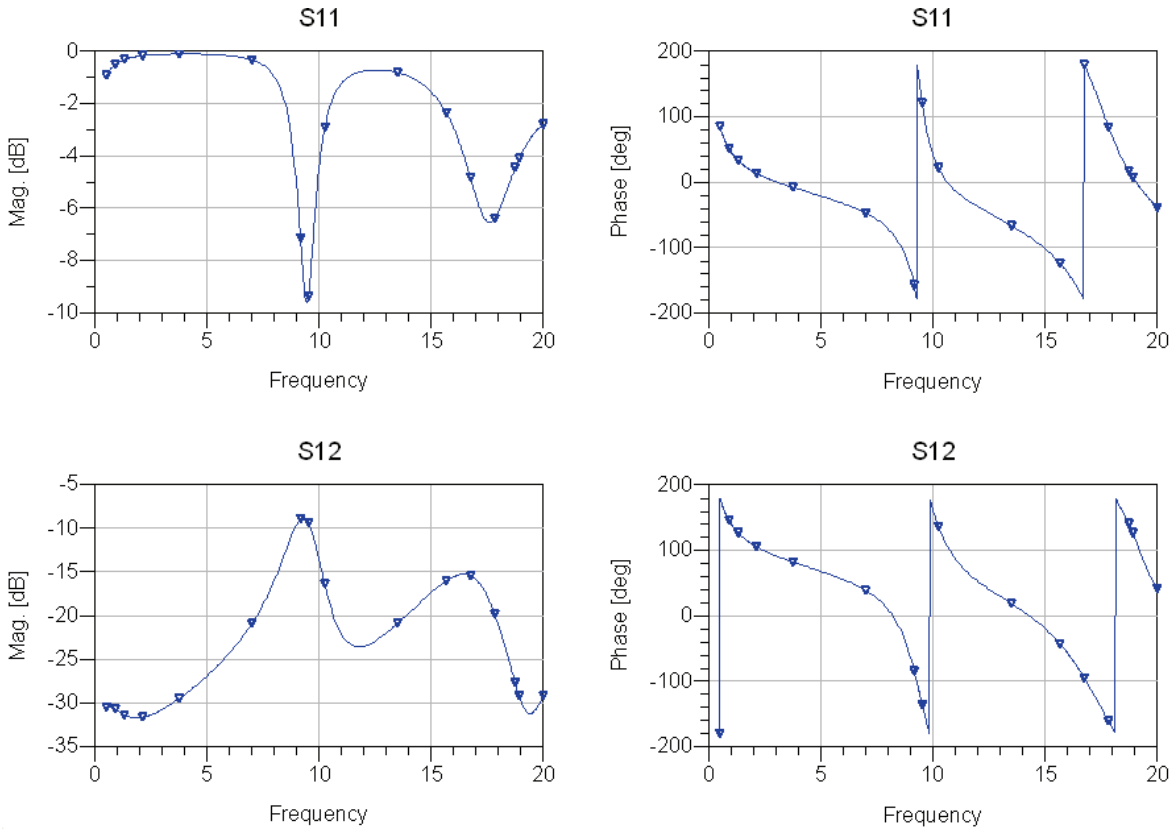

Figure 77: S-parameters from Momentum simulation of electromagnetically coupled inductors – three line widths spacing.

Figure 76 above shows how the s-parameter response from the closely spaced inductors is, according to ADS's Momentum. We see that the $|S_{12}|$ response has two peaks; at 9.2 and 16.4 GHz, and that the magnitude of coupling is fairly high with -6.2 dB at maximum.

From Figure 77 we read off the equivalent peak values of -8.8 dB at 9.3 GHz and -15.3 dB at 16.5 GHz.

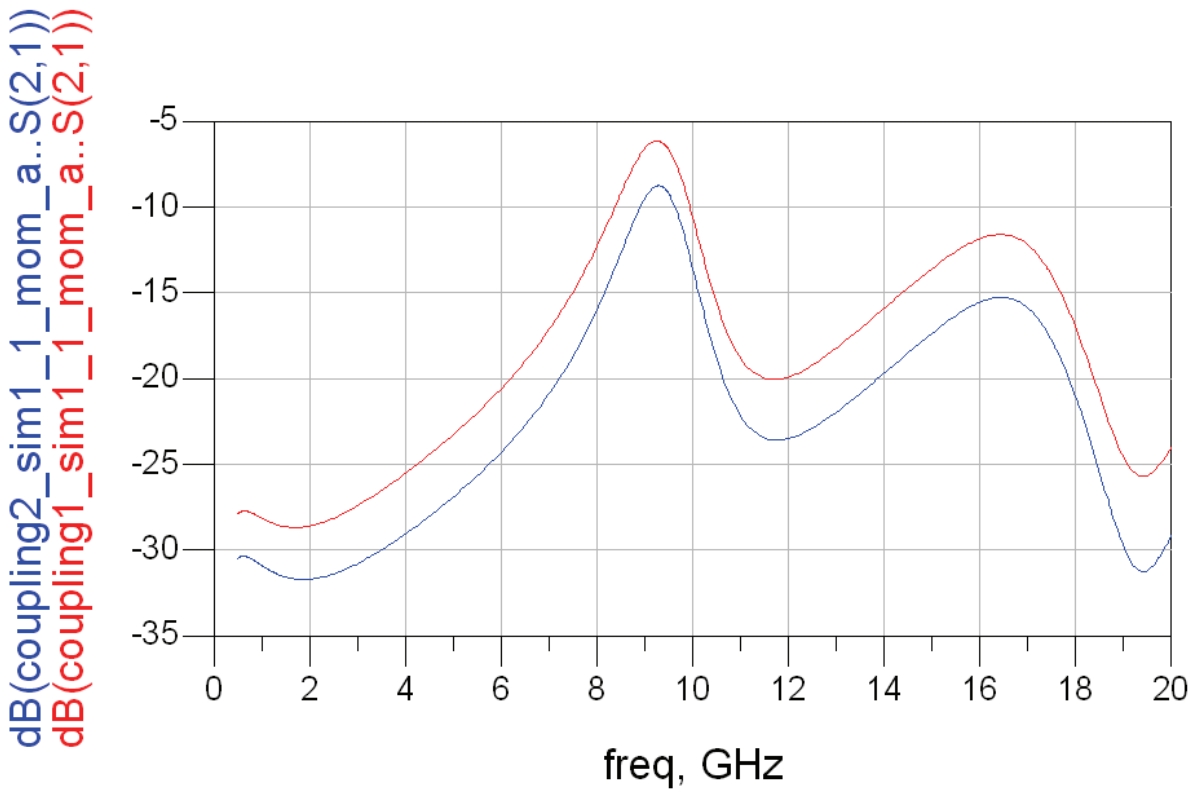

Figure 78: Decibel plot of both coupled inductors Momentum simulations.

In Figures 79 and 80, the S_{11} and S_{21} results from Momentum is displayed in Smith Charts. Figure 78 shows the coupling (in decibel) between the two inductors for both the close and far apart case. It is clear that the coupling has two peaks at 9.2 and 16.4 GHz, where S21 is -6.2 and -11.6 dB, respectively. We also notice that the closely spaced inductors has stronger coupling over the whole frequency range.

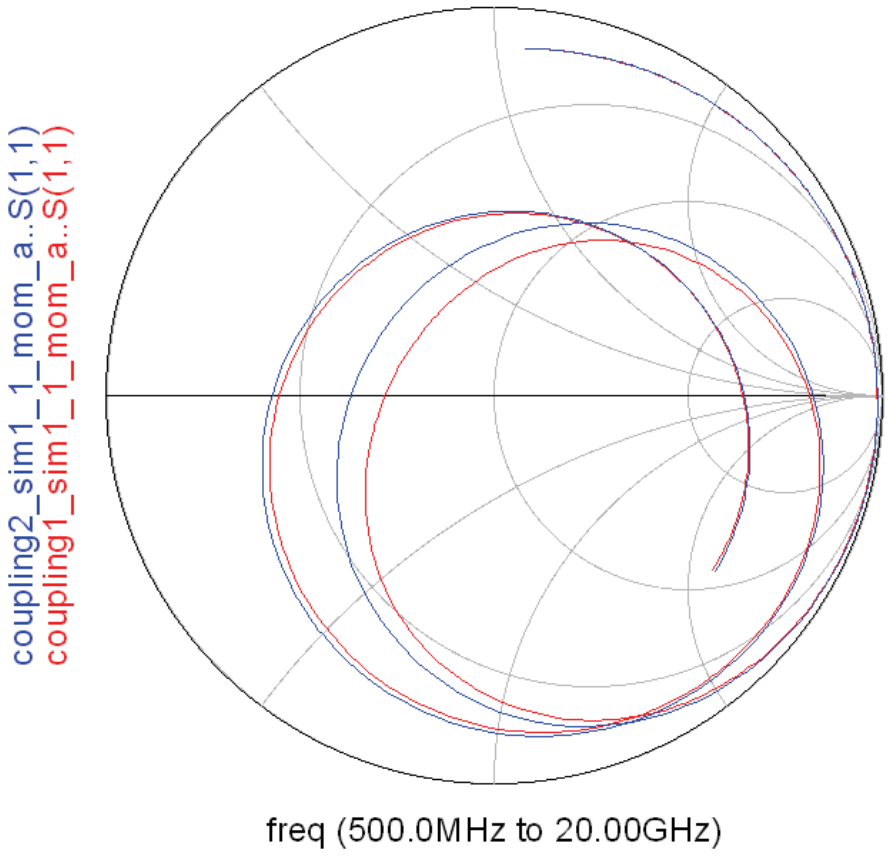

Figure 79: Momentum S_{11} parameters in Smith Chart.

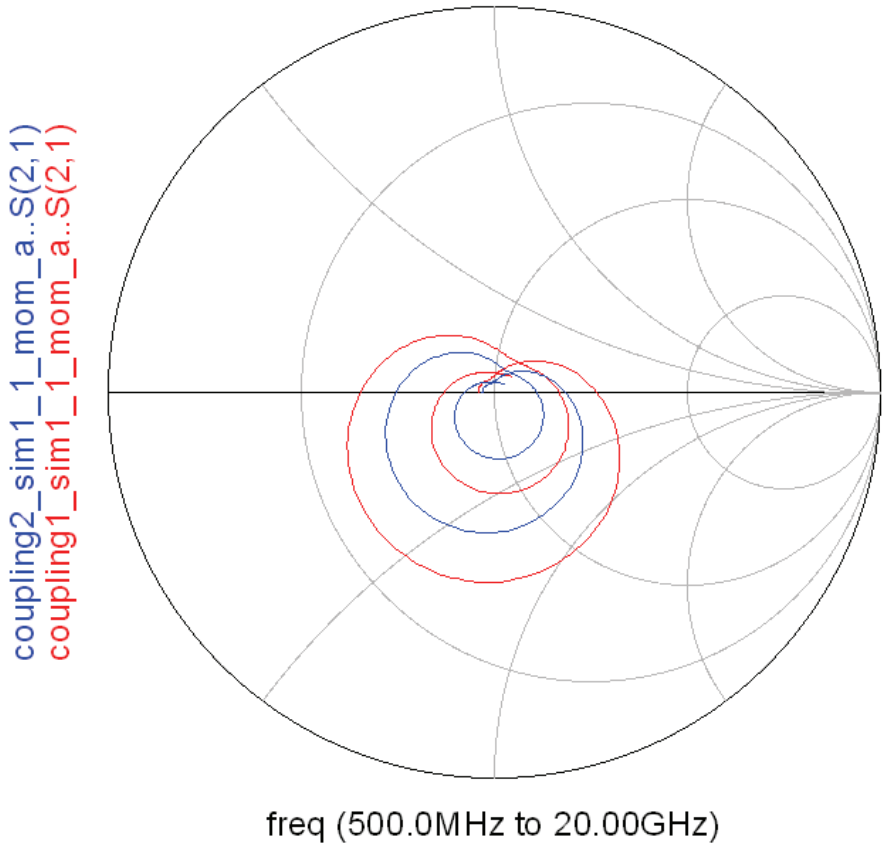

Figure 80: Momentum S_{21} parameters in Smith Chart.

Conclusion

Measurement Vs. Simulation

Single Inductors

The following pages shows the s-parameters of all the inductors, both from the models and from Momentum simulations plotted in the same plots as the measurement results. We concentrate on the S_{11} parameter, and the decibel and phase is plotted in separate plots.

The measurement results is named inductor_w_s_n, where w=width, s=spacing and n=number of segments (#turns*4). The simulation results indicates the inductor number (see Appendix A4), while an ending of mom_a indicates Momentum simulation.

We notice that inductor 1 has the poorest agreement between the measurement and simulation results. Different data set sizes from the simulations and measurement makes it difficult to get accurate numerical differences between the various results, but the maximum deviations from measurement results is approximately 3.0 dB for the Momentum simulation and 3.1 dB for the TriQuint model simulation. The Momentum results agree best with the measured phase, with the model S_{11} phase having a 10.3˚ deviation at 15.5 GHz.

In the case of inductor 3 (width=5, spacing=5 and segments=6) the TriQuint model results seems to agree better with the measurement results than the Momentum results does. The magnitude of the model agrees extremely well with the measurement results with only a few tenths of a decibel deviation at the most.

The results from inductor 5 shows that both Momentum and model results agree very well with the measured results. The phase from the model agrees a bit better than the Momentum one at higher frequencies.

S-parameters for inductor 6 are displayed in Figures 88, 91 and92. Also in this case there is good agreement between the results, with the phase of the model being more accurate than that of Momentum simulation at higher frequencies.

The S_{21} parameters also agree well for both the model and the Momentum simulation results. The model results seems to agree better over most of the frequency range for all but inductor 6, where the two simulation results is approximately equally accurate.

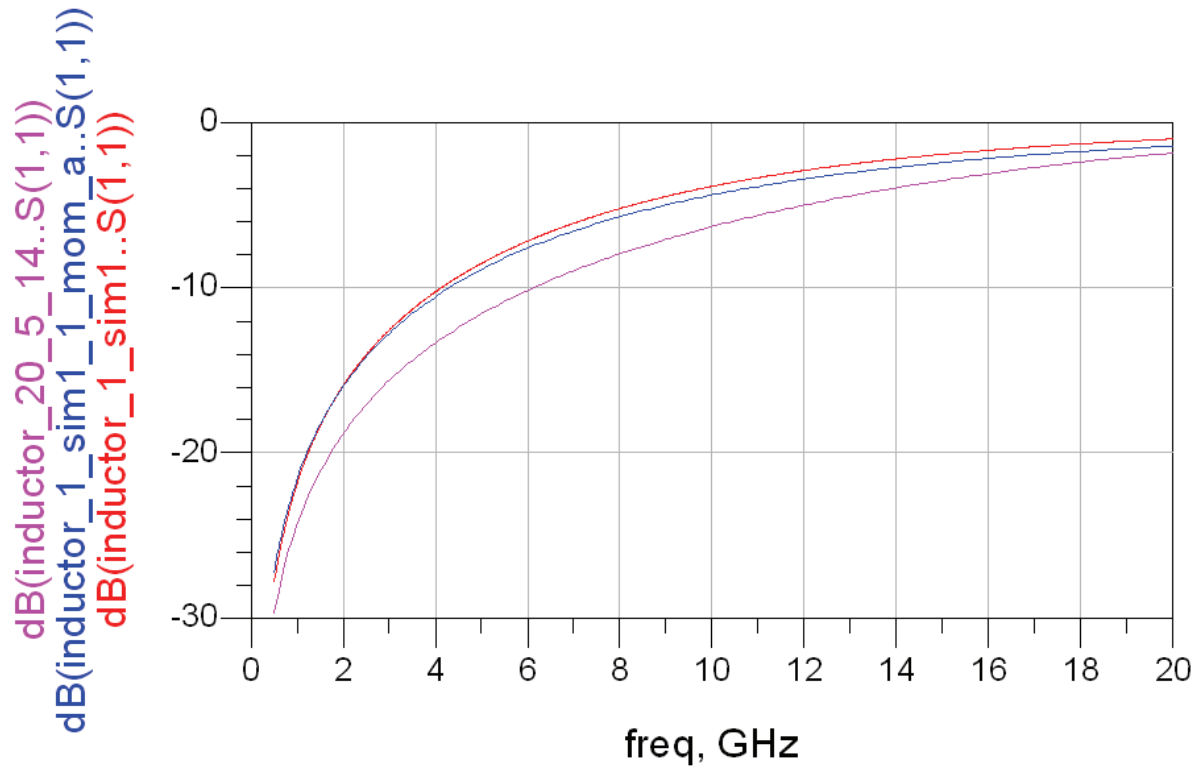

Figure 81: Decibel plot for inductor 1.

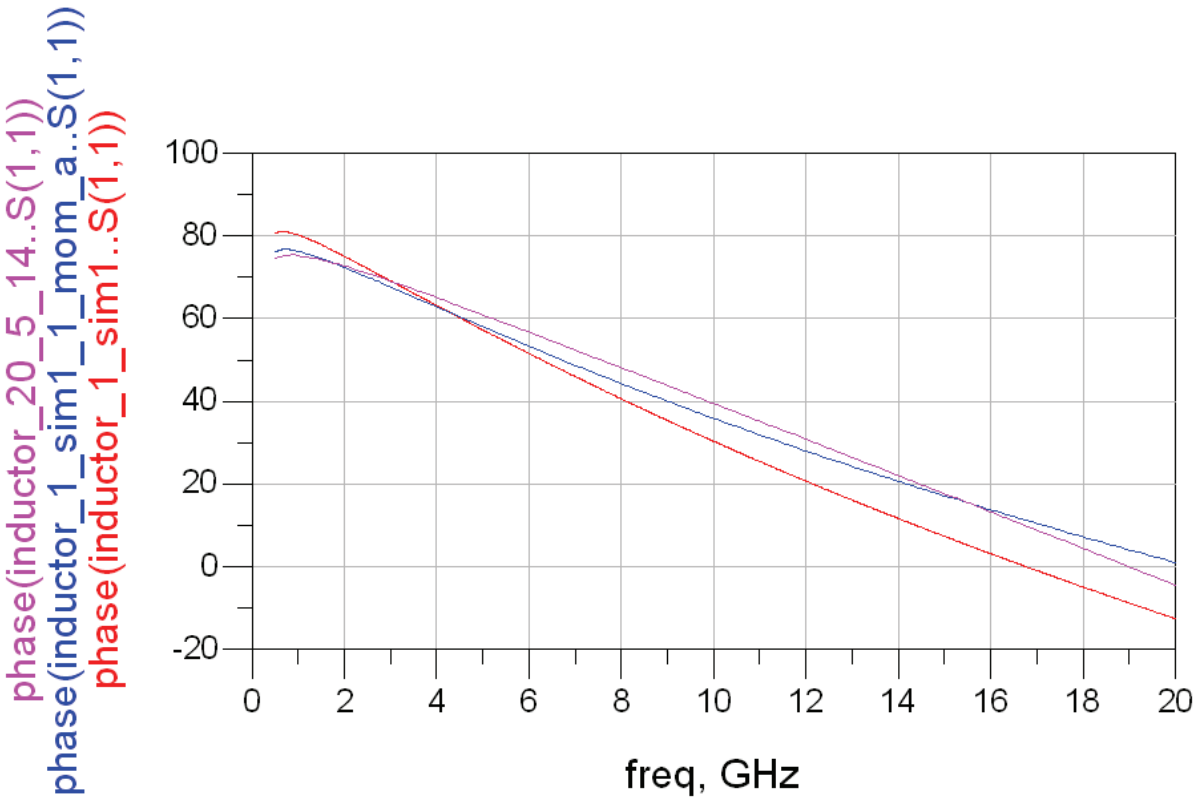

Figure 82: Phase plot for inductor 1.

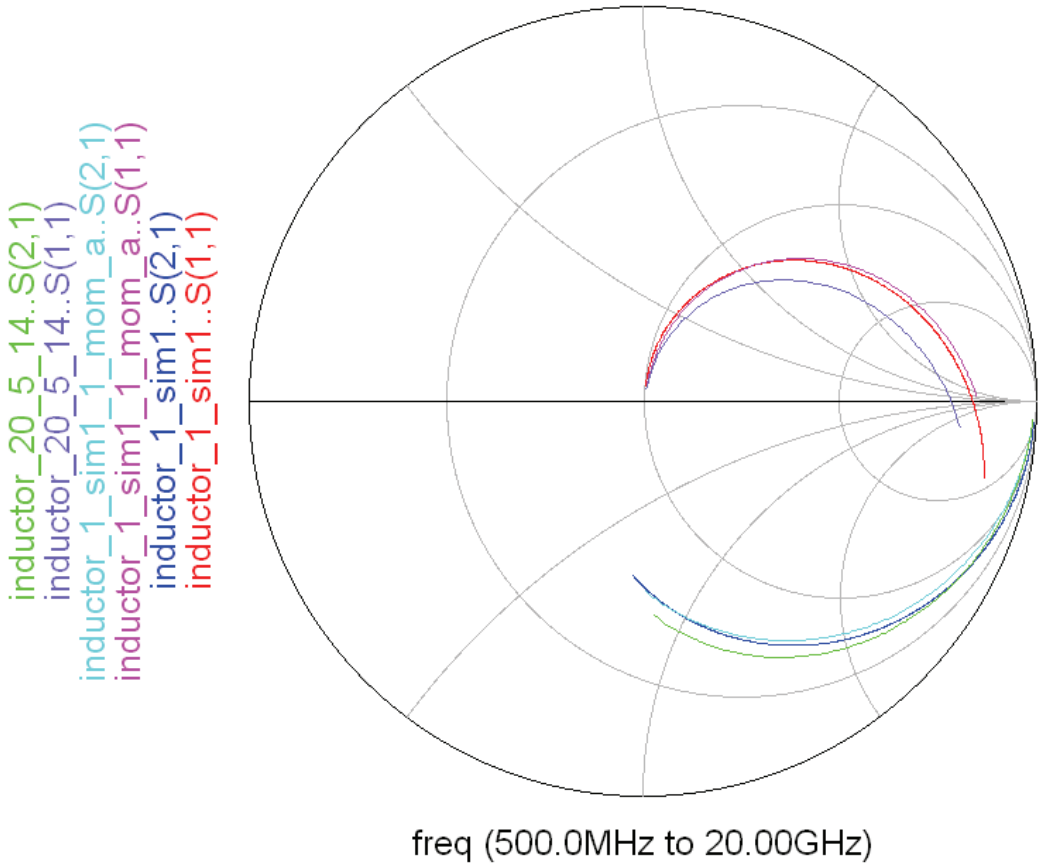

Figure 83: Smith Chart for inductor 1.

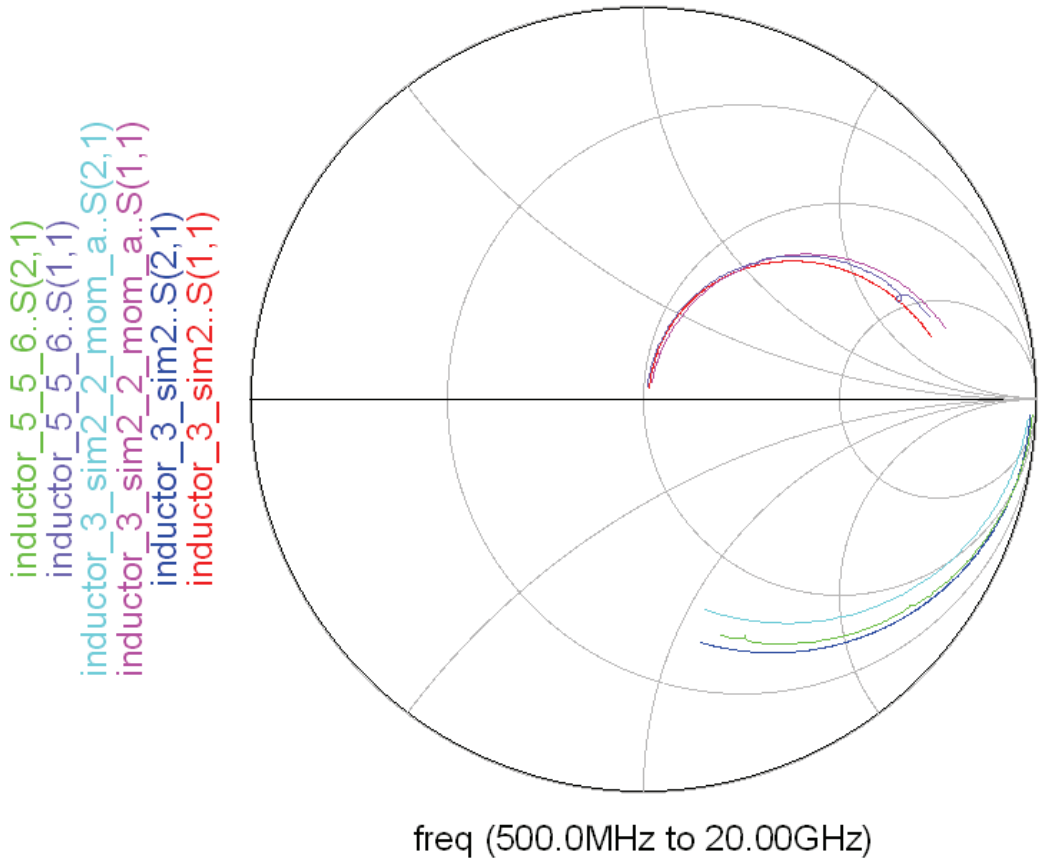

Figure 84: Smith Chart for inductor 3.

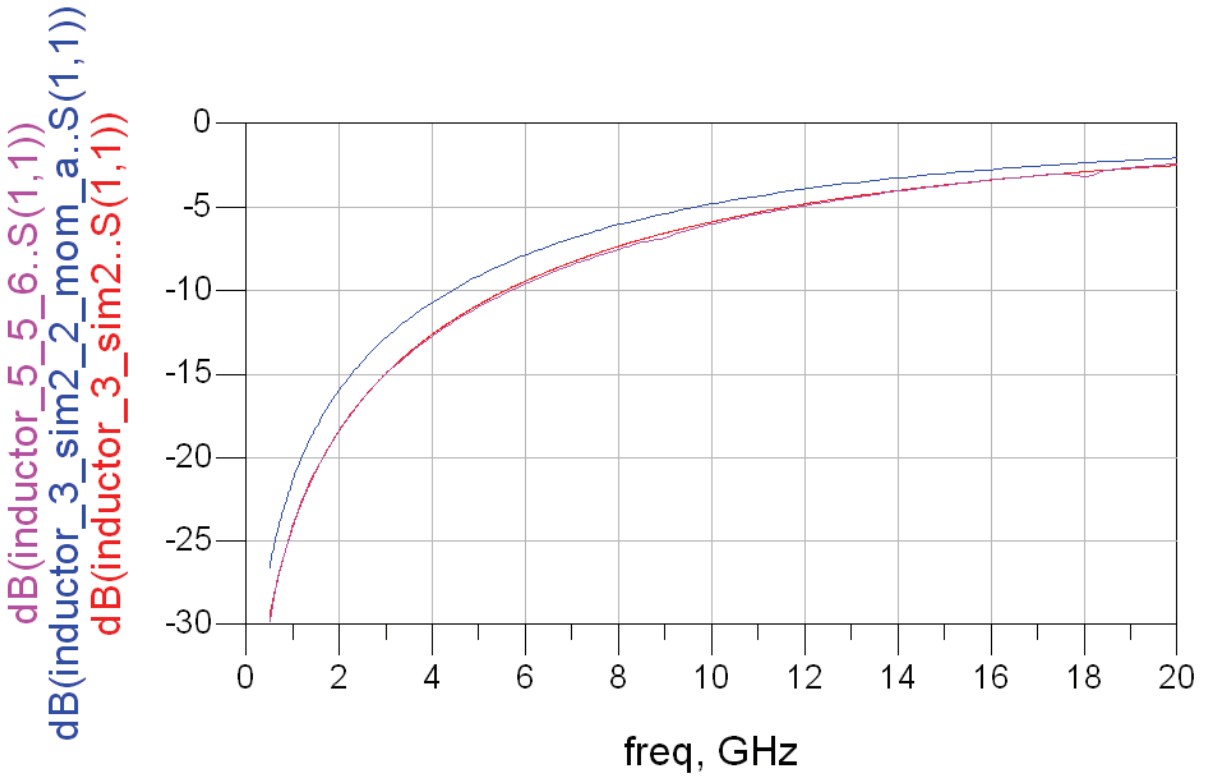

Figure 85: Decibel plot for inductor 3.

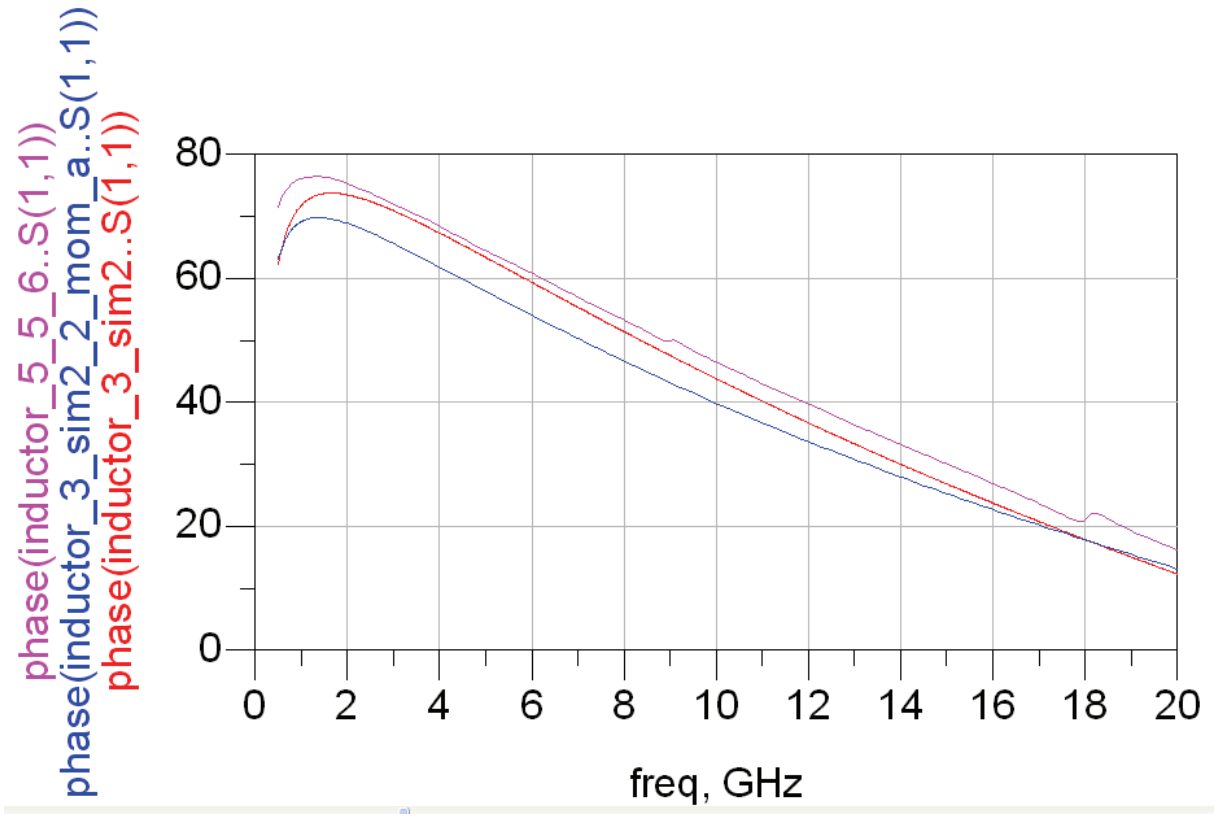

Figure 86: Phase plot for inductor 3.

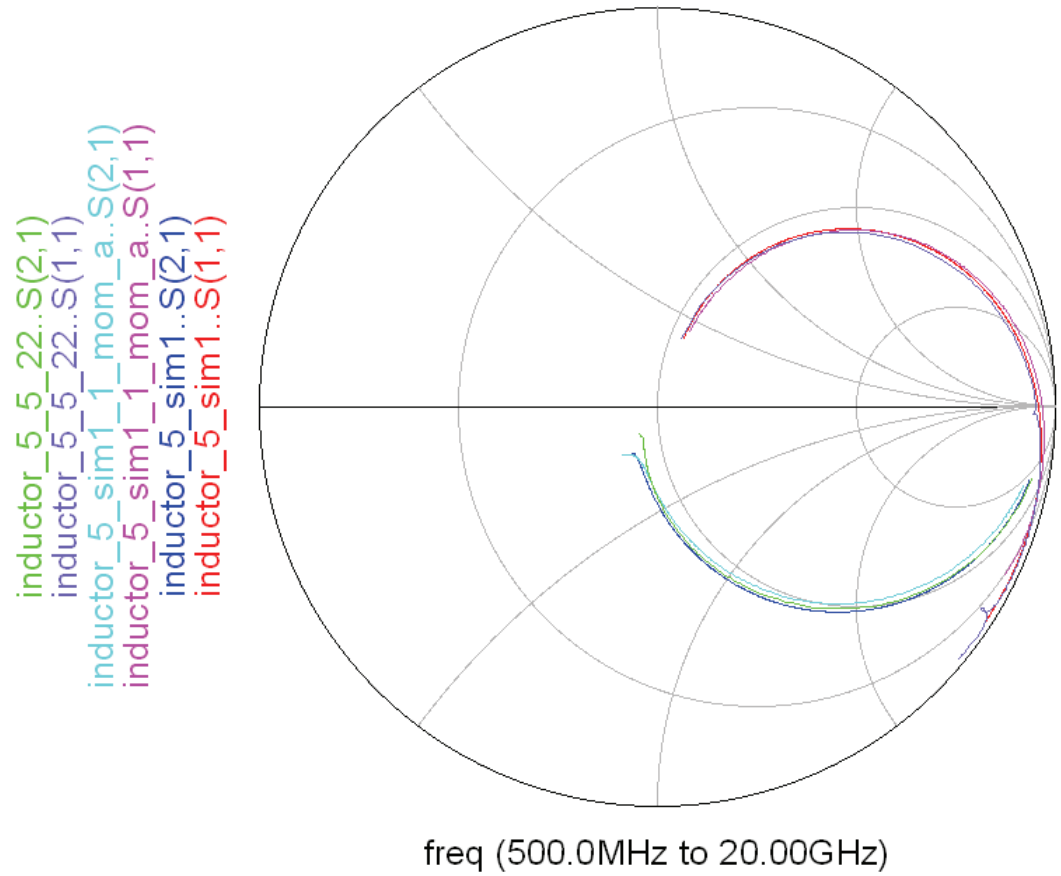

Figure 87: Smith Chart for inductor 5.

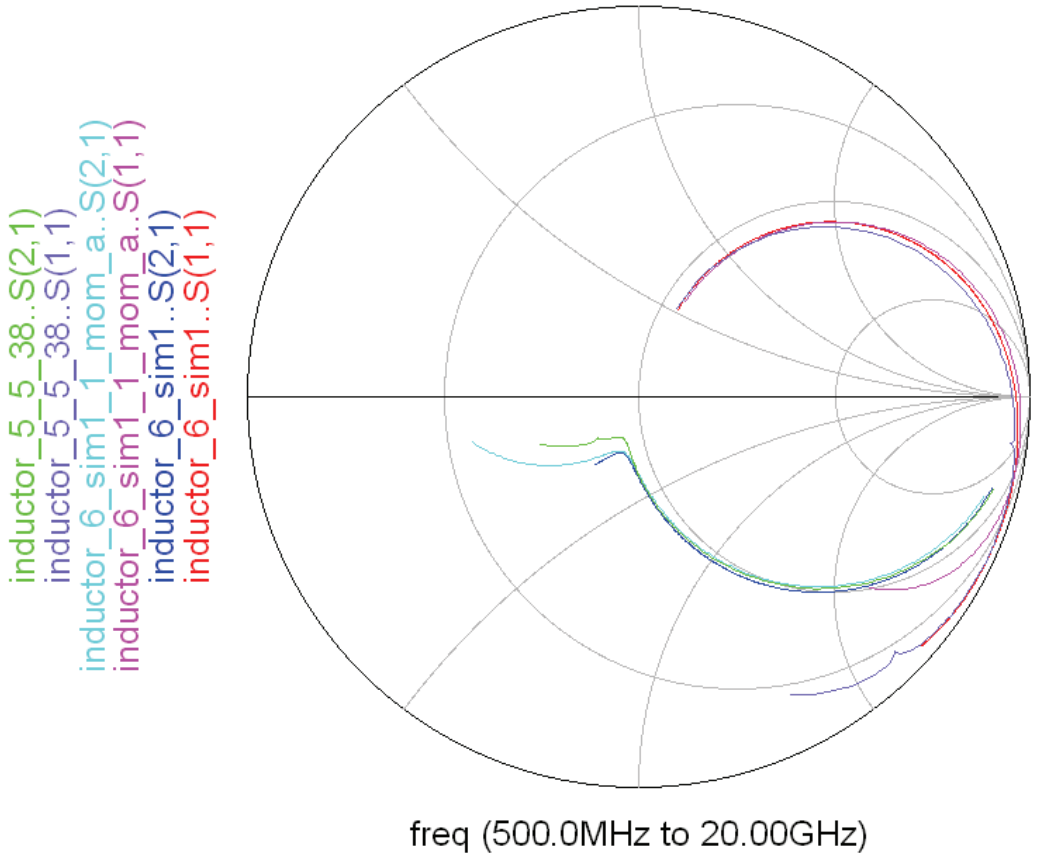

Figure 88: Smith Chart for inductor 6.

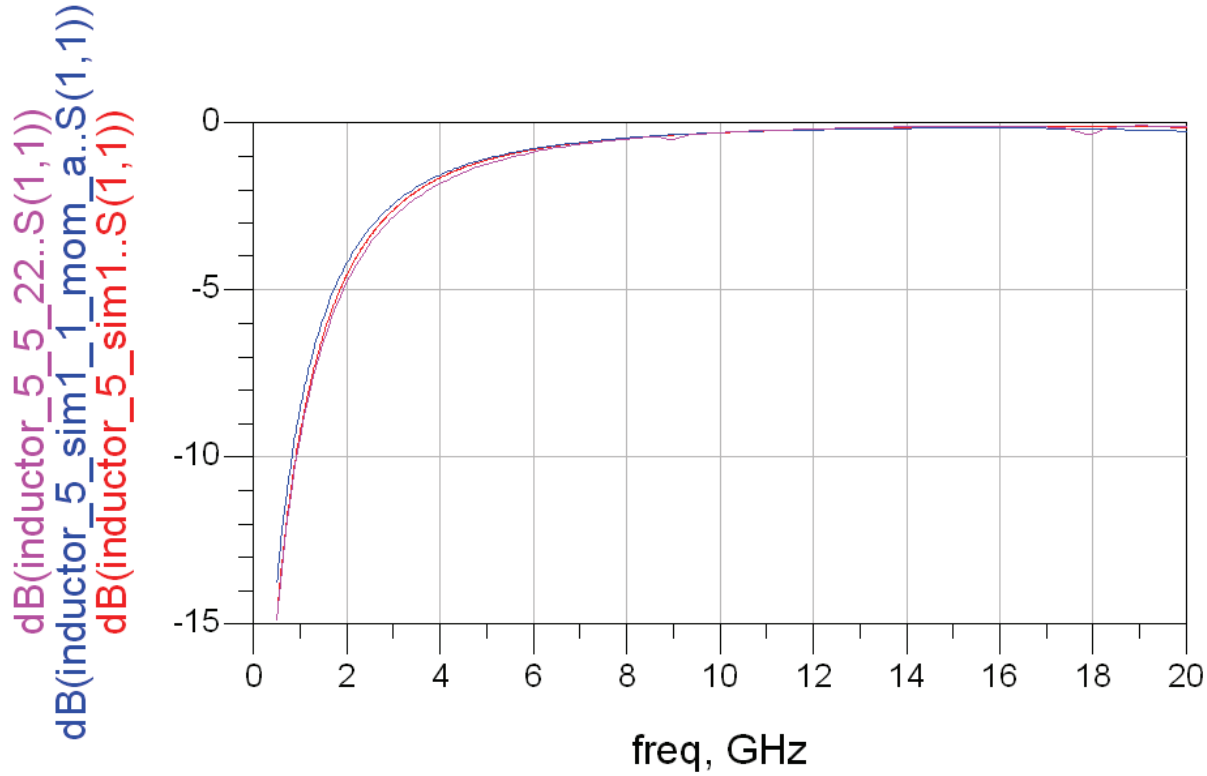

Figure 89: Decibel plot for inductor 5.

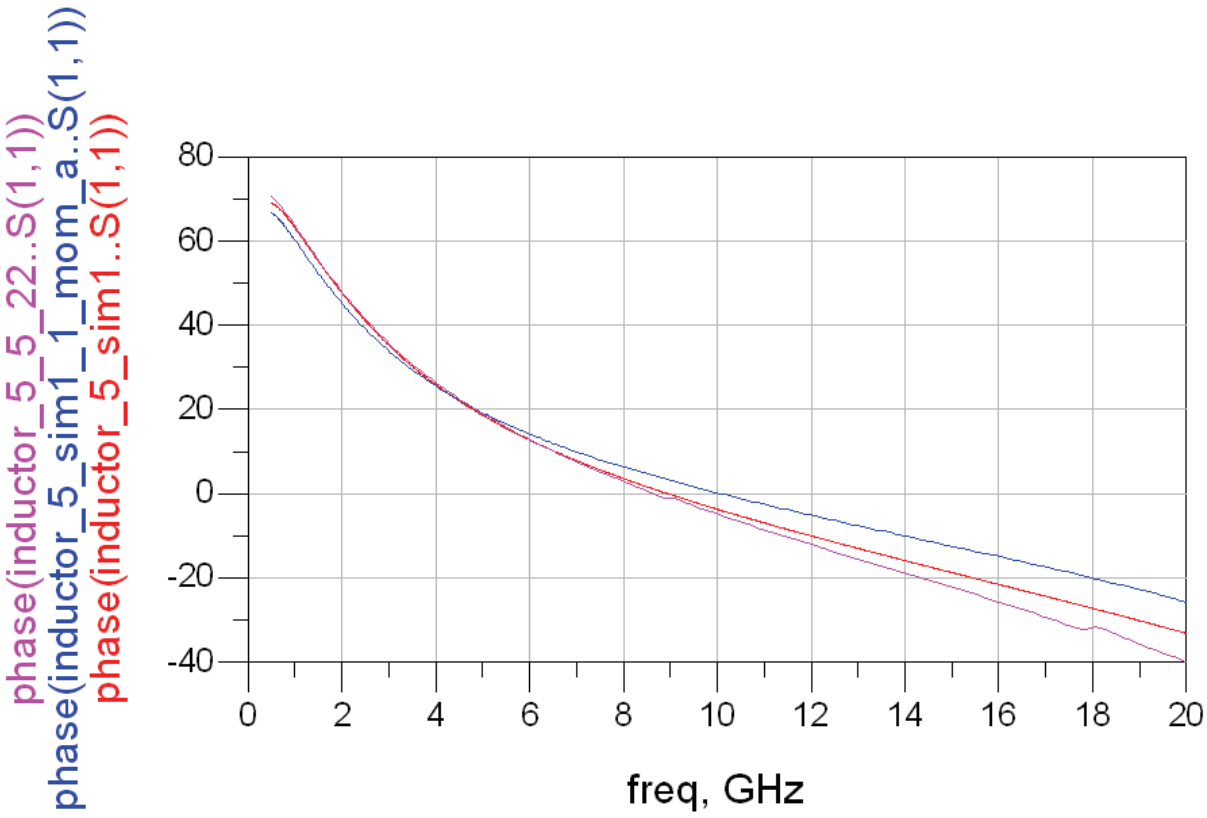

Figure 90: Phase plot for inductor 5.

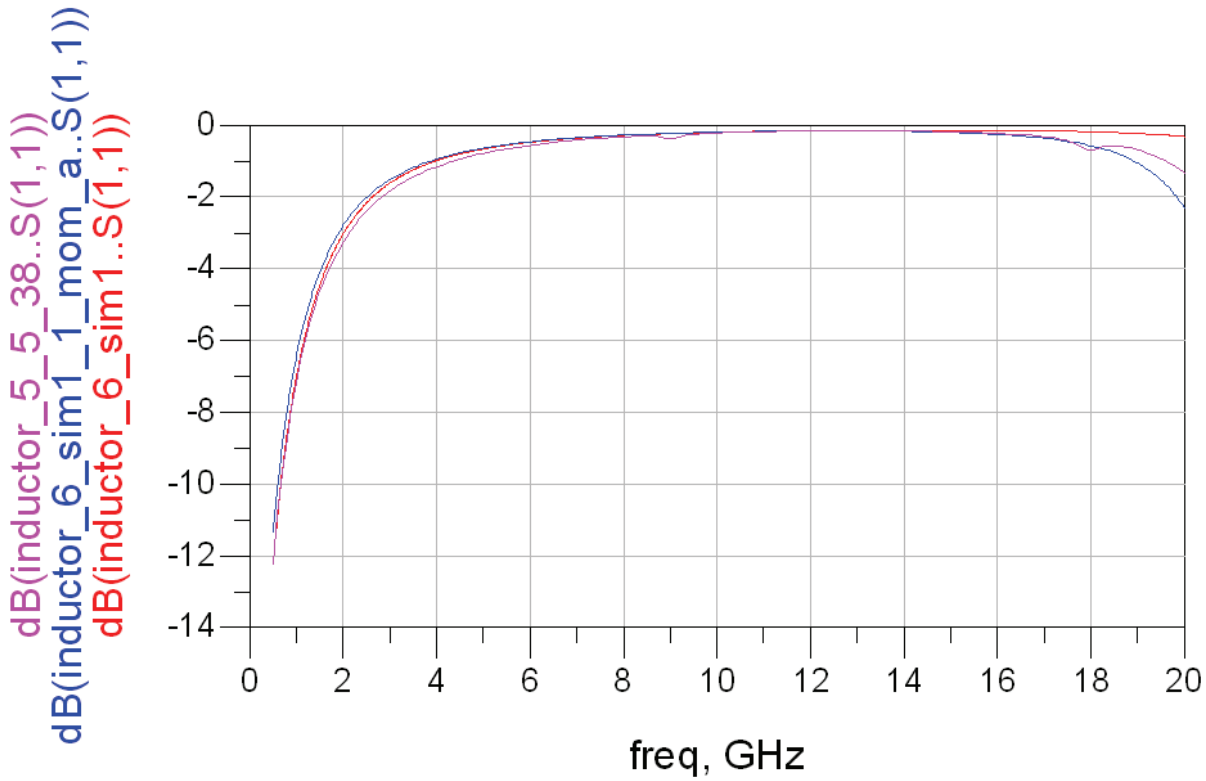

Figure 91: Decibel plot for inductor 6.

Figure 92: Phase plot for inductor 6.

Coupled Inductors

We first study the s-parameters for the single inductor with shorted output. Both Momentum and measurement results is plotted in the Smith Chart below, while Figure 94 and Figure 95 shows the magnitude (in dB) and phase.

We see from Figure 94 that Momentum simulation predicts a minimum of $|S_{11}|$=-7.5 dB at 9.5 GHz, while the measurements gives -5.8 dB at 9.8 GHz. The agreement between measurement and simulation gets worse at higher frequencies. Momentum gives a resonance at 16.8 GHz, while measurements give resonance at 18.0 GHz. The magnitude response from Momentum at high frequencies is also inaccurate. Momentum predicts a valley at 17.7 GHz, while measurements show a valley at 19.3 GHz.

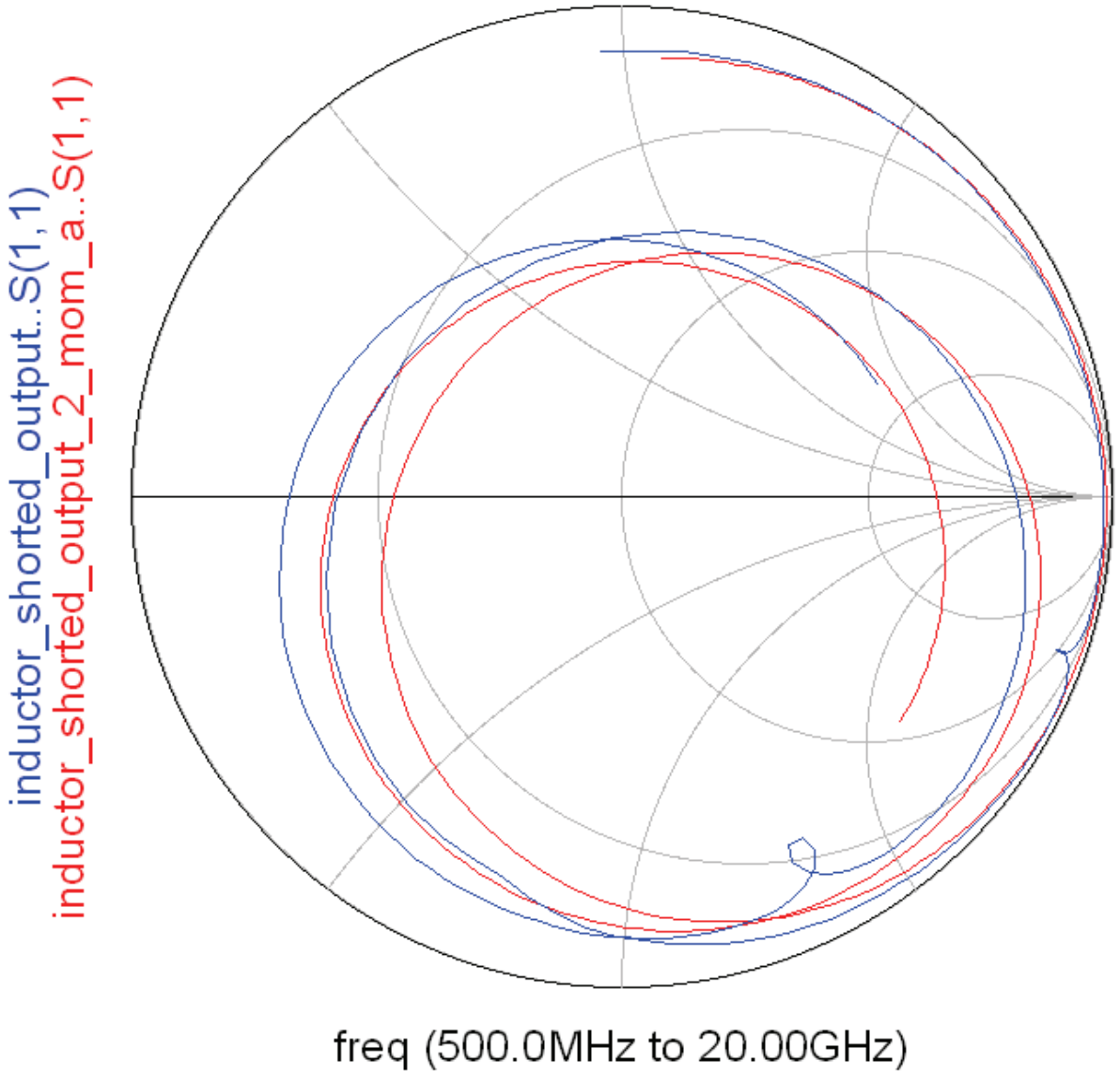

Figure 93: Smith Chart showing measured and simulated s-parameter from single inductor.

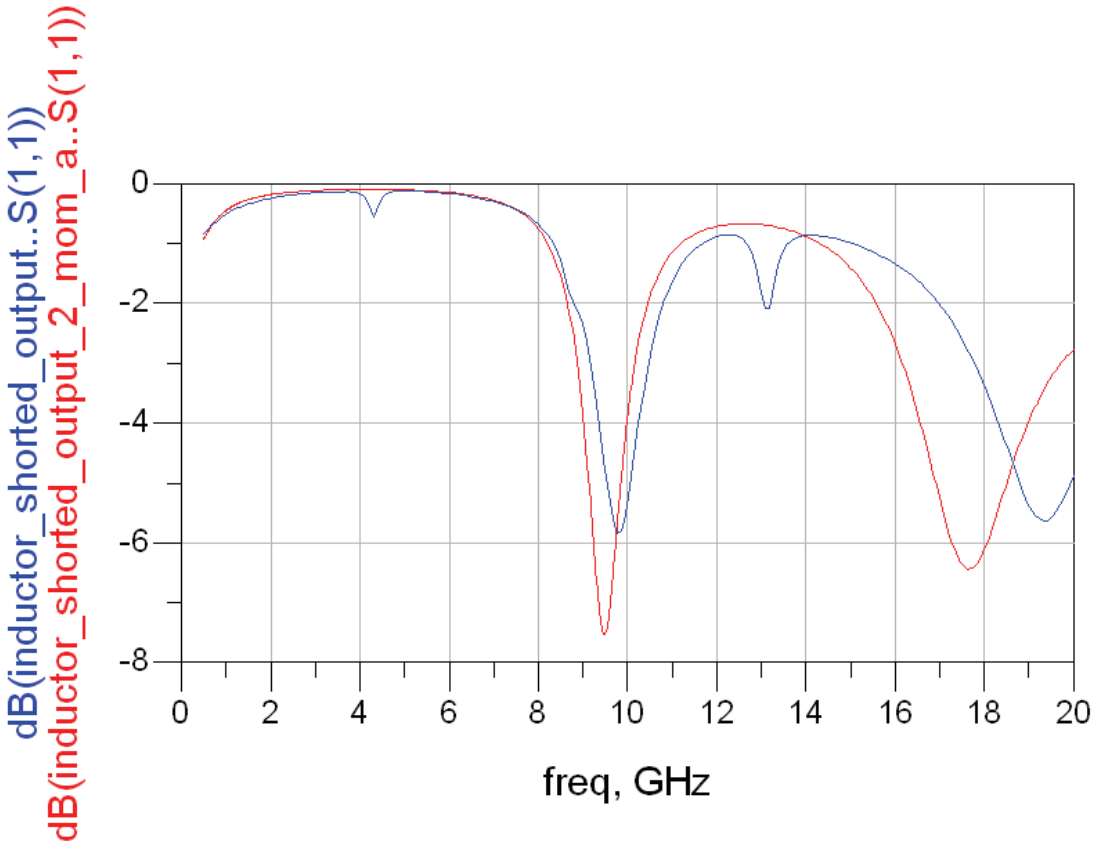

Figure 94: Graph comparing the measured and simulated dB value from single inductor.

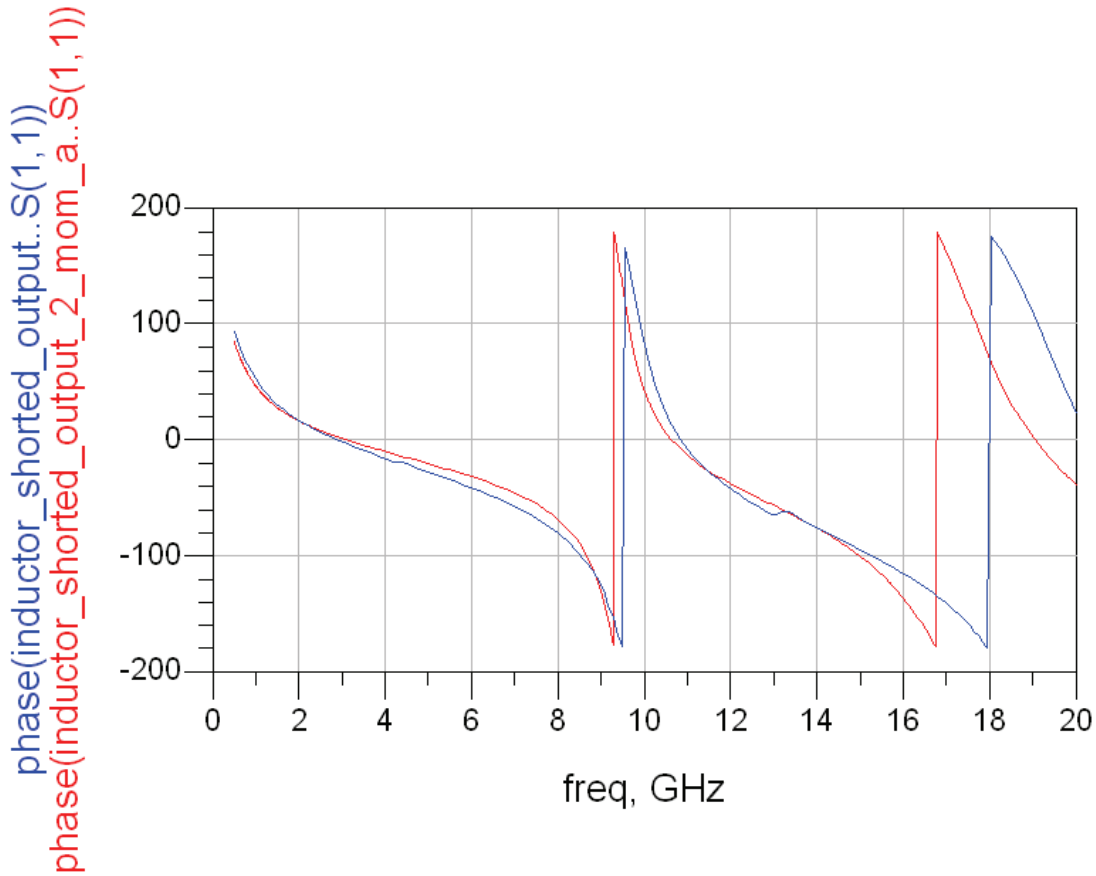

Figure 95: Graph comparing the measured and simulated phase from single inductor.

We will now focus on the coupled inductors measurement and Momentum simulation results. S-parameters (both S_{11} and S_{21}) from both cases are plotted in the same plots below. inductor_coupling_close and inductor_coupling_far is the measurement results, while coupling1_sim1_1_mom_a is the (adapted) simulation results from the closely spaced inductors and coupling2_sim1_1_mom_a is the results from the more distantly spaced inductors.

We can see that the results equal those from the single inductor in that the agreement between measurement and simulation is best at low frequencies. Momentum simulation predicts better matching and higher coupling at a lower frequency than the measurement results shows.

Appendix A6 shows the key data from the coupled inductors s-parameters displayed in tables.

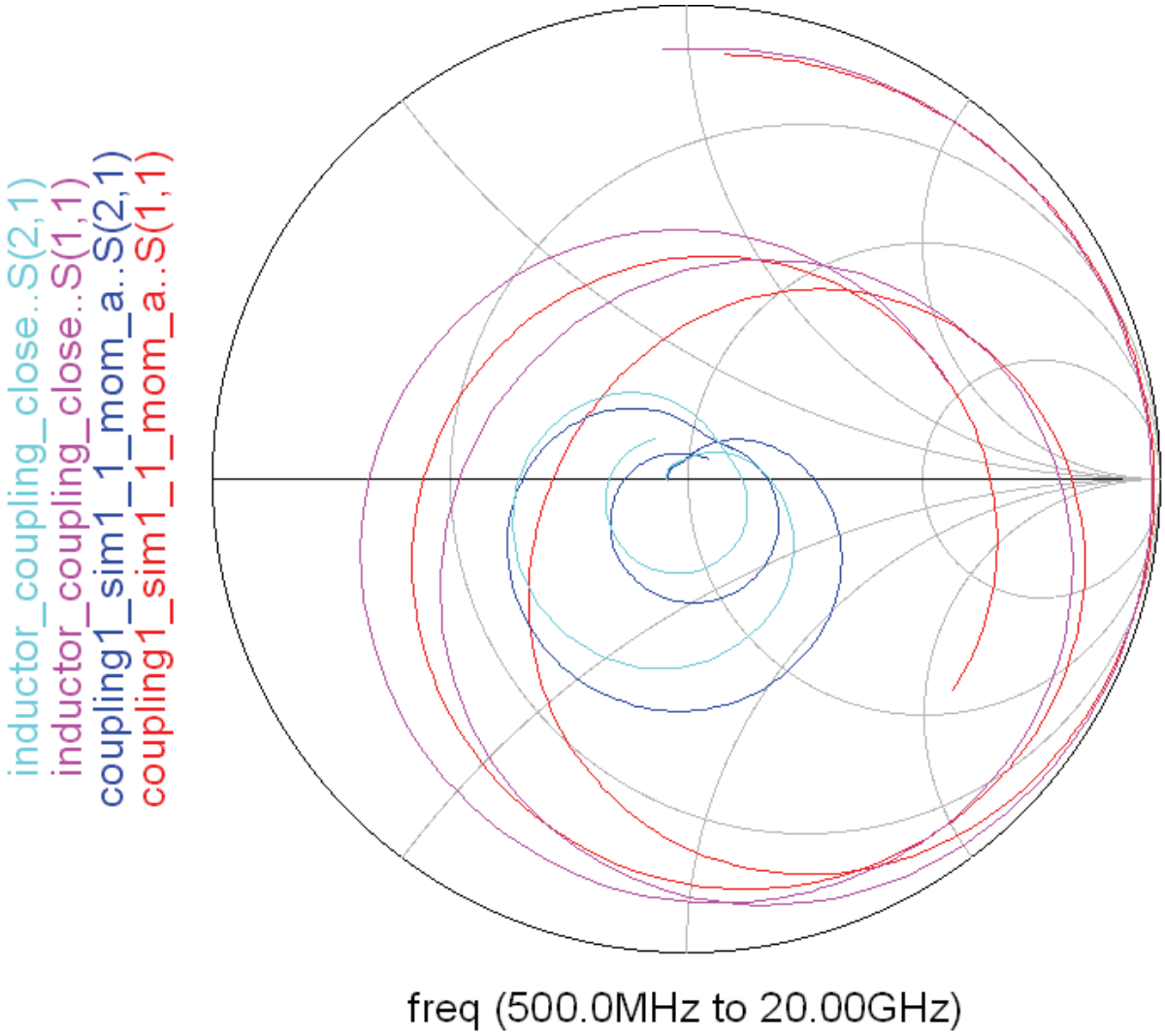

Figure 96: Smith Cart showing s-parameters from both Momentum simulation and measurements – closely spaced inductors.

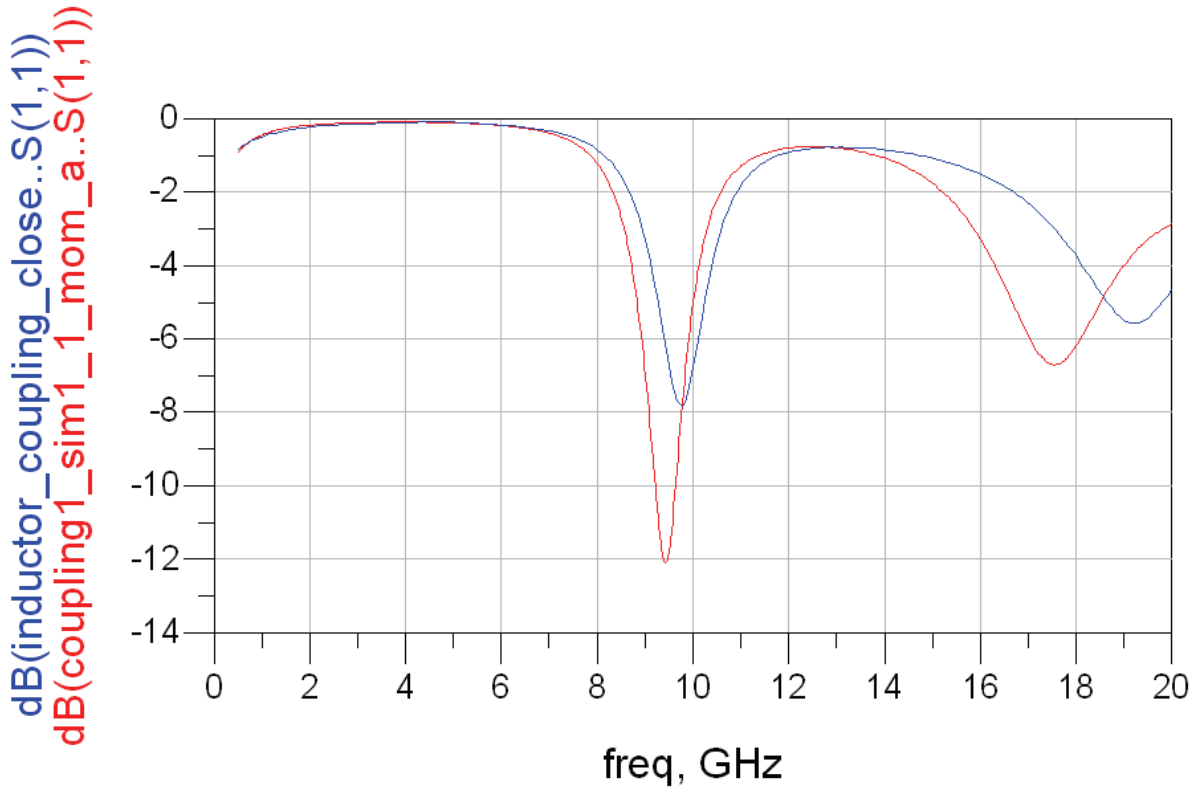

Figure 97: Decibel plot of S_{11} from measurements and simulation - closely spaced inductors.

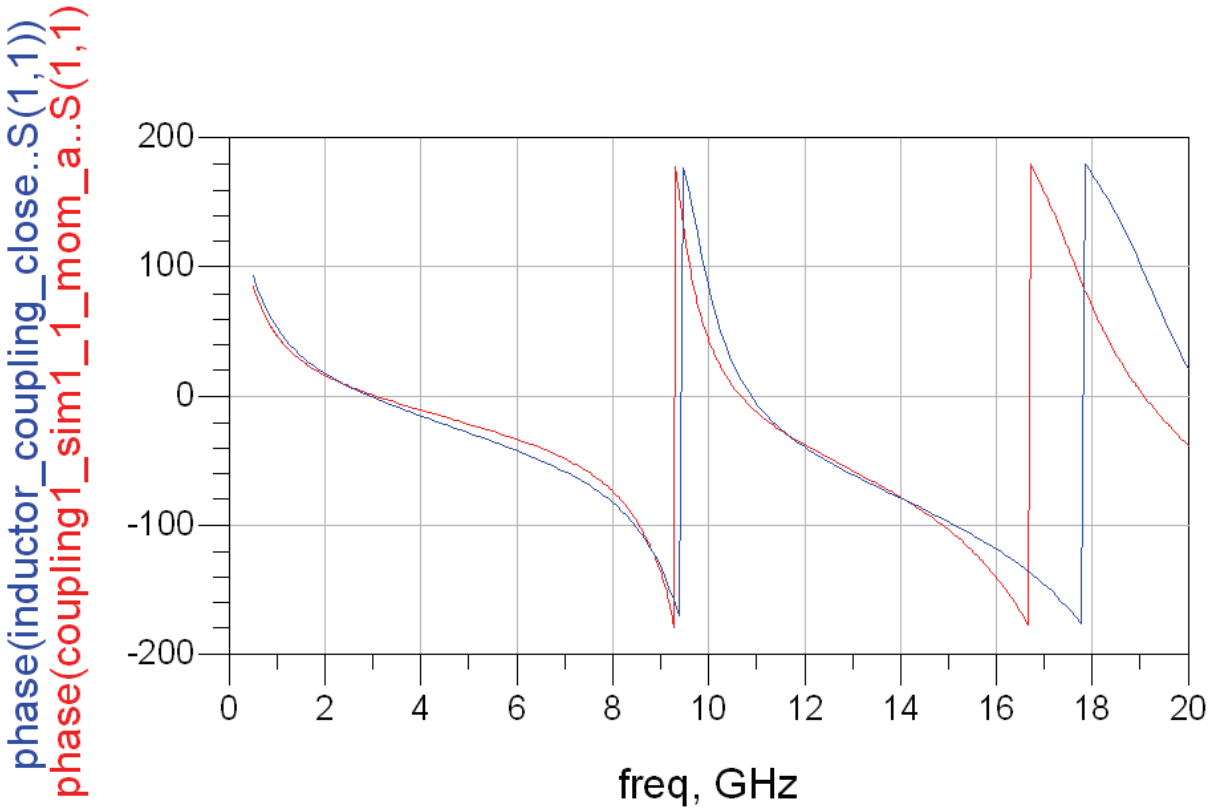

Figure 98: Phase plot of S_{11} from measurements and simulation - closely spaced inductors.

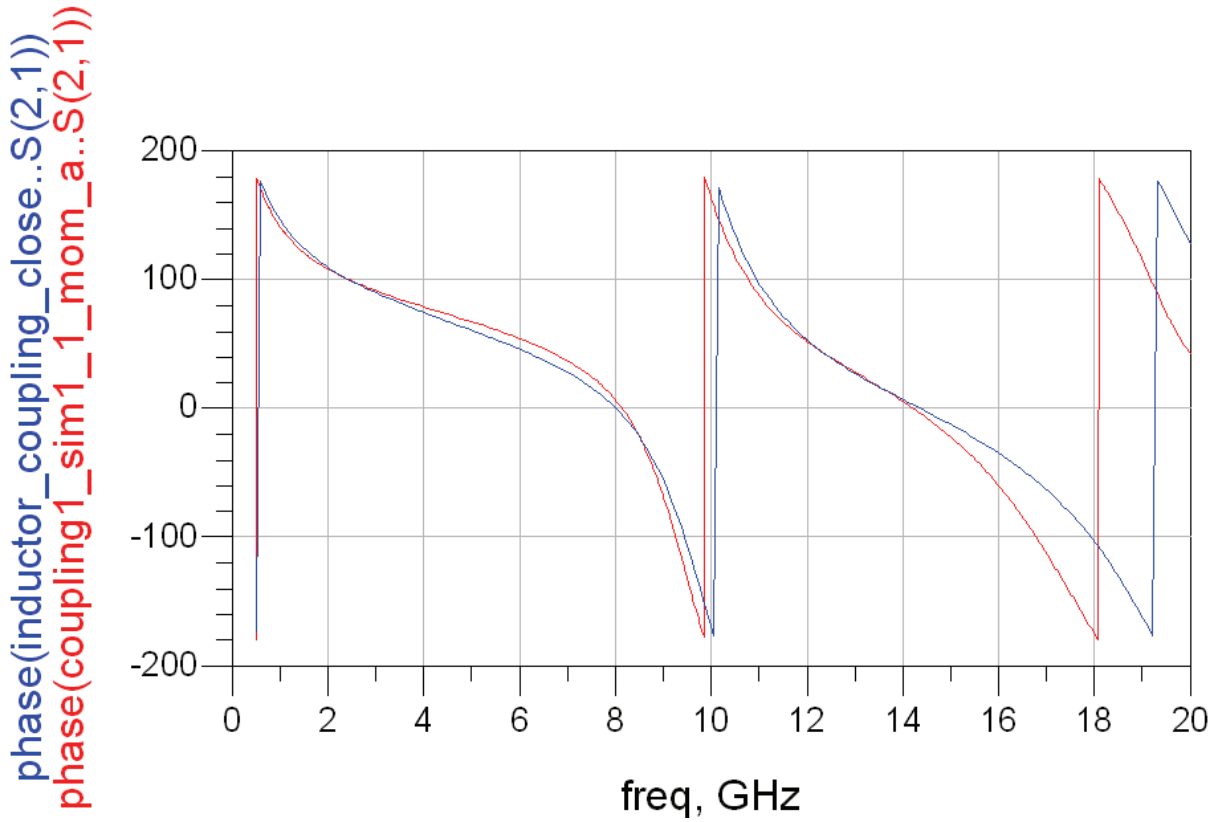

Figure 99: Decibel plot of S_{21} from measurements and simulation - closely spaced inductors.

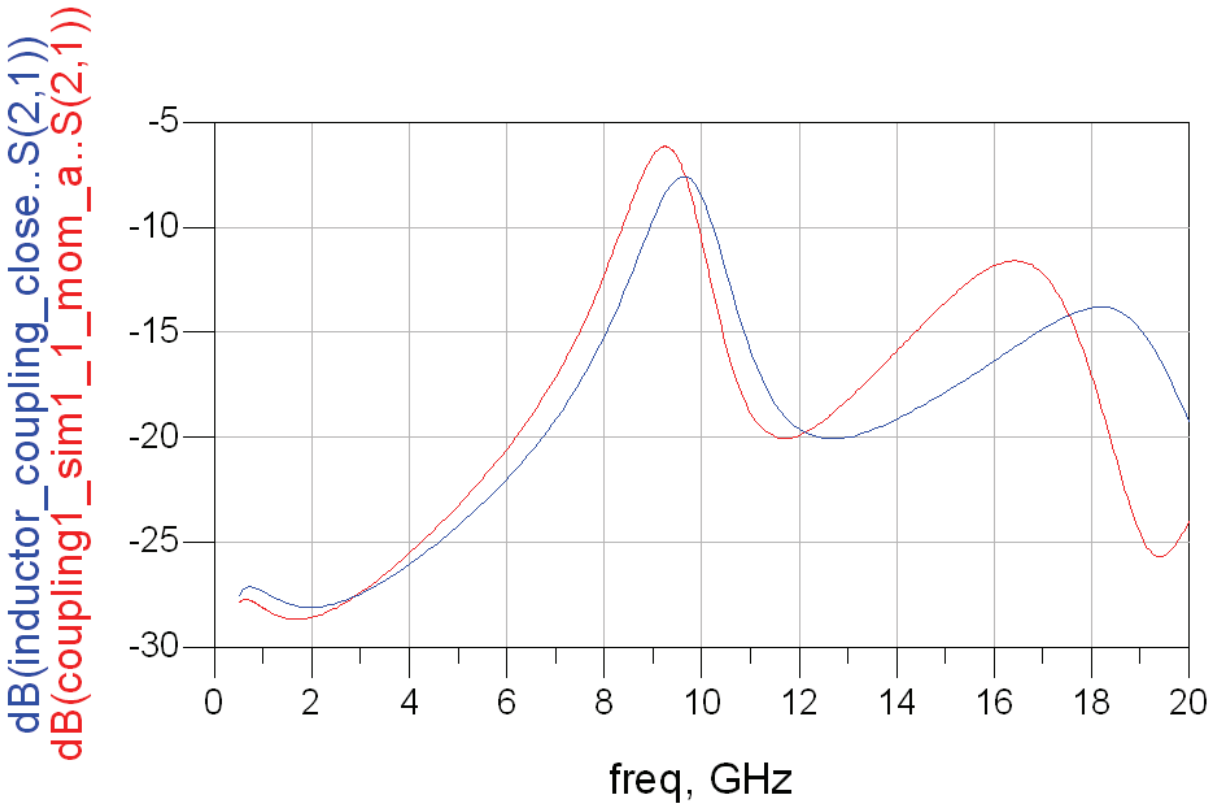

Figure 100: Phase plot of S_{21} from measurements and simulation - closely spaced inductors.

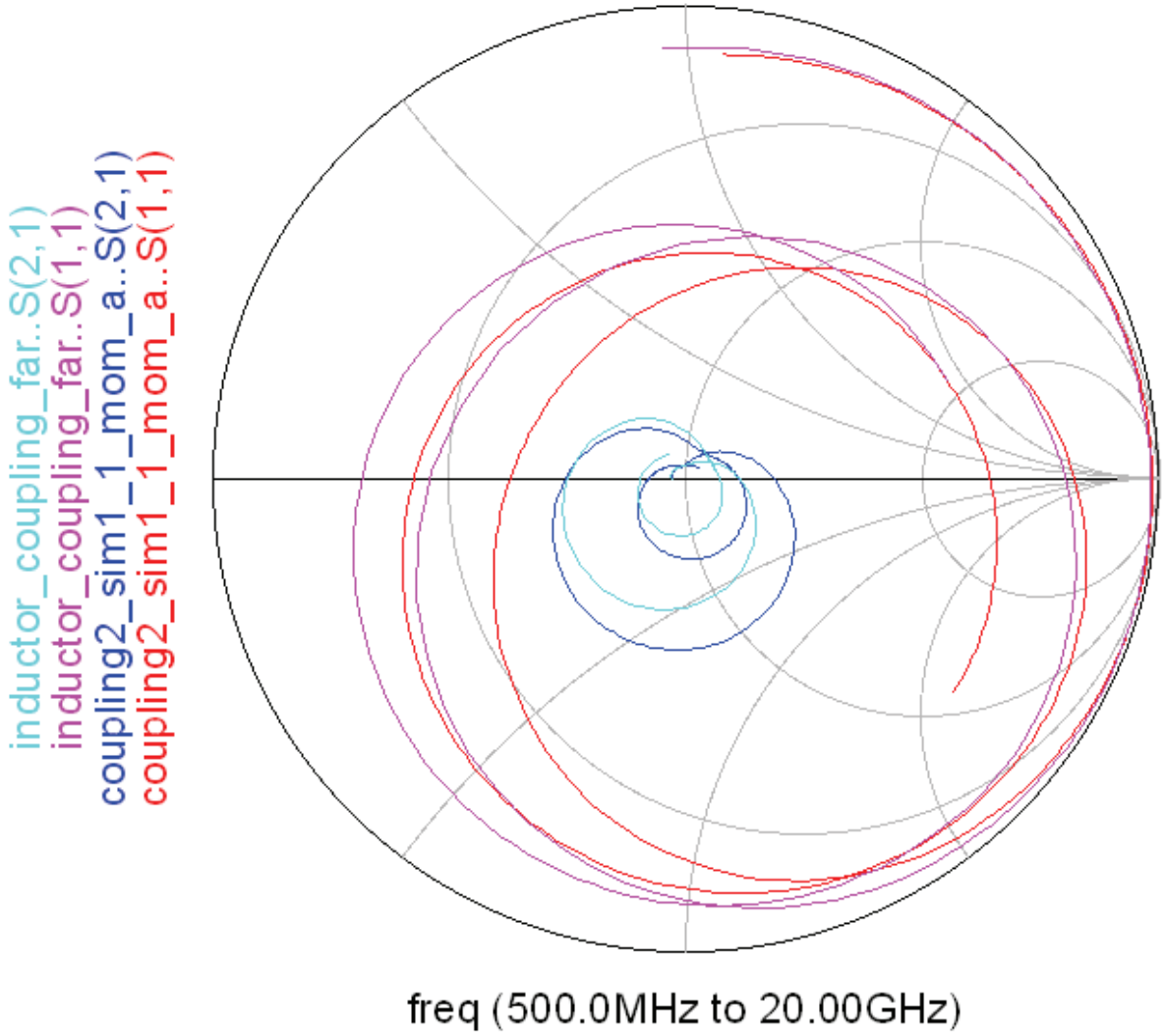

Figure 101: Smith Cart showing s-parameters from both Momentum simulation and measurements – far spaced inductors.

The Momentum vs. measurement data from the far spaced inductors has roughly the same deviations as in the case of the closely spaced inductors. See Tables 3 and 4 in Appendix A6 for numerical values.

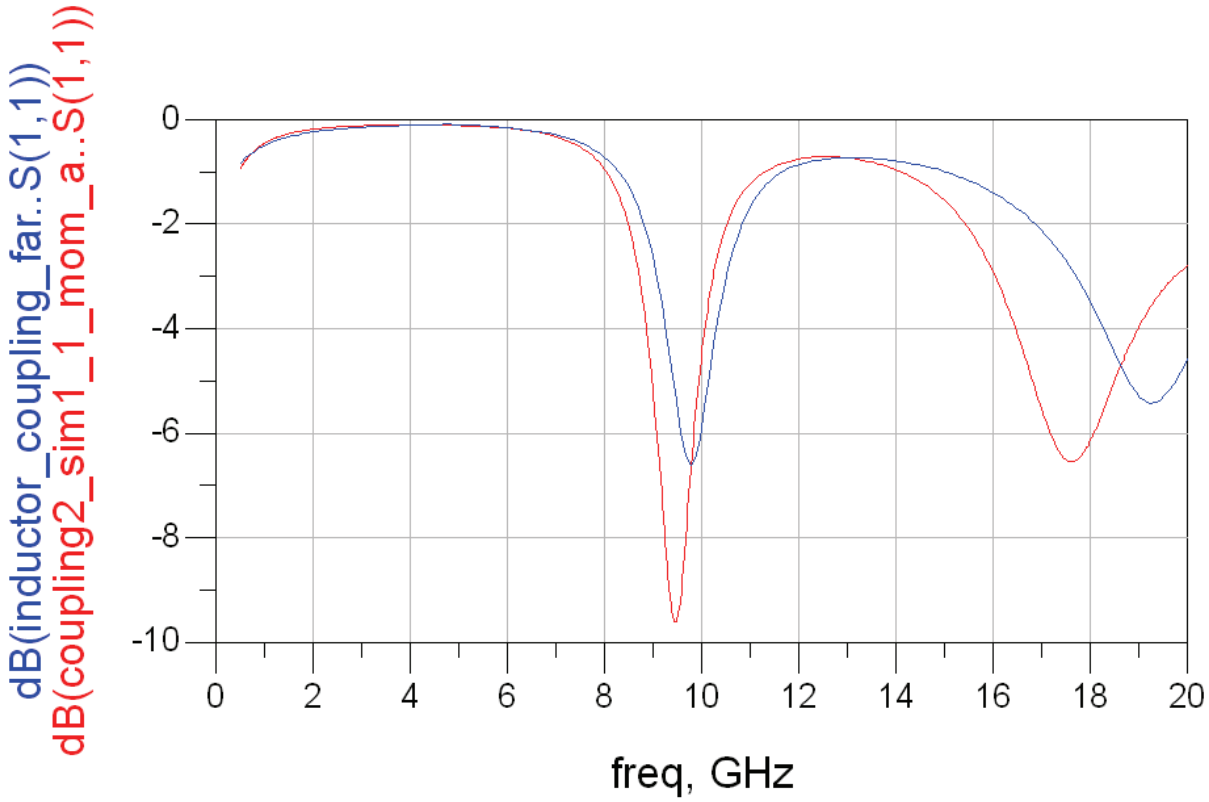

Figure 102: Decibel plot of S_{11} from measurements and simulation - far spaced inductors.

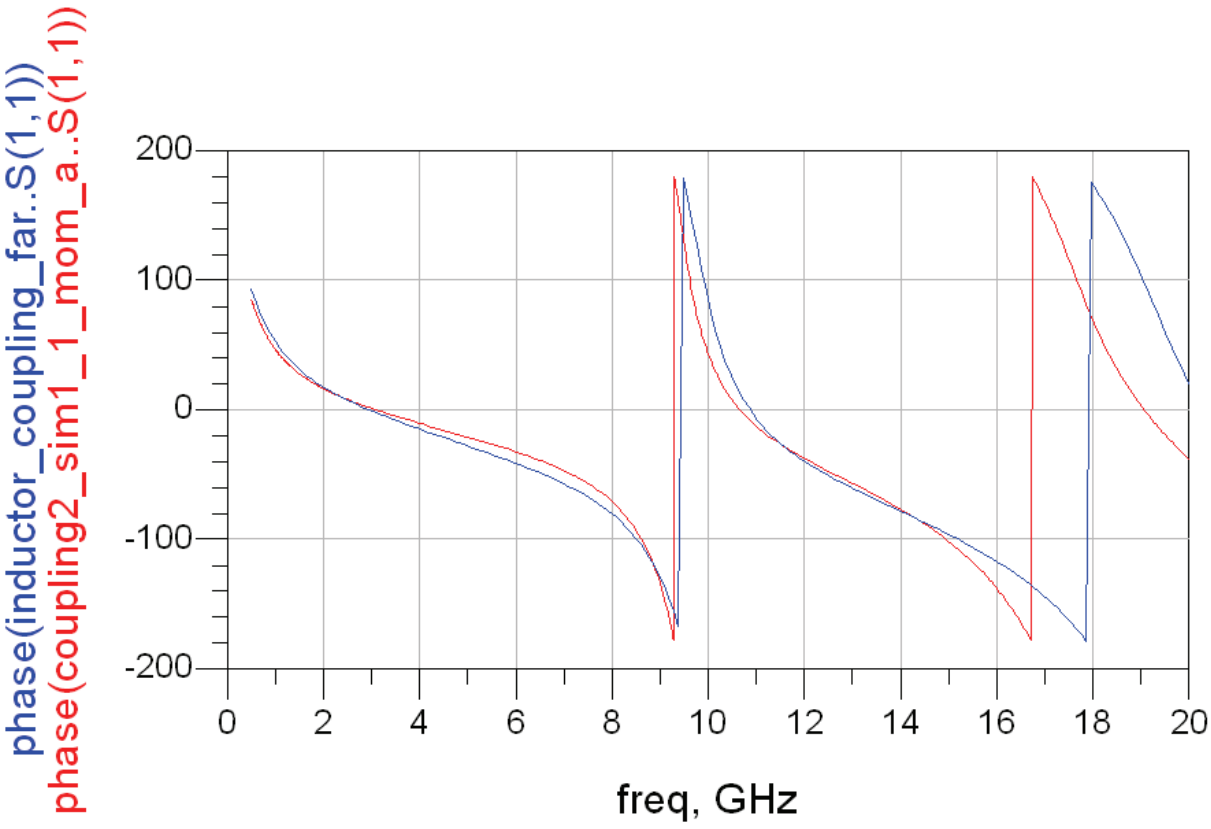

Figure 103: Phase plot of S_{11} from measurements and simulation - far spaced inductors.

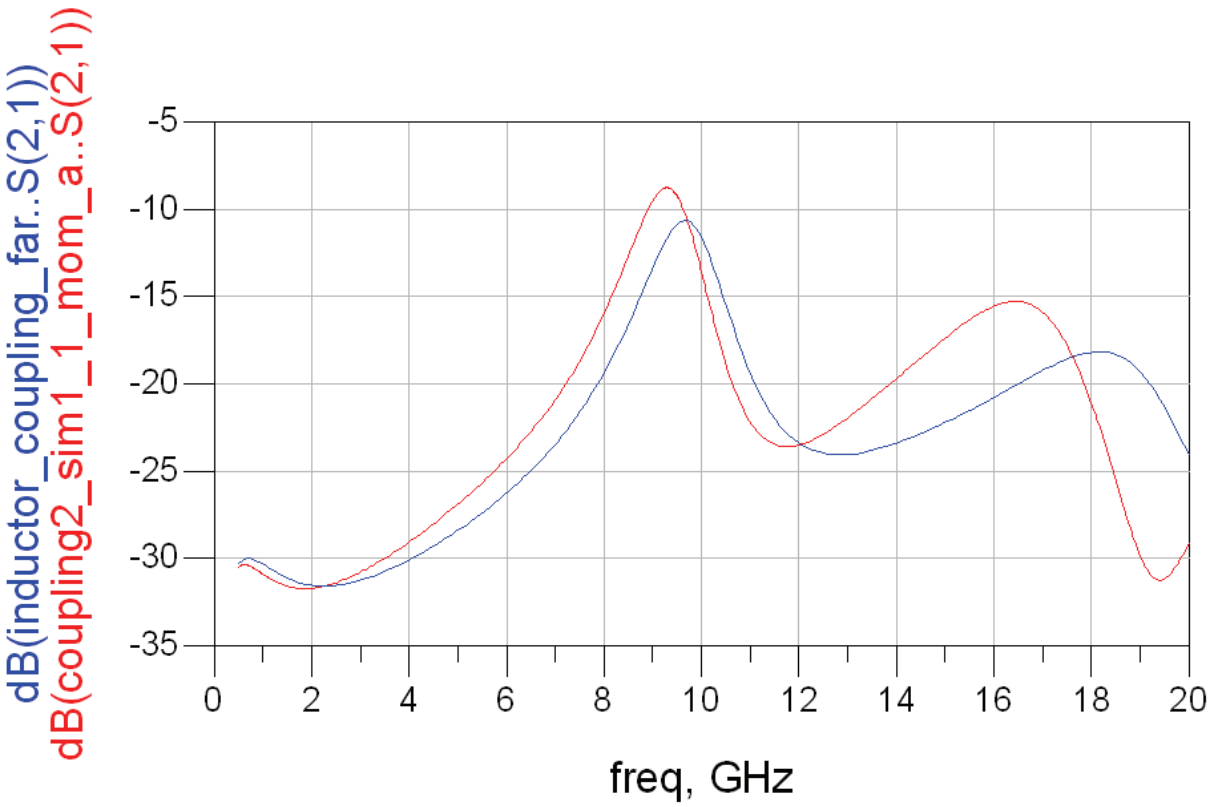

Figure 104: Decibel plot of S_{21} from measurements and simulation - far spaced inductors.

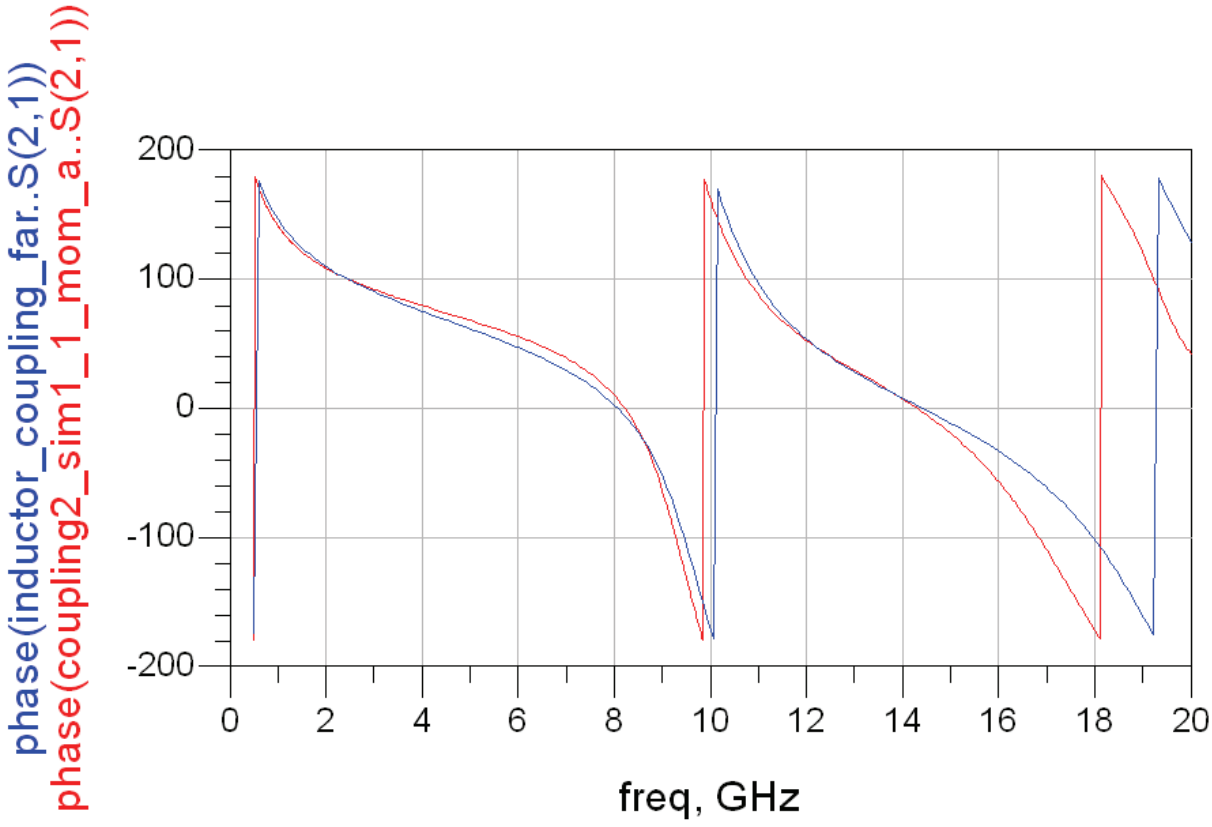

Figure 105: Phase plot of S_{21} from measurements and simulation - far spaced inductors.

Sources of Error

As we have seen in the measurement vs. simulation section, the agreement between measurement and simulation results is generally good, but can deviate in some cases and at some frequencies.

The results obtained from the TriQuint model seems to generally agree better with the measurements than those obtained from running ADS's Momentum. The differences between the two seems to be greatest in the case of inductors with few turns (i.e. inductor 3 of Appendix A4), in favour of the TriQuint model. In the case of inductor 1, which has thick lines (width=20 μm) the simulation results from both the model and Momentum is relatively inaccurate.

The coupled inductors show worse agreement between measurement and simulation than what is the case for single inductors. The difference between the two gets particularly large at higher frequencies.

One possible cause of deviation between measurement and simulation is process variations in the wafer production. Dimensions of the wafer and its structures, like transmission lines can vary from production to production. Also the thickness of the substrate can vary, causing deviations from the predicted behaviour. Each wafer is tested, and only accepted if it passes relatively strict tests, but process deviations can still occur.

Inaccuracies in the calibration process can also cause errors in the results. The reference plane needs to be the same in both simulation and measurement, or the results will differ. Another factor is the ports. These are ignored in the simulation, because they are calibrated out (de-embedded) in the measurements. The via holes are not ideal though, since they have a small inductance and resistance. In the simulations the signal is applied directly between the reference plane of the transmission line and the ground plane. This difference can cause deviation between measurement and simulation results.

If the reference plane is not equal in measurement and simulation there will be an extra inductance (and small resistance and capacitance) in the case where the reference plane is farthest from the component. This could also be a cause of error, especially in the case of the coupled inductors, where a separate calibration chip had to be used.

Predicted Accuracy of Fabricated Wilkinson Power Divider

From the above discussion and the conclusions we arrived at in the Measurement Vs. Simulation section it is apparent that we can not expect perfect agreement between the simulation and the produced circuit.

The results show that simulation predicts stronger coupling than what actually is the case, so this should not be a problem in the Wilkinson Power Divider circuit. They also show that the coupling depends on the separation distance between the inductors. The separation distance in the power divider is a lot bigger than that of the coupled inductors in Appendix A5, so cross-talk between the inductors should not be a problem in the produced circuit.

The Measurement Vs. Simulation section also shows that the accuracy of simulation results is good, indicating that the inductors of the produced circuit should show the same behaviour as in the simulations.

Since only inductor measurements are tested against ADS simulations, it is difficult to predict the accuracy of the overall circuit. The via holes, resistor, capacitors, transmission lines, ports etc. could cause inaccurate agreement between measurement and simulation. It is therefore impossible to predict the behaviour of the produced Wilkinson Power Divider based on the simulation results, though the Measurement Vs. Simulation section indicates that the agreement should be fairly good.

Effect of Momentum Meshing

Before running a Momentum simulation in ADS, the mesh needs to be set up. This setup is of key importance to the accuracy of the simulation result. One of the most important parameters is the mesh density (along with the mesh frequency). This decides the size of the mesh cells. All the simulations in this report use a 20 cells/wavelength setting for the mesh density. Since the components used are very small compared to a wavelength, this setting results in fairly large cells.

To examine what effect the mesh density setting can have on Momentum simulations, we compare a mesh density of 100 cells/wavelength to the original results obtained with a setting of 20 cells/wavelength. The circuit we use is inductor 1 from Appendix A4, and test whether increased mesh density leads to more accurate results. This inductor is chosen because the simulation results were fairly inaccurate, with room for improvement.

Figures 106 and 107 shows the magnitude (in decibel) and phase of both simulations along with actual measurements, while Figure 108 shows the same data plotted in a Smith Chart. sim1_2 is the simulation with high mesh density, while sim1_1 is the results from Momentum using a low mesh density.

From Figure 108 we can see that the simulation with increased mesh density gives a marginally better result for both S_{11} and S_{21} over the whole frequency range. This is true also for the phase of S_{21}, while there is an improvement in the phase of S_{11} for nearly the whole frequency range with increased mesh density.

As we can see, the improvement in simulation accuracy is small, and comes at the expense of increased simulation time (and memory usage). The mesh density of 20 cells/wavelength resulted in 98 rectangular cells, 169 triangular cells, 40 via cells and 444 edge currents, while a mesh density of 100 cells/wavelength gave 203 rectangular cells, 265 triangular cells, 91 via cells and 851 edge currents. The meshing of the component with a mesh density of 100 cells/wavelength can be seen in Figure 109.

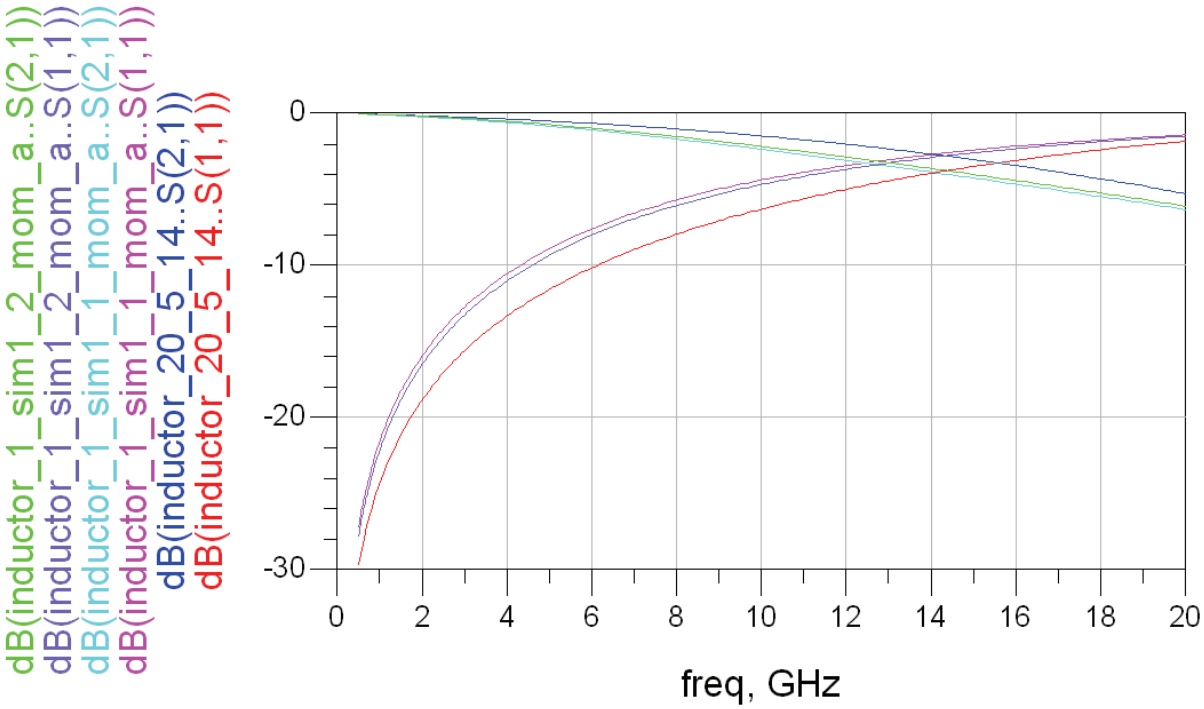

Figure 106: Decibel plot comparing the two mesh settings for inductor 1.

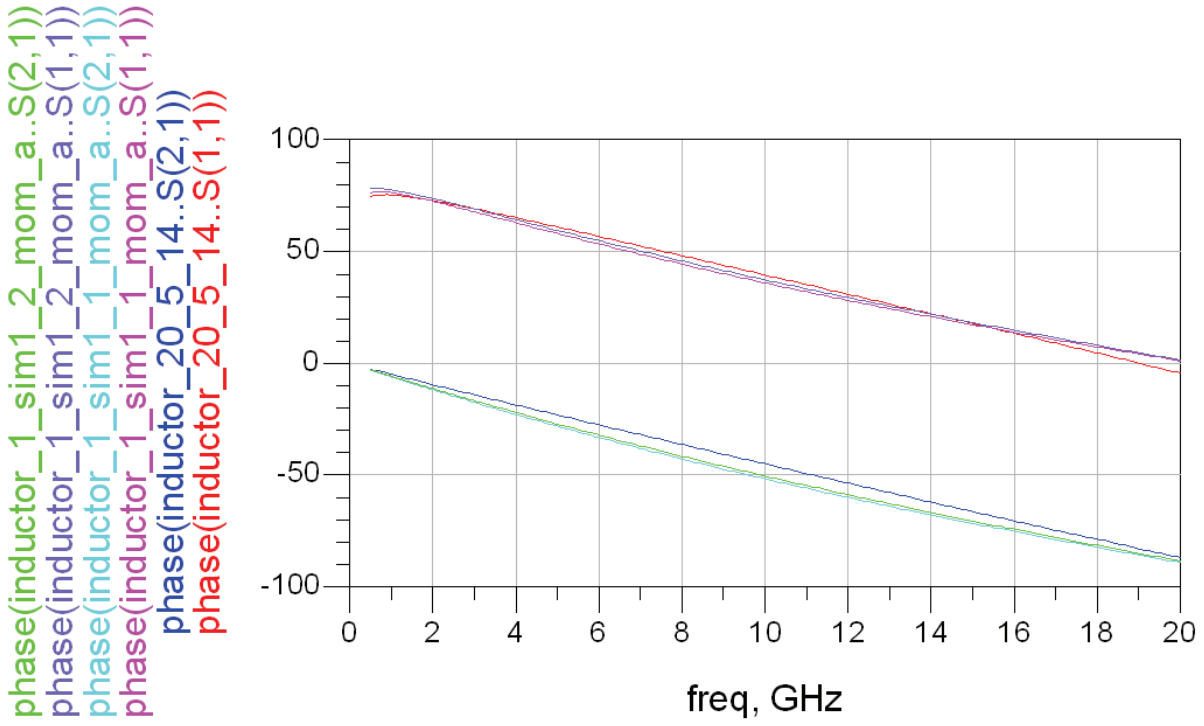

Figure 107: Phase plot comparing the two mesh settings for inductor 1.

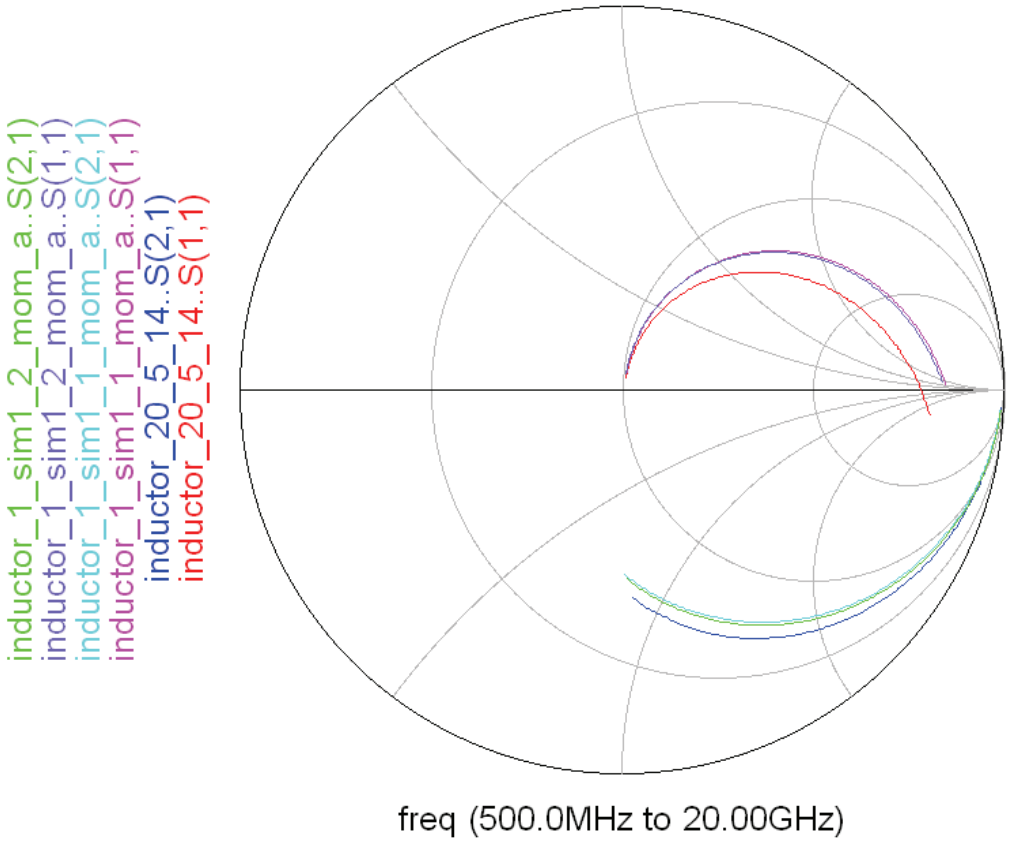

Figure 108: Smith Chart displaying the Momentum results using two different mesh densities for inductor 1.

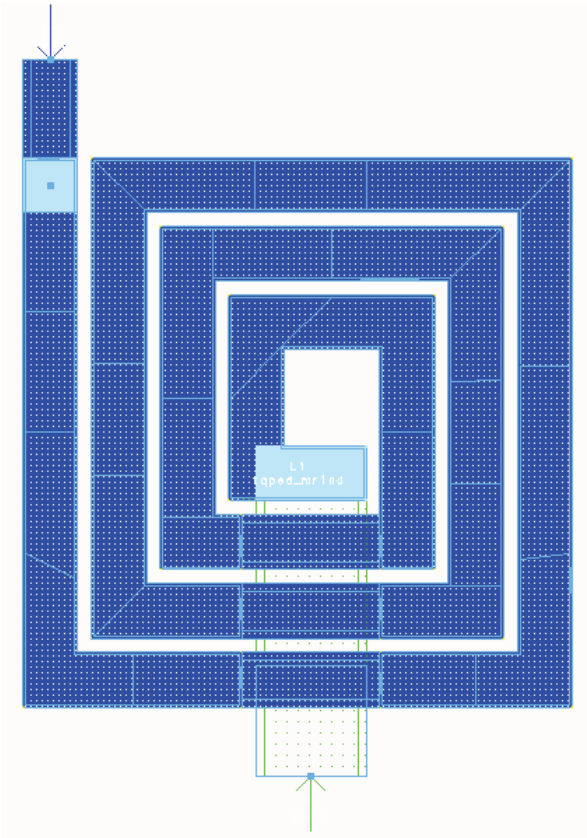

Figure 109: Inductor 1 (see Appendix A4) with a mesh density of 100 cells/wavelength. Meshing is displayed with light blue/green lines.

Summary

As space reduction of modern microwave circuits becomes more and more important, this report should be of relevance to RF designers. The Wilkinson Power Divider is a commonly used circuit and is therefore a good choice for learning the relevant techniques.

This report has described in detail all the steps involved in the process of designing a distributed Wilkinson Power Divider. The final circuit shows good performance while occupying a small area on the substrate (403 μm * 271 μm). The matching of the ports has been shown to be particularly good, at the expense of the isolation between ports 2 and 3. The loss from port 1 to ports 2 and 3 is reasonably low.

All relevant simulation results has been included and compared to the desired results. Deviations from these wanted results have been discussed, and the probable causes of these explained. The circuit has been simulated in both the frequency (s-parameters) domain and time domain.

Accurate measurement of single and coupled inductors has been performed using Automatic Network Analyzer and Probe Station. These measurement results has been compared to ADS's Momentum simulation results from the same component, and in most cases also the s-parameters from supplied TriQuint models for ADS. The deviations have been pointed out and the most probable causes have been described in the sources of error section.

After reading this report the reader should have a good understanding of how to use computer software tools to design MMIC circuits as well as a deep understanding of the technology and circuit used. The thorough theory part should make all aspects of the design process in the practical part clear to the reader.

The final layout should be ready for production. If it is to be used as a stand-alone unit, ports have to be added to the points where the signals are applied. This would normally involve some sort of coplanar waveguide to mictrostrip transmission line transition.

References

1. S. Lucyszyn and I.D. Robertson; RFIC and MMIC Design and Technology; London; Institution of Electrical Engineers; 2001
2. Günter Kompa; Practical Microstrip Design and Applications; Boston; Artech House; 2005
3. James W. Nilson and Susan A. Riedel; Electric Circuits; Upper Saddle River, N.J.; Pearson/Prentice Hall; 2005
4. Constantine A. Balanis; Antenna Theory – Analysis and Design; Hoboken, N.J.; John Wiley & Sons; 2005
5. Inder J. Bahl; Lumped Elements for RF and Microwave Circuits; Boston; Artech House; 2003
6. David J. Griffiths; Introduction to Electrodynamics; Upper Saddle River, N.J.; Prentice Hall; 1999
7. David K. Cheng; Field and Wave Electromagnetics; Reading, M.A.; Addison-Wesley; 1989
8. http://ieeexplore.ieee.org/stamp/stamp.jsp?tp=&arnumber=1124668&isnumber=24846
9. http://archive.evaluationengineering.com/archive/articles/0307/images/rf_fig3.jpg
10. http://www.microwaves101.com/encyclopedia/Network_theory.cfm#threeport
11. http://ieeexplore.ieee.org/stamp/stamp.jsp?tp=&arnumber=1126617&isnumber=24930
12. http://en.wikipedia.org/wiki/LC_circuit
13. http://www.ittc.ku.edu/~jstiles/723/handouts/Wilkinson%20Divider%20Even%20and%20Odd%20Mode%20Analysis.pdf
14. http://www.trilithic.com/RF%20and%20Microwave%20Components/Products/Power%20Dividers%20and%20Directional%20Couplers%20for%20Communications/Power%20Dividers%20and%20Directional%20Couplers%20for%20Communications.html
15. http://en.wikipedia.org/wiki/Wilkinson_power_divider
16. http://ieeexplore.ieee.org/stamp/stamp.jsp?tp=&arnumber=4395805
17. http://ursi-france.institut-telecom.fr/pages/pages_ursi/URSIGA08/papers/BP20p8.pdf
18. http://www.instockwireless.com/power_divider_pd1020.htm
19. http://en.wikipedia.org/wiki/Electrical_conductivity
20. http://ieeexplore.ieee.org/stamp/stamp.jsp?arnumber=596892&isnumber=13055
21. http://en.wikipedia.org/wiki/Michael_Faraday
22. http://mcalc.sourceforge.net/mstrip.gif
23. http://www.triquint.com/prodserv/foundry/docs/TQPEDv2_2.pdf
24. http://cp.literature.agilent.com/litweb/pdf/5988-3326EN.pdf
25. http://cp.literature.agilent.com/litweb/pdf/5965-7917E.pdf
26. http://www.microwaves101.com/encyclopedia/networkanalyzermeasurements.cfm
27. http://en.wikipedia.org/wiki/Probe_station
28. http://www.microwaves101.com/encyclopedia/rfprobe.cfm
29. http://images.pennnet.com/article_images/sst/org/edge-open_25percent.jpg
30. http://www.signatone.com/products/probestations/checkmate.asp
31. http://www.ittc.ku.edu/~jstiles/723/handouts/Odd%20Even%20Mode%20Analysis.pdf
32. http://en.wikipedia.org/wiki/Superposition_theorem
33. http://personal.ee.surrey.ac.uk/Personal/D.Jefferies/mmethod.html

34. http://en.wikipedia.org/wiki/Inductor
35. http://en.wikipedia.org/wiki/S-parameters
36. Guennadi Kouzaev; MMIC_2 handout; Course: TTT14 @ NTNU fall 2008
37. Guennadi Kouzaev; MMIC_3 handout; Course: TTT14 @ NTNU fall 2008
38. Guennadi Kouzaev; Components_VII_2 handout; Cource: TTT4205 @ NTNU fall 2007

Appendixes

Appendix A1 – Smith Chart

Appendix A2 – TriQuint 0.5 um TQPED Process

Appendix A3 – Two-Port Twelve-Term Error Correction Formulas for Vector Network Analyzers

Appendix A4 – Layout for Single Inductors

Appendix A5 – Layout for Coupled Inductors

Appendix A6 – Coupled Inductors Data

Appendix A7 – Inductor Inductance List

Appendix A8 – Inductor Resistance List

NAME	TITLE	DWG. NO.
SMITH CHART FORM ZY-01-N	ANALOG INSTRUMENTS COMPANY, NEW PROVIDENCE, N.J. 07974	DATE

NORMALIZED IMPEDANCE AND ADMITTANCE COORDINATES

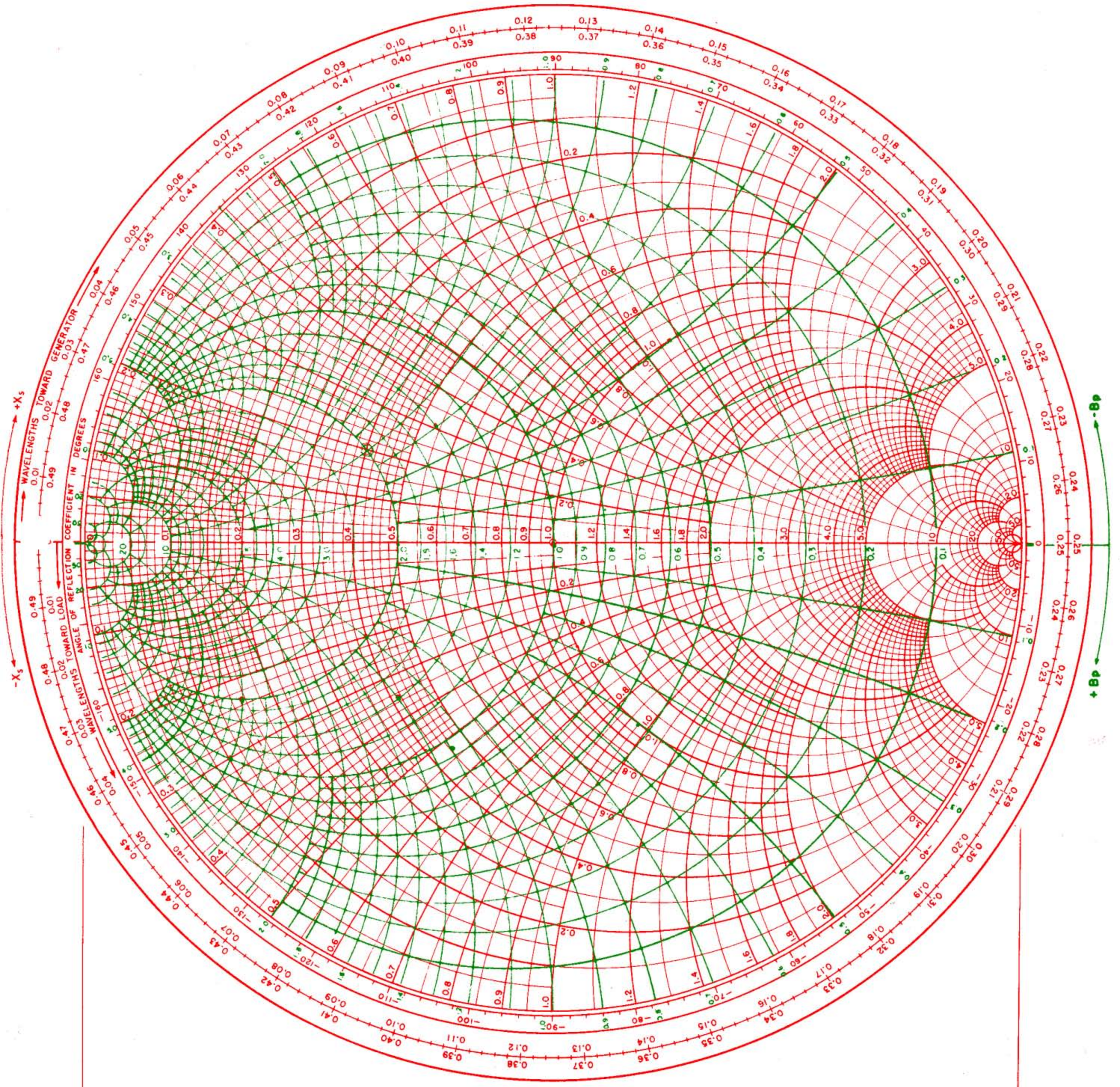

A1

TQPED

0.5 um E/D pHEMT Foundry Service

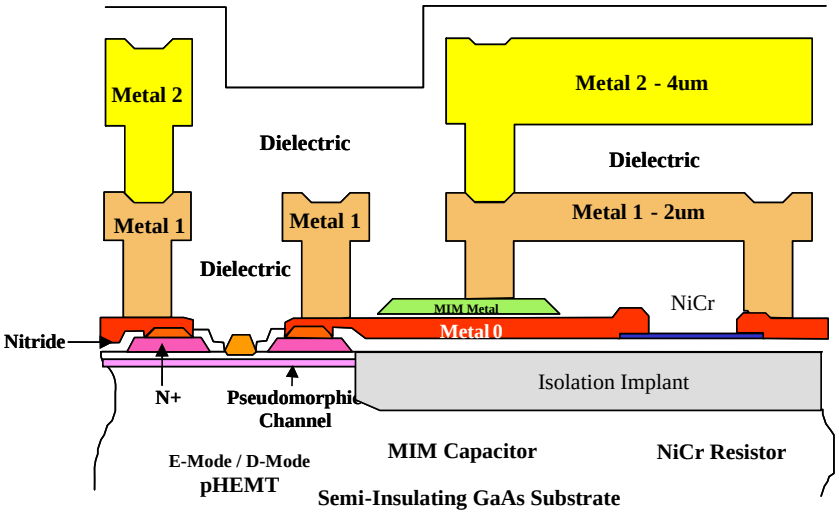

0.5 um pHEMT Device Cross-Section

General Description

TriQuint's TQPED process is based on our production-released 0.5 µm TQPHT process. TQPED partners an E-Mode pHEMT device with our TQPHT D-Mode transistors to be the first foundry pHEMT process to integrate E-Mode and D-Mode transistors on the same wafer. This process is targeted for low noise amplifiers, linear, low loss and high isolation RF switch applications, converters and integrated RF Front Ends. The TQPED process offers a D-Mode pHEMT with a –0.8 V pinch off, and an E-Mode pHEMT with a +0.35 V threshold voltage. The three metal interconnecting layers are encapsulated in a high performance dielectric that allows wiring flexibility, optimized die size and plastic packaging simplicity. Precision NiCr resistors and high value MIM capacitors are included allowing higher levels of integration, while maintaining smaller, cost –effective die sizes.

Features

- E-Mode, 0.35 V, Vth
- D-Mode, -0.8 V Vp
- InGaAs Active Layer pHEMT Process
- 0.5 um Optical Lithography Gates
- High Density Interconnects:
  - 2 Global
  - 1 Local
- High-Q Passives
- Thin Film Resistors
- High Value Capacitors
- Backside Vias Optional
- Based on Production TQPHT pHEMT and Interconnect
- Nominal TOM3 FET Models Available

Applications

- Highly Efficient, and Linear Power Amplifiers
- Low Loss, High Isolation, Low-Harmonic Content Switches
- Integrated digital control logic for Switches and Transceivers
- Converters
- Integrated RF Front Ends– LNA, SW, PA
- Wireless Transceivers, Base stations, Direct Broadcast Satellite Radars, Digital Radios, RF / Mixed Signal ICs
- Power Detectors and Couplers

TQPED

0.5 um E/D pHEMT Foundry Service

TQPED Process Details

Process Details @ Vds = 3.0V			
Element	Parameter	Value	Units
D-Mode pHEMT	Vp (1uA/um)	-0.8	V
	Idss (3V)	230	mA/mm
	Imax (3V)	515	mA/mm
	Breakdown, Vdg	15 min, 20 typ	V
	Ft @ 50% Idss	27	GHz
	Fmax @ 50% Idss	90	GHz
	Gm (50% Idss)	365	mS/mm
	Ron	1.4	Ohms * mm
E-Mode pHEMT	Vth (1uA/um)	+0.35	V
	Idss	0.1	uA/um
	Imax	320	mA/mm
	Breakdown, Vdg	15 min, 18 typ	V
	Ft @ 50% Idss	33	GHz
	Fmax @ 50% Idss	100	GHz
	Gm (50% Idss)	600	mS/mm
	Ron	2.5	Ohms * mm
Common Process Element Details			
Gate Length		0.5	µm
Interconnect		3	Metal Layers
MIM Caps	Value	630	pF/mm2
Resistors	NiCr	50	Ohms/sq
	Bulk	320	Ohms/sq

Maximum Ratings

Storage Temperature Range	-65 to +150	Deg C
Operating Temperature Range	-55 to +150	Deg C
EFET/DFET Transistor (Vs open; Idg = 1uA/um)	15	V
Capacitor	40	V

TriQuint Semiconductor
2300 NE Brookwood Pkwy
Hillsboro, Oregon 97124

Phone: 503-615-9000
Fax: 503-615-8905
Email: info@triquint.com

TQPED

0.5 um E/D pHEMT Foundry Service

Prototyping and Development

- Prototype Development Quick Turn (PDQ):
  - Shared mask set
  - Run monthly
  - Hot Lot cycle time
- Prototype Wafer Option (PWO):
  - Customer-specific masks; Customer schedule
  - 2 wafers delivered
  - Hot Lot cycle time
  - With thinning and sawing; optional backside vias

Design Tool Status

- Complete Design Manual Now
- Device Library of circuit elements: FETs, diodes, thin film resistors, capacitors, inductors
- Design Kit for Agilent's ADS design environment
- Design Kit planned for AWR Microwave Office
- Layout Library in GSD II format
- Cadence Development Kit with PCells in Preliminary Release
- Layout Rule Sets for Design Rule Check for ICED, Cadence
- Qualified package models for supported package styles
- Noise parameters on specific device sizes available

Training

- GaAs Design Classes:
  - Half-Day Introduction; Upon request
  - Four-Day Technical Training; Fall and Spring at TriQuint Oregon facility
- For Training & PDQ Schedules, please visit: www.triquint.com/foundry/

Process Qualification Status

- Mature process based on TQPHT 150-mm process
- Process fully released to production
- Full 150mm wafer Process Qualification complete
- For more information on Quality and Reliability, contact TriQuint or visit: www.triquint.com/manufacturing/QR/

Applications Support Services

- Tiling of GDSII stream files including PCM
- Design Rule Check services
- Layout Versus Schematic check services
- Packaging Development Engineering
- Test Development Engineering:
  - On-wafer
  - Packaged parts
- Thermal Analysis Engineering
- Yield Enhancement Engineering
- Part Qualification Services
- Failure Analysis

Manufacturing Services

- Mask making
- Production 150-mm wafer fab
- Wafer Thinning
- Wafer Sawing
- Substrate Vias
- DC Diesort Testing
- RF On-wafer testing
- Plastic Packaging
- RF Packaged Part Testing

Please contact your local TriQuint Semiconductor Representative/ Distributor or Foundry Services Division for Additional information:
E-mail: sales@triquint.com Phone: (503) 615-9000 Fax: (503) 615-8905

TriQuint Semiconductor
2300 NE Brookwood Pkwy
Hillsboro, Oregon 97124

Phone: 503-615-9000
Fax: 503-615-8905
Email: info@triquint.com

$$S_{11A} = \frac{\left[\left(\frac{S_{11M} - E_{DF}}{E_{RF}}\right)\left[1 + \left(\frac{S_{22M} - E_{DR}}{E_{RR}}\right)E_{SR}\right]\right] - \left[\left(\frac{S_{21M} - E_{XF}}{E_{TF}}\right)\left(\frac{S_{12M} - E_{XR}}{E_{TR}}\right)E_{LF}\right]}{\left[1 + \left(\frac{S_{11M} - E_{DF}}{E_{RF}}\right)E_{SF}\right]\left[1 + \left(\frac{S_{22M} - E_{DR}}{E_{RR}}\right)E_{SR}\right] - \left[\left(\frac{S_{21M} - E_{XF}}{E_{TF}}\right)\left(\frac{S_{12M} - E_{XR}}{E_{TR}}\right)E_{LF}E_{LR}\right]}$$

$$S_{21A} = \frac{\left[1 + \left(\frac{S_{22M} - E_{DR}}{E_{RR}}\right)\left(E_{SR} - E_{LF}\right)\right]\left(\frac{S_{21M} - E_{XF}}{E_{TF}}\right)}{\left[1 + \left(\frac{S_{11M} - E_{DF}}{E_{RF}}\right)E_{SF}\right]\left[1 + \left(\frac{S_{22M} - E_{DR}}{E_{RR}}\right)E_{SR}\right] - \left[\left(\frac{S_{21M} - E_{XF}}{E_{TF}}\right)\left(\frac{S_{12M} - E_{XR}}{E_{TR}}\right)E_{LF}E_{LR}\right]}$$

$$S_{12A} = \frac{\left[1 + \left(\frac{S_{11M} - E_{DF}}{E_{RF}}\right)\left(E_{SF} - E_{LR}\right)\right]\left(\frac{S_{12M} - E_{XR}}{E_{TR}}\right)}{\left[1 + \left(\frac{S_{11M} - E_{DF}}{E_{RF}}\right)E_{SF}\right]\left[1 + \left(\frac{S_{22M} - E_{DR}}{E_{RR}}\right)E_{SR}\right] - \left[\left(\frac{S_{21M} - E_{XF}}{E_{TF}}\right)\left(\frac{S_{12M} - E_{XR}}{E_{TR}}\right)E_{LF}E_{LR}\right]}$$

$$S_{22A} = \frac{\left[\left(\frac{S_{22M} - E_{DR}}{E_{RR}}\right)\left[1 + \left(\frac{S_{11M} - E_{DF}}{E_{RF}}\right)E_{SF}\right]\right] - \left[\left(\frac{S_{21M} - E_{XF}}{E_{TF}}\right)\left(\frac{S_{12M} - E_{XR}}{E_{TR}}\right)E_{LR}\right]}{\left[1 + \left(\frac{S_{11M} - E_{DF}}{E_{RF}}\right)E_{SF}\right]\left[1 + \left(\frac{S_{22M} - E_{DR}}{E_{RR}}\right)E_{SR}\right] - \left[\left(\frac{S_{21M} - E_{XF}}{E_{TF}}\right)\left(\frac{S_{12M} - E_{XR}}{E_{TR}}\right)E_{LF}E_{LR}\right]}$$

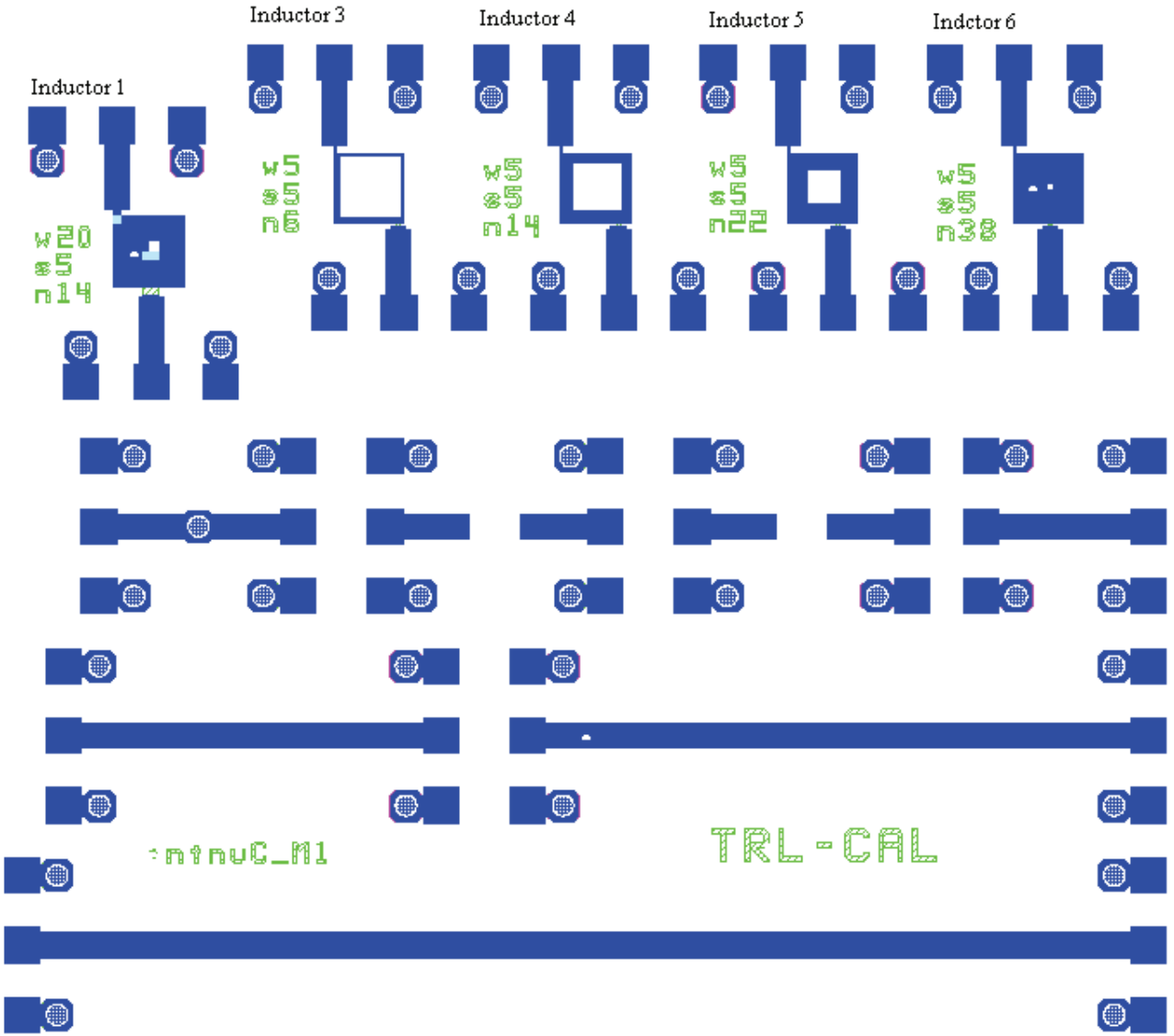
Inductor 1
Inductor 3
Inductor 4
Inductor 5
Indctor 6
w20
s5
n14
w5
s5
n6
w5
s5
n14
w5
s5
n22
w5
s5
n38
TRL-CAL

A4

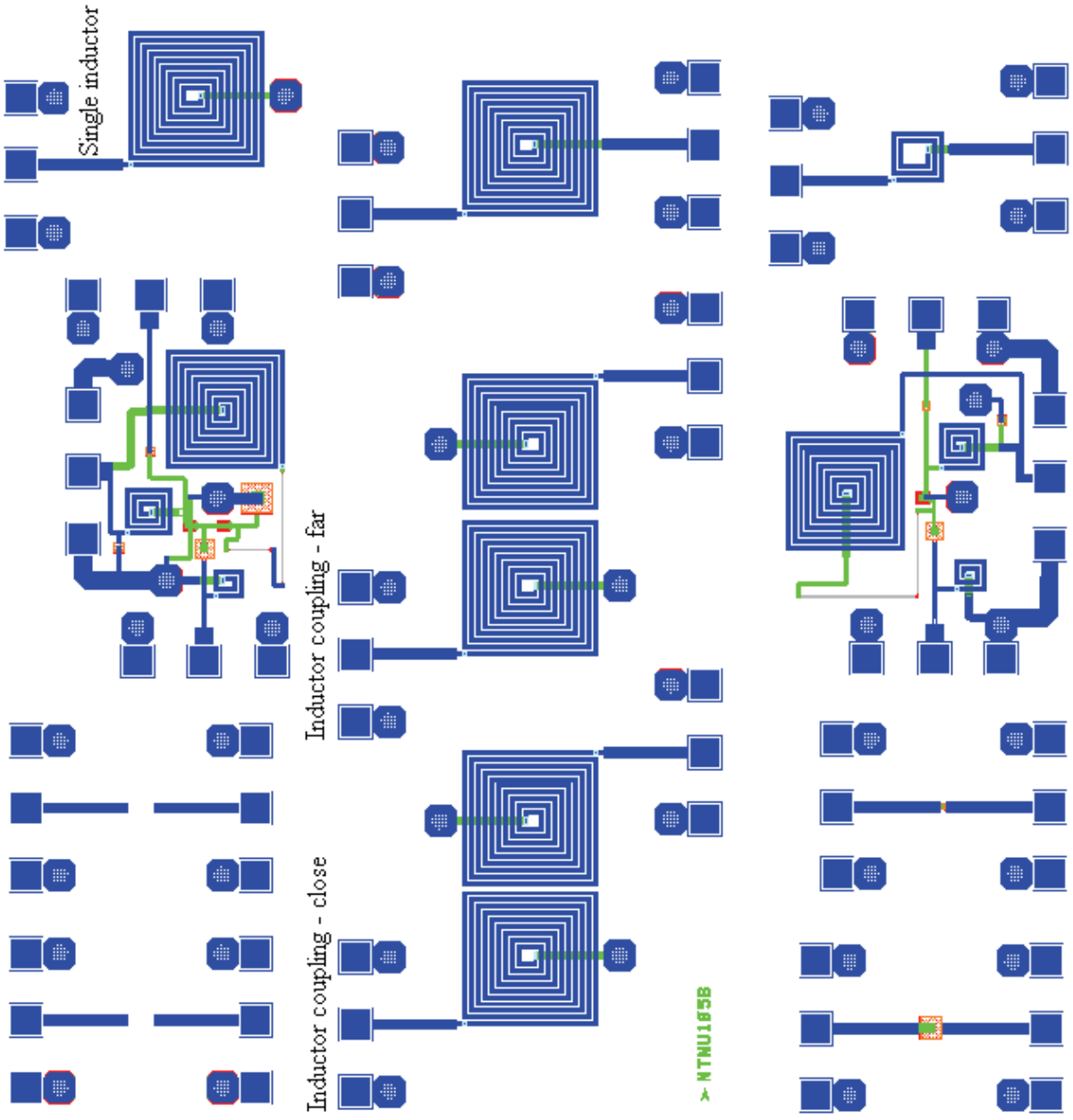
Single inductor
Inductor coupling - far
Inductor coupling - close
NTNU185B

Coupled inductors data

Close - S_{11}	*Meassurement freq.*	*Momentum freq.*	*Meassurement amplitude*	*Momentum amplitude*
Valley 1	9.8 GHz	9.4 GHz	-7.8 dB	-12.1 dB
Valley 2	19.2 GHz	17.5 GHz	-5.6 dB	-6.7 dB
Resonance 1	2.9 GHz	3.0 GHz	X	X
Resonance 2	9.4 GHz	9.3 GHz	X	X
Resonance 3	10.9 GHz	10.7 GHz	X	X
Resonance 4	17.8 GHz	16.7 GHz	X	X

Table 1: One line width spacing coupled inductors – S_{11} data.

Close - S_{21}	*Meassurement freq.*	*Momentum freq.*	*Meassurement amplitude*	*Momentum amplitude*
Peak 1	9.7 GHz	9.2 GHz	-7.6 dB	-6.2 dB
Peak 2	18.2 GHz	16.4 GHz	-13.8 dB	-11.6 dB
Resonance 1	0.5 GHz	0.5 GHz	X	X
Resonance 2	8.0 GHz	8.1 GHz	X	X
Resonance 3	10.1 GHz	9.9 GHz	X	X
Resonance 4	14.4 GHz	14.2 GHz	X	X
Resonance 5	19.3 GHz	18.1 GHz	X	X

Table 2: One line width spacing coupled inductors – S_{21} data.

Far - S_{11}	*Meassurement freq.*	*Momentum freq.*	*Meassurement amplitude*	*Momentum amplitude*
Valley 1	9.8 GHz	9.4 GHz	-6.6 dB	-9.6 dB
Valley 2	19.2 GHz	17.5 GHz	-5.4 dB	-6.5 dB
Resonance 1	2.9 GHz	3.0 GHz	X	X
Resonance 2	9.5 GHz	9.3 GHz	X	X
Resonance 3	10.8 GHz	10.7 GHz	X	X
Resonance 4	17.9 GHz	16.7 GHz	X	X

Table 3: Three line widths spacing coupled inductors – S_{11} data.

Far - S_{21}	*Meassurement freq.*	*Momentum freq.*	*Meassurement amplitude*	*Momentum amplitude*
Peak 1	9.7 GHz	9.3 GHz	-10.6 dB	-8.8 dB
Peak 2	18.2 GHz	16.5 GHz	-18.2 dB	-15.3 dB
Resonance 1	0.5 GHz	0.5 GHz	X	X
Resonance 2	8.1 GHz	8.2 GHz	X	X
Resonance 3	10.1 GHz	9.9 GHz	X	X
Resonance 4	14.4 GHz	14.3 GHz	X	X
Resonance 5	19.3 GHz	18.1 GHz	X	X

Table 4: Three line widths spacing coupled inductors – S_{21} data.

Inductance

freq	inductance1	inductance3	inductance5	inductance6
500.0 MHz	1.019E-9	9.929E-10	5.941E-9	8.231E-9
597.5 MHz	1.003E-9	9.922E-10	5.947E-9	8.237E-9
695.0 MHz	9.910E-10	9.929E-10	5.953E-9	8.251E-9
792.5 MHz	9.800E-10	9.928E-10	5.956E-9	8.255E-9
890.0 MHz	9.718E-10	9.927E-10	5.962E-9	8.269E-9
987.5 MHz	9.635E-10	9.913E-10	5.967E-9	8.276E-9
1.085 GHz	9.566E-10	9.894E-10	5.973E-9	8.285E-9
1.183 GHz	9.503E-10	9.883E-10	5.977E-9	8.299E-9
1.280 GHz	9.447E-10	9.857E-10	5.986E-9	8.318E-9
1.377 GHz	9.404E-10	9.848E-10	5.993E-9	8.336E-9
1.475 GHz	9.355E-10	9.831E-10	6.001E-9	8.357E-9
1.573 GHz	9.316E-10	9.809E-10	6.016E-9	8.385E-9
1.670 GHz	9.281E-10	9.800E-10	6.028E-9	8.412E-9
1.768 GHz	9.245E-10	9.780E-10	6.044E-9	8.447E-9
1.865 GHz	9.211E-10	9.774E-10	6.059E-9	8.483E-9
1.962 GHz	9.185E-10	9.761E-10	6.077E-9	8.520E-9
2.060 GHz	9.159E-10	9.751E-10	6.102E-9	8.571E-9
2.158 GHz	9.147E-10	9.759E-10	6.127E-9	8.627E-9
2.255 GHz	9.123E-10	9.748E-10	6.153E-9	8.679E-9
2.353 GHz	9.104E-10	9.744E-10	6.180E-9	8.739E-9
2.450 GHz	9.089E-10	9.743E-10	6.208E-9	8.796E-9
2.547 GHz	9.079E-10	9.752E-10	6.242E-9	8.871E-9
2.645 GHz	9.063E-10	9.750E-10	6.280E-9	8.955E-9
2.743 GHz	9.054E-10	9.749E-10	6.309E-9	9.025E-9
2.840 GHz	9.051E-10	9.746E-10	6.350E-9	9.110E-9
2.938 GHz	9.041E-10	9.738E-10	6.398E-9	9.215E-9
3.035 GHz	9.027E-10	9.736E-10	6.433E-9	9.300E-9
3.132 GHz	9.009E-10	9.716E-10	6.475E-9	9.397E-9
3.230 GHz	9.007E-10	9.719E-10	6.529E-9	9.517E-9
3.328 GHz	8.992E-10	9.704E-10	6.573E-9	9.621E-9
3.425 GHz	8.991E-10	9.703E-10	6.631E-9	9.752E-9
3.523 GHz	8.987E-10	9.701E-10	6.690E-9	9.893E-9
3.620 GHz	8.978E-10	9.692E-10	6.747E-9	1.002E-8
3.717 GHz	8.975E-10	9.685E-10	6.818E-9	1.018E-8
3.815 GHz	8.978E-10	9.685E-10	6.881E-9	1.034E-8
3.913 GHz	8.974E-10	9.681E-10	6.955E-9	1.052E-8
4.010 GHz	8.968E-10	9.680E-10	7.032E-9	1.070E-8
4.107 GHz	8.971E-10	9.684E-10	7.106E-9	1.089E-8
4.205 GHz	8.974E-10	9.690E-10	7.188E-9	1.109E-8
4.303 GHz	8.980E-10	9.698E-10	7.285E-9	1.132E-8
4.400 GHz	8.984E-10	9.699E-10	7.371E-9	1.156E-8
4.497 GHz	8.985E-10	9.703E-10	7.462E-9	1.180E-8
4.595 GHz	8.996E-10	9.713E-10	7.579E-9	1.210E-8
4.692 GHz	9.002E-10	9.721E-10	7.682E-9	1.238E-8
4.790 GHz	9.007E-10	9.725E-10	7.798E-9	1.269E-8
4.888 GHz	9.013E-10	9.726E-10	7.916E-9	1.302E-8
4.985 GHz	9.014E-10	9.725E-10	8.036E-9	1.336E-8
5.082 GHz	9.021E-10	9.730E-10	8.165E-9	1.373E-8
5.180 GHz	9.027E-10	9.731E-10	8.290E-9	1.411E-8
5.277 GHz	9.028E-10	9.730E-10	8.436E-9	1.454E-8
5.375 GHz	9.039E-10	9.737E-10	8.583E-9	1.498E-8
5.473 GHz	9.043E-10	9.737E-10	8.735E-9	1.543E-8
5.570 GHz	9.056E-10	9.748E-10	8.906E-9	1.598E-8
5.668 GHz	9.066E-10	9.750E-10	9.088E-9	1.652E-8
5.765 GHz	9.071E-10	9.751E-10	9.275E-9	1.712E-8
5.862 GHz	9.088E-10	9.767E-10	9.474E-9	1.773E-8
5.960 GHz	9.095E-10	9.767E-10	9.688E-9	1.842E-8
6.058 GHz	9.103E-10	9.773E-10	9.905E-9	1.908E-8
6.155 GHz	9.123E-10	9.785E-10	1.016E-8	1.989E-8
6.253 GHz	9.142E-10	9.801E-10	1.042E-8	2.060E-8
6.350 GHz	9.153E-10	9.804E-10	1.070E-8	2.133E-8
6.447 GHz	9.175E-10	9.825E-10	1.100E-8	2.198E-8
6.545 GHz	9.188E-10	9.830E-10	1.132E-8	2.233E-8
6.643 GHz	9.209E-10	9.838E-10	1.166E-8	2.237E-8
6.740 GHz	9.229E-10	9.853E-10	1.202E-8	2.164E-8
6.838 GHz	9.249E-10	9.866E-10	1.240E-8	1.976E-8
6.935 GHz	9.270E-10	9.876E-10	1.284E-8	1.674E-8
7.032 GHz	9.276E-10	9.876E-10	1.323E-8	1.145E-8
7.130 GHz	9.286E-10	9.875E-10	1.367E-8	4.595E-9
7.228 GHz	9.301E-10	9.882E-10	1.415E-8	-3.438E-9
7.325 GHz	9.316E-10	9.885E-10	1.461E-8	-1.144E-8
7.423 GHz	9.329E-10	9.890E-10	1.508E-8	-1.781E-8
7.520 GHz	9.353E-10	9.905E-10	1.562E-8	-2.235E-8
7.617 GHz	9.377E-10	9.918E-10	1.605E-8	-2.458E-8
7.715 GHz	9.391E-10	9.925E-10	1.649E-8	-2.551E-8
7.813 GHz	9.414E-10	9.942E-10	1.687E-8	-2.538E-8
7.910 GHz	9.437E-10	9.952E-10	1.710E-8	-2.459E-8
8.008 GHz	9.455E-10	9.960E-10	1.710E-8	-2.341E-8
8.105 GHz	9.485E-10	9.977E-10	1.677E-8	-2.209E-8
8.203 GHz	9.502E-10	9.984E-10	1.572E-8	-2.073E-8
8.300 GHz	9.535E-10	1.000E-9	1.397E-8	-1.942E-8
8.398 GHz	9.560E-10	1.001E-9	1.114E-8	-1.816E-8
8.495 GHz	9.584E-10	1.002E-9	6.999E-9	-1.696E-8
8.592 GHz	9.612E-10	1.003E-9	1.402E-9	-1.575E-8
8.690 GHz	9.638E-10	1.002E-9	-4.307E-9	-1.462E-8
8.787 GHz	9.662E-10	9.995E-10	-8.528E-9	-1.354E-8
8.885 GHz	9.692E-10	9.948E-10	-9.879E-9	-1.272E-8
8.982 GHz	9.718E-10	9.893E-10	-8.962E-9	-1.244E-8
9.080 GHz	9.747E-10	9.947E-10	-1.038E-8	-1.242E-8
9.178 GHz	9.782E-10	1.005E-9	-1.453E-8	-1.220E-8
9.275 GHz	9.802E-10	1.010E-9	-1.807E-8	-1.170E-8
9.373 GHz	9.830E-10	1.014E-9	-1.984E-8	-1.111E-8
9.470 GHz	9.857E-10	1.017E-9	-2.011E-8	-1.053E-8
9.568 GHz	9.889E-10	1.019E-9	-1.976E-8	-1.002E-8
9.665 GHz	9.917E-10	1.021E-9	-1.904E-8	-9.548E-9
9.762 GHz	9.952E-10	1.023E-9	-1.821E-8	-9.119E-9
9.860 GHz	9.978E-10	1.025E-9	-1.725E-8	-8.716E-9
9.957 GHz	1.002E-9	1.028E-9	-1.631E-8	-8.342E-9

10.06 GHz	1.005E-9	1.030E-9	-1.541E-8	-7.991E-9
10.15 GHz	1.009E-9	1.032E-9	-1.459E-8	-7.690E-9
10.25 GHz	1.012E-9	1.034E-9	-1.378E-8	-7.379E-9
10.35 GHz	1.016E-9	1.036E-9	-1.303E-8	-7.103E-9
10.45 GHz	1.020E-9	1.038E-9	-1.237E-8	-6.846E-9
10.54 GHz	1.025E-9	1.041E-9	-1.174E-8	-6.588E-9
10.64 GHz	1.028E-9	1.043E-9	-1.112E-8	-6.348E-9
10.74 GHz	1.031E-9	1.044E-9	-1.056E-8	-6.122E-9
10.84 GHz	1.036E-9	1.047E-9	-1.003E-8	-5.908E-9
10.93 GHz	1.038E-9	1.048E-9	-9.590E-9	-5.715E-9
11.03 GHz	1.043E-9	1.050E-9	-9.145E-9	-5.526E-9
11.13 GHz	1.047E-9	1.052E-9	-8.761E-9	-5.353E-9
11.23 GHz	1.050E-9	1.053E-9	-8.382E-9	-5.178E-9
11.32 GHz	1.054E-9	1.056E-9	-8.033E-9	-5.015E-9
11.42 GHz	1.059E-9	1.058E-9	-7.712E-9	-4.865E-9
11.52 GHz	1.063E-9	1.060E-9	-7.410E-9	-4.715E-9
11.62 GHz	1.068E-9	1.063E-9	-7.118E-9	-4.576E-9
11.71 GHz	1.073E-9	1.066E-9	-6.863E-9	-4.444E-9
11.81 GHz	1.077E-9	1.068E-9	-6.618E-9	-4.317E-9
11.91 GHz	1.083E-9	1.072E-9	-6.373E-9	-4.192E-9
12.01 GHz	1.088E-9	1.074E-9	-6.158E-9	-4.078E-9
12.10 GHz	1.092E-9	1.077E-9	-5.951E-9	-3.966E-9
12.20 GHz	1.098E-9	1.080E-9	-5.748E-9	-3.862E-9
12.30 GHz	1.103E-9	1.083E-9	-5.561E-9	-3.756E-9
12.40 GHz	1.108E-9	1.086E-9	-5.378E-9	-3.656E-9
12.49 GHz	1.114E-9	1.089E-9	-5.212E-9	-3.563E-9
12.59 GHz	1.119E-9	1.092E-9	-5.051E-9	-3.471E-9
12.69 GHz	1.126E-9	1.096E-9	-4.901E-9	-3.385E-9
12.79 GHz	1.132E-9	1.100E-9	-4.761E-9	-3.304E-9
12.88 GHz	1.136E-9	1.102E-9	-4.622E-9	-3.221E-9
12.98 GHz	1.140E-9	1.104E-9	-4.491E-9	-3.142E-9
13.08 GHz	1.143E-9	1.106E-9	-4.362E-9	-3.066E-9
13.18 GHz	1.147E-9	1.109E-9	-4.242E-9	-2.993E-9
13.27 GHz	1.153E-9	1.112E-9	-4.126E-9	-2.921E-9
13.37 GHz	1.157E-9	1.115E-9	-4.023E-9	-2.856E-9
13.47 GHz	1.163E-9	1.119E-9	-3.914E-9	-2.788E-9
13.57 GHz	1.169E-9	1.122E-9	-3.813E-9	-2.723E-9
13.66 GHz	1.173E-9	1.126E-9	-3.716E-9	-2.661E-9
13.76 GHz	1.180E-9	1.129E-9	-3.619E-9	-2.598E-9
13.86 GHz	1.185E-9	1.133E-9	-3.535E-9	-2.542E-9
13.96 GHz	1.190E-9	1.136E-9	-3.439E-9	-2.481E-9
14.05 GHz	1.195E-9	1.140E-9	-3.356E-9	-2.427E-9
14.15 GHz	1.199E-9	1.143E-9	-3.269E-9	-2.371E-9
14.25 GHz	1.204E-9	1.146E-9	-3.195E-9	-2.318E-9
14.35 GHz	1.208E-9	1.149E-9	-3.114E-9	-2.267E-9
14.44 GHz	1.214E-9	1.154E-9	-3.045E-9	-2.218E-9
14.54 GHz	1.217E-9	1.156E-9	-2.979E-9	-2.174E-9
14.64 GHz	1.222E-9	1.160E-9	-2.917E-9	-2.129E-9
14.73 GHz	1.226E-9	1.163E-9	-2.850E-9	-2.084E-9
14.83 GHz	1.228E-9	1.166E-9	-2.784E-9	-2.038E-9
14.93 GHz	1.231E-9	1.171E-9	-2.728E-9	-1.998E-9
15.03 GHz	1.235E-9	1.175E-9	-2.670E-9	-1.956E-9
15.13 GHz	1.236E-9	1.177E-9	-2.611E-9	-1.915E-9
15.22 GHz	1.240E-9	1.183E-9	-2.558E-9	-1.876E-9
15.32 GHz	1.243E-9	1.187E-9	-2.509E-9	-1.840E-9
15.42 GHz	1.246E-9	1.192E-9	-2.453E-9	-1.801E-9
15.52 GHz	1.247E-9	1.196E-9	-2.403E-9	-1.764E-9
15.61 GHz	1.247E-9	1.200E-9	-2.354E-9	-1.728E-9
15.71 GHz	1.247E-9	1.205E-9	-2.304E-9	-1.691E-9
15.81 GHz	1.248E-9	1.210E-9	-2.259E-9	-1.658E-9
15.90 GHz	1.245E-9	1.214E-9	-2.214E-9	-1.623E-9
16.00 GHz	1.245E-9	1.219E-9	-2.170E-9	-1.589E-9
16.10 GHz	1.241E-9	1.222E-9	-2.126E-9	-1.558E-9
16.20 GHz	1.238E-9	1.226E-9	-2.086E-9	-1.526E-9
16.30 GHz	1.234E-9	1.231E-9	-2.044E-9	-1.494E-9
16.39 GHz	1.228E-9	1.235E-9	-2.005E-9	-1.463E-9
16.49 GHz	1.220E-9	1.239E-9	-1.968E-9	-1.434E-9
16.59 GHz	1.208E-9	1.241E-9	-1.929E-9	-1.404E-9
16.68 GHz	1.199E-9	1.247E-9	-1.893E-9	-1.376E-9
16.78 GHz	1.185E-9	1.250E-9	-1.857E-9	-1.347E-9
16.88 GHz	1.167E-9	1.253E-9	-1.820E-9	-1.318E-9
16.98 GHz	1.153E-9	1.258E-9	-1.786E-9	-1.291E-9
17.07 GHz	1.131E-9	1.259E-9	-1.752E-9	-1.264E-9
17.17 GHz	1.112E-9	1.262E-9	-1.719E-9	-1.237E-9
17.27 GHz	1.090E-9	1.265E-9	-1.687E-9	-1.210E-9
17.37 GHz	1.058E-9	1.264E-9	-1.654E-9	-1.184E-9
17.47 GHz	1.033E-9	1.264E-9	-1.623E-9	-1.158E-9
17.56 GHz	1.004E-9	1.261E-9	-1.592E-9	-1.132E-9
17.66 GHz	9.686E-10	1.251E-9	-1.564E-9	-1.108E-9
17.76 GHz	9.299E-10	1.237E-9	-1.544E-9	-1.086E-9
17.86 GHz	8.823E-10	1.210E-9	-1.537E-9	-1.068E-9
17.95 GHz	8.357E-10	1.182E-9	-1.544E-9	-1.060E-9
18.05 GHz	7.817E-10	1.167E-9	-1.545E-9	-1.052E-9
18.15 GHz	7.306E-10	1.186E-9	-1.532E-9	-1.040E-9
18.25 GHz	6.594E-10	1.220E-9	-1.505E-9	-1.021E-9
18.34 GHz	5.933E-10	1.256E-9	-1.476E-9	-9.976E-10
18.44 GHz	5.161E-10	1.281E-9	-1.447E-9	-9.738E-10
18.54 GHz	4.357E-10	1.302E-9	-1.418E-9	-9.496E-10
18.64 GHz	3.499E-10	1.318E-9	-1.391E-9	-9.262E-10
18.73 GHz	2.529E-10	1.331E-9	-1.365E-9	-9.026E-10
18.83 GHz	1.606E-10	1.341E-9	-1.340E-9	-8.804E-10
18.93 GHz	4.983E-11	1.350E-9	-1.314E-9	-8.574E-10
19.02 GHz	-5.749E-11	1.359E-9	-1.291E-9	-8.362E-10
19.12 GHz	-1.842E-10	1.366E-9	-1.266E-9	-8.139E-10
19.22 GHz	-2.936E-10	1.369E-9	-1.245E-9	-7.929E-10
19.32 GHz	-4.085E-10	1.376E-9	-1.223E-9	-7.722E-10
19.41 GHz	-5.221E-10	1.379E-9	-1.204E-9	-7.521E-10
19.51 GHz	-6.319E-10	1.384E-9	-1.184E-9	-7.323E-10
19.61 GHz	-7.468E-10	1.390E-9	-1.166E-9	-7.127E-10
19.71 GHz	-8.641E-10	1.399E-9	-1.147E-9	-6.925E-10
19.81 GHz	-9.803E-10	1.402E-9	-1.129E-9	-6.735E-10
19.90 GHz	-1.095E-9	1.408E-9	-1.112E-9	-6.540E-10
20.00 GHz	-1.215E-9	1.414E-9	-1.094E-9	-6.344E-10

Resistance

freq	resistance1	resistance3	resistance5	resistance6
500.0 MHz	1.015	1.019	1.061	1.082
597.5 MHz	1.017	1.019	1.065	1.090
695.0 MHz	1.019	1.020	1.070	1.098
792.5 MHz	1.021	1.021	1.076	1.107
890.0 MHz	1.022	1.022	1.081	1.117
987.5 MHz	1.024	1.023	1.088	1.128
1.085 GHz	1.026	1.024	1.095	1.141
1.183 GHz	1.028	1.025	1.102	1.154
1.280 GHz	1.030	1.025	1.111	1.168
1.377 GHz	1.031	1.026	1.120	1.185
1.475 GHz	1.033	1.027	1.129	1.200
1.573 GHz	1.035	1.029	1.140	1.220
1.670 GHz	1.037	1.030	1.151	1.239
1.768 GHz	1.039	1.031	1.162	1.259
1.865 GHz	1.041	1.032	1.175	1.282
1.962 GHz	1.044	1.033	1.187	1.305
2.060 GHz	1.046	1.035	1.200	1.327
2.158 GHz	1.048	1.036	1.215	1.355
2.255 GHz	1.050	1.038	1.230	1.381
2.353 GHz	1.053	1.039	1.244	1.408
2.450 GHz	1.055	1.041	1.261	1.440
2.547 GHz	1.058	1.042	1.275	1.467
2.645 GHz	1.060	1.044	1.295	1.503
2.743 GHz	1.063	1.046	1.316	1.544
2.840 GHz	1.066	1.048	1.332	1.576
2.938 GHz	1.068	1.050	1.355	1.617
3.035 GHz	1.071	1.051	1.379	1.668
3.132 GHz	1.074	1.053	1.400	1.712
3.230 GHz	1.077	1.055	1.427	1.762
3.328 GHz	1.080	1.057	1.455	1.822
3.425 GHz	1.083	1.059	1.479	1.873
3.523 GHz	1.086	1.061	1.511	1.940
3.620 GHz	1.089	1.063	1.542	2.011
3.717 GHz	1.093	1.065	1.573	2.080
3.815 GHz	1.097	1.068	1.612	2.164
3.913 GHz	1.100	1.069	1.645	2.246
4.010 GHz	1.104	1.073	1.688	2.342
4.107 GHz	1.107	1.075	1.729	2.444
4.205 GHz	1.111	1.077	1.768	2.543
4.303 GHz	1.115	1.081	1.814	2.660
4.400 GHz	1.119	1.083	1.865	2.792
4.497 GHz	1.123	1.086	1.910	2.917
4.595 GHz	1.128	1.089	1.967	3.067
4.692 GHz	1.132	1.091	2.024	3.238
4.790 GHz	1.136	1.095	2.085	3.413
4.888 GHz	1.141	1.098	2.158	3.633
4.985 GHz	1.145	1.100	2.231	3.863
5.082 GHz	1.150	1.103	2.307	4.125
5.180 GHz	1.154	1.106	2.393	4.427
5.277 GHz	1.158	1.108	2.485	4.752
5.375 GHz	1.163	1.112	2.577	5.111
5.473 GHz	1.168	1.114	2.687	5.549
5.570 GHz	1.173	1.117	2.794	6.027
5.668 GHz	1.179	1.121	2.918	6.581
5.765 GHz	1.184	1.124	3.062	7.247
5.862 GHz	1.189	1.127	3.190	7.947
5.960 GHz	1.195	1.131	3.356	8.866
6.058 GHz	1.200	1.134	3.524	9.886
6.155 GHz	1.206	1.137	3.703	11.088
6.253 GHz	1.212	1.142	3.914	12.534
6.350 GHz	1.218	1.145	4.152	14.377
6.447 GHz	1.225	1.150	4.384	16.454
6.545 GHz	1.231	1.153	4.687	19.199
6.643 GHz	1.238	1.158	5.017	22.419
6.740 GHz	1.244	1.162	5.375	26.105
6.838 GHz	1.251	1.166	5.811	30.501
6.935 GHz	1.259	1.171	6.276	35.600
7.032 GHz	1.267	1.176	6.834	39.533
7.130 GHz	1.274	1.180	7.467	42.865
7.228 GHz	1.281	1.184	8.145	44.359
7.325 GHz	1.288	1.189	8.978	42.677
7.423 GHz	1.295	1.193	9.931	39.218
7.520 GHz	1.303	1.197	11.041	34.685
7.617 GHz	1.311	1.202	12.321	29.692
7.715 GHz	1.319	1.207	13.891	24.760
7.813 GHz	1.327	1.212	15.701	20.612
7.910 GHz	1.336	1.217	17.841	17.318
8.008 GHz	1.344	1.222	20.394	14.297
8.105 GHz	1.353	1.228	23.268	12.143
8.203 GHz	1.363	1.233	26.686	10.224
8.300 GHz	1.372	1.239	30.468	8.713
8.398 GHz	1.382	1.246	34.176	7.500
8.495 GHz	1.392	1.252	37.335	6.486
8.592 GHz	1.402	1.259	39.298	5.627
8.690 GHz	1.412	1.267	38.375	5.067
8.787 GHz	1.422	1.274	35.118	4.800
8.885 GHz	1.434	1.279	31.257	4.835
8.982 GHz	1.444	1.277	30.013	5.033
9.080 GHz	1.456	1.270	31.837	4.641
9.178 GHz	1.467	1.273	31.889	3.930
9.275 GHz	1.479	1.281	28.705	3.263
9.373 GHz	1.491	1.289	24.266	2.755
9.470 GHz	1.503	1.297	20.347	2.398
9.568 GHz	1.516	1.304	16.994	2.119
9.665 GHz	1.529	1.312	14.175	1.890
9.762 GHz	1.542	1.319	12.040	1.709
9.860 GHz	1.555	1.326	10.232	1.558
9.957 GHz	1.569	1.334	8.703	1.408

10.06 GHz	1.583	1.341	7.534	1.297
10.15 GHz	1.597	1.348	6.559	1.194
10.25 GHz	1.612	1.355	5.731	1.105
10.35 GHz	1.627	1.363	4.999	1.011
10.45 GHz	1.642	1.370	4.465	0.948
10.54 GHz	1.659	1.378	3.917	0.873
10.64 GHz	1.675	1.387	3.480	0.810
10.74 GHz	1.693	1.396	3.113	0.763
10.84 GHz	1.710	1.404	2.798	0.712
10.93 GHz	1.727	1.412	2.558	0.673
11.03 GHz	1.746	1.421	2.310	0.635
11.13 GHz	1.764	1.429	2.124	0.600
11.23 GHz	1.783	1.438	1.927	0.566
11.32 GHz	1.804	1.448	1.759	0.533
11.42 GHz	1.822	1.454	1.608	0.501
11.52 GHz	1.843	1.464	1.486	0.480
11.62 GHz	1.864	1.473	1.359	0.454
11.71 GHz	1.885	1.481	1.265	0.436
11.81 GHz	1.906	1.490	1.169	0.412
11.91 GHz	1.931	1.501	1.087	0.394
12.01 GHz	1.953	1.510	0.995	0.372
12.10 GHz	1.979	1.521	0.927	0.359
12.20 GHz	2.004	1.531	0.856	0.339
12.30 GHz	2.030	1.541	0.802	0.327
12.40 GHz	2.057	1.554	0.759	0.314
12.49 GHz	2.083	1.564	0.700	0.299
12.59 GHz	2.113	1.576	0.653	0.291
12.69 GHz	2.142	1.587	0.620	0.282
12.79 GHz	2.174	1.599	0.575	0.265
12.88 GHz	2.209	1.614	0.539	0.257
12.98 GHz	2.242	1.628	0.509	0.247
13.08 GHz	2.275	1.640	0.477	0.236
13.18 GHz	2.309	1.653	0.458	0.229
13.27 GHz	2.344	1.665	0.430	0.225
13.37 GHz	2.379	1.676	0.404	0.215
13.47 GHz	2.417	1.691	0.377	0.207
13.57 GHz	2.453	1.702	0.359	0.202
13.66 GHz	2.494	1.717	0.333	0.192
13.76 GHz	2.534	1.729	0.311	0.186
13.86 GHz	2.577	1.743	0.301	0.184
13.96 GHz	2.624	1.761	0.280	0.178
14.05 GHz	2.667	1.774	0.264	0.177
14.15 GHz	2.716	1.791	0.258	0.176
14.25 GHz	2.763	1.806	0.246	0.174
14.35 GHz	2.814	1.824	0.245	0.175
14.44 GHz	2.866	1.839	0.222	0.165
14.54 GHz	2.920	1.854	0.221	0.169
14.64 GHz	2.974	1.871	0.223	0.170
14.73 GHz	3.030	1.884	0.211	0.167
14.83 GHz	3.096	1.908	0.204	0.165
14.93 GHz	3.156	1.926	0.194	0.164
15.03 GHz	3.216	1.940	0.188	0.161
15.13 GHz	3.285	1.962	0.186	0.160
15.22 GHz	3.356	1.983	0.176	0.159
15.32 GHz	3.423	2.000	0.167	0.156
15.42 GHz	3.500	2.021	0.167	0.156
15.52 GHz	3.576	2.041	0.150	0.150
15.61 GHz	3.657	2.064	0.145	0.148
15.71 GHz	3.742	2.088	0.147	0.150
15.81 GHz	3.828	2.109	0.134	0.146
15.90 GHz	3.919	2.136	0.133	0.146
16.00 GHz	4.008	2.158	0.129	0.147
16.10 GHz	4.109	2.185	0.125	0.145
16.20 GHz	4.203	2.209	0.130	0.150
16.30 GHz	4.309	2.235	0.126	0.149
16.39 GHz	4.419	2.264	0.122	0.149
16.49 GHz	4.526	2.290	0.123	0.152
16.59 GHz	4.643	2.321	0.122	0.154
16.68 GHz	4.772	2.354	0.118	0.152
16.78 GHz	4.886	2.382	0.121	0.155
16.88 GHz	5.017	2.420	0.117	0.155
16.98 GHz	5.150	2.452	0.122	0.159
17.07 GHz	5.275	2.486	0.124	0.162
17.17 GHz	5.414	2.524	0.125	0.165
17.27 GHz	5.559	2.565	0.131	0.168
17.37 GHz	5.701	2.608	0.138	0.174
17.47 GHz	5.852	2.652	0.149	0.181
17.56 GHz	6.001	2.697	0.170	0.193
17.66 GHz	6.150	2.745	0.200	0.208
17.76 GHz	6.325	2.795	0.236	0.226
17.86 GHz	6.480	2.820	0.277	0.252
17.95 GHz	6.657	2.804	0.286	0.270
18.05 GHz	6.823	2.737	0.243	0.266
18.15 GHz	6.990	2.659	0.192	0.249
18.25 GHz	7.153	2.638	0.149	0.227
18.34 GHz	7.329	2.658	0.117	0.210
18.44 GHz	7.478	2.699	0.099	0.201
18.54 GHz	7.649	2.749	0.085	0.196
18.64 GHz	7.797	2.802	0.074	0.194
18.73 GHz	7.940	2.859	0.070	0.195
18.83 GHz	8.074	2.911	0.065	0.197
18.93 GHz	8.187	2.967	0.060	0.199
19.02 GHz	8.306	3.022	0.059	0.203
19.12 GHz	8.364	3.088	0.059	0.208
19.22 GHz	8.417	3.137	0.062	0.215
19.32 GHz	8.455	3.193	0.064	0.221
19.41 GHz	8.488	3.241	0.063	0.228
19.51 GHz	8.491	3.299	0.065	0.235
19.61 GHz	8.492	3.353	0.064	0.243
19.71 GHz	8.483	3.405	0.062	0.250
19.81 GHz	8.428	3.469	0.062	0.258
19.90 GHz	8.364	3.525	0.061	0.268
20.00 GHz	8.283	3.590	0.059	0.277